Institute for Photogrammetry and GeoInformation University of Hannover

European Organization for Experimental Photogrammetric Research

OEEPE-Workshop

Integrated Sensor Orientation

17.9.-18.9.2001 Hannover, Germany

Content :

M. Mostafa, APPLANIX Corp., Richmond Hill,Ont., Canada:
Boresight Calibration without Ground Control

L. Pinto, Technical University of Milano, **G. Forlani**, University of Parma, Italy:
Integrated INS/DGPS Systesms: Calibration and combined block adjustment

C. Ressl, Institute for Photogrammetry and Remote Sensing, Vienna Technical University, Austria:
The OEEPE-Test 'Integrated Sensor Orientation' and its handling within the hybrid-block adjustment program ORIENT

M. Schmitz, G. Wübbena, A. Bagge, Geo++, Garbsen, **E. Kruck**, GIP, Aalen, Germany:
Benefit of Rigorous Modeling of GPS in Combined AT/GPS/IMU-Bundle Block Adjustment

A.J. Seara, The National Geodetic Mapping and Cadastre Agency of Portugal (IPCC), Lisboa, Portugal:
Comparison Between Direct Camera Orientation Measurement and Bundle Block Adjustment Determination

J. Vallet, Swiss Federal Institute of Technology, Lausanne, Switzerland:
Handheld Mobile Mapping System for Helicopter-based Avalanche Monitoring

Integrated Sensor Orientation at ICC, mathematical models and experiences

R.Alamús, A.Baron, J.Talaya
Institut Cartogràfic de Catalunya, Spain.

Abstract

The Institut Cartogràfic de Catalunya (ICC) has been involved in integrated sensor orientation for several years, since the integration of an INS to a line scanner sensor (CASI) in 1997, up to the acquisition of an orientation system that has been installed on a photogrammetric camera in 2000.

On the paper the mathematical models used for the assimilation of the GPS/IMU data in a general adjustment procedure will be explained, especially focusing on the determination of the auxiliary parameters needed for directed georeferencing such as boresight misalignment, camera selfcalibration or linear drift parameters. A tentative combination of GPS/IMU and aerial triangulation, currently under study, will also be explained.

Then the experiences of ICC on the integration of GPS/INS data for sensor orientation, together with the work carried out with the OEEPE experiment will be presented.

1. Introduction

Direct orientation of aerial photogrammetric images is an emergent technology that is gaining ground to the conventional aerial triangulation. However, direct orientation is not just the combination of GPS and IMU observations; a successful orientation depends also on the correct determination of all the elements that participate on the transformation from the image space to the object space. Those elements such as the boresight misalignment matrix, nodal distance, antennas offset, drift parameters… should be determined in order to allow a direct georeferencing. The robustness of the image orientation is a critical issue on a production environment; the ICC has been studying different mathematical models and workflows for a robust determination of the auxiliary parameters.

2. Mathematical model for GPS/IMU sensor orientation

A traditional way for defining the orientation of an aerial photograph has been providing the exterior orientation parameters through the photograph projection centre position (x,y,z) and the angles that define its attitude (ω,ϕ,κ). The integration of GPS and inertial observations allows the determination of the inertial sensor position and attitude. The results of the GPS/IMU integration should be related to the exterior orientation parameters together with some auxiliary parameters through a mathematical model. At the ICC two different models have been studied, a geocentric model that is less intuitive on the results analysis, and a UTM model that is more intuitive, and therefore more suitable in a production environment. Both models have been implemented in the ICC GeoTeX/ACX software, [2].

2.1 General description

As stated above, a correct orientation of photogrammetric images implies the correct determination of some auxiliary parameters that are needed in order to propagate the orientation observations measured

by the IMU and GPS sensors to the image sensor [4], [6]. Those auxiliary parameters can be divided as camera dependent (nodal distance, camera calibration parameters), mounting dependent (antenna offset, boresight misalignment matrix) or mission dependent (camera selfcalibration parameters, drift parameters). The camera dependent and mounting dependent can be well determined in a calibration flight, however special attention has to be paid to the stability of those parameters, in particular to the boresight misalignment matrix. In the models used at the ICC two groups of drift parameters are implemented, the traditional drift parameters for the GPS observations and a set of drift parameters for the IMU observations. If there are enough satellites in view, the distance to the reference station is not very high and the IMU observations have a very good quality the GPS/IMU integration have the capability to provide position and angular information without drifts, however our experience shows that in a production environment position and angular drift parameters still play a significant role on the orientation of the images.

2.2 Geocentric case

The photogrammetric observations are modelled in the usual way through collinearity equations whose image rotation matrix is parameterised in terms of (ω,ϕ,κ). Concerning the GPS aerial control observations the model used is, [3]:

$$\begin{pmatrix} X_{GPS} \\ Y_{GPS} \\ Z_{GPS} \end{pmatrix} = \begin{pmatrix} X_{DT} \\ Y_{DT} \\ Z_{DT} \end{pmatrix} + (1+\mu_{DT})\, R_{DT} \left(\begin{pmatrix} X \\ Y \\ Z \end{pmatrix} + T(\lambda,\varphi)\, R^{j}(\omega\phi\kappa) \begin{pmatrix} X_a^j \\ Y_a^j \\ Z_a^j \end{pmatrix} \right) + \begin{pmatrix} X_s \\ Y_s \\ Z_s \end{pmatrix} + \begin{pmatrix} V_{xs} \\ V_{ys} \\ V_{zs} \end{pmatrix} (t^j - t_0)$$

where

X_{DT} , Y_{DT} , Z_{DT} ,μ_{DT} , R_{DT} are the translation, scale and rotation matrix which defines the datum transfer (it is usually set to the identity transformation).
T is the matrix to transform from a local level frame to an ECEF frame.
X, Y, Z are the geocentric coordinates of the projection centre
X_a, Y_a, Z_a are the antenna offset parameters.
X_s, Y_s, Z_s, V_{xs}, V_{ys}, V_{zs} are the linear drift parameters (position, velocity).
t^j is time when the photograph was taken.
t_0 is the auxiliary reference time.

The IMU data (attitude observations) are modelled as:

$$R_{Roll,Pitch,Heading} = \begin{pmatrix} 0 & 1 & 0 \\ 1 & 0 & 0 \\ 0 & 0 & -1 \end{pmatrix} R(\omega\phi\kappa) \begin{pmatrix} 1 & 0 & 0 \\ 0 & -1 & 0 \\ 0 & 0 & -1 \end{pmatrix} R^{t}_{mis}$$

defining :

$$L_{i,j} := R_{Roll,Pitch,Heading}$$

we have :

$$\begin{aligned} \text{Roll} &= \arctan(L_{3,2}, L_{3,3}) + DR_0 + DR_1 (t^j - t_0) \\ \text{Pitch} &= \arcsin(-L_{3,1}) + DP_0 + DP_1 (t^j - t_0) \\ \text{Heading} &= \arctan(L_{2,1}, L_{1,1}) + DH_0 + DH_1 (t^j - t_0) \end{aligned}$$

where

$R_{Roll,Pitch,Heading}$ is the direction cosine matrix defining the relative orientation of the IMU body frame to the local level frame defined by the sequence of rotations of roll, pitch and heading.

R_{mis} is the fixed direction cosine matrix defining the boresight misalignment matrix.

DR_0, DP_0, DH_0 are the offset of roll, pitch and heading

DR_1, DP_1, DH_1 are the drift of roll, pitch and heading

t^j is time when the photograph was taken.

t_0 is the auxiliary reference time.

2.3 Map projection case

The photogrammetric observations are modelled in the usual way through collinearity equations whose image rotation matrix is parametrized in terms of (ω,ϕ,κ). Concerning the GPS aerial control observations the model used is:

$$\begin{pmatrix} X_{GPS} \\ Y_{GPS} \\ H_{GPS} \end{pmatrix} = \begin{pmatrix} X_{DT} \\ Y_{DT} \\ H_{DT} \end{pmatrix} + (1+\mu_{DT})\, R_{DT} \left(\begin{pmatrix} X_{UTM} \\ Y_{UTM} \\ H \end{pmatrix} + R(\mu^j)\, R^j(\omega\phi\kappa) \begin{pmatrix} X_a^j \\ Y_a^j \\ Z_a^j \end{pmatrix} \right) + \begin{pmatrix} X_s \\ Y_s \\ H_s \end{pmatrix} + \begin{pmatrix} V_{xs} \\ V_{ys} \\ V_{Hs} \end{pmatrix} (t^j - t_0)$$

where

X_{DT} , Y_{DT} , H_{DT} ,μ_{DT} , R_{DT} are the translation, scale and rotation matrix which defines the datum transfer (it is usually set to the identity transformation).

X_{UTM}, Y_{UTM}, H are the projected coordinates of the projection centre

X_a, Y_a, Z_a are the antenna offset parameters.

X_s, Y_s, H_s, V_{xs}, V_{ys}, V_{Hs} are the linear drift parameters (position, velocity).

t^j is time when the photograph was taken.

t_0 is the auxiliary reference time.

$R(\mu^j)$ is $\begin{pmatrix} \mu^j & 0 & 0 \\ 0 & \mu^j & 0 \\ 0 & 0 & 1 \end{pmatrix}$, and μ^j is a scale factor depending on map projection scale factor and flight altitude.

The IMU data (attitude observations) are modelled as:

$$R_{Roll,Pitch,Heading} = \begin{pmatrix} 0 & 1 & 0 \\ 1 & 0 & 0 \\ 0 & 0 & -1 \end{pmatrix} T^t(\lambda,\varphi)\, J_{geo}^{gc}\, J_{utm}^{geo}\, R(\mu^j)\, R\ (\omega\phi\kappa) \begin{pmatrix} 1 & 0 & 0 \\ 0 & -1 & 0 \\ 0 & 0 & -1 \end{pmatrix} R_{mis}^t$$

defining :

$$L_{i,j} := R_{Roll,Pitch,Heading}$$

then:

$$\begin{aligned} \text{Roll} &= \arctan(L_{3,2}, L_{3,3}) + DR_0 + DR_1 (t^j - t_0) \\ \text{Pitch} &= \arcsin(-L_{3,1}) + DP_0 + DP_1 (t^j - t_0) \\ \text{Heading} &= \arctan(L_{2,1}, L_{1,1}) + DH_0 + DH_1 (t^j - t_0) \end{aligned}$$

where

$R_{Roll,Pitch,Heading}$ is the direction cosine matrix defining the relative orientation of the IMU body frame to the local level frame defined by the sequence of rotations roll, pitch and heading.

R_{mis} is the fixed direction cosine matrix defining the boresight misalignment matrix.

DR_0, DP_0, DH_0 are the drift of roll, pitch and heading

DR_1, DP_1, DH_1 are the velocity drift of roll, pitch and heading

t^j is time when the photograph was taken.

t_0 is the auxiliary reference time.

3. ICC experiences

3.1 First experiments

ICC started its experiences on GPS/IMU integration for direct georeferencing with a first successful experiment in 1997. Two projects were done, one block (Linyola) flown at a photo scale 1:32000 containing 80 photos distributed in 5 parallel strips and two cross strips (figure 1) and one linear mapping project (Guissona) consisting in 42 photos flown in 5 strips at a photo scale 1:5000 (figure 2).

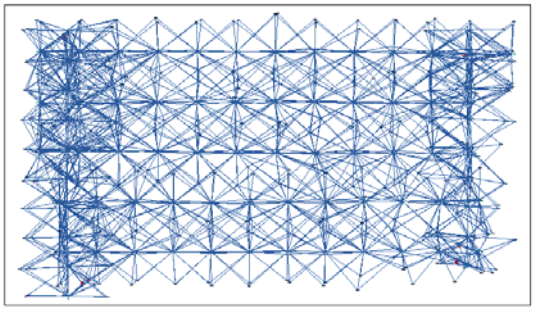

Figure 1: Linyola[1]

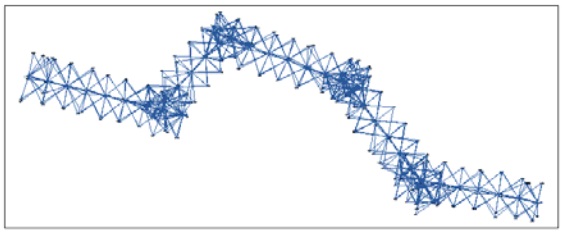

Figure 2: Guissona[1]

The comparison of the photogrammetric points coordinates derived from the classical aerialtriangulation with the ones obtained using direct georeferencing can be seen in table 1, it has to be mentioned that some systematic error on the GPS trajectory were removed by using drift parameters.

Block	X (m)	Y (m)	H (m)
Linyola (1:32000)	0.58	0.65	0.67
Guissona (1 : 5000)	0.12	0.22	0.13

Table 1: RMS of the difference between AT points and points obtained by direct georeferencing

[1] In this plots, photogrammetric observations are shown. Each blue line represents the connection between a projection centre of a photo and a tie point measured in the photo. So, the start of a blue segment represents a tie point and the end represents the photo projection centre in which the tie point has been measured.

3.2 Operational system for Direct Georeferencing

In late 2000 ICC started to operate an Applanix system in a production environment. In order to define an acceptable workflow for a production environment two blocks at flight scale 1:60000 have been flown with the Applanix system and aerotriangulated. The first one (figure 1) had 255 photos in 6 strips in east/west direction and 3 more in north/south direction, while the second one (figure 2) had 368 photos in 11 east/west direction, 5 in north/west direction and 3 following the coast

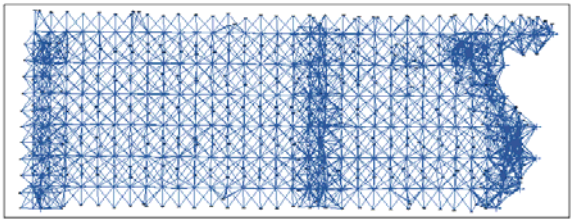

Figure 3: block 1[1]

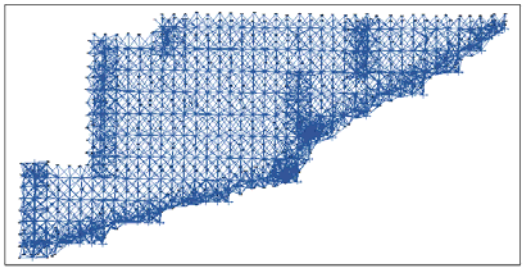

Figure 4: block 2[1]

Thus, once the blocks were aerotriangulated, a calibration adjustment using all information available (photogrammetric, ground control points, GPS and attitude observations) was made in order to compute the boresight misalignment matrix, the camera selfcalibration parameters and to see the attitude residuals. The results obtained in these adjustments were:

	ω	(σ_ω)	φ	(σ_φ)	κ	(σ_κ)
Block 1	0º 4' 25.57"	(2.12")	-0º 1' 52.35"	(1.63")	180º 1' 14.64"	(1.53")
Block 2	0º 4' 22.71"	(1.57")	-0º 1' 54.70"	(1.27")	180º 1' 31.28"	(1.20")

Table 2: boresight misalignment matrices adjusted for each block and standard deviations

Both blocks were flown in 7 days and as it can be observed, the values obtained are equivalents in roll and pitch angles. Only in heading the difference is statistically significant. The reason for such difference can be the drift observed on the heading observations (see figures 5 and 6).

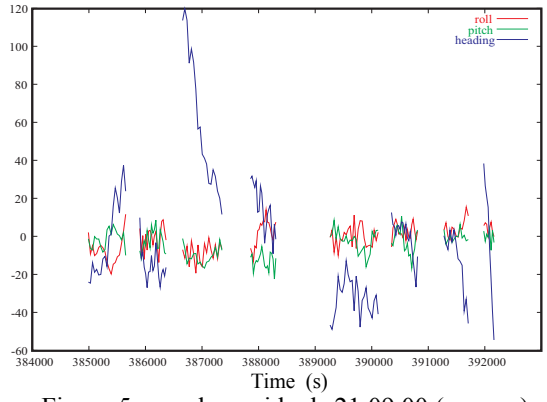

Figure 5: angular residuals 21.09.00 (arc-sec)

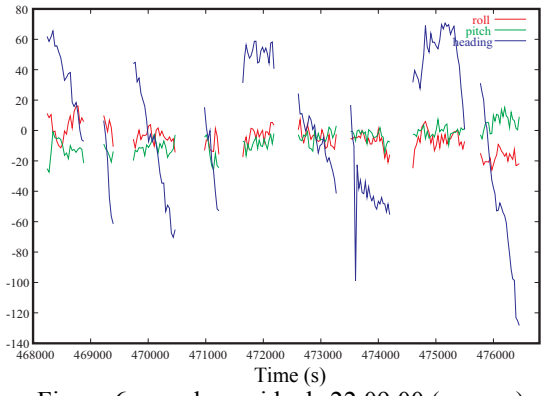

Figure 6: angular residuals 22.09.00 (arc-sec)

From these values it can be seen that roll and pitch accuracies are good enough, but the heading angle residuals are showing a systematic behaviour and can rise as big as 2 arc-minutes. So, according to our experience and at least when flying long photo lines, the heading determination is not accurate enough for robust direct orientation. Therefore, it is necessary to aerotriangulate some photographs for allowing the estimation of a heading drift, in order to correct the systematic errors.

Different configurations using regular sub-blocks for obtaining a robust configuration in order to compute the heading drift and, at the same time, saving a great part of AT were studied. The configuration that showed a good performance consists in measuring tie points in only one model at the beginning and at the end of each strip as shown in figure 7.

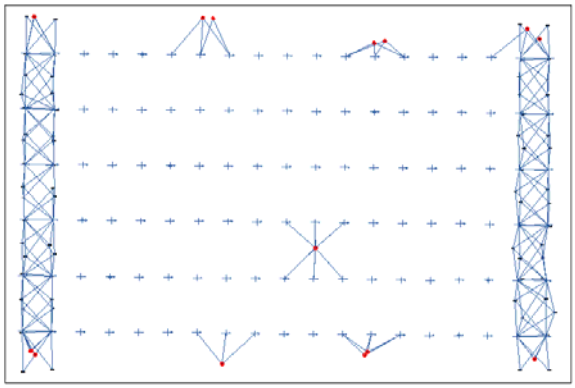

Figure 7: configuration chosen to orient regular blocks[2]

Using this configuration the camera parameters and heading drift can be estimated and so this angular drift corrects the high heading residuals. The angular residuals of this adjustment are shown in figures 8 and 9. As can be seen in figure 9 after applying the angular drift parameters there are still some isolated peaks on the heading residuals, those peaks are reported also in other experiments and can only be identified by measuring some tie points or by a visual determination of the parallax. Those effects can be a problem for stereo plotting and are a serious handicap on the robustness of the method.

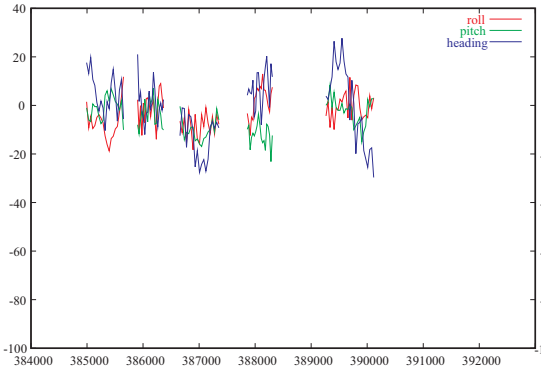

Figure 8: angular residuals 21.09.00 (arc-sec)

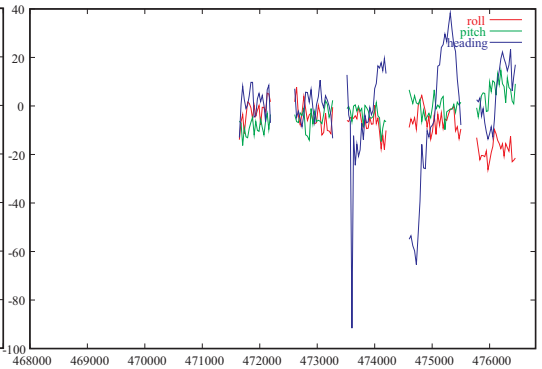

Figure 9: angular residuals 22.09.00 (arc-sec)

To check the accuracies on the ground given by the exterior orientation obtained using this configuration, a forward intersection adjustment was computed. The ground coordinates points obtained have been compared with those given by the AT of each blocks.

The differences obtained are similar for both blocks and quite good. Following the differences for block 1 are plotted:

---

[2] Each cross represents a photo projection centre. Blue lines represent the connection between a photo projection centre and a tie point measured in the photo. Red points represent ground control points observed in a photo.

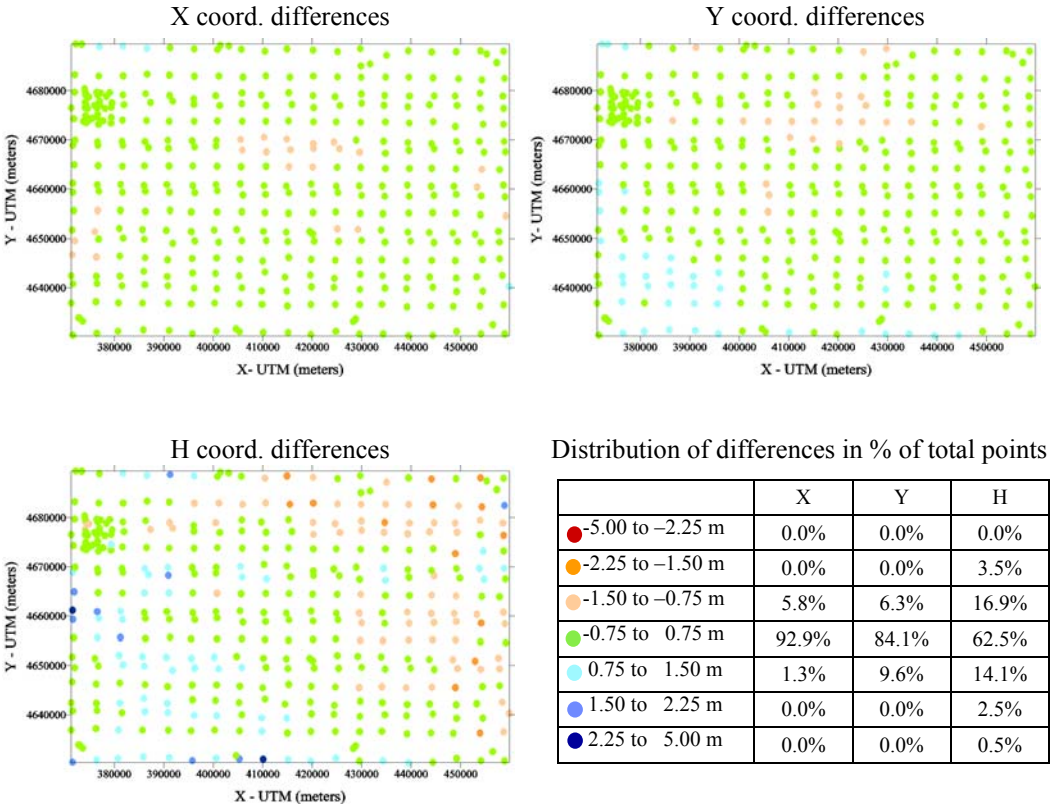

Distribution of differences in % of total points

	X	Y	H
-5.00 to –2.25 m	0.0%	0.0%	0.0%
-2.25 to –1.50 m	0.0%	0.0%	3.5%
-1.50 to –0.75 m	5.8%	6.3%	16.9%
-0.75 to 0.75 m	92.9%	84.1%	62.5%
0.75 to 1.50 m	1.3%	9.6%	14.1%
1.50 to 2.25 m	0.0%	0.0%	2.5%
2.25 to 5.00 m	0.0%	0.0%	0.5%

Figure 10: differences on ground coordinates in X_{UTM}, Y_{UTM} and H between AT points and points obtained by configuration chosen

Another aspect that has to be considered is if the configuration chosen allows the estimation of the camera focal length and the principal point corrections. The values for this parameters obtained in the calibration adjustment and those obtained on the proposed configuration are statistically equivalent.

3.3 Stability of the boresight calibration

Efficiency of direct orientation depends on a good knowledge of the geometric relationship between the involved sensors (boresight misalignment matrix). The determination of the misalignment matrix is done though a well controlled calibration flight. It is important to use an updated misalignment matrix to get acceptable results, however, calibration are very expensive and time consuming. So it is very important to study the stability of the misalignment matrix and perform calibration flighst every certain period.

As explained on the previous section the stability of the boresight misalignment matrix has been studied on two independent flights, the time period between the first and the last flight was just 20 days and the misalignment matrix was found the be stable, more studies will be carried out when more blocks with GPS/IMU data will available

Since 1998 ICC is operating a CASI (Compact Airborne Spectographic Imager) and orienting its images by using a GPS/INS system Although the orientation of this sensor is much less demanding that a photogrammetric sensor, [the IFOV (Instantaneous Field Of View) of one CASI pixel is about 300 arcsec while the IFOV of one photo pixel scanned at 15 microns is about 20”] ICC has been

studying the stability of the boresight misalignment between the CASI sensor and the INS system, the results are presented on the following table.

Block	ω (σ_ω)	φ (σ_φ)	κ (σ_κ)	Date
Garrotxa	0º 5'54''(33'')	0º 4'59''(35'')	-0º 1'38''(57'')	1998.07.23
Benifallet	0º 3'36''(50'')	0º 0' 1''(54'')	-0º 4' 2''(165'')	1998.08.04
Bellmunt	0º 5'31''(37'')	0º 5'24''(37'')	-0º 5'24''(96'')	1998.08.19
Paris 1	-0º15'35''(35'')	-0º18'57''(38'')	-0º30' 3''(84'')	2000.04.07
Paris 2	-0º16'30''(35'')	-0º21'24''(36'')	-0º27' 7''(87'')	2000.04.25
Paris 3	-0º15'37''(31'')	-0º22'45''(33'')	-0º36'38''(88'')	2000.05.06
Paris 4	-0º16'24''(37'')	-0º18'15''(36'')	-0º34'22''(104'')	2000.06.02

Table 3: adjusted boresight calibration parameters for several blocks (CASI sensor)

Table 3 shows the results concerning the stability of the boresight (note that the misalignment matrix has been expressed with the ω,φ and κ parameterisation). For these flights it was carried out a bundle block adjustment per flight in order to compute the boresight misalignment matrix. In Garrotxa, Benifallet and Bellmunt blocks the CASI-INS platform was detached between flights and moved from an airplane to another, despite these changes the matrix is fairly stable (specially considering that the IFOV of the sensor is about 5 arc-minutes). Before Paris flights the CASI sensor was upgraded, this explains differences in the boresight calibration due to modifications on the sensor electronics. Adjusted values for κ shows larger differences up to 7 arc-minutes. Due to the narrow FOV of the sensor and the not so accurate available control κ was not possible to determine better (for a deeper discussion on the orientation of the CASI see [1]).

4. **OEEPE experiment**

The ICC has participated in the OEEPE Test Integrated Sensor Orientation, whose purpose was to investigate integrated sensor orientation using GPS and IMU in comparison and in combination with aerial triangulation [5].

Two sets of GPS/IMU data from two different companies were provided, both of them describing the same configuration of a calibration block flown at scales 1:5000 and 1:10000. The goal of the calibration flight was to estimate, though a combined adjustment, the auxiliary parameters needed for a correct direct georeferencing. At ICC the auxiliary parameters adjusted were: boresight misalignment matrix, antenna offset and camera selfcalibration.

4.1 Determination of the boresight misalignment matrix

The boresight misalignment matrices obtained for each company are:

	ω (σ_ω)	φ (σ_φ)	κ (σ_κ)
company 1	0º 5' 26.101" (1.35")	-0º 0' 31.896" (1.33")	0º 3' 36.160" (1.53")
company 2	0º 6' 56.990" (2.11")	0º 3' 16.028" (2.08")	179º 49' 21.521" (1.20")

Table 4: boresight misalignment matrices adjusted and their standard deviations

Analysing these results, it can be commented that it was possible to perform a good determination of the boresight misalignment in both cases. This says that the configuration of the block is robust enough to allow the determination of the relation between the camera system and the IMU system. It can be observed that the standard deviations for company 2 are a little worse that for company 1. This

can be partially explained by a poorer quality of the photogrammetric observations from company 2 block. In fact, the RMS of the photogrammetric residuals obtained in the adjustments have been:

	x image coordinate	y image coordinate
company 1	3.6 μ	3.7 μ
company 2	4.0 μ	4.2 μ

Table 5 : RMS of photogrammetric residuals for each company

4.2 Determination of the antenna offset

The antenna offset, between the camera and the GPS, antenna can be precisely measured using topographic techniques, however, in the calibration flight adjustment done by ICC a correction to the nominal value was also computed. When interpreting the corrections to the nominal antenna offset it has to be kept in mind the strong correlation between its components and other system parameters. (the flight direction component of the antenna offset is highly correlated with an error in the synchronization of the photographs and the height component has the same effect that an error in the nodal distance used in the computations).

The antenna offsets adjusted, for company 1 shows a displacement of 6.5 cm in flight direction and 10.0 cm in height. For company 2, the values were 7.5 cm in flight direction and 8.3 cm in height. As stated above, it is not possible to know if the height correction of the antenna offset is due to an incorrect measurement of the antenna offset or to the use of a wrong value of the nodal distance. Also, as the block were flown at nearly constant velocity (variation of only 10% were observed) a constant error on the synchronization will show up as a correction of the antenna offset on the flight direction (7 cm correction on the flight direction is equivalent to a synchronization error of about 0.0008 seconds). A block with strips flown at significantly different velocities would help to decorrelate these two error types. Moreover, a parameter modelling a synchronization error cannot be adjusted because the position and attitude observations were only available at the exposures time (time span was 5 seconds for photos at 1:5000 and 10 seconds for photos at 1:10000 approximately). It would be desired to have the data at 200 Hz in order to be able to estimate this parameter.

The best way for determining a correct nodal distance is by doing a laboratory calibration of the lens cone. As the blocks were flown at two different scales (1:5000 and 1:10000), it has to be mentioned that the focal length parameter has been decorrelated from the nodal distance or height component of the antenna offset

4.3 Angular drift parameters

Looking at the angular residuals (figures 11 and 12) obtained in the calibration adjustments for both companies, a systematic behaviour is observed in some strips. So, some problems on the determination of the kappa can be identified for both companies. This confirms the behaviour that has been detected in the blocks at flight scale 1:60000 processed by ICC and explained before. The use of angular drift parameters per strip for correcting the heading behaviour can be helpful.

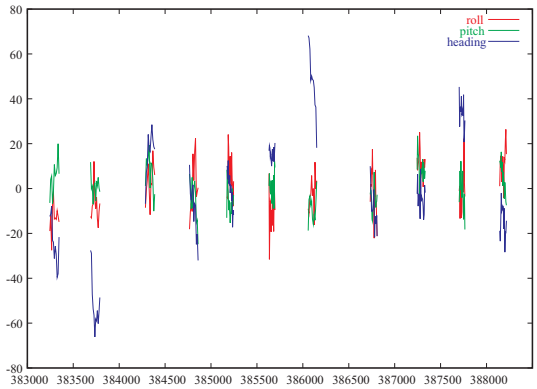

Figure 11: angular residuals obtained for company_1

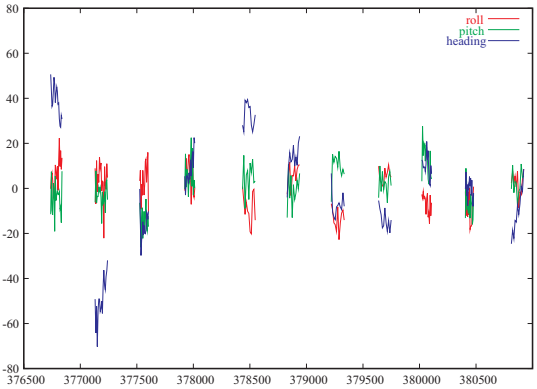

Figure 12: angular residuals obtained for company_2

5. Practical conclusions

Direct georeferencing is showing an acceptable performance, however, there are still some aspects that have to be improved in order to increase the robustness of the technique. The principal aspects to be taken into account in direct georefrencing can be summarized on:

- Calibration flights should be done for a correct determination of all the auxiliary parameters needed on direct georeferencing.
- Studies on the stability of the auxiliary parameters should be carried for determining a recommended recurrence of the calibration flights.
- As the determination of kappa shows sometimes a systematic error that can be corrected using angular drift parameters, minimal aerotriangulation of the block is still necessary to model angular observations errors.
- It is desirable to estimate/calibrate a synchronization offset as well as the nodal distance, this parameters show a high correlation with the flight direction component and the height component of the antenna offset respectively.
- Further studies should be carried out on the integration of GPS/IMU georeferencing and automatic aerotriangulation. This would be helpful to increase the robustness of both methods.

6. References

[1] Alamús R. and Talaya J. 2000: *Airborne sensor integration and direct orientation of the CASI system. International* Archives of Photogrammetry and Remote Sensing, Vol. 33, B1, pp. 5-11.
[2] Colomina I., Navarro J.A. and Térmens A. 1992: *GeoTeX: A general point determination system*. International Archives of Photogrammetry, Vol. 29, Comm. III, pp. 656-664.
[3] Colomina I., 1993: *A note on the analytics of aerial triangulation with GPS aerial control.* Photogrammetric Engineering & Remote Sensing, Vol. 59, No. 11, November 1993, pp. 1619-1624.
[4] Cramer M. 1999: *Direct geocoding – is aerial triangulation obsolete?* in: Fritsch D., Spiller R. (Eds.), Photogrammetric Week ´99, pp. 59-70.
[5] Heipke C., Jacobsen K., Wegmann H. 2001: *OEEPE test on integrated sensor orientation – statusreport*, ASPRS Annual Convention St. Louis, on CD-ROM, 5 p.
[6] Skaloud J. (1999): *Problems in sensor orientation by INS/DGPS in the airborne environment*, Proceedings, ISPRS Workshop "Direct versus indirect methods of sensor orientation", Barcelona.

Ø. Andersen, B. Nilsen
Department of Mapping Sciences
P.O. Box 5034
N-1432 Aas, Norway
Phone : +47 64 94 88 77
Fax : +47 64 94 88 56
E-mail. : ikfbn@ikf.nlh.no
Web : http://www.nlh.no/ikf

Can map compilation rely on GPS/INS alone?

One way of using the GPS/INS data, is to leave out the aerial triangulation. In that case we determine the exterior orientation elements without using aerial triangulation. This is very interesting from an economical point of view.
But does aerial triangulation only determine the exterior orientation elements? Or does the triangulation also determine parameters for the interior of the camera?

GPS/INS may be used in different ways; for example to improve an aerial triangulation. In this paper, however, we have taken an opposite starting point; namely that GPS/INS replaces the triangulation completely. This starting point raises serious questions about reliability since we do not get any terrain points to check the model orientation against. This problem has caught some interest during the recent years.

This investigation deals with another important problem that has got less attention; namely self-calibration. Modern, high quality triangulation/block adjustment includes self-calibration to correct for deformations in the interior of the camera. The correction parameters are not obtained if we instead use GPS/INS for the determination of the exterior orientation elements. Aerial triangulation enables us to compensate for systematic errors in the images that may be considered as film distortion. The utilization of GPS/INS on the other hand, gives no such opportunity. Another aspect is that during map compilation one does not take into consideration the self-calibration parameters calculated in the triangulation. We do compensate for radial distortion, but not for film distortion, which can be a lager source of error.

In this paper, the magnitudes of the model deformations will be investigated, using empirical values for self-calibration parameters obtained in several different blocks.

New Calibration and Computing Method for Direct Georeferencing of Image and Scanner Data Using the Position and Angular Data of an Hybrid Inertial Navigation System

by

M. Bäumker and F.J. Heimes
FH Bochum
University of Applied Sciences

e-mails: manfred.baeumker@fh-bochum.de
franz-josef.heimes@fh-bochum.de

Abstract

The direct georeferencing of images or other photogrammetric data requires accurate angles and positions of the site of the expose. Recently these data will be measured by an inertial reference system augmented by a GPS sensor. While the definitions of the angles derived by the inertial reference system differ from those needed for the georeferencing, appropriate transformation formulas are evident. These formulas also have to consider the small misalignments between the image coordinate system and the body coordinate system established by the inertial instruments. The new transformation algorithms in respect to these misalignments as well as a new method to calibrate the misalignments are described.

1 Introduction

Direct georeferencing of image-, video- and scanner data by means of GPS-augmented inertial systems is of growing importance for photogrammetric applications (*Schwarz* 1995, *Hutton et al.* 1998, *Cramer* 1999). Special attention and considerations have to be focussed to the angular data determined by inertial reference systems which are defined according to the aviation standard ARINC 705 [*Airlines Electronic Engineering Committe* 1982] and to their transformation into the individual photogrammetric system used.

Today's state-of-the-art inertial reference systems are either based on laser gyros or on fibre optical gyros in a so-called strapdown configuration in which the inertial sensors (normally three gyros and three accelerometers) are fixed in respect to a body coordinate system which normally coincides with the principal axes of the aircraft. The inertially determined heading and attitude data according to the aviation norm ARINC 705 as well as other navigational parameters are usually used for flight control, flight management purposes and for the transformations of the velocity increments determined in the body coordinate system into the navigation coordinate system (*Bäumker* 1995). The definition of these coordinate systems and their corresponding angles do not comply with the coordinate systems and angles (omega, phi and kappa) used in photogrammetry. Besides the different definitions, the axes of the body coordinate system and of the camera or image system have to be mounted parallel to each other. But in practice there still remains small angular discrepancies (± 1° or more) after their mounting. These so-called misalignments affect and limit the overall accuracy of the photogrammetric angles. The definition of the different coordinate systems as well as the definition of the different angles are presented in the paper. Furthermore the necessary transformations including the rigorous treatment of the misalignments are derived for some standard application cases in photogrammetry. Besides these fundamental aspects a new adjustment and calibration method to determine the misalignments has been worked out.

2 Fundamentels of the coordinate systems and angles used in inertial navigation

Inertial navigation is based on the continuous integration of the accelerations measured by the accelerometers. In a strapdown configuration the accelerations are measured in a body fixed coordinate system (index b; axes: x^b: along, positive forward, y^b: across, positive to the right, z^b: vertical, positive down). Besides the correction due to gravity and other effects the accelerations have to be transformed prior to its integration into a local level coordinate system – the so-called navigation coordinate system (index n; axes: x^n: northward, y^n: eastward, z^n: vertical in direction of the plumb line). This transformation is performed by a rotation matrix which includes three rotations of the Euler angles according to ARINC 705 (heading: ψ, roll: ϕ, pitch: θ). The angles and rotation matrix have to be continuously updated by means of the gyro measurements and are used for flight control and other navigational or stabilisation purposes. Figure 1 shows the definitions of the coordinate systems and the corresponding Euler angles.

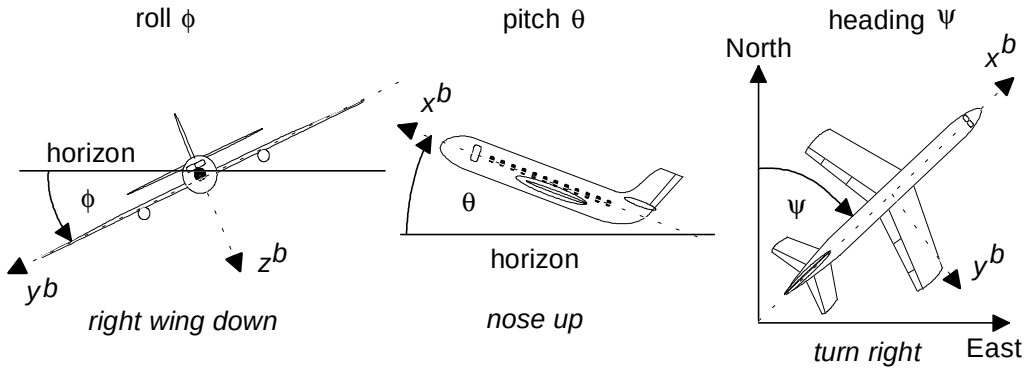

Figure 1: Definition of the body and the navigation coordinate systems and of the Euler angles ϕ, θ, ψ

The roll, pitch and heading angles are used to transform a vector from the body coordinate system into the navigation system or vice versa. The transformation matrix itself is calculated by three consecutive rotation matrices in the following order: 1st rotation: roll around x-axis; 2nd rotation: pitch around y-axis; 3rd rotation: heading (yaw) around z-axis. The combination of the three rotations results in the following orthogonal transformation matrix:

$$\boldsymbol{C}_b^n = \boldsymbol{R}_z(\psi)\cdot\boldsymbol{R}_y(\theta)\cdot\boldsymbol{R}_x(\phi) = \begin{bmatrix} \cos\psi & -\sin\psi & 0 \\ \sin\psi & \cos\psi & 0 \\ 0 & 0 & 1 \end{bmatrix}\cdot\begin{bmatrix} \cos\theta & 0 & \sin\theta \\ 0 & 1 & 0 \\ -\sin\theta & 0 & \cos\theta \end{bmatrix}\cdot\begin{bmatrix} 1 & 0 & 0 \\ 0 & \cos\phi & -\sin\phi \\ 0 & \sin\phi & \cos\phi \end{bmatrix}$$

$$\boldsymbol{C}_b^n = \begin{bmatrix} \cos\psi\cdot\cos\theta & \cos\psi\cdot\sin\theta\cdot\sin\phi-\sin\psi\cdot\cos\phi & \cos\psi\cdot\sin\theta\cdot\cos\phi+\sin\psi\cdot\sin\phi \\ \sin\psi\cdot\cos\theta & \sin\psi\cdot\sin\theta\cdot\sin\phi+\cos\psi\cdot\cos\phi & \sin\psi\cdot\sin\theta\cdot\cos\phi-\cos\psi\cdot\sin\phi \\ -\sin\theta & \cos\theta\cdot\sin\phi & \cos\theta\cdot\cos\phi \end{bmatrix}$$

The inverse transformation (from the navigation coordinate system into the body coordinate system can be easily performed by:

$$C_n^b = (C_b^n)^{-1} = (C_b^n)^T$$

The notation used for the indices directly indicates the transformation direction: the lower index represents the original system and the upper index the target system. Example: If the origin of a camera or a GPS antenna are mounted at different sites a lever arm transformation is needed to transfer the position of the GPS antenna to the camera. As the lever arm $\mathbf{r}^b$ is measured in the body

coordinate system a transformation into the navigation coordinate system $\mathbf{r}^n$ has to be applied. This is done by:

$$\boldsymbol{r}^n = C_b^n \cdot \boldsymbol{r}^b$$

The inverse transformation is performed by:

$$\boldsymbol{r}^b = C_n^b \cdot \boldsymbol{r}^n = (C_b^n)^{-1} \cdot \boldsymbol{r}^n$$

If the transformation matrix is known the Euler angles (roll ϕ, pitch θ, heading ψ) can be directly recalculated from its elements C_{ij} (i = column, j = row):

$$\phi = \arctan \frac{C_{32}}{C_{33}} \qquad \theta = \arcsin -C_{31} = \arctan \frac{-C_{31}}{\sqrt{C_{32}^2 + C_{33}^2}} \qquad \psi = \arctan \frac{C_{21}}{C_{11}}$$

As already mentioned the navigation coordinate system is related to the local level and the direction to the North. In case of a roving craft this coordinate system is not fixed but changes with respect to the velocity of the craft (see Figure 2).

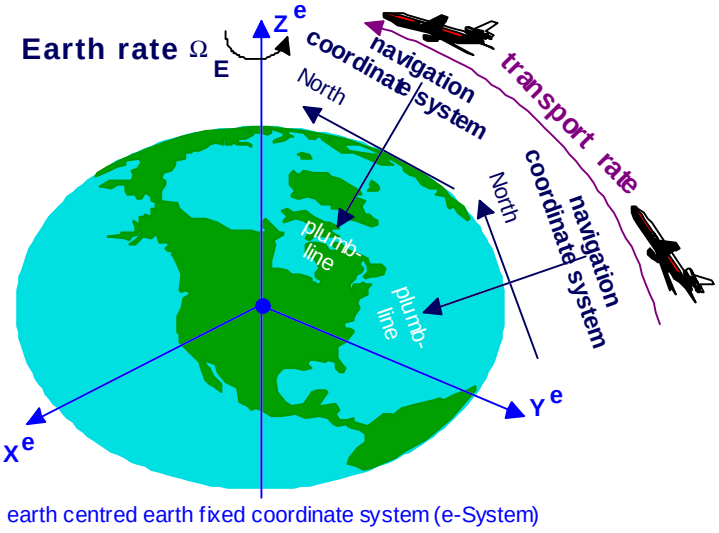

Figure 2: Transport rate, earth rate, navigation coordinate system and its relation to the earth centred earth fixed coordinate (ECEF) system.

These changes are called transport rate Ω_{en}^n and its vector can be calculated by:

$$\Omega_{en}^n = \begin{bmatrix} \dot{\lambda} \cdot \cos\varphi \\ -\dot{\varphi} \\ -\dot{\lambda} \cdot \sin\varphi \end{bmatrix} = \begin{bmatrix} \frac{V_E}{R_E+h} \\ -\frac{V_N}{R_N+h} \\ -\frac{V_E \cdot \tan\varphi}{R_E+h} \end{bmatrix} = \begin{bmatrix} \omega_{en_x}^n \\ \omega_{en_y}^n \\ \omega_{en_z}^n \end{bmatrix}$$

V_N: north velocity
V_E: east velocity
φ, λ, h: ellipsoidal geographic coordinates (latitude, longitude, height)
R_N, R_E: mean radii of the earth ellipsoid

The relation between the varying navigation systems and its axes orientations can be realised with the help of an earth centred earth fixed coordinate system (ECEF, Index e). This is performed by the following two rotation matrices containing the ellipsoidal geographic coordinates φ, λ:

$$\boldsymbol{C}_e^n = \boldsymbol{R}_y(\varphi + 90^\circ) \cdot \boldsymbol{R}_z(\lambda) = \begin{bmatrix} \cos(\varphi+90^\circ) & 0 & \sin(\varphi+90^\circ) \\ 0 & 1 & 0 \\ -\sin(\varphi+90^\circ) & 0 & \cos(\varphi+90^\circ) \end{bmatrix} \cdot \begin{bmatrix} \cos\lambda & -\sin\lambda & 0 \\ -\sin\lambda & \cos\lambda & 0 \\ 0 & 0 & 1 \end{bmatrix} =$$

$$= \begin{bmatrix} -\sin\varphi & 0 & \cos\varphi \\ 0 & 1 & 0 \\ -\cos\varphi & 0 & -\sin\varphi \end{bmatrix} \cdot \begin{bmatrix} \cos\lambda & -\sin\lambda & 0 \\ -\sin\lambda & \cos\lambda & 0 \\ 0 & 0 & 1 \end{bmatrix} = \begin{bmatrix} -\sin\varphi\cdot\cos\lambda & -\sin\varphi\cdot\sin\lambda & \cos\varphi \\ -\sin\lambda & \cos\lambda & 0 \\ -\cos\varphi & -\cos\varphi\cdot\sin\lambda & -\sin\varphi \end{bmatrix}$$

The result is a transformation matrix to transform a vector from the ECEF-System (e-system) to any navigation system (n-system) or vice versa:

ECEF system → navigation system: $\boldsymbol{r}^n = \boldsymbol{C}_e^n \cdot \boldsymbol{r}^e = (\boldsymbol{C}_n^e)^T \cdot \boldsymbol{r}^e$

navigation system → ECEF system: $\boldsymbol{r}^e = \boldsymbol{C}_n^e \cdot \boldsymbol{r}^n = (\boldsymbol{C}_e^n)^{-1} \cdot \boldsymbol{r}^n$

All coordinate systems (b-system, n-system, e-system) are right handed three dimensional cartesian coordinate systems.

3 Fundamentels of the coordinate systems and angles used in photogrammetry

The body coordinate system (b-System) used in inertial navigation seems to be similar to the image coordinate system (B-System) used in photogrammetry. The image coordinate system is realised by the fiducial marks of the camera or the CCD sensor. The origin is the projection centre O in the distance of the focus length c to the principal point (see Figure 3). Instead of the navigation system (n-system) in photogrammetry the quite similar earth fixed terrain or object coordinate system (E-System) is used. Besides the different orientations of the coordinate systems the rotation angles (φ, ω, κ) are defined in very different orders additionally depending on the photogrammetric mapping system.

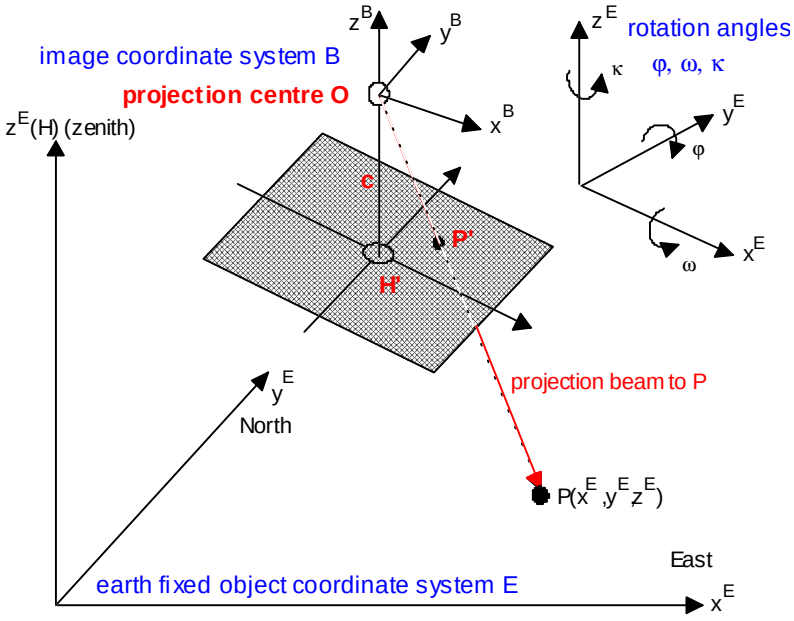

Figure 3: Definitions of the coordinate systems and rotation angles used in photogrammetry: image coordinate system B, terrain or object coordinate system E, and rotation angles φ, ω, κ

A typical candidate of an object coordinate system is the Gauß-Krüger-coordinate system or an equivalent mapping system. But to avoid a left handed orientated coordinate system the x-axis is pointing eastward and the y-axis northward while the direction of the z-axis (height) is aligned to the zenith. Such mapping systems of the earth ellipsoid have a non unique scaling and nevertheless the

meridian deviation is affecting the orientation in respect to the geographic orientation. These difficulties can be avoided by using a spatial cartesian coordinate system tangent to the level surface.

The transformations needed are established for various photogrammetric bundle adjustment systems like BLUH developed at the university Hannover (*Jacobsen* 1996) and like PATB of the university Stuttgart (*INPHO* GmbH 1999) which have different definitions of the order of the rotation angles. Other orders are described in (Kraus 1997 a, b) to which the following transformation algorithms can be easily adopted if necessary. The definition of the rotation angles and its rotation order of the bundle adjustment systems mentioned above (BLUH, PATB) are as follows:

$$\boldsymbol{C}^{B}_{E_{BLUH}} = \boldsymbol{R}_z(\chi)\cdot\boldsymbol{R}_x(\omega)\cdot\boldsymbol{R}_y(\varphi) = \begin{bmatrix} \cos\chi & \sin\chi & 0 \\ -\sin\chi & \cos\chi & 0 \\ 0 & 0 & 1 \end{bmatrix}\cdot\begin{bmatrix} 1 & 0 & 0 \\ 0 & \cos\omega & \sin\omega \\ 0 & -\sin\omega & \cos\omega \end{bmatrix}\cdot\begin{bmatrix} \cos\varphi & 0 & -\sin\varphi \\ 0 & 1 & 0 \\ \sin\varphi & 0 & \cos\varphi \end{bmatrix}$$

$$\boldsymbol{C}^{B}_{E_{PATB}} = \boldsymbol{R}_x(\omega)\cdot\boldsymbol{R}_y(\varphi)\cdot\boldsymbol{R}_z(\chi) = \begin{bmatrix} 1 & 0 & 0 \\ 0 & \cos\omega & -\sin\omega \\ 0 & \sin\omega & \cos\omega \end{bmatrix}\cdot\begin{bmatrix} \cos\varphi & 0 & \sin\varphi \\ 0 & 1 & 0 \\ -\sin\varphi & 0 & \cos\varphi \end{bmatrix}\cdot\begin{bmatrix} \cos\chi & -\sin\chi & 0 \\ \sin\chi & \cos\chi & 0 \\ 0 & 0 & 1 \end{bmatrix}$$

The results of the matrix multiplication are:

$$\boldsymbol{C}^{B}_{E_{BLUH}} = \begin{bmatrix} \cos\kappa\cdot\cos\varphi+\sin\kappa\cdot\sin\omega\cdot\sin\varphi & \sin\kappa\cdot\cos\omega & -\cos\kappa\cdot\sin\varphi+\sin\kappa\cdot\sin\omega\cdot\cos\varphi \\ -\sin\kappa\cdot\cos\varphi+\cos\kappa\cdot\sin\omega\cdot\sin\varphi & \cos\kappa\cdot\cos\omega & \sin\kappa\cdot\sin\varphi+\cos\kappa\cdot\sin\omega\cdot\cos\varphi \\ \cos\omega\cdot\sin\varphi & -\sin\omega & \cos\omega\cdot\cos\varphi \end{bmatrix}$$

$$\boldsymbol{C}^{B}_{E_{PATB}} = \begin{bmatrix} \cos\varphi\cdot\cos\chi & -\cos\varphi\cdot\sin\kappa & \sin\varphi \\ \cos\omega\cdot\sin\chi+\sin\omega\cdot\sin\varphi\cdot\cos\chi & \cos\omega\cdot\cos\chi-\sin\omega\cdot\sin\varphi\cdot\sin\chi & -\sin\omega\cdot\cos\varphi \\ \sin\omega\cdot\sin\chi-\cos\omega\cdot\sin\varphi\cdot\cos\chi & \sin\omega\cdot\cos\chi+\cos\omega\cdot\sin\varphi\cdot\sin\chi & \cos\omega\cdot\cos\varphi \end{bmatrix}$$

Both matrices are orthogonal matrices. Thus its inverse transformation is given by

$$(\boldsymbol{C}^{B}_{E})^{-1} = (\boldsymbol{C}^{B}_{E})^{T} = \boldsymbol{C}^{E}_{B}.$$

While the aeronautical standards are clearly defined in photogrammetry each system has its own specific definition, e.g. for BLUH and PATB the orientation of the axes of the image coordinate system are shown in Figure 4. Its definitions are different from the body coordinate system used in navigation (see Figure 5).

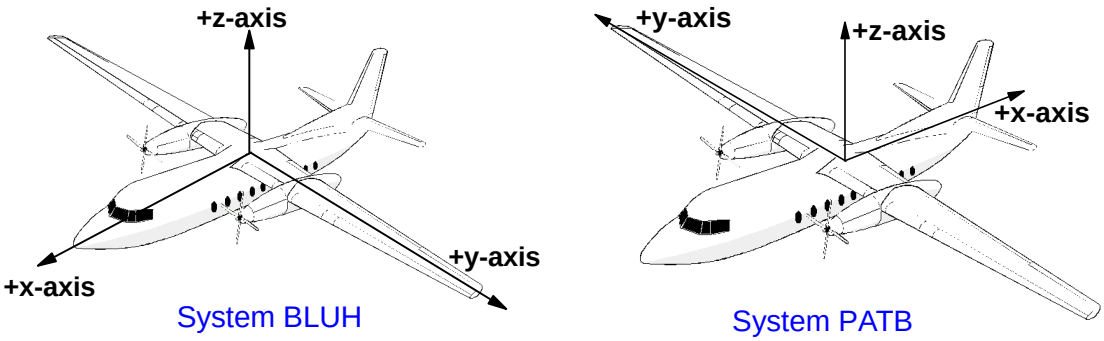

Figure 4: Definition of the orientation of the image coordinate system for BLUH (left) and PATB (right)

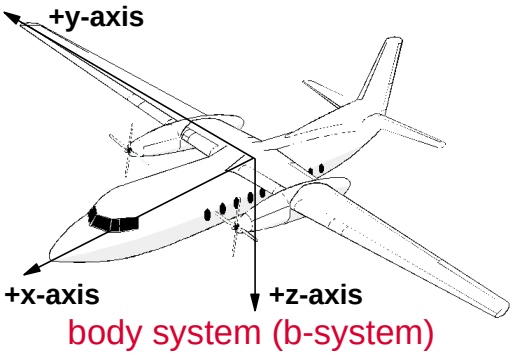

Figure 5: Definition of the body coordinate system used in navigation

After establishing the appropriate matrices either a vector from the image coordinate system into the object coordinate system or vice versa can be transformed by

$$\boldsymbol{r}^B = \boldsymbol{C}_E^B \cdot \boldsymbol{r}^E = (\boldsymbol{C}_B^E)^T \cdot \boldsymbol{r}^E$$ object to image coordinate system (E- to B-system)

$$\boldsymbol{r}^E = \boldsymbol{C}_B^E \cdot \boldsymbol{r}^B = (\boldsymbol{C}_E^B)^{-1} \cdot \boldsymbol{r}^B$$ image to object coordinate system (B- to E-system)

In this notation the vector to be transformed (input) is situated on the right side of the equation and the vector of the target system (output) on the left side. The upper index of the vector on the right must coincide with the lower index of the transformation matrix to be multiplied while its upper index indicates the target system. Note that the indices of the transposed or inverse matrices in brackets are vice versa. This will simplify the following derivations.

If one of the transformation matrices is known the rotation angles (φ, ω, κ) can be recalculated from its matrix elements C_{ij} for which the definition of the rotation order is essential. The results are shown for the two systems BLUH and PATB in Table 1:

System BLUH	System PATB
$\varphi = \arctan \frac{C_{31}}{C_{33}}$	$\varphi = \arcsin C_{13} = \arctan \frac{C_{13}}{\sqrt{C_{23}^2+C_{33}^2}}$
$\omega = \arcsin -C_{32} = \arctan \frac{-C_{32}}{\sqrt{C_{12}^2+C_{22}^2}}$	$\omega = \arctan \frac{-C_{23}}{C_{33}}$
$\chi = \arctan \frac{C_{12}}{C_{22}}$	$\chi = \arctan \frac{-C_{12}}{C_{11}}$

Table 1: Calculation of the rotation angles φ, ω, κ from the matrix elements of the rotation matrix

4 Derivation of the formulas to convert the attitude and heading angles of an INS for direct georeferencing

The subjects of the previous two chapters are focussed on the individual treatment of the rotation and transformation matrices and the corresponding rotation angles used in navigation and in photogrammetry to transform a vector from one system to another system. Table 2 shows a management synopsis of the results.

To convert the attitude and heading angles (ϕ, θ, ψ) of an INS into the photogrammetric angles (φ, ω, κ) the different coordinate systems and rotation angles definitions have to be considered. Furthermore the mapping system used and whether a correction due to earth curvature and meridian deviation has been applied in the photogrammetric system must be considered. For this reason a

spatial cartesian tangent plane coordinate system is recommended as object coordinate system. The origin of this coordinate system should coincide with the centre of the image block.

Navigation	Photogrammetry
roll, pitch and heading angles: ψ, ϕ, θ	phi, omega and kappa : φ, ω, κ
vector in body coordinate system (b-System): $\boldsymbol{r}^b = \begin{bmatrix} x^b \\ y^b \\ z^b \end{bmatrix}$	vector in image coordinate system (B-System) $\boldsymbol{r}^B = \begin{bmatrix} x^B \\ y^B \\ z^B \end{bmatrix}$
vector in navigation coordinate system (n-system): $\boldsymbol{r}^n = \begin{bmatrix} x^n \\ y^n \\ z^n \end{bmatrix}$	vector in terrain or object coordinate system (E-system) $\boldsymbol{r}^E = \begin{bmatrix} x^E \\ y^E \\ z^E \end{bmatrix}$
transformation matrix from body to navigation system $\boldsymbol{C}_b^n = (\boldsymbol{C}_n^b)^T$	transformation matrix from terrain to image system $\boldsymbol{C}_E^B = (\boldsymbol{C}_B^E)^T$
vector in earth centred earth fixed coordinate system (ECEF) $\boldsymbol{r}^e = \begin{bmatrix} X^e \\ Y^e \\ Z^e \end{bmatrix}$	
direction of the plumb line approximated by the ellipsoidal geographic coordinates $\begin{bmatrix} \varphi \\ \lambda \\ h \end{bmatrix}$	
transformation matrix from ECEF to navigation system $\boldsymbol{C}_e^n = (\boldsymbol{C}_n^e)^T$	

Table 2: Concise overview of the different coordinate systems, vectors, angles and transformations matrices used in navigation and in photogrammetry

Because of the different orientation of the coordinate axes in navigation and in photogrammetry two additional transformation matrices are required to get equivalently orientated systems. These are:

1. matrix to convert a vector from b-System to B-system and vice versa: T_b^B
2. matrix to convert a vector form n-System to E-System and vice versa : T_n^E

The matrices consist of the following elements:

System BLUH

$$\boldsymbol{T}_{b_{BLUH}}^B = \begin{bmatrix} 1 & 0 & 0 \\ 0 & -1 & 0 \\ 0 & 0 & -1 \end{bmatrix}$$

System PATB

$$\boldsymbol{T}_{b_{PATB}}^B = \begin{bmatrix} -1 & 0 & 0 \\ 0 & 1 & 0 \\ 0 & 0 & -1 \end{bmatrix}$$

n-System to E-System

$$\boldsymbol{T}_n^E = \begin{bmatrix} 0 & 1 & 0 \\ 1 & 0 & 0 \\ 0 & 0 & -1 \end{bmatrix}$$

Using these matrices the following four vector transformations can be performed:

Body to image coordinate system (b to B): $\boldsymbol{r}^B = \boldsymbol{T}_b^B \cdot \boldsymbol{r}^b$

Image to body coordinate system (B to b): $\boldsymbol{r}^b = \boldsymbol{T}_B^b \cdot \boldsymbol{r}^B = (\boldsymbol{T}_b^B)^T \cdot \boldsymbol{r}^B$

Navigation to object coordinate system (n to E): $\boldsymbol{r}^E = \boldsymbol{T}_n^E \cdot \boldsymbol{r}^n$

Object to navigation coordinate system (E to n): $\boldsymbol{r}^n = \boldsymbol{T}_E^n \cdot \boldsymbol{r}^E = (\boldsymbol{T}_n^E)^T \cdot \boldsymbol{r}^E$

The last mentioned transformation is only valid if a tangent plane coordinate system is used as E-system or if corrections due to earth curvature and meridian deviation are applied in case of Gauß-Krüger-coordinates. Otherwise a further transformation matrix is required to compensate for these effects:

$$\boldsymbol{C}_n^{n'} = \begin{bmatrix} 1 & e_v & -e_e \\ -e_v & 1 & e_n \\ e_e & -e_n & 1 \end{bmatrix} \quad \text{with} \quad \begin{aligned} e_n &= -(\lambda_i - \lambda_0) \cdot \cos\varphi \\ e_e &= (\varphi_i - \varphi_0) \\ e_v &= (\lambda_i - \lambda_0^{GK}) \cdot \sin\varphi \end{aligned}$$

λ_0^{GK}: mean meridian of the Gauß-Krüger-coordinate system

For direct georeferencing the transformation matrix from the image coordinate system (B-system) in which the image coordinates are measured to the terrain system (E-system) (or its inverse matrix) has to be derived for each image from the inertially determined coordinates of the projection centre and the corresponding attitude and headings angles (ϕ, θ, ψ). Then, in the last step, the photogrammetric angles phi, omega and kappa (φ, ω, κ) have to be additionally calculated from the derived matrix.

For each exposure site i the following matrices have to be calculated from the attitude and heading angles (ϕ_i, θ_i, ψ_i), the ellipsoidal geographic coordinates (φ_i, λ_i) and the ellipsoidal geographic coordinates (φ_0, λ_0) of the origin P_0 of the tangent plane system:

$$\boldsymbol{C}_b^{n_i} = f(\phi_i, \theta_i, \psi_i) \qquad \boldsymbol{C}_e^{n_0} = f(\varphi_0, \lambda_0) \qquad \boldsymbol{C}_e^{n_i} = f(\varphi_i, \lambda_i)$$

In case of Gauß-Krüger-coordinates an additional matrix is required

$\boldsymbol{C}_{n_0}^{n'} = f(\varphi_i, \lambda_i, \varphi_0, \lambda_0, \lambda_0^{GK})$ otherwise this matrix has to be replaced by the identity matrix **I**.

Now the following five transformations can be performed:

1. $\boldsymbol{C}_b^e = (\boldsymbol{C}_e^{n_i})^T \cdot \boldsymbol{C}_b^{n_i}$ result: b-system to e-system
2. $\boldsymbol{C}_b^{n_0} = \boldsymbol{C}_e^{n_0} \cdot \boldsymbol{C}_b^e$ result: b-system to n_0-system (navigation system in P_0)
3. $\boldsymbol{C}_b^{n'} = \boldsymbol{C}_{n_0}^{n'} \cdot \boldsymbol{C}_b^{n_0}$ result: b-system to n-system
4. $\boldsymbol{T}_n^B = \boldsymbol{T}_b^B \cdot (\boldsymbol{C}_b^{n'})^T$ result: n'-system to B-system
5. $\boldsymbol{C}_E^B = \boldsymbol{T}_n^B \cdot (\boldsymbol{T}_n^E)^T$ result: E-system to B-system

Combining all transformation matrices one gets after some matrix operations:

$$\boldsymbol{C}_E^B = \boldsymbol{T}_b^B \cdot \left(\boldsymbol{C}_{n_0}^{n'} \cdot \boldsymbol{C}_e^{n_0} \cdot (\boldsymbol{C}_e^{n_i})^T \cdot \boldsymbol{C}_b^{n_i}\right)^T \cdot (\boldsymbol{T}_n^E)^T$$

The photogrammetric rotation angles phi, omega, kappa (φ, ω, κ) have to be calculated as already shown above.

5 Treatment and adjustment of misalignments between INS and camera

High accurate applications (better 0.1°) require an special treatment of the misalignments between INS and camera. For such applications the INS should be mounted firmly at the camera. In practice, the ideal case of exactly parallel axes of INS and camera cannot be achieved with the necessary accuracy. Thus the small error angles (misalignments, see Figure 6) have to be calibrated and considered additionally in the transformations.

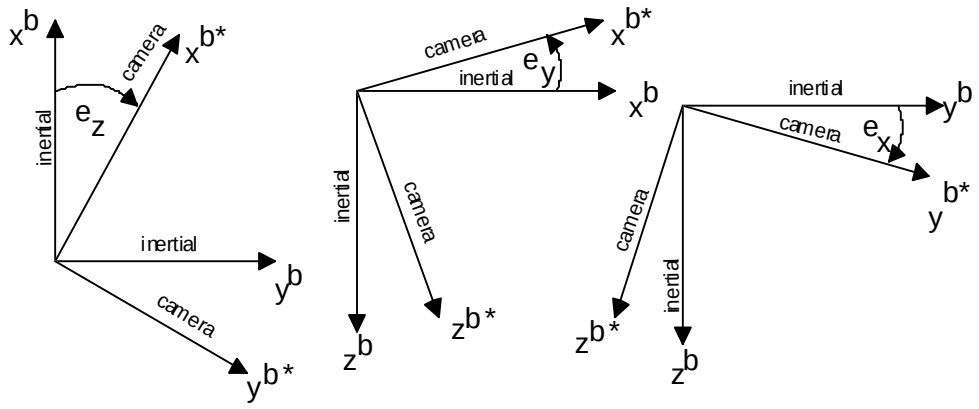

Figure 6: Misalignments e_x, e_y, e_z between INS and camera

Due to the misalignments the body coordinate system b in which the attitude and heading angles are defined the camera refers to a slightly rotated body coordinate system b*. Normally the misalignments e_x, e_y, e_z around the three axes are small angles (< 3°) and a differential rotation matrix is sufficient. This differential rotation matrix is additionally used to convert the original transformation matrix $\boldsymbol{C}_b^n$ prior to its further use. This is done as follows:

$$\boldsymbol{C}_{b^*}^n = \boldsymbol{C}_b^n \cdot \boldsymbol{T}_{b^*}^b$$

with the differential rotation matrix $\boldsymbol{T}_b^{b^*} = \begin{bmatrix} 1 & e_z & -e_y \\ -e_z & 1 & e_x \\ e_y & -e_x & 1 \end{bmatrix}$ (1)

This leads to the following complete transformation matrix in which the misalignments are included:

$$\boldsymbol{C}_E^B = \boldsymbol{T}_b^B \cdot \left(\boldsymbol{C}_{n_0}^{n'} \cdot \boldsymbol{C}_e^{n_0} \cdot (\boldsymbol{C}_e^{n_i})^T \cdot \boldsymbol{C}_b^{n_i} \cdot (\boldsymbol{T}_b^{b^*})^T \right)^T \cdot (\boldsymbol{T}_n^E)^T \qquad (2)$$

If the INS is fixed at the camera the misalignments e_x, e_y, e_z should stay constant. In general neither the axes of the INS nor the axes of the camera defined by the fiducial marks can be easily measured with conventional geodetic methods, For this reason the determination of the misalignments is performed with a specific *on-the-job-calibration* procedure. In this procedure the complete system with camera and INS is put in a test flight over a test area with well surveyed control points. Then in a bundle adjustment for each photo the angles phi, omega and kappa (φ, ω, κ) are determined. These angles and the corresponding angles and positions of the projection centres measured by the INS are used to estimate the misalignments.

The estimation of the misalignments is performed in an adjustment for which the following data of each image are used:

- inertially derived angles: ϕ, θ, ψ
- photogrammetric angles determined in the bundle adjustment: φ, ω, κ
- three dimensional coordinates of the projection centre (ellipsoidal geographic coordinates φ, λ, h, geocentric coordinates X, Y, Z, or Gauß-Krüger-coordinates E, N, H)

The unknown of the adjustment model are formed by the misalignments e_x, e_y, e_z contained in the misalignment matrix (1). When regarding equation (2) the $\boldsymbol{C}_{E}^{B}$- matrix on the left side can be computed from the photogrammetrically determined angles. On the right side all matrices with the exception of the misalignment matrix can be derived from the inertially determined data. To apply the adjustment model the matrix containing the misalignments have to be isolated. After some transformations equation (2) can be written as

$$(\boldsymbol{T}_b^B)^T \cdot \boldsymbol{C}_E^B = \boldsymbol{T}_b^{b^*} \cdot (\boldsymbol{C}_b^{n_i})^T \cdot \boldsymbol{C}_e^{n_i} \cdot \left(\boldsymbol{T}_n^E \cdot \boldsymbol{C}_{n_0}^{n'} \cdot \boldsymbol{C}_e^{n_0}\right)^T \qquad (3)$$

or abbreviated to

$$\boldsymbol{B} = \boldsymbol{T}_b^{b^*} \cdot \boldsymbol{D} \qquad (4)$$

with

$$\boldsymbol{B} = \begin{bmatrix} b_{11} & b_{12} & b_{13} \\ b_{21} & b_{22} & b_{23} \\ b_{31} & b_{32} & b_{33} \end{bmatrix} = (\boldsymbol{T}_b^B)^T \cdot \boldsymbol{C}_E^B$$

and

$$\boldsymbol{D} = \begin{bmatrix} d_{11} & d_{12} & d_{13} \\ d_{21} & d_{22} & d_{23} \\ d_{31} & d_{32} & d_{33} \end{bmatrix} = (\boldsymbol{C}_b^{n_i})^T \cdot \boldsymbol{C}_e^{n_i} \cdot \left(\boldsymbol{T}_n^E \cdot \boldsymbol{C}_{n_0}^{n'} \cdot \boldsymbol{C}_e^{n_0}\right)^T$$

The reconstruction of equation (4) results in:

$$\begin{bmatrix} b_{11} & b_{12} & b_{13} \\ b_{21} & b_{22} & b_{23} \\ b_{31} & b_{32} & b_{33} \end{bmatrix} = \begin{bmatrix} 1 & e_z & -e_y \\ -e_z & 1 & e_x \\ e_y & -e_x & 1 \end{bmatrix} \cdot \begin{bmatrix} d_{11} & d_{12} & d_{13} \\ d_{21} & d_{22} & d_{23} \\ d_{31} & d_{32} & d_{33} \end{bmatrix}$$

Each matrix element on the left side defines a single equation. Thus the following 9 equations can be formed for each photo i:

$$\begin{aligned}
b_{11} &= d_{11} + d_{21} \cdot e_z - d_{31} \cdot e_y & b_{11} - d_{11} &= d_{21} \cdot e_z - d_{31} \cdot e_y \\
b_{12} &= d_{12} + d_{22} \cdot e_z - d_{32} \cdot e_y & b_{12} - d_{12} &= d_{22} \cdot e_z - d_{32} \cdot e_y \\
b_{13} &= d_{13} + d_{23} \cdot e_z - d_{33} \cdot e_y & b_{13} - d_{13} &= d_{23} \cdot e_z - d_{33} \cdot e_y \\
b_{21} &= -d_{11} \cdot e_z + d_{21} + d_{31} \cdot e_x & b_{21} - d_{21} &= -d_{11} \cdot e_z + d_{31} \cdot e_x \\
b_{22} &= -d_{12} \cdot e_z + d_{22} + d_{32} \cdot e_x \quad \text{or} & b_{22} - d_{22} &= -d_{12} \cdot e_z + d_{32} \cdot e_x \\
b_{23} &= -d_{13} \cdot e_z + d_{23} + d_{33} \cdot e_x & b_{23} - d_{23} &= -d_{13} \cdot e_z + d_{33} \cdot e_x \\
b_{31} &= d_{11} \cdot e_y - d_{21} \cdot e_x + d_{31} & b_{31} - d_{31} &= d_{11} \cdot e_y - d_{21} \cdot e_x \\
b_{32} &= d_{12} \cdot e_y - d_{22} \cdot e_x + d_{32} & b_{32} - d_{32} &= d_{12} \cdot e_y - d_{22} \cdot e_x \\
b_{33} &= d_{13} \cdot e_y - d_{23} \cdot e_x + d_{33} & b_{33} - d_{33} &= d_{13} \cdot e_y - d_{23} \cdot e_x
\end{aligned}$$

The equations on the right are equivalent to the well-known adjustment model when disregarding the vector with the residuals **v**:

$$\boldsymbol{l}_i + \boldsymbol{v}_i = \boldsymbol{A}_i \cdot \boldsymbol{x} \qquad (5)$$

with

$$\boldsymbol{l}_i = \begin{bmatrix} b_{11}-d_{11} \\ b_{12}-d_{12} \\ b_{13}-d_{13} \\ b_{21}-d_{21} \\ b_{22}-d_{22} \\ b_{23}-d_{23} \\ b_{31}-d_{31} \\ b_{32}-d_{32} \\ b_{33}-d_{33} \end{bmatrix} \quad \boldsymbol{A}_i = \begin{bmatrix} 0 & -d_{31} & d_{21} \\ 0 & -d_{32} & d_{22} \\ 0 & -d_{33} & d_{23} \\ d_{31} & 0 & -d_{11} \\ d_{32} & 0 & -d_{12} \\ d_{33} & 0 & -d_{13} \\ -d_{21} & d_{11} & 0 \\ -d_{22} & d_{12} & 0 \\ -d_{23} & d_{13} & 0 \end{bmatrix} \quad \boldsymbol{x} = \begin{bmatrix} e_x \\ e_y \\ e_z \end{bmatrix}$$

After applying this equation system to each photo the total normal equations including all measurement are established and solved for the misalignments:

$$\boldsymbol{x} = \left(\sum_{i=1}^{n} (\boldsymbol{A}_i^T \cdot \boldsymbol{A}_i) \right)^{-1} \cdot \left(\sum_{i=1}^{n} (\boldsymbol{A}_i^T \cdot \boldsymbol{l}_i) \right) \qquad \text{n: total number of photos}$$

The standard deviation derived form the residuals in (5) indicates the quality of the adjustment.

6 In situ calibration of the Local Earth Observation system LEO

In the last years at the University of Applied Sciences Bochum the Local Earth Observation system LEO has been developed (*Bäumker et al.* 1998, *Bäumker et al*. 1999, *Bäumker et al.* 2000). The most recent development is based on a state-of-the-art strapdown INS (LLN-G1, see Figure 7) equipped with three fibre optical gyros (FOG) and three pendulum accelerometers and a differential single frequency C/A-Code GPS receiver (LEICA 9400) to augment and to improve the inertial measurements providing an accuracy in positioning of appr. 0.30 m in the DGPS mode. The accuracies of the inertial instruments used are described in Table 3. For best accuracy the modified INS (removal of the power supply) is firmly mounted on a digital camera (at present a Kodak DCS 420 or KODAK DCS 460) and controlled by a stabilised platform (see Figure 8) to guarantee perfect photos even under turbulent flight conditions.

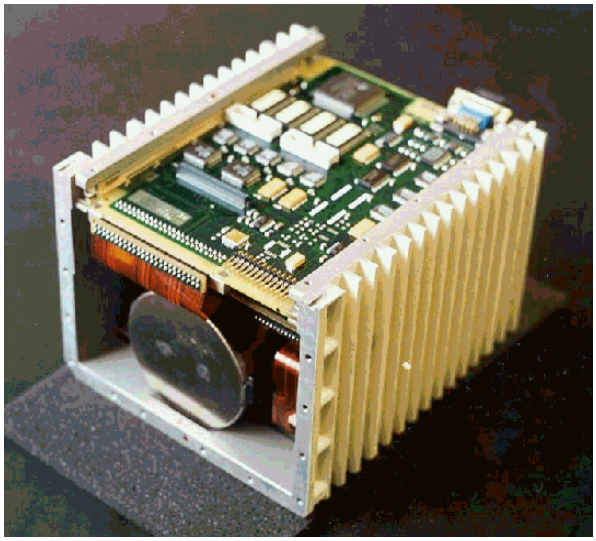

Figure 7: Modified inertial navigation system LLN-G1 with fibre optical gyros; at the front: one of the three coils with 500 m fibre length

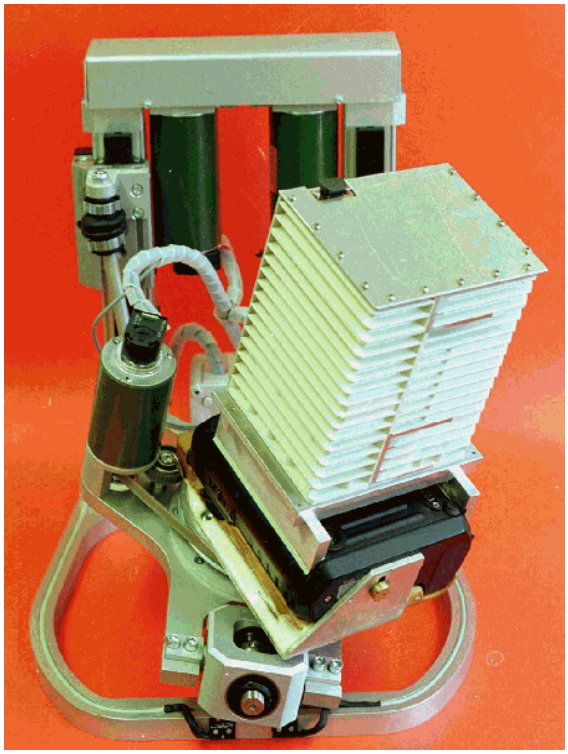

	FOG Gyro	accelero-meter
drift/bias	0.1°/h	0.5 mg
scale factor	100 ppm	1000 ppm
noise	0.02 $°/\sqrt{h}$	0.01 mg

Table 3: Accuracies of the inertial sensors

Camera and INS are mounted in such a way that their principal axes are almost parallel. The remaining small angle differences (misalignments) are determined during a special in situ or *on-the-job-calibration* as already mentioned and will be later additionally considered in the direct georeferencing of the image or scanner data.

Figure 8: Controlled platform with digital camera Kodak DCS 460 (f = 28 mm, 2000 x 3000 pixel) and the FOG-INS LLN-G1 modified (LITEF Germany)

Normally the determination of the misalignments has to be performed with the complete equipment during an extra test flight over an area with sufficient control points. A major disadvantage of this procedure is its dependency from the whether and from the availability of a suited aircraft and test area. For this reason at the University of Applied Sciences Bochum a special indoor calibration procedure has been developed and already carried out. The procedure enables an *on-job-calibration* of the misalignments during a simulated flight in the laboratory. The procedure is based on a test field with 40 control points. The three-dimensional test field has been established in the laboratory of the department of civil engineering with a size of appr. 10 m x 6 m (Figure 9).

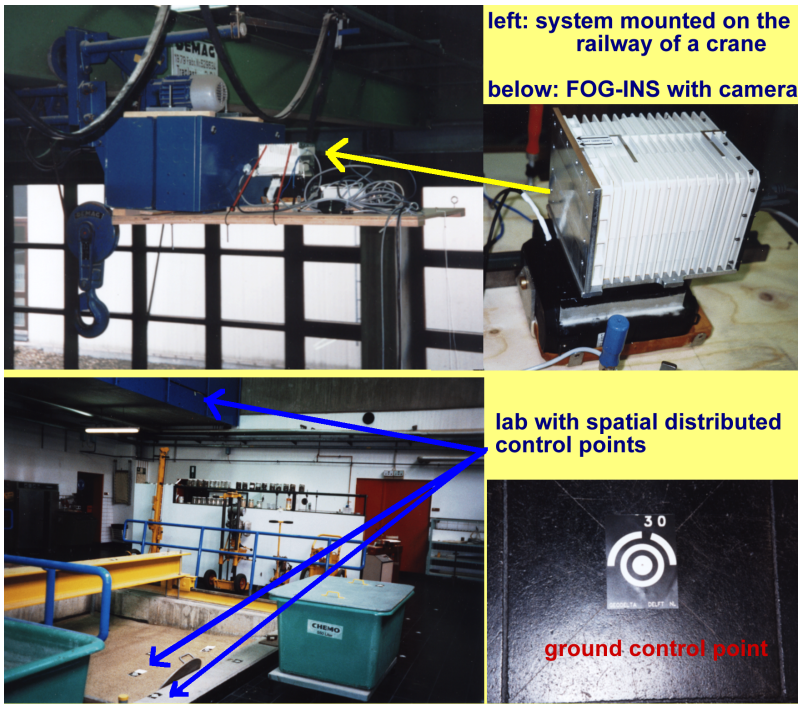

Figure 9: Laboratory of the department of civil engineering with crane, INS, camera and ground control points

The coordinates of the control points were determined by tachymeter and precise level in system WGS84 (accuracy < 1mm). Additionally signalled points are used as tie points in the bundle block adjustment. The *calibration flight* took place without the controlled platform in a height of 3.5 m up to 7 m above ground yielding image scales between 1:250 to 1:125. The remotely controlled steering of the crane with its equipment considered an overlap of the images of 60% forward and 40% across.

While in a real flight the images have to be taken during the motion of the aircraft with this procedure the crane can be exactly stopped at the predetermined exposure positions. During this time the INS is switched to the navigation mode *on-ground* in which a zero velocity update (ZUPT) is performed in the Kalman Filter to estimate the system and sensor errors and to improve the system performance of the INS because in the laboratory no GPS signals are available to augment the system. Thus the INS must operate the other time in the *free inertial mode*.

Another distinctive feature of the lab calibration is the determination of the initial heading from the earth rate estimations during the two minutes self alignment. In general, the initial heading accuracy depends on the gyro biases and on the amount of the horizontal earth rate component resulting in an initial heading accuracy of 0.5 ° at mid latitudes. During an GPS-augmented flight this accuracy is considerably improved to < 0.05 ° soon after some accelerations and the take off of the aircraft with the help of the GPS measurements used as observations in the Kalman Filter. To achieve the required initial heading accuracy in the lab a special two position alignment is performed in which the gyro and accelerometer biases and the earth rate components can be estimated and separated. After this alignment procedure the accuracy of the attitude angles is < 0.005° and of the heading angle < 0.025°.

During the following lab flight 28 photos were taken, one of them is shown in Figure 10. The image coordinates of the signalled control and tie points (see Figure 11) were automatically measured (coded bar marks) with an accuracy of < 2 µm. The bundle adjustment provides for each image the photogrammetric angles (φ, ω, κ) which are fed together with the inertially derived quantities into the above described adjustment model. Table 3 is showing in extracts the coordinates of the projection centres (north, east, height) and the roll, pitch and heading angles (ϕ, θ, ψ) determined by the INS. The adjusted misalignments (e_x, e_y, e_z) and the residuals of the adjustment are listed together with the photogrammetric determined angles (φ, ω, κ) in Table 4. From the residuals a standard deviation of 0.003° Gon for φ, ω and of 0.011° Gon for κ have been estimated.

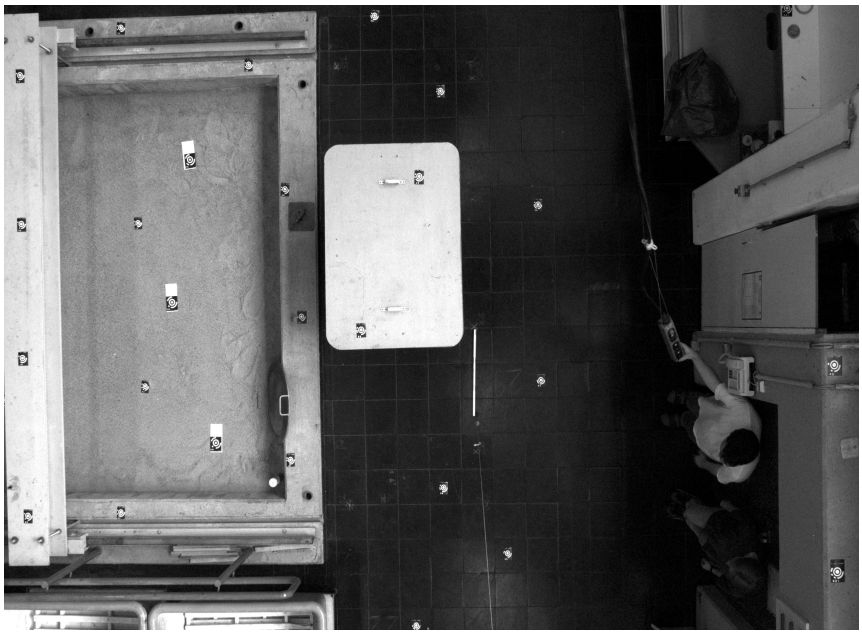

Figure 10 (left): Photo taken at the lab test flight

Figure 11 (below): Signalled ground control point (coded bar mark for automatic measurement of image coordinates)

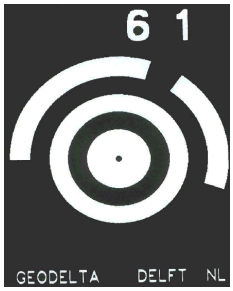

The results show the powerful capability of the lab calibration method to determine the misalignments between camera and INS to be used for direct georeferencing. There is no need for an expensive calibration flight over a test field with well surveyed control points and nevertheless the system is calibrated in situ.

Point	Northing [m]	Easting[m]	height [m]	Roll[°]	Pitch[°]	Head[°]
0	5700085.0	2580116.0	107.0	(origin of the test field)		
101	5700088.2209	2580117.1066	107.2483	-1.45	-0.32	-28.68
102	5700087.7932	2580117.8857	107.2492	-1.45	-0.29	-28.81
103	5700087.3698	2580118.6747	107.2496	-1.45	-0.29	-29.08
104	5700086.9704	2580119.4247	107.2512	-1.45	-0.27	-28.99
....						
401	5700082.0422	2580119.2659	107.2381	-1.37	-0.71	-28.43
402	5700082.9423	2580119.7544	107.2400	-1.45	-0.57	-28.47
403	5700083.9653	2580120.3192	107.2447	-1.55	-0.45	-28.56
404	5700084.8925	2580120.8238	107.2474	-1.39	-0.44	-28.55
405	5700085.9316	2580121.3922	107.2486	-1.43	-0.49	-29.16

Table 4: Coordinates of the projection centres and roll, pitch and heading angles (ϕ, θ, ψ) of the INS (in extracts)

adjusted misalignments: e_x = 0.2126°, e_y = 0.3138°, e_z = 0.0989°

Point	φ [Gon]	ω [Gon]	κ [Gon]	δφ [Gon]	δω [Gon]	δκ [Gon]
101	-1.2100	0.6500	131.7700	-0.0005	-0.0038	0.0117
102	-1.1900	0.6900	131.9000	0.0020	0.0043	-0.0022
103	-1.1900	0.6900	132.2000	-0.0013	-0.0013	-0.0022
104	-1.1800	0.7100	132.1000	-0.0010	0.0011	-0.0018
....						
401	-1.3400	0.2300	131.5000	0.0004	0.0048	0.0117
402	-1.3400	0.4100	131.5100	0.0043	0.0048	-0.0199
403	-1.3800	0.5800	131.6300	-0.0025	0.0025	0.0027
404	-1.2200	0.5000	131.6100	-0.0039	-0.0021	-0.0063
405	-1.2800	0.4900	132.2800	-0.0034	0.0019	-0.0149
Std.dev. (Phi,Omega,Kappa) [Gon]:				0.0026	0.0030	0.0107

Table 5: Adjusted misalignments, photogrammetric angles (φ, ω, κ) and their residuals (in extracts)

7 Results of direct georeferencing

After completion of the system's laboratory calibration as described above a test flight over the test area of the University of Applied Sciences Bochum has been carried out to evaluate the performance of direct georeferencing. The flight parameters have been as follows:

- camera: Kodak DCS 460 CIR (appr. 2000 x 3000 pixel)
- image size: 18,4 mm x 27,6 mm
- focal length: 28 mm
- image scale: 1 : 25.000
- forward overlap: 60 %
- sidelap: 25 %, four flight lines
- base to height ratio: 0,25
- flight height: 700 m
- total number of images: 70

First of all a reference bundle adjustment has been carried out to determine the coordinates of appr. 500 tie points. These tie points (standard deviation in planimetric coordinates appr. 0.25 m, in height appr. 1.0 m) were used as check points in the investigations of the accuracy performance of direct georeferencing.

With the elements of exterior orientation as determined in-flight (angles already corrected for misalignments) forward intersections were carried out with the image coordinates measured – an independent direct georeferencing. From the comparison of both sets of coordinates the following standard deviations were obtained:

$$\sigma_X = 0{,}30 \text{ m}; \sigma_Y = 0{,}43 \text{ m}; \sigma_Z = 1{,}50 \text{ m}$$

It should be mentioned that the calculated standard deviations contain the uncertainties of the bundle adjustment and those of the direct georeferencing.

8 Practical Conclusions

In recent years the aerial survey system LEO (Local Earth Observation) for direct georeferencing of image data has been developed at the University of Applied Sciences Bochum. In the latest stage of development the system is based on a highly dynamic stabilising platform on which the digital camera (Kodak DCS 460) as well as the inertial system (state-of-the-art fibre optical gyros (FOG) and pendulum accelerometers) are mounted.

For direct georeferencing of image data the angles roll, pitch and heading (ϕ, θ, ψ) determined in-flight by the inertial system have to be transformed into the angles omega, phi and kappa (φ, ϕ, κ) of the photogrammetric system used. The transformations additionally have to consider that the image coordinate systems as well as the object coordinate systems in photogrammetry are defined in different ways. In any case the misalignments (non-parallelism) between the principal axes of the camera system and the inertial system have to be corrected for. In general the misalignments are determined from a special calibration flight over a test field with a sufficient number of ground control points.

To avoid extra effort and cost a calibration procedure has been developed which provides the misalignment values from laboratory calibration and which is also independent from weather conditions. The laboratory calibration procedure is based on a three-dimensional test field with 40 ground control points. The *calibration flight* is performed with the help of a remotely controlled travelling crane on which the complete system (camera and inertial system) is mounted in situ. The adjustment for the determination of the calibration data as well as the transformation of the angles is carried out according to mathematically rigorous algorithms. These algorithms can be easily adapted to other photogrammetric coordinate systems.

Due to the lack of GPS measurements in the laboratory a special heading alignment procedure is applied to estimate initial heading and the biases of the inertial sensors. Photos are taken whilst the travelling crane stops. During this time period the inertial system changes into the *on ground mode* in which the system is continuously improved by zero velocity updates (ZUPTs) performed in the Kalman Filter.

The results demonstrate that with the procedure described an accuracy of 0.003 Gon for omega and phi and of 0.011 Gon for kappa is obtainable after calibration of the misalignments. Herewith an efficient procedure is available for the calibration of the misalignments between inertial system and camera and for the transformation of the inertial angles into the photogrammetric system. Besides the

angles omega, phi and kappa the system delivers positional data with an accuracy of 0.3 m (horizontal) resp. 1.5 m (vertical) for direct georeferencing of all kinds of image or scanner data.

References

Airlines Electronic Engineering Committe (1982): ARINC Characteristic 705 - Attitude and Heading Reference System. Aeronautical Radio INC., Annapolis, Maryland 1982.

Bäumker, M. (1995): Basiswissen Inertial- und Sensortechnik. In: Journal for Satellite-Based Positioning, Navigation and Communication, Vol. 4/95, pp. 147-152, December 1995.

Bäumker, M., R. Brechtken, F.-J. Heimes, T. Richter (1998): Hochgenaue Stabilisierung einer Sensorplattform mit den Daten eines (D)GPS-gestützten Inertialsystems. Zeitschrift für Photogrammetrie und Fernerkundung ZPF, Heft 1/98, S. 15-22.

Bäumker, M., R. Brechtken, F.-J. Heimes, T. Richter (1999): Direkte Georeferenzierung mit dem Luftaufnahmesystem LEO. In: Proceedings 10. Internationale Geodätische Woche, Obergurgl, 21.2.-27.2.1999.

Bäumker, M., F.-J. Heimes, H. Hahn, W. Klier, R. Brechtken, T. Richter (2000): Mathematical Modeling, Computer Simulation, Control and Applications of a Stabilized Platform of an Airborne Sensor. In: Proceedings ISPRS 2000 Amsterdam, Volume XXXIII, Part B2, pp. 278-286, Amsterdam, The Netherlands, 16 -23 July 2000.

Cramer, M. (1999): Direct Geocoding - Is Aerial Triangulation Obsolete? In: Photogrammetric Week '99 Stuttgart, S. 59 - 70. H. Wichmann Verlag Heidelberg 1999.

Hutton, J. und E. Lithopoulus (1998): Airborne Photogrammetry Using Direct Camera Orientation Measurements. In: Photogrammetrie - Fernerkundung - Geoinformation 6/1998, pp. 363-370, 1998.

INPHO GmbH (1999): FAQ - PATB-GPS. In: Firmen Website unter http://www.inpho.de (1999).

Jacobsen, K. (1996): User Manual Programm System BLUH. Institute for Photogrammetrie and Engineering Surveys, University Hannover, 1996.

Kraus, K. (1997a): Photogrammetrie, Band 1: Grundlagen und Standardverfahren. 6. Aufl., Dümmlers Verlag, ISBN: 3-427-78646-3, 1997.

Kraus, K. (1997b): Photogrammetry, Vol. 2: Advanced Methods and Applications. 4th ed., Dümmlers Verlag, ISBN: 3-427-78694-3, 1997.

Schwarz, K.P. (1995): Integrated airborne navigation system for photogrammetry. In Photogrammetric Week 1995, pp. 139-154, Wichmann Verlag Heidelberg 1995.

Addresses of the authors:

Prof. Dr.-Ing. M. Bäumker
University of Applied Sciences Bochum
Department of Surveying and Geoinformatics
Lennershofstr. 140
D-44801 Bochum
e-Mail: Manfred.Baeumker@FH-Bochum.de

Prof. Dr.-Ing. F.-J. Heimes
University of Applied Sciences Bochum
Department of Surveying and Geoinformatics
Lennershofstr. 140
D-44801 Bochum
e-Mail: Franz-Josef.Heimes@FH-Bochum.de

Keynote Address

Modern Sensor Orientation Technologies and Procedures

Ismael Colomina
Institute of Geomatic,
Generalitat de Catalunya & Universitat Politècnica de Catalunya
Barcelona, Spain
ismael.colomina@IdeG.es

Abstract

The discipline of sensor orientation, both in photogrammetry and airborne remote sensing, has experienced a remarkable progress by the use of two technologies, satellite precise positioning and its combination with inertial attitude and trajectory determination.

Satellite/inertial attitude and point determination are extremely sophisticated and powerful tools. They involve radio frequency ranging over thousands of kilometers, complex models for orbit determination, precise measurement of angular velocities and linear accelerations, atomic clocks, etc. Today, the ring laser gyro, for instance, is regarded as one of the technology achievements of the past century.

Satellite positioning and inertial attitude and trajectory determination are enabling technologies – like others in the context of contemporary photogrammetry- which were designed with other applications in mind. Their use in photogrammetric [and geodetic] applications pushes them to their very limit which asks for a number of things: understanding of the technologies' principles; familiarity with their behavior; and operational procedures consistent with the application domain context.

The paper will elaborate in the above issues. It will conclude exploring the potential for improvement in the next future.

On the use of GPS/inertial exterior orientation parameters in airborne photogrammetry [1]

Michael Cramer & Dirk Stallmann

Institute for Photogrammetry (ifp)
University of Stuttgart

michael.cramer@ifp.uni-stuttgart.de

Abstract

Within the last five years extensive research was done using integrated GPS/inertial systems for the direct georeferencing of airborne sensors for high-end applications. Pushed by the development and practical use of digital sensor systems, originally started with laser scanner systems and followed by imaging multi-line pushbroom scanners, direct georeferencing offers the only way for an efficient sensor orientation process. Nonetheless, even for standard frame based camera systems, digital or analogue, the use of direct orientation measurements is useful in especially in – from a photogrammetric point of view – unfavourable applications like corridor surveys or single model orientation. In the ideal case using direct exterior orientation elements with sufficient accuracy image orientation without any ground control is possible. Within this paper the use of integrated systems in airborne environments is discussed, where the main emphasis is laid on the combination with standard analogue frame cameras. The empirical results of different well controlled test flights are used to illustrate the today's performance of direct georeferencing based on high-end integrated systems. Additionally, a combined GPS/inertial-AT or integrated sensor orientation approach is presented which allows the in-situ calibration of certain system parameters even without ground control and therefore provides highest flexibility to overcome the most limiting factor of direct georeferencing: uncorrected errors in the overall system calibration. Finally, the use of directly measured exterior orientations in model orientation and DEM generation is investigated.

1. Introduction

Since the last several years the georeferencing of airborne sensors based on direct GPS/inertial measurements of the exterior orientation parameters was a major task at the Institute for Photogrammetry (ifp). Originally initiated by the Digital Photogrammetric Assembly (DPA) digital pushbroom line scanner research project started in 1995 an extended triangulation program was developed where positioning and orientation data obtained from GPS/inertial integration are used as additional observations of the camera air station and attitude. The approach is based on the well known bundle adjustment and its fundamental collinearity equation. Besides standard functionalities like camera self-calibration using different parameter sets the adjustment approach is expanded with additional correction terms to handle systematic errors in the direct exterior orientation elements. In the best case this additional unknowns are used to estimate the inherent boresight-alignment angles to correct the misalignment between sensor coordinate frame and inertial body frame. Otherwise, offsets or linear correction terms are introduced to eliminate the influence of systematic positioning or

[1] Except of the first introductory section this paper closely follows the publication Cramer, M. (2001): Performance of GPS/inertial solutions in photogrammetry, in *Photogrammetric Week 2001*, Fritsch/Spiller (eds.), Wichmann Verlag, Heidelberg, Germany.

attitude offsets or linear errors for example due to incorrectly determined phase ambiguities or remaining gyro biases. Based on the data from the OEEPE test flights the potential of the software is demonstrated.

2. GPS/inertial integration and sensor orientation

2.1. GPS/inertial integration

The benefits of GPS/inertial integration are well known in the meantime: Since both sensor systems are of almost complementary error behaviour the ideal combination will provide not only higher positioning, velocity and attitude accuracy but also a significant increase in reliability, as both systems are supporting each other: The inertial system can help GPS by providing accurate initial position and velocity information after signal loss of lock. Even during satellite outages where the number of visible satellites drops below four INS will provide continuous trajectory information. On the other hand the high absolute performance from GPS can help the inertial navigation system with accurate estimates on the current behaviour of its error statistics. In Kalman filtering used in traditional navigation approaches the internal INS errors are modelled as gyro drifts and accelerometer offsets. These sensor specific errors are estimated together with additional error states describing the navigation errors in position, velocity and attitude. In more enhanced approaches the 15 state error model mentioned before is refined with e.g. gyro and accelerometer scale factors, time variable drifts and error terms describing the non-orthogonality of the inertial sensor axes. Using integrated GPS/inertial systems for high-quality direct georeferencing, models consisting of 15-25 error states are generally used.

2.2. Sensor georeferencing

With the availability of integrated GPS/inertial systems of sufficient accuracy the direct measurement of the fully exterior orientation of any sensor during data recording becomes feasible, which offers an interesting alternative to the standard indirect approach of image orientation based on classical aerial triangulation. Unfortunately, since the GPS/inertial orientation module is physically separated from the sensor to be oriented translational offsets and rotations are existent and have to be considered in addition to the correct time alignment between the different sensor components. Except for the additional misalignment correction (so-called boresight alignment) between inertial sensor axes and corresponding image coordinate frame the correction of time and spatial eccentricities is similar to the general practice in GPS-supported aerial triangulation, where the lever arm has to be determined to reduce the GPS position related to the antenna phase centre on top of the aircraft's fuselage to the desired camera perspective centre. Most likely, the lever arm components between the GPS antenna, the centre of the inertial measurement unit and the camera perspective centre are measured a priori and the appropriate translational offsets are already considered during GPS/inertial data processing. Therefore, the final positioning information from GPS/inertial integration mostly directly refers to the camera perspective centre. Taking this assumption into account the general equation for direct georeferencing which transforms points from the sensor or imaging frame *P* to the corresponding points defined in a local cartesian object coordinate frame *L* is given as follows (Equation (1)).

$$\begin{bmatrix} X_P \\ Y_P \\ Z_P \end{bmatrix}_L = \begin{bmatrix} X_0 \\ Y_0 \\ Z_0 \end{bmatrix}_L + \lambda \cdot R_B^L(\omega,\varphi,\kappa) \cdot \Delta R_P^B(\Delta\omega,\Delta\varphi,\Delta\kappa) \cdot \begin{bmatrix} x_p \\ y_p \\ -f \end{bmatrix}_P \qquad (1)$$

This equation is based on the well known spatial similarity transformation also used for standard indirect image orientation supplemented with an additional rotation matrix ΔR_P^B as a function of the boresight alignment angles $\Delta\omega, \Delta\varphi, \Delta\kappa$ rotating the image vector $(x_p, y_p, -f)^T$ from the photo

coordinates *P* to the body-frame system *B*. The rotation is necessary since the directly measured orientation angles refer to the body-frame system defined by the inertial sensor axes and not to the image coordinate system. This is different from the indirect approach. Although a first raw alignment of both coordinate frames is tried during system installation manually, misorientations – typically in the size of a few tenth of a degree – remain and have to be compensated numerically during boresight correction. The final rotation angles ω, φ, κ are derived from the GPS/inertial attitude data. After R_B^L rotation and subsequent scaling of the image vector the translation $(X_0, Y_0, Z_0)^T$ based on the reduced and transformed GPS/inertial position measurements results in the final object point coordinates. This modified spatial similarity transformation describes the basic mathematical model not only for direct georeferencing but also for a general combined GPS/inertial-AT approach for image orientation. Similar to standard aerial triangulation the modified model may be expanded with additional unknowns to allow the overall system calibration which will be illustrated in more details in Section 2.4.

2.3. Coordinate frames and attitude transformation

Within the previous sub-section one major point was not considered: The orientation angles from GPS/inertial are not comparable to the photogrammetric angles ω, φ, κ and therefore cannot be used to build up the R_B^L matrix directly. Since INS and integrated GPS/inertial systems originally were designed for navigation purposes the computed attitudes are interpreted as navigation angles roll r, pitch p, yaw y. At a certain epoch t_i these navigation angles are obtained from a matrix $R_B^{N(t_i)}$ at time t_i rotating the inertial body frame to the so-called navigation frame N which is a local system whose origin is located in the centre of the inertial sensor axes triad. Since the INS is moving relatively to the earth's surface this local frame is not constant but moving with time, therefore the x-axis of this local navigation frame always points to the local north direction where the z-axis follows the local plumb line pointing down and the y-axis completes the right hand frame. In contrary to this, the photogrammetric image orientation angles from indirect image orientation based on the collinearity equation are obtained from a transformation between the sensor frame (photo coordinates) and a fixed cartesian earth related local system normally defined as an east-north-up coordinate system. The origin of this local frame is given with its geographic coordinates Λ_0, Φ_0 and therefore clearly differs from the moving local navigation frame. Hence, the conversion of navigation angles is necessary to enable the image orientation based on the equation mentioned above.
One possible way to transform the navigation angles to photogrammetric attitudes is realized via the cartesian earth-centred earth-fixed coordinate system to connect the time variable local navigation frame $N(t_i)$ with moving origin (time varying position Λ_i, Φ_i), and the fixed photogrammetric local coordinate system *L*. Now, the following Equation (2)

$$R_B^L(\omega,\varphi,\kappa) = R_{N(t_0)}^L(\pi,0,-\frac{\pi}{2}) \cdot R_E^{N(t_o)}(\Lambda_0,\Phi_0) \cdot R_{N(t_i)}^E(\Lambda_i,\Phi_i) \cdot R_B^{N(t_i)}(r,p,y) \qquad (2)$$

is found defining the transformation from the observed navigation angles *r, p, y* to the photogrammetric angles ω, φ, κ. The rotation matrix $R_{N(t_0)}^L$ is obtained from the composed two elementary rotations $R_1(\pi) \cdot R_3(-\pi/2)$ to align the different axes directions between the local navigation system *N* and the photogrammetric local frame *L*. In case the axes directions between inertial body frame *B* and imaging coordinate frame *P* do not coincide an additional correction matrix R_P^B similar to the axes alignment rotation before has to be considered at the right end of the matrix product. A slightly different solution to this transformation problem and additional information on the definition of the different coordinate frames is given in *Bäumker & Heimes* (2001).

2.4. System calibration

One inherent problem in image orientation is the overall system calibration. Any discrepancies between the assumed mathematical model used in the orientation process and the true physical reality during image exposure will cause errors in object point determination. This problem appears in traditional indirect as well as in direct image orientation but in the second approach based on GPS/inertial measurements system calibration gains in importance significantly. In classical aerial triangulation additional parameters like mathematical polynomials (e.g. *Ebner* 1976, *Grün* 1978) or – alternatively – physical relevant parameters (e.g. *Brown* 1971, originally designed for use in terrestrial photogrammetry) are used to fit the physical process of image formation with the assumed mathematical model of central perspective. For direct georeferencing especially the modelling of the interior geometry of the imaging sensor is of major importance since GPS/inertial now provides direct measurements of the true physical camera position and orientation during exposure whereas in bundle adjustment the exterior orientations are estimated values only. Although these values are optimal values from an adjustment point of view they might differ significantly from the physically valid parameters due to the strong correlation with the interior orientation of the camera and the additional parameters for self-calibration. Due to the perfect correlation between camera focal length and vertical component a small difference of about 20µm between assumed focal length from lab-calibration and true focal length during camera exposure for example will result in a systematic height offset of about 20cm for 1:10000 image scale. Besides the already mentioned parameters for self-calibration and boresight alignment calibration, additional corrections for subsequent correction of directly measured positioning or attitude data are considered. This is similar to standard GPS-supported aerial triangulation where additional constant offsets or linear drifts are used to compensate systematic errors in the GPS positions – if present. Therefore, Equation (1) is completed like follows (Equation (3)),

$$\begin{bmatrix} X_0 \\ Y_0 \\ Z_0 \end{bmatrix} = \begin{bmatrix} X'_0 \\ Y'_0 \\ Z'_0 \end{bmatrix} + \sum_{i=0}^{n} \begin{bmatrix} a_i \\ b_i \\ b_i \end{bmatrix} \cdot t^i \qquad \begin{bmatrix} \omega \\ \varphi \\ \kappa \end{bmatrix} = \begin{bmatrix} \omega' \\ \varphi' \\ \kappa' \end{bmatrix} + \sum_{i=0}^{n} \begin{bmatrix} u_i \\ v_i \\ w_i \end{bmatrix} \cdot t^i \qquad (3)$$

where t^i denotes the time and $(a_i, b_i, c_i), (u_i, v_i, w_i)$ are the terms for position and attitude correction, respectively. The index n determines the order of the correction polynomial. Such offsets or linear correction terms are introduced to eliminate remaining influences of systematic positioning and attitude offsets or first order effects if necessary. Although such errors should not be expected for high quality integrated systems, unfavourable GPS satellite constellations during data acquisition, longer base lines or – very simple – errors in the GPS reference station coordinates or antenna phase centre correction can cause errors in the integrated positions. Additionally, if the quality of the GPS data is not sufficient to completely eliminate the internal systematic inertial errors this will affect the quality of GPS/inertial attitude determination. This scenario shows the relevance of the correction terms given in Equation (3). Under ideal circumstances, if optimal GPS/inertial data are available, the unknowns (u_0, v_0, w_0) are used to estimate the boresight alignment angles. In case Equation (1) is expanded with low order correction polynomials given in Equation (3) the boresight alignment can be replaced with the attitude offset correction since both values are redundant and non separable from the $R_B^L \cdot \Delta R_P^B$ rotation matrix product. Equations (1) and (3) are the basic mathematical formulas to realize a combined GPS/inertial bundle adjustment. In combination with the usual additional parameter sets (preferable modelled as physical relevant and interpretable parameters as proposed by Brown) such a general approach provides the best opportunity for an optimal overall system calibration. The potential of such a combined or integrated approach of sensor orientation is discussed in Section 4.

3. Performance of direct sensor orientation

The investigation of the accuracy performance of integrated GPS/inertial systems for direct sensor orientation was one major topic of research during the last years. In especially at the Institute for Photogrammetry (ifp) extensive test flights were done since 1998 to evaluate the potential and accuracy performance of GPS/inertial systems, where the main focus was laid on the combination of commercial high-end systems with standard analogue aerial frame cameras. Since the images were captured over a well surveyed test site close to Stuttgart (Vaihingen/Enz, size 7km x 5km), the standard method of aerial triangulation was applied to provide independent values for comparison with the exterior orientations from GPS/inertial. Nonetheless, one has to be very careful calling these values reference values since they are estimated values highly correlated with the interior orientation of the camera or non-corrected systematic errors in the model and might differ from the true physical orientation parameters as already mentioned. Therefore, the overall system quality is obtained from check point analysis, where object points are re-calculated using spatial forward intersection based on the known exterior orientations from GPS/inertial and compared to their pre-surveyed reference coordinates. Within this spatial intersection the directly measured exterior orientations are handled as fixed values, i.e. with very small standard deviations $\rightarrow 0$. Before direct georeferencing is performed the boresight alignment is determined from analyzing the attitude differences at a certain number of camera stations. Since for the ifp test flights no spatially separated calibration test site was available this boresight calibration was done within the actual test area which might result in slightly too optimistic accuracy numbers. Generally the calibration site is different from the desired mission area. This topic is discussed in Section 4.

Within the ifp test flights the two only currently available commercial high-end GPS/inertial systems were tested under similar airborne environments. During the first campaign in December 1998 the POS/AV 510 DG – formerly called POS/DG 310 – from Applanix, Canada (*Reid & Lithopoulos* 1998) was flown, about 15 months later in June 2000 a similar test was done using the AEROcontrol IId system from IGI, Germany (*Kremer* 2001). Both systems were also used within the OEEPE test as described in more details in *Heipke et al.* (2001). Since the test configurations and results from the Vaihingen/Enz test flights are already published in detail (*Cramer* 1999, *Cramer et al.* 2000, *Cramer* 2001) only the main results and conclusions are summed up here.

- The tests have shown, that for medium image scales (1:13000, wide-angle camera), the obtained accuracy (RMS) in object space is about 5-20cm for the horizontal and 10-25cm for the vertical component. Using large scale imagery from lower flying heights above ground (1:6000, wide-angle camera) results in slightly better object point quality. The accuracy numbers mentioned above are obtained from the Vaihingen/Enz test site and are reconfirmed with similar results from the OEEPE flight data. Most likely, both independently checked GPS/inertial systems provided quite similar accuracy performance.
- The quality of object point coordinates from direct georeferencing is dependent on the number of image rays used for object point determination. A large image overlap providing a strong block geometry positively influences the point accuracy since multiple image rays can compensate remaining errors in the orientation parameters. From the object point accuracy mentioned above the higher accuracy bound corresponds to blocks with high overlaps where the lower accuracy should be expected from object point determination from 2-3 folded points from single flight strips.
- The overall system quality is mainly dependent on the correct overall system calibration, including the orientation module and the imaging component. In this case especially the vertical component seems to be critical. In several test flights systematic and, moreover, scale dependent offsets in the vertical coordinate of object points were present, which might be due to small inconsistencies between the assumed camera focal length from calibration and the true focal length during the flight. Additionally, uncorrected influences of refraction will cause the same systematic effects. Besides the essential boresight alignment calibration the precise determination of these effects is mandatory before the system is used for direct georeferencing, otherwise they will affect the system performance significantly. Most likely, this calibration will be determined

within a small calibration block and then used for the subsequent test areas, unfortunately the stability of system calibration over a longer time period and the quality of calibration transfer between calibration site and mission area is not proven yet and is under current investigation. Nonetheless, in an ideal scenario the calibration should be performed in the mission area directly, preferable without any ground control. Such an in-situ calibration results not only in significant cost savings since no additional effort for flight and data processing is necessary for the calibration blocks, also the optimal calibration parameters valid for the desired test area could be determined.

4. Performance of integrated sensor orientation

The combined georeferencing using AT and integrated GPS/inertial exterior orientation measurements is based on the mathematical formulas given in Equations (1) and (3). As already pointed out, this model is expanded with additional parameter sets used for self-calibration like in traditional aerial triangulation. This approach provides highest flexibility for system calibration and combined object point determination. The potential and requirements are illustrated within the following example and compared to standard AT and direct georeferencing.

4.1. Test data set

To show the potential of combined GPS/INS-AT for system calibration and point determination the results of one of the calibration blocks from the OEEPE test data sets are depicted in the following. This medium scale (1:10000) image block consists of 5 strips, two of them flown twice. Altogether 85 images (60% long and side overlap, wide-angle camera) were captured during the flight using an analogue aerial camera. For direct georeferencing high quality GPS/inertial data are available, where the boresight angles have been corrected already. Within this paper the results from the GPS/inertial data provided by the Applanix POS/AV system are given only. For quality tests the coordinates of 13 well distributed independent object points with a positioning accuracy of 1cm were available. These points were used for the estimation of the overall exterior system performance. Within the empirical tests object point determination is done in different versions. The results of the several test runs are given in Table 1 and discussed in the following.

4.2. Results from aerial triangulation

Following the rule of thumb (*Kraus* 1990) the theoretical accuracy to be expected from aerial triangulation assuming a wide-angle camera and signalized points is in the range of $\sigma_{X,Y} = \pm 4\mu m$ (in image scale) and $\sigma_Z = \pm 0.005\%$ of flying height above ground corresponding to an object point quality of 4cm (horizontal) and 8cm (vertical). For the chosen test data set these theoretical values are verified from the empirical accuracy based on a GPS-supported AT (Version #1a). Nonetheless, the aspired vertical accuracy is worse since a systematic offset about 20cm in the height component affects the accuracy significantly. This error corresponds for example to a change in camera focal length of 20µm and is compensated if appropriate additional unknowns are introduced into the adjustment. Applying an additional self-calibration using the physically interpretable additional parameter set proposed by *Brown* (1971) the vertical accuracy is in the aspired range (Version #1b, Figure 1). Since there is a perfect correlation between focal length and vertical component similar results are obtained if an additional height offset ΔZ is considered instead of focal length correction Δc. This shows quite clearly that if the data of one image scale corresponding to one flying height are available only, the error source cannot be separated between these two effects. Nevertheless, from further analysis of the 1:5000 image scale blocks from the OEEPE test material a scale dependent variation of the vertical offset is indicated. Since such an effect should be quite unusual for GPS positioning this systematic is caused most likely from the imaging component, due to focal length variations as shown before or non-corrected influences of refraction. Similar scale dependent height variations are already known from earlier test material for example the Vaihingen/Enz test data (*Cramer* 1999).

#	Configuration (+ additional parameters)	GCP/ ChP	$\hat{\sigma}_0$ [µm]	RMS [cm]			Max.Dev. [cm]		
				ΔX	ΔY	ΔZ	ΔX	ΔY	ΔZ
1a	GPS-AT	4/9	6.5	5.6	4.8	21.0	9.6	7.9	31.7
1b	GPS-AT + self-calibrat. (SC)	4/9	4.7	4.2	5.3	9.0	8.3	10.3	18.4
2a	DG	0/13	23.0	16.6	18.6	23.2	29.0	37.7	44.9
2b	DG + boresight alignm. (BA)	0/13	10.8	9.0	7.8	23.0	16.4	16.8	39.5
2c	DG + SC (no focal length c)	0/13	9.7	8.9	7.3	19.9	13.6	12.9	39.6
2d	DG + c, x_p, y_p	1/12	9.8	8.8	7.1	13.7	12.9	13.3	30.8
2e	DG + SC	1/12	9.7	8.6	7.2	13.2	13.5	12.8	29.9
3a	GPS/INS-AT	0/13	6.4	8.2	7.8	18.2	13.3	20.5	30.1
3b	GPS/INS-AT + BA	0/13	6.4	7.6	7.4	18.5	13.3	19.4	29.0
3c	GPS/INS-AT + SC (no c)	0/13	5.4	5.2	6.5	16.5	10.5	15.6	23.9
3d	GPS/INS-AT + c, x_p, y_p	1/12	5.9	6.1	6.1	7.4	13.5	12.6	16.1
3e	GPS/INS-AT + SC	1/12	5.4	5.5	7.3	6.0	10.7	16.4	9.9

Table 1: Accuracy of object point determination (OEEPE test, block Cali10, Applanix POS/AV).

4.3. Results from direct georeferencing

In the second step the point determination is repeated using direct georeferencing (DG, Version #2a, Figure 2) where the GPS/inertial exterior orientations are used as fixed parameters and the object point coordinates are obtained from forward intersection only. The accuracy obtained from DG is about 15-20cm which should be expected for such medium scale blocks. The difference vectors at every single check point are depicted in Figure 2. Since no adjustment is performed the obtained $\hat{\sigma}_0$ is worse compared to standard AT, indicating that the image rays do not intersect in object space due to remaining errors in the exterior orientations or the mathematical model. To estimate the influence of such present errors the object point determination is repeated introducing additional unknowns in the mathematical model. The additional introduction of boresight correction parameters (BA, Version #2b) and the refinement of system self-calibration (SC, Version #2c) results in a significant increase in $\hat{\sigma}_0$ by a factor of 2. Now the horizontal quality from check points is well below 1dm. This shows the potential of the general expanded mathematical model for in-site system refinement. In the ideal case no additional flights for calibration are necessary because the estimation of boresight angles and the camera calibration can be realized in the test site directly even without knowledge of any ground control. Nevertheless, such an efficient in-site calibration is only possible for image blocks providing strong geometry and with overlapping flight lines. This are some limitations for the flight planning, but even more important, the following has to be taken into account: Not all errors can be corrected without ground control. In especially constant shifts in the GPS/inertial positioning and offsets in the height component due to sub-optimal camera calibration have to be mentioned in this context. In standard airborne photogrammetric applications, where image data of one area are available in one certain image scale mostly, the refinement of the camera focal length is not possible without ground information due to the poor intersection geometry of image rays. Therefore the focal length c (Version #2c) was excluded from the self-calibration parameter set. Quite clearly, this shows the limits of direct georeferencing. If the system conditions between calibration and mission flight significantly change and position or height offsets are introduced due to any reason, the compensation of such systematic errors is only possible if at least one single GCP is available in the test area. In other words, such errors are non-detectable without any check points in the mission area and therefore will deteriorate the accuracy significantly, especially if an object accuracy in the sub-decimetre range is aspired. From a reliability point of view such a situation has to be avoided strictly. This indirectly gives an answer to one of the main motivations for direct georeferencing whether sensor orientation without any check

points is really desirable. With one check point that can be introduced as ground control point – if necessary – these systematic errors are compensated. In our case one point located in the middle of the block was used to model the height offset within a refined interior orientation of the camera which increases the vertical accuracy up to 13cm (RMS). Comparing the results from Versions #2d and #2e no significant differences are seen which indicates that the three interior orientation parameters are sufficient to model the systematic effects. Nevertheless, it has to be mentioned that for the final two versions the term DG in its narrower sense is not correctly any more, since the results are obtained with the use of one ground control point now.

4.4. Results from combined GPS/inertial-AT or integrated sensor orientation

Within the final test runs (Versions #3a - #3e) the same calculations from Versions #2a - #2e are repeated again, but one major difference is applied: The GPS/inertial orientations are not used as fixed values any more but appropriate standard deviations are introduced in the adjustment procedure. This approach is similar to the general strategy used in GPS-supported AT where the directly measured coordinates from GPS are used with certain standard deviations corresponding to their expected accuracy. Typically, values of 5-10cm are introduced for the quality of the GPS positioning. Within the data set presented here corresponding standard deviations for GPS/inertial positioning and attitude of 5cm and 0.003deg are introduced, respectively. These values are derived from the comparison to the exterior orientations from standard AT and therefore should represent a realistic estimation of the expected positioning and attitude accuracy. Taking these standard deviations into account the exterior orientations are no fixed values any longer and corrections are estimated within the adjustment. The difference to the DG versions presented before is quite obvious: The reached values for $\hat{\sigma}_0$ are enhanced significantly. Consequently, the empirical accuracy from check point analysis is improved. In especially in Version #3a (Figure 3) the large difference to the RMS values from DG (Version #2a, Figure 2) is visible: the horizontal accuracy increases by a factor of two, although no additional parameters are introduced. The strong image geometry provided from standard frame cameras positively influences the quality of object point determination. The quality of the intersection of image rays in object space is improved since remaining tensions are interpreted as remaining errors in the orientation parameters. Additionally, the comparison of Figures 3 and 2 shows the interesting fact that the existing systematic errors are more clearly visible in Version #3a. Besides the almost constant height offset a horizontal shift in north-west direction seems to be existent. Assuming the exterior orientation as error free and constant, all tensions are projected into the object point determination resulting in a more disturbed difference vector plot. The introduction of additional corrections for the boresight angles and an additional self-calibration (without focal length correction) further improves the accuracy and compensates parts of the error budget. Nevertheless, similar to the previous results the existent vertical offset can only be eliminated with the usage of at least one ground control point which has been done in the final two versions. The best overall accuracy in the range of 6cm (RMS) for all three coordinate components is obtained when all self-calibration parameters are introduced in the adjustment approach (Version #3e, Figure 4). Although the results are only based on one GCP the accuracy is almost similar to the accuracy from GPS-supported AT as calculated in Version #1b and seen in Figure 1.

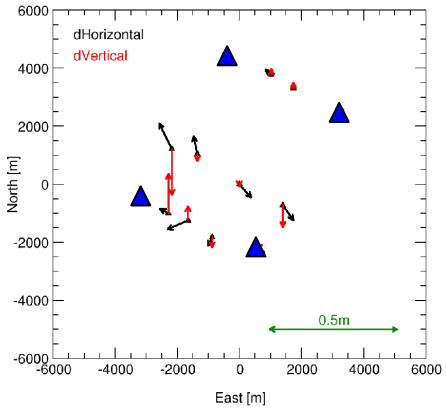

Figure 1: Residuals after GPS-supported AT with self-calibration, 4 GCP (Version #1b).

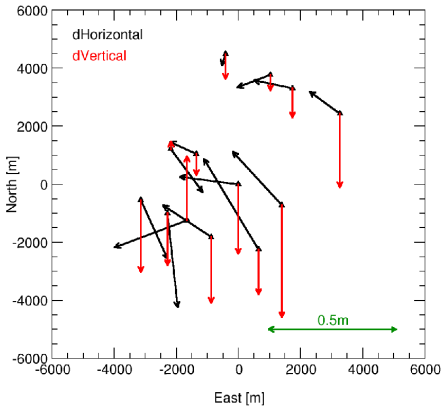

Figure 2: Residuals after direct georeferencing, fixed exterior orientation (EO, Version #2a).

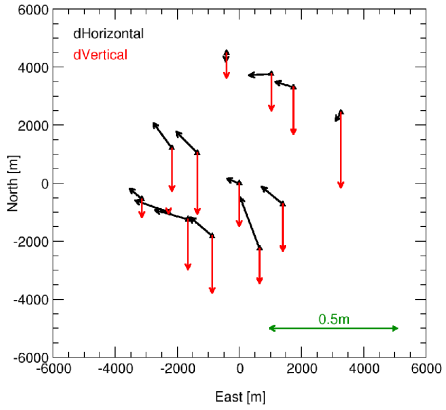

Figure 3: Residuals after GPS/inertial-AT, EO with Std.Dev. (Version #3a).

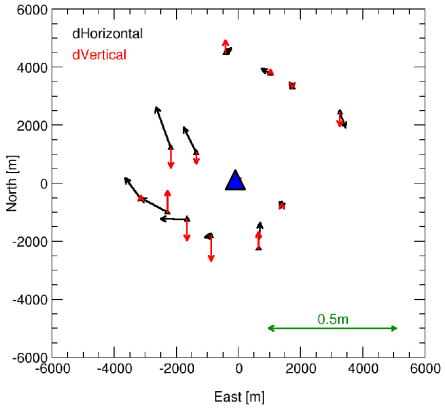

Figure 4: GPS/inertial-AT with self-calibration, 1 GCP, EO with Std.Dev. (Version #3e).

From the results obtained in the integrated or combined GPS/inertial-AT approach the following conclusions can be drawn, showing the possible application fields of GPS/inertial technology in aerial photogrammetry. These conclusions have to be seen in addition to the statements already given at the end of Section 3.

- The quality of object point determination increases if appropriate standard deviations are assumed for the GPS/inertial exterior orientations. The strong image geometry of standard frame cameras compensates remaining errors in the exterior orientation parameters.
- The overall sensor system calibration is a quite demanding task, therefore an in-site calibration is realized in a combined GPS/inertial-AT approach. The exclusive and a priori correction of the three boresight angles does not seem to be sufficient in some cases. The additional use of self-calibration and/or additional boresight refinement parameters yields in better results. This negative influence of non-corrected systematic errors is not only valid for the orientation based on GPS/inertial data but also for traditional AT.
- Using the combined GPS/inertial AT the alignment of boresight angles and sub-sets of the additional self-calibration parameters can be determined within the test area even without ground control if certain requirements related to the flight planning and block geometry are fulfilled.

- Constant position shifts and vertical offsets are the most critical errors since they are non detectable without any check point information. In case such errors occur after system calibration and no ground control is available in the mission area they will decrease the object point accuracy.
- Using an overall sensor system optimally calibrated for the mission area realized with an combined GPS/inertial AT – based on a minimum number of ground control, if necessary – the obtained object point quality is quite similar to the results from GPS-supported or standard AT.

5. DEM generation

Up to now the main focus in GPS/inertial performance tests was laid on the estimation of the overall and absolute system quality obtained and quantified from the empirical check point residuals. Nonetheless, major photogrammetric tasks still are in the field of stereo plotting and automatic DEM generation from stereo models where the results from AT – especially the estimated exterior orientations – in the traditional way serve as input data for the single model orientation. In contrary to the absolute system quality now the relative performance is of interest and the question whether the short term quality of the directly measured GPS/inertial exterior orientations is good enough to generate parallax-free stereo models has to be responded. The current work at ifp is focussed on this topic and first results are given in the following.

The typical accuracy of direct georeferencing based on fixed orientation elements for image blocks reaches values about 15-30µm in image space as shown above and verified for example from the results from the OEEPE test. Since a certain amount of this value can be interpreted a remaining y-parallax such a high $\hat{\sigma}_0$ will prevent stereo measuring capabilities. Nevertheless, the situation changes if only single models or single strips are taken into account. A typical example is shown in Figure 5, where the differences between the GPS/inertial attitudes and the orientation angles from standard AT are depicted for two parallel flight lines (image scale 1:6500, flying height 1000m). These data are part of the Vaihingen/Enz test June 2000, where the IGI AEROcontrol integrated GPS/inertial system was flown in combination with an analogue airborne camera (*Cramer* 2001).

As it can be seen from Figure 5 there is a large jump in the heading angle differences between the two different strips. If this jump is interpreted as an error in the GPS/inertial attitude determination such non-corrected systematic will induce high $\hat{\sigma}_0$ values if points from both strips are used for object point determination. But concentrating on the differences between neighbouring images within one single strip only, the attitude variations are significant smaller.

To estimate the influence of orientation errors on the subsequent DEM generation from stereo images a synthetic stereo pair was simulated (assumed image scale 1:10000, wide-angle camera) where both images consist of the same radiometric information. This synthetic image pair was generated to provide optimal requirements for the automatic point transfer, otherwise the influence of remaining errors in the exterior orientations on the generated DEM is superimposed with effects from erroneous image matching. Thus, the automatic point matching within this stereo pair reconstructed from correct exterior orientation parameters should result in an exact horizontal plane in object space since

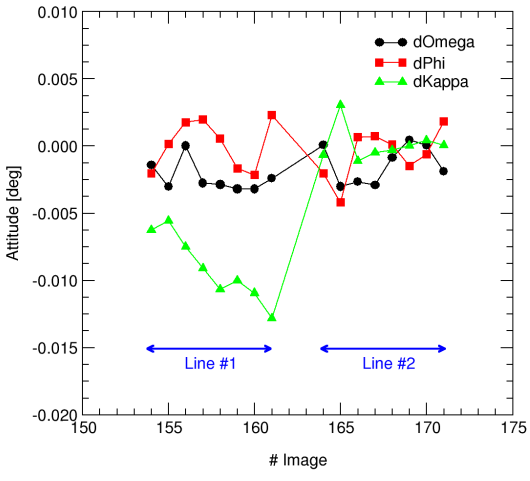

Figure 5: Differences between attitudes from GPS/inertial and AT (Vaihingen/Enz test).

all image points provide the same and constant x-parallax. In the next step additional errors in the exterior orientations are introduced and the image matching is repeated. To get realistic values for the orientation errors the differences in the exterior orientation parameters between neighbouring images are analyzed. Within this example the exterior orientation of the first image was falsified by the following numbers: ΔEast=2cm, ΔNorth=8cm, ΔVertical=12cm, Δω=0.0003deg, Δφ=0.005deg, Δκ=-0.004deg. The values correspond to the orientation differences between the images #165 and #166 from the test data set depicted in Figure 5 and will result in certain y-parallaxes if the automatic image matching is repeated on this mis-oriented stereo pair. In our case the subsequent image matching based on the Match-T program (*Krzystek* 1991) reaches a theoretical 3D point height accuracy of 18cm and an estimated internal height accuracy of the interpolated DEM points of about 3cm. From the internal Match-T classification about 43% of the matched points are classified as regular grid points within the accuracy bounds. The remaining points are classified as so-called lower redundancy points where less than 4 points are used for mesh interpolation or the obtained height accuracy of the interpolated DEM point is below the selected accuracy bound. Although significant y-parallaxes due to orientation errors are present within the images the automatic image matching seems to deliver reasonable results. Nevertheless, this internal accuracy does not necessarily reflect the exterior quality of the obtained surface model. Therefore the resulting surface model obtained from Match-T is shown in Figure 6 together with the true surface plane to be expected from correct matching based on non-erroneous orientation parameters. As one can see the obtained surface shows systematic differences compared to the expected horizontal plane, that can be divided into a global and a local systematic error effect. The global effect more or less represents the model deformation due to the introduced errors in the exterior orientation of the first image. These systematic and well known effects from the theory of relative orientation can also be estimated from the mathematical relation known from relative orientation, where the influence of orientation errors on the obtained height deformation is expressed (*Kraus* 1990). As a first approximation the obtained surface can be described as a plane that shows a negative systematic shift compared to the true horizontal plane and additionally is tilted from south-east to north-west. The size of the vertical errors vary from approximately -1dm to -4dm. Besides this global and low-frequency systematic error representing the influence of model deformation additional higher-frequency local errors are seen as a topography on the surface. For example in the south-eastern part of the model a raise in the heights of about 15cm is clearly visible. Such vertical errors correspond to errors in the automatic image matching which shows the negative effect of the existent parallaxes. Besides the height errors horizontal deformations are present (non-

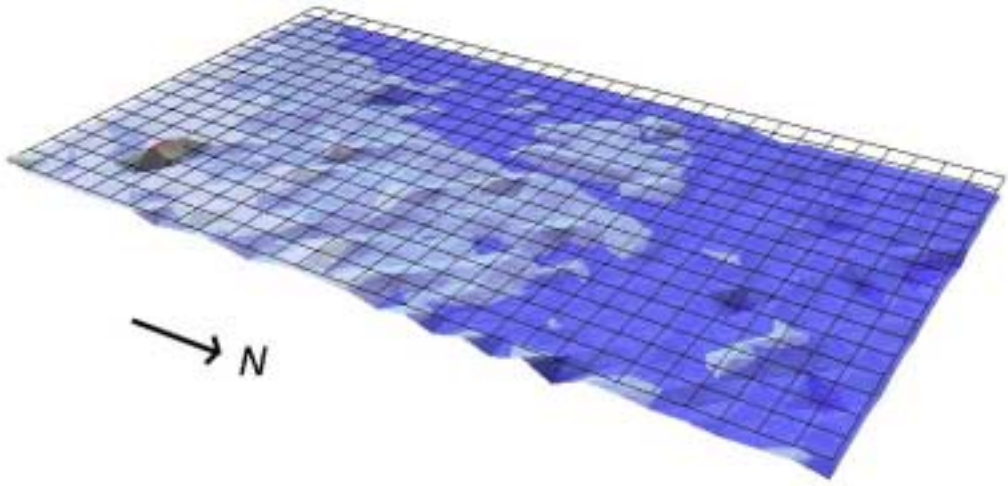

Figure 6: DEM from automatic image matching based on mis-oriented synthetic stereo model.

visible from Figure 6). Further detailed analysis proves that the horizontal displacement errors mainly occur in a star-shaped form pointing in north, north-east direction in the northern half and in south, south-east direction in the southern part of the model. The maximum horizontal errors are in the range of approximately 2dm and therefore quite similar to the mean height offset.
These first and preliminary tests are only based on simulations with a synthetic stereo pair, where the orientation of one image is falsified by a certain amount, which should correspond to an orientation error that can be expected within two subsequently measured GPS/inertial orientation parameter sets. The results have shown that for this specific test data set the DEM generation from stereo models based on automatic image matching obtains acceptable results, although remaining orientation errors are present. Nevertheless, the generated surface model is superimposed with the model deformations. This effect has to be taken into account, if no ground control is available. Alternatively a certain portion of the model deformation can be eliminated with an additional absolute orientation process which is similar to the procedure in relative/absolute image orientation. Further work has to be focussed on the effect and size of height errors due to incorrect automatic point matching. In this case in especially the robustness of the automatic image matching on remaining orientation errors has to be determined. Based on more detailed future investigations recommendations on maximum tolerances for the orientation errors resulting in errors in the surface model should be given for different configurations and image scales, finally.

6. Conclusions

The extensive tests performed in the last years have shown that the GPS/inertial technology is mature for practical use in operational environments. The obtained accuracy based on GPS/inertial data still has remaining potential of improvement. Especially the refinement of the integrated sensor orientation software where the GPS/inertial data are introduced and processed plays a significant role for the obtained overall system quality from imaging and orientation component. Today the integration of direct exterior orientation measurements in the photogrammetric reconstruction process is done on the GPS/inertial positions and attitude level. Nevertheless, in future "true" integrated processing software approaches might be available directly based on the GPS phase measurements and the inertial angular rates and linear accelerations. Within such an integrated evaluation the photogrammetric constraints are used to support the GPS/inertial data processing. Such an approach, similar to the centralized Kalman filtering in GPS/inertial integration, will result in higher overall system reliability and accuracy. To resume, in future, GPS/inertial technology will be used in all parts of the photogrammetric reconstruction process. GPS/inertial systems will become a standard tool for airborne image orientation. The acceptance of this technology will be pushed by the growing use of new digital airborne sensors with their need for a very flexible and fast data evaluation.

References

Bäumker, M. and Heimes, F.-J. (2001): Neue Kalibrations- und Rechenverfahren zur direkten Georeferenenzierung von Bild- und Scannerdaten mittels der Positions- und Winkelmessungen eines hybriden Navigationssystems, in Mitteilungen Institut für Geodäsie, Heft 19, Universität Innsbruck, pp. 3-16.

Brown, D. C. (1971): Close-range camera calibration, Photogrammetric Engineering 37(8), pp. 855-866.

Cramer, M. (2001): On the use of direct georeferencing in airborne photogrammetry, in Proceedings 3rd. International Symposium on Mobile Mapping Technology, January 2001, Cairo, digital publication on CD, 13 pages.

Cramer, M., Stallmann, D. and Haala, N. (2000): Direct georeferencing using GPS/inertial exterior orientations for photogrammetric applications, in International Archives of Photogrammetry and Remote Sensing, Vol. 33 Part B3, pp. 198-205.

Cramer, M. (1999): Direct geocoding – is aerial triangulation obsolete?, in Fritsch/Spiller (eds.): Photogrammetric Week 1999, Wichmann Verlag, Heidelberg, Germany, pp. 59-70.

Ebner, H. (1976): Self-calibrating block adjustment, Congress of the International Society for Photogrammetry, Invited Paper of Commission III, Helsinki, Finland.

Grün, A. (1978): Accuracy, reliability and statistics in close-range photogrammetry, Inter-congress symposium, International Society for Photogrammetry, Commission V, Stockholm, Sweden.

Heipke, C., Jacobsen, K. and Wegmann, H. (2001): The OEEPE test on integrated sensor orientation - results of phase 1, in Fritsch/Spiller (eds.): Photogrammetric Week 2001, Wichmann Verlag, Heidelberg, Germany, to be published.

Kraus, K. (1990): Photogrammetrie (Band 1), Dümmler Verlag, Bonn, Germany, 348 pages.

Kremer, J. (2001): CCNS and AEROcontrol: Products for efficient photogrammetric data collection, in Fritsch/Spiller (eds.): Photogrammetric Week 2001, Wichmann Verlag, Heidelberg, Germany, to be published.

Krzystek, P. (1991): Fully automatic measurement of digital elevation models, in Proceedings of the 43rd Photogrammetric Week, Stuttgart, pp. 203-214.

Reid, D. B. and Lithopoulos, E. (1998): High precision pointing system for airborne sensors, in Proceedings IEEE Position Location and Navigation Symposium (PLANS), pp. 303-308.

Specifications and Operational Results from AEROcontrol – IId, the GPS/Fibre-optic Based Positioning and Attitude Determination System

by
Albrecht Grimm
IGI mbH
D-57223 Kreuztal, Germany
info@igi-cons.com

Abstract

Since years, IGI has defined three accuracy classes for its AEROcontrol systems:

AEROcontrol - I
position: 0.5m RMS
phi/omega/kappa: 0.5deg RMS

AEROcontrol - II
position: 0.2m RMS
phi/omega: 0.01deg RMS
kappa: 0.1deg RMS

AEROcontrol - III
position: 0.1m RMS
phi/omega: 0.001deg RMS
kappa: 0.01deg RMS

The aerial survey industry has addressed their interest to the mid-class system, because of its accuracy, weight/dimensions and pricing. Till end of 1999 the AEROcontrol - IIb system, a dry-tuned gyro based system has been offered and operated for aerial photography, SAR / IF-SAR and scanner operations. The accuracies achieved fit into the given range. This system has been operated during the OEEPE Test Norway 1999. The accuracies achieved during this test under unfavourable conditions (50% with 7 to 8 GPS satellites, 50% with 5 and less satellites) have been computed by OEEPE participants. They are

position: 0.1m RMS
height: 0.2m RMS

derived from ground control points.

Since the year 2000, the
AEROcontrol - IId system,
a fibre-optic gyro based system, is available. This system has been tested by ifp-Stuttgart during the Vaihingen/Enz Test-2000. The following accuracies have been found:

position: 0.05 - 0.1m RMS (depending on photo scale)
phi/omega: 0.003deg RMS
kappa: 0.007deg RMS

As can be seen, the reached accuracies for the AEROcontrol - IId system fit well with the set up specifications given by IGI for its class and nearly reach the values given for the most accurate AEROcontrol - III system.

After bore-sight alignment, GPS and IMU post-processing the results from the AEROcontrol - IId system directly can be used for LIDAR operations and orthophoto production or may be introduced as additional observations for AT and speeding up the AAT.

Some aspects from operated aerial photography projects
project Saudi Arabia,
project Mecklenburg-Vorpommern and
project LVA Nordrhein-Westfalen
followed by the LIDAR
project Baerwalde
will be discussed.

IGI's contribution will end with some remarks on the OEEPE Test Norway 1999.

Accuracy Analysis of Reconstructed Points in Object Space From Direct and Indirect Exterior Orientation Methods

Ayman Habib and Toni Schenk
Department of Civil and Environmental Engineering
The Ohio State University
Columbus, OH 43135
Habib.1@osu.edu, Schenk.2@osu.edu

1 Introduction

Recent advances of direct orientation systems achieve accuracies in the orientation parameters that are comparable to those obtained by aerial triangulation (indirect orientation). Some photogrammetric organizations report successful applications of direct orientation. For example, *Abdullah* (2000) describes results obtained with an integrated system, consisting of a carrier phase dual-frequency GPS receiver, a strapdown Inertial Navigation System, and a RC30 aerial camera. While in some cases the direct orientation parameters were comparable with those obtained by aerial triangulation, in a number of projects the required quality of the orientation parameters was not reached with the integrated system. The author attributes these mixed results to a possible mechanical instability of the IMU and camera mount, to the GPS quality and the internal IMU performance, and to the internal instability of the camera. *Jacobsen* (2000) points to the intriguing problem of determining the misalignment of the different system components. The limited separation of the different error components, caused by the high correlation among the respective parameters, requires special procedures to determine such errors. The author also recommends to determine the misalignment components very frequently. Another potential problem is the reliability.

Crucial to the success of direct orientation systems is a rigorous system calibration. *Cramer et al.* (2000) suggest to establish special calibration sites, but refer to the different environment between calibration site and project area. Differences in temperature, pressure, and refraction may render calibration parameters that are not valid for the project area. Ultimately, only aerial with self-calibration can determine the actual systematic errors.

Superficial discussions about direct vs. indirect orientation focus on the accuracy of the orientation parameters. This is only one part of the story, however. The determination of the exterior orientation parameters—direct or indirect—is an absolute prerequisite for subsequent photogrammetric processes, such as reconstructing the object space from images. In this paper we examine the question on how accurately object points can be determined from orientation parameters obtained by aerial triangulation or by direct platform orientation systems. The experiments fall into three categories: classical aerial triangulation with ground control points, aerial triangulation with GPS/INS information of the perspective centers, and direct reconstruction of object points with platform orientation data by way of intersecting conjugate bundle rays from multiple images. The major objective is to study the impact of random errors and biases of the interior and exterior orientation parameters on reconstructed object points. In order to restrict the error analysis to the assumed errors, we only use synthetic data.

The next section describes the experiments, starting with a comparison of classical aerial triangulation using ground control points with aerial triangulation using GPS/INS observations at the perspective centers. We then describe another set of experiments where reconstructed object points with the exterior orientation data from the platform orientation system, that is, without aerial triangulation, by way of spatial intersection from multiple bundle rays are used.

2 Experiments

In this section we describe the experiments performed and discuss the results. The primary goal is to compare the precision of object points obtained in different scenarios, such as block configuration, density and distribution of control points, and presence of random and systematic errors. This comparison is accomplished by comparing the computed position of object points with their known values.

2.1 Test Data, Configurations

The first part of the experiments is concerned with comparing object points obtained by way of aerial triangulation. In the second part we use direct orientation data to intersect points in object space. This reflects the situation where the exterior orientation is directly derived from platform orientation systems.

We have performed all experiments with synthetic data. This controlled environment assures that the point accuracy is solely a function of the block configuration and the errors introduced. The Multi Sensor Aerial Triangulation program MSAT, developed at OSU, was used to generate synthetic data and to conduct the experiments.

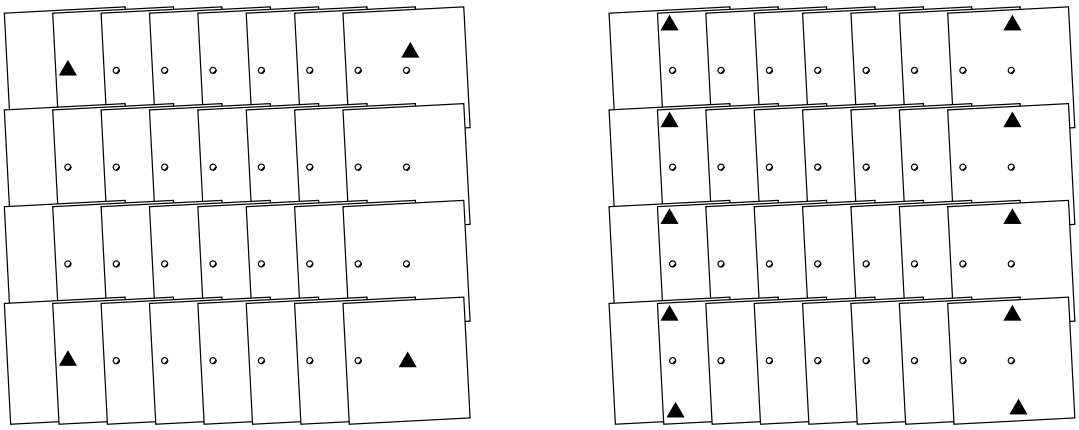

Figure 1: A synthetic block of 4 strips, 8 photographs per strip was used for the experiments. In (a), four control points were introduced and in (b) 10 control points. For aerial triangulation with GPS, all 32 exposure centers are assumed to be known.

Fig. 1 shows the test block, consisting of 4 strips, each with 8 photographs. For simulating a classical aerial triangulation scenario we have used 4 control points as illustrated in Fig. 1(a) and 10 control points (b), respectively. In addition to the traditional 20% sidelap we also performed experiments with 60% sidelap. The forward overlap was in all cases 60% and a 5×5 point pattern per photograph determines the point density. To complete the technical information on the synthetic block: focal length $c = 150$ mm, flight height $H = 2000$ m.

Table 1 contains random and systematic errors introduced to the synthetic data. One may argue about the nature and magnitude of the systematic errors we have introduced. However, our primary objective is to study the impact of systematic errors on the reconstructed points in object space. As shown in Table 1, we introduced a bias in the interior orientation parameters (IOP). The IOP bias comprises a shift of the principal point $\Delta x_p = \Delta y_p = 50\,\mu$m and a change of the focal length ($\Delta c = 50\,\mu$m). Another systematic error source is related to the position of the perspective center of the camera, derived from GPS measurements. Here, we only assume a bias in the GPS offset vector (perspective center to GPS antenna, ΔGPS $= 10$ cm). In direct platform orientation systems, one must also expect a bias in the

attitude, derived from INS, although the nature of this error is quite complex. For simplicity we have assumed a constant bias, $\Delta\text{INS} = 0.05^o$. Note that in all experiments, the random errors listed in Table 1 were always present.

Table 1: Assumed random and systematic errors. A — indicates that this particular error source was not modeled, that is, no error was considered in the block adjustment.

source	**random error**	**systematic error**
ground control points (gcp)	± 10 cm	—
photo coordinates	$\pm 5\,\mu$m	—
principal point $x_p,\ y_p$	$\pm 5\,\mu$m	$50\,\mu$m
focal length c	$\pm 5\,\mu$m	$50\,\mu$m
GPS	± 10 cm	—
GPS offset vector	—	± 10 cm
INS (attitude)	$\pm 10''$	0.05^o

There are several statistical properties suitable to express the precision and accuracy of reconstructed object points. One such measure is the Root Mean Square (RMS) error, derived from the differences between computed object points and their known position. The variance-covariance matrix of reconstructed points is another useful quantity. We use mainly the RMS error in the following comparisons.

2.2 Results with Aerial Triangulation

The first set of experiments involves a comparison between classical aerial triangulation (AT) with ground control points and aerial GPS triangulation without ground control points (GPS-AT). Table 2 lists the RMS errors for several configurations. The first two rows of the table are related to aerial triangulation with 4 and 10 ground control points. The third configuration is a pure GPS triangulation where all 32 perspective centers were assumed to be known. No additional ground control point was used. The fourth row is a slight modification in that the attitude of the exposure stations is introduced as additional observation. Columns 2–4 contain the RMS errors under the assumption that only random errors were present. For the magnitude of these random errors the reader is referred to Table 1. The remaining three columns of Table 2 show the RMS errors obtained by introducing a bias in the IOP, namely a shift of the principal point ($\Delta x_p = \Delta y_p = 50\,\mu$m), and a change in the focal length $\Delta c = 50\,\mu$m.

Table 2: Comparison between classical AT with control points and GPS AT without ground control points, measured by RMS of object points.

configuration	**no bias** RMS [m]			**IOP bias** RMS [m]		
	x	y	z	x	y	z
AT, 4 gcp	0.11	0.14	1.74	0.11	0.15	1.73
AT, 10 gcp	0.07	0.10	0.20	0.07	0.11	0.20
GPS-AT	0.08	0.13	0.17	0.63	0.79	0.71
GPS-INS-AT	0.06	0.11	0.14	0.64	0.77	0.69

The analysis of the results without bias confirms the expectation that a GPS-AT is superior to traditional AT if the control points are not dense enough. With only four control points in the corner of the block, we bridge 8 baselines with an anticipated poor result for elevations. In the case of 10 control points, GPS-AT performs only marginally better. Interestingly enough, the inclusion of the orientation angles as additional observations to the GPS-AT barely improves the RMS errors. Incidentally, the configuration with 60% sidelap and four control points (not listed in Table 2) yields nearly the same results as GPS-AT.

When introducing an IOP bias (shift of the principal point, change of focal length), we notice a drastic change in the comparison classical vs. GPS-AT. Classical AT almost completely absorbs the bias while the object points obtained in GPS-AT and GPS/INS-AT are fully impacted by the bias. A shift of $50\,\mu$m in the $x-$ and $y-$direction of the perspective center translates into a shift on the ground linearly to the photo scale ($H/c \approx 13333$), that is ≈ 0.67 m. Likewise, a change in the focal length affects the elevations by similar magnitudes. *Schenk* (1999) shows in detail the reasons for this different behavior of direct and indirect orientation procedures. In a nutshell, the indirect orientation determines exterior orientation parameters based on a fixed interior orientation. Remaining systematic IO errors affect directly the EO parameters. But the reconstruction of object points, using the same IO, is virtually free of systematic IO errors.

2.3 Intersection of Object Points Using Direct Orientation Data

In this section we discuss the results obtained by intersecting conjugate points in object space based on known exterior orientation parameters. Table 3 lists the RMS numbers obtained for different scenarios. We distinguish between $2-$ and $n-$point intersection where n can reach 6 points in a 60%/20% overlap configuration. The numbers listed in Table 3 are not very different, though. The significant difference between $2-$ and $n-$point intersections is the redundancy which amounts to an increased robustness of the computed object point positions.

Table 3: Intersection with direct orientation parameters (no AT).

configuration	**RMS [m] with 2 intersecting pts.**			**RMS [m] with N intersecting pts.**		
	x	y	z	x	y	z
no biases	0.15	0.21	0.37	0.13	0.21	0.34
$\Delta x_p = \Delta y_p = \Delta c = 50\,\mu$m	0.68	0.78	0.78	0.66	0.79	0.77
only $\Delta c = 50\,\mu$m	0.15	0.22	0.78	0.13	0.22	0.76
ΔGPS $= 10$ cm	0.17	0.21	0.39	0.16	0.20	0.36
ΔINS $= 0.05^o$	2.00	2.11	1.08	1.96	1.71	0.76

The first row lists the RMS numbers for the ideal unbiased situation where only random errors of the photo coordinates ($\pm 5\,\mu$m) and random errors of the exterior orientation parameters (± 10 cm for GPS and $\pm 10''$ for the attitude) are considered. The second row shows the impact of an IOP bias on the intersected points. A shift of the principal point directly affects the $X-$ and $Y-$coordinates of the object points, while a change in the focal length affects the $Z-$component. This is clearly manifested by the results in the third row. Here, only a bias in the focal length is assumed. There is virtually no effect in planimetry. As shown in the previous section, a shift of the principal point causes a planimetric error on the ground of ≈ 67 cm.

The introduction of a bias in the GPS offset vector has no noticeable effect on the intersected points. In contrast, an INS bias greatly affects the reconstructed object points. By and large, the effect amounts

to a rotation of the vector from the exposure stations to the object point by a rotation matrix containing the INS bias. With this geometrical interpretation in mind it stands to reason that predominantly $x-$ and $y-$ are affected.

Finally, we compare the precision of objects points determined by direct orientation parameters with the results obtained by GPS-AT, assuming that systematic errors are present.

Table 4: Comparison of precision of points obtained by GPS-AT and by intersection with direct orientation parameters in the presence of systematic errors.

bias	**GPS-AT** RMS [m]			**intersection** RMS [m]		
	x	y	z	x	y	z
no biases	0.08	0.13	0.17	0.15	0.21	0.37
Δ IOP	0.63	0.79	0.71	0.68	0.78	0.78
Δ GPS	0.10	0.07	0.18	0.17	0.21	0.39
Δ INS	1.16	1.54	1.14	2.00	2.11	1.08

Table 4 shows the results. In case of a bias in the interior orientation parameters (Δ IOP) there is no difference in the RMS values between GPS-AT and intersection. This result implies that aerial triangulation does not improve the precision of object points. In contrast, a GPS-AT significantly improves the point precision if either a bias in the GPS offset vector or in the INS attitude data is present.

3 Conclusions

In many discussions related to direct vs. indirect orientation, emphasis is placed on the precision of the orientation parameters. This is not very relevant, however, because the orientation data are just an intermediate result in photogrammetric processes. Thus, it is more meaningful to compare the precision of object points. We performed several experiments with synthetic data with the goal to understand the influence of various systematic errors on object points. The use of synthetic data in a block adjustment is comparable to a numerical modeling of the propagation of systematic errors. Hence, we can generalize the results as follows:

1. In the absence of systematic errors, GPS aerial triangulation (GPS-AT) performs equal or better than classical aerial triangulation with ground control points (AT).

2. Adding the attitude as additional observations to GPS-AT only marginally yields better results.

3. In case of systematic errors in the interior orientation parameters (IOP), e.g. a shift of the principal point and a change in the focal length, greatly affects GPS-AT. The error propagates linearly into object space. The planimetric errors of object points is approximately the error in image space, multiplied by the photo scale. Classical AT “absorbs" an IOP bias. This situation can be symbolically represented as follows:

$$\begin{aligned} \text{AT with (IOP} + \Delta\text{IOP)} &= \text{EOP} + \Delta\text{EOP} \\ \text{EOP} + \Delta\text{EOP} + \text{IOP} + \Delta\text{IOP} &\approx \text{correct } X, Y, Z \text{ object points} \\ \text{GPS-AT:} \quad \text{EOP} + \text{IOP} + \Delta\text{IOP} &= \text{wrong } X, Y, Z \text{ object points} \end{aligned}$$

4. Comparing $2-$point intersection with the point position determined by GPS-AT reveals that the latter yields substantially better point precisions, except in situations where only systematic IOP errors are present. This suggests to perform GPS-AT with direct orientation data.

5. The systematic errors analyzed in this paper are difficult to detect in GPS-AT, because of the low redundancy of the point computation.

References

Abdullah, Q. (2000). Camera Orientation without Aerotriangulation: System Performance and Productivity. In *International Archives of Photogrammetry and Remote Sensing*, **33**(B3/1), 4–11.

Cramer, M., D. Stallmann and N. Haala (2000). Direct Geo-referencing Using GPS/Inertial Exterior orientations for Photogrammetric Applications. In *International Archives of Photogrammetry and Remote Sensing*, **33**(B3/1), 198–205.

Jacobsen, K. (2000). Potential and Limitation of Direct Sensor Orientation. In *International Archives of Photogrammetry and Remote Sensing*, **33**(B3/1), 429–435.

Mostafa, M., J. Hutton and E. Lithopoulos (2001). Airborne Direct Geo-referencing of Frame Imagery: An Error Budget. In *Proc. Mobile Mapping System Symposium*, Cairo.

Schenk, T. (1999b). *Digital Photogrammetry*. TerraScience, Laurelville, OH 43135, 428 pages.

THE OEEPE TEST ON INTEGRATED SENSOR ORIENTATION[1]

Christian Heipke, Karsten Jacobsen, Helge Wegmann, Hannover

ABSTRACT

The European Organisation for Experimental Photogrammetric Research (OEEPE) has embarked on a test investigating sensor orientation using GPS and IMU in comparison and in combination with aerial triangulation. The test consists of two phases. The first phase comprises the system calibration and direct georeferencing. The second phase deals with the integrated sensor orientation, i. e. the integration of the GPS/IMU data into the bundle adjustment.13 test participants processed the distributed data and returned their results.

In this paper we describe the test incl. the data acquisition and report about the results of phase I. The accuracy potential of direct georeferencing for 1:5.000 imagery was found to lie at approximately 5-10 cm in planimetry and 10 – 15 cm in height in object space and at 15 - 20 mm in image space. The most important finding is the fact, that while these values are larger by a factor of 2 - 3 when compared to standard photogrammetric results, direct georeferencing has proven to be a serious alternative to conventional bundle adjustment and currently allows for the generation of orthophotos and other applications with less stringent accuracy requirements. However, stereo plotting is not always possible due to the sometimes relatively large remaining model y-parallaxes. Future developments in the areas of GPS and IMU sensors and data processing will probably also reduce this problem. The best results in terms of accuracy and in particular in terms of reliability are expected from an integration of GPS/IMU data into the bundle adjustment which is the topic of test phase II.

1 INTRODUCTION

Image orientation is a key element in any photogrammetric project, since the determination of three-dimensional coordinates from images requires the image orientation to be known. In aerial photogrammetry this task has been exclusively and very successfully solved using aerial triangulation since many decades. Over the years, a number of additional sensors were used to directly determine at least some exterior orientation parameters, albeit with little success until the advent of GPS in the eighties and the pioneering work of Mader (1986). In this regard it is interesting to note that in the same year Ackermann predicted that "the performance of new navigation systems will allow in-flight measurements of carrier position and attitude to an accuracy with will change the photogrammetric methods fundamentally" (Ackermann 1986, p. 93).

Today differential kinematic GPS positioning is a standard tool for determining the camera exposure centres for aerial triangulation. Using the GPS measurements as additional observations in the bundle adjustment a geometrically stable block based on tie points alone can be formed, and ground control points (GCP) are essentially only necessary for calibration, for detecting and eliminating GPS errors such as cycle slips, for reliability purposes, and possibly for datum transformations. One can distinguish between a loose coupling of photogrammetric and GPS observations, sometimes called the "shift and drift approach" (Ackermann 1994; Jacobsen 1997) and a rigorous GPS/AT combination (Jacobsen, Schmitz 1996; Kruck et al. 1996; Schmitz 1998).

Gyroscopes and accelerometers are the components of an inertial measurement unit (IMU)[2]. Using gyroscopes, one is able to determine the rotation elements of the exterior orientation, the accelerome-

[1] A short version of this paper has been published in the proceedings of the Photogrammetric Week 2001.

[2] We use the term IMU instead of INS (Inertial navigation system). Following Colomina (1999), an INS contains an IMU as a measurement device plus positioning and guidance functions, mainly realised in software.

ters provide sensor velocity and position. Thus, in principle a GPS/IMU sensor combination can yield the exterior orientation elements of each image without aerial triangulation. This technology, called direct sensor orientation[3], opens up many new applications (Schwarz et al. 1993; Colomina 1999; Skaloud 1999). GPS/IMU measurement can also be used as additional observations within a bundle adjustment; this concept is referred to as integrated sensor orientation.

A series of tests and pilot projects has been conducted and has convincingly shown the potential of direct georeferencing and integrated sensor orientation (Skaloud, Schwarz 1998; Wewel et al. 1998; Abdullah, Tuttle 1999; Burman 1999; Colomina 1999; Cramer 1999; Toth 1999; Jacobsen 2000). At independent checkpoints on the ground root mean square errors of down to 0.1 to 0.2 m were obtained. These results have proven that both technologies are serious alternatives to conventional aerial triangulation. In addition, potential error sources have been identified. These include the Kalman filtering of the GPS/IMU data for noise reduction, the determination of parameters for systematic position and attitude corrections of the GPS/IMU data (system calibration parameters), the stability of these parameters over time, especially the stability of the attitude values between the IMU and the camera, and the time synchronisation between the various sensors.

In bundle adjustment the control information in the form of ground control point coordinates and the quantities to be determined (the coordinates of tie points) are both located on the object surface, and the computation of the unknowns can be thought of as an interpolation task. In direct georeferencing, on the other hand, the control information is measured at the height of the sensors and subsequently transferred down to the object surface. Therefore, direct georeferencing must be considered as an extrapolation, and thus a compensation of different error sources due to a high correlation between the related parameters is much less effective. This fact is particularly true for possible changes in the interior orientation of the camera, which no longer can be compensated for by a change in the exterior orientation (e. g. Schenk 1999; Habib; Schenk 2001). In this light, also the choice of the object space coordinate system needs a closer look (see e. g. Jacobsen, Wegmann 2001), since the photogrammetric collinearity equations need a Cartesian system, a requirement the mapping systems do not fulfil.

2 TEST OBJECTIVES AND EXPECTED RESULTS

The European Organisation for Experimental Photogrammetric Research (OEEPE) has embarked on a multi-site test investigating sensor orientation using GPS and IMU in comparison and in combination with aerial triangulation (see also Heipke et al., 2000; 2001). The Institute for Photogrammetry and GeoInformation (IPI), University of Hannover, acts as pilot centre. Data acquisition for the test including the organisation of test flights and the necessary fieldwork was carried out by the Department of Mapping Sciences (IKF), Agricultural University of Norway in Ås.

The focus of the test is on the obtainable accuracy for large scale topographic mapping using photogrammetric film cameras. The accuracy of the results is assessed with the help of independent check points on the ground in the following scenarios:

- conventional aerial triangulation,
- GPS/IMU observation for the projection centres only (direct georeferencing),
- combination of aerial triangulation with GPS/IMU (integrated sensor orientation).

The test is expected to demonstrate to which extent direct georeferencing and integrated sensor orientation are accurate and efficient methods for the determination of the exterior orientation parameters for large scale topographic mapping.

Another test goal is to transfer the technology recently developed within the research arena to potential users. This goal is in line with the mission of OEEPE, and it is the main reason for choosing a multi-site test approach. As a consequence, the duration of the test is somewhat lengthy when compared to a single site investigation. This disadvantage can be tolerated, however, because we believe that in the long run the technology transfer issue is more important.

[3] In contrast to “direct sensor orientation” the term “direct georeferencing” includes not only the determination of the exterior orientation elements but also the subsequent computation of object space coordinates.

3 DATA ACQUISITION AND GPS/IMU DATA PRE-PROCESSING

3.1 Criteria for selecting test data

The test was carried out based on especially acquired imagery and GPS/IMU data. In order to enable a fair and meaningful test between the two competing technologies the following selection criteria for the data acquisition were set forward:

- geometrically stable photogrammetric block,
- modern photogrammetric film camera,
- dual frequency GPS receivers using differential carrier phase measurements with a data rate of 0.5 sec, preferably identical receivers for the aircraft and reference station,
- a short base line between aircraft and reference station,
- high quality off-the-shelf navigation grade IMU as typically used in precise airborne attitude determination,
- different image scales suitable for large scale topographic mapping,
- a well-controlled test field with a large number of ground control points.

Given these criteria and a few practical constraints a test field in Fredrikstad, Norway, was selected. The test field Fredrikstad (see figure 1) lies in the south of Norway near the capital Oslo. It is maintained by IKF. The test field has already been used in a prior OEEPE test on GPS-assisted bundle adjustment (Andersen, Ackermann 2001), its size is approximately 5 x 6 km^2. 51 well distributed signalised ground control points with UTM/EUREF89 coordinates and ellipsoidal heights known to better than 0.01 m are available. The ground control point targets have a size of 40 x 40 cm^2.
In order to eliminate influences of long GPS base lines, it was decided to place the stationary receiver necessary for the differential GPS solution directly is the test field. For reasons of redundancy, additional receivers were operated at various distances from the test field.

Figure 1: Test field Fredrikstad, the black triangles indicate the position of the ground control points

3.2 Acqusition of aerial imagery and GPS/IMU data

Two companies producing suitable GPS/IMU equipment agreed to participate in the test, namely Applanix of Toronto, Canada, using their system POS/AV 510-DG (Hutton, Lithopoulos 1998; Applanix 2001), and IGI mbH of Kreuztal (formerly of Hilchenbach), Germany, with the system AEROcontrol IIb (IGI mbH 2001). The test imagery was acquired in October 1999 by the Norwegian companies Fotonor AS and Fjellanger Widerøe (FW) Aviation AS using photogrammetric cameras equipped with a wide angle lens. For each GPS/IMU system calibration flights in two different scales (1:5.000 and 1:10.000) followed by the actual test flight in 1:5.000 were carried out; see also table 1). The flight axes of the two calibration flights are presented in figures 2 and 3, those of the actual test flights in figures 4 and 5. These figures also show the ground control points (GCP) and check points. The object space coordinates of the GCP visible in the figures 2 and 3 were distributed to the participants in order to carry out the system calibration (for further detail see below).
Both flying companies had the IMU tightly attached to the photogrammetric camera and have used gyro-stabilised camera platforms. While Fotonor had the PAV30 switched on during the complete

		Applanix	IGI
Flying company		Fotonor	Fjellanger Widerøe Aviation
Photogrammetric camera		Leica RC30	Zeiss RMK Top
Focal length [mm]		153	153
Date of calibration protocol		February-22-1999	Aug-03-1998
Gyro-stabilised camera platform		PAV30, switched on during the complete mission	T-AS, switched on during parts of the mission
Film material		Panchromatic (AP 200)	Panchromatic (AP200)
GPS reference station		Fredrikstad	
GPS receiver		Ashtec Z Surveyor, (L1 and L2)	
data rate		0.5 sec	
GPS/IMU-System		POS / AV 510-DG	AEROcontrol IIb
Accuracies of GPS/ IMU post-processing according to companies	Position	< 0.1 m	< 0.1 m
	roll, pitch	0.005 deg.	0.005 deg.
	yaw	0.008 deg.	0.010 deg.
GPS receiver		Ashtech Z Surveyor, (L1 and L2)	Ashtech Z XII, (L1 and L2)
Data rate		0.5 sec	0.5 sec
Gyroscopes		Litton LN-200	Litef LCR-88
data rate		200 Hz	50 Hz
Flight mission		Oct.-07-99, 7:39-12:43	Oct. -07-99, 9:38-13:17
Sequence of data acquisition		Cal. flight 1:5.000, cal. flight 1:10.000, test flight	Cal. flight 1:10.000, cal. flight 1:5.000, test flight
Calibration flight 1:5.000		2 strips North/South, 2 strips East/West (in opposite dir.)	2 strips North/South, 2 strips East/West (in opposite dir.)
No. of images		2*17 + 2*14 = 62	2*17 + 2*14 = 62
End overlap		l = 60 %	l = 60 %
Flying height [m]		800	800
No. of visible ground control points		25	25
Calibration flight 1:10.000		block with 5 strips followed by 2 strips at a 90 degree angle	block with 5 strips followed by 2 strips at a 90 degree angle
No. of images		5*11 + 2*15 = 85	5*11 + 2*14 = 83
Overlap		l = 60 %, q = 60 %	l = 60 %, q = 60 %
Flying height [m]		1600	1600
No. of visible ground control points		50	50
Actual test flight		block with 9 strips followed by 2 strips at a 90 degree angle	block with 7 strips followed by 1 strip at a 90 degree angle
No. of images		9*17 + 2*14 = 181	7*17 + 1*14 = 133
Overlap		l = 60 %, q = 60 %	l = 60 %, q = 60 %
Flying height [m]		800	800
No. of visible ground control points		50	50

Table 1: Data acquisition details[4]

[4] It should be noted that the GPS/IMU system used for the test represents the state-of-the-art technology of 1999, and is a little out of date at the time of writing (Summer 2001). For instance, while in the AEROcontrol IIb from IGI dry-tuned gyros were used, they have been replaced by fibre optics gyros in the current system AEROcontrol IId. Similar developments have taken place at Applanix.

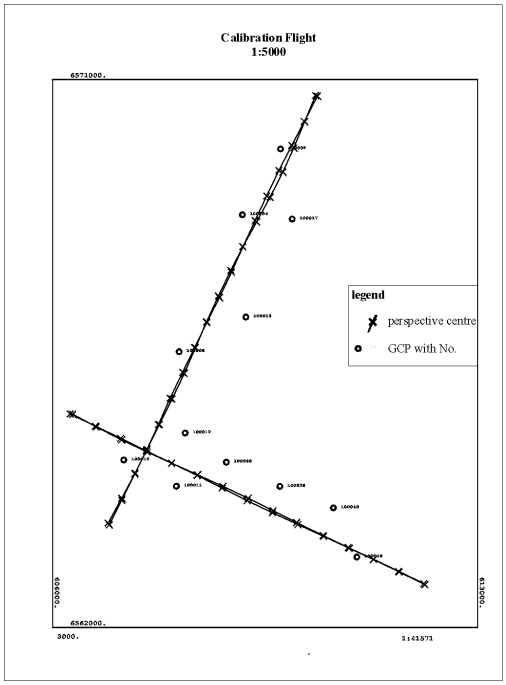

Figure 2: Flight axes of calibration flight 1:5.000

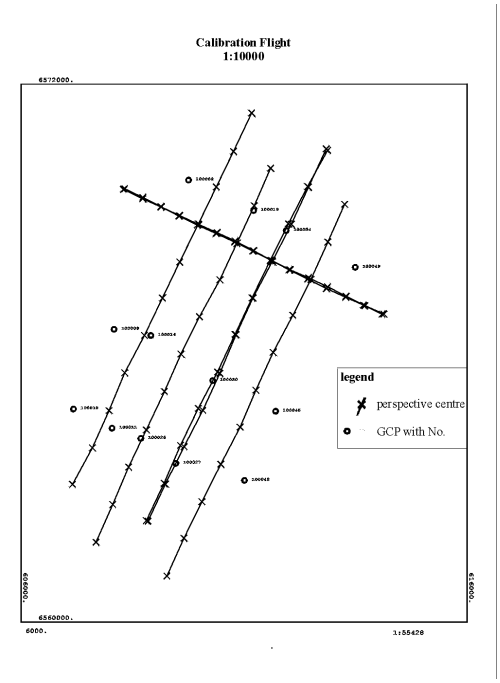

Figure 3: Flight axes of calibration flight 1:10.000

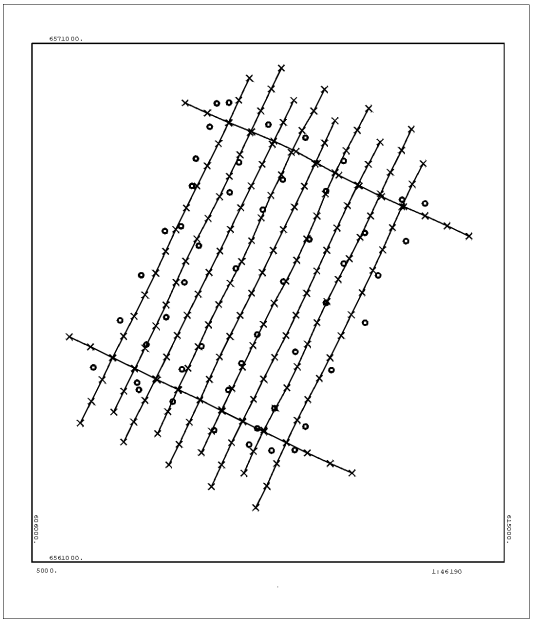

Figure 4: Fotonor/Applanix test flight, 1:5.000

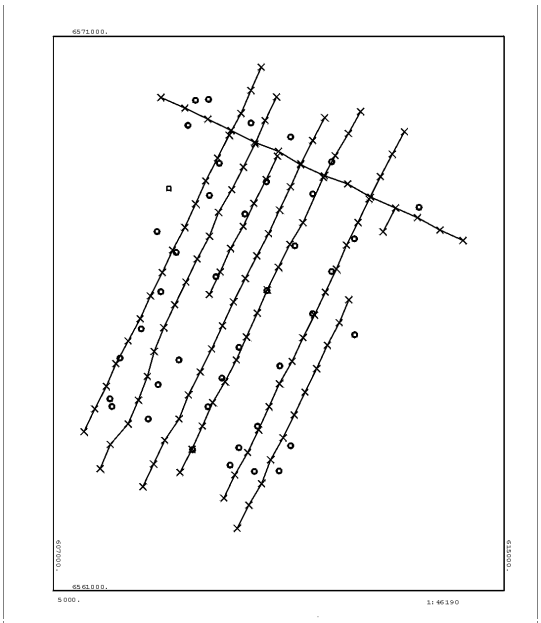

Figure 5: FW/IGI test flight, 1:5.000

mission, FW had turned on the T-AS for parts of the flight only. In both cases movements of the camera with respect to the aircraft were registered and accounted for in post-processing.
Unfortunately, the weather did not permit to have identical conditions for the two test flights. The Fotonor/Applanix flight could be carried out according to plan, all scheduled images were captured, and apart from a short period of time during the calibration flight 1:10.000, a minimum of 9 GPS satellite was visible during the mission. As a result the PDOP value indicating the quality of the GPS observations was below 2 except for parts of the 1:10.000 calibration flight (see also figure 6). The memory card of the on-board IMU become full shortly before the end of the actual test flight and was changed, apparently without any consequences for the data acquisition.
The FW aircraft with the IGI system was operated from an airport further away from the test field. Fog prevented a start as scheduled, and during the second half of the flight clouds started to move into the test field area. The crew slightly changed sequence of image capture, but some of images could not be acquired at all. This fact explains the different number of images of the test flight (see again table 1) and also differences between figures 4 and 5. Also, the film cassette had to be changed during the flight. Finally, for about 50 % of the FW/IGI test flight the number of visible satellites dropped down to 6, resulting in a PDOP value of up to 3.5 (see figure 7). These difficulties during data acquisition have to be taken into account in the interpretation of the test results (see below).

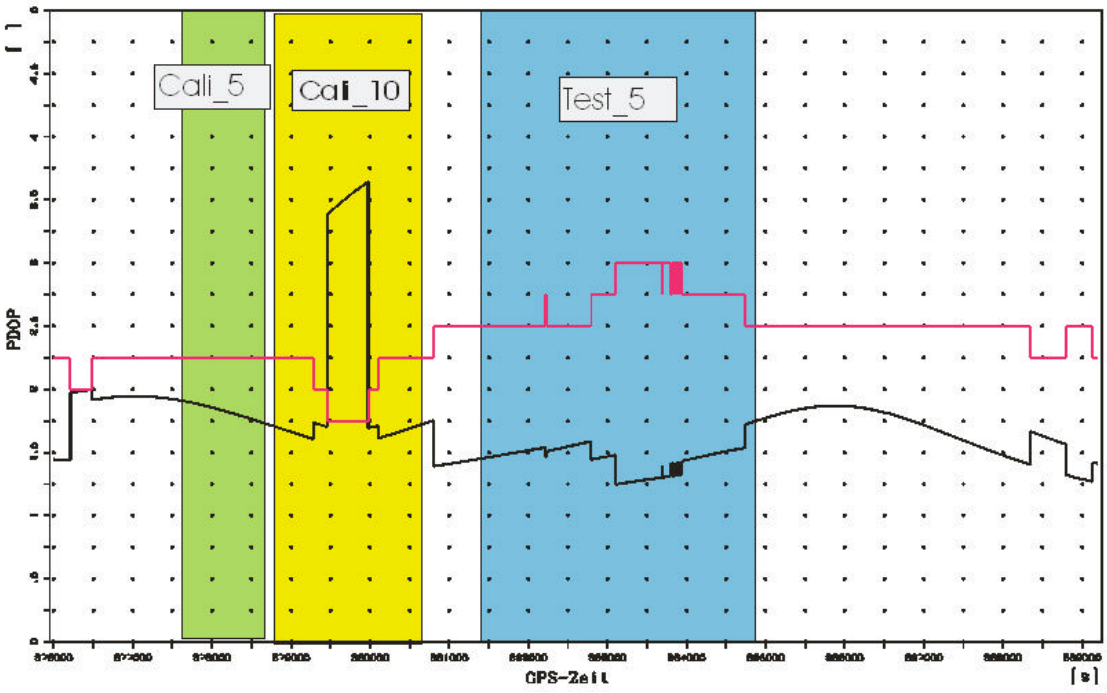

Figure 6: Number of visible satellites (red) and resulting PDOP value (black), Fotonor/Applanix flight (elevation mask 5°, SNR >2, signals actually received simultaneously at the reference station and the receiver in the aircraft)

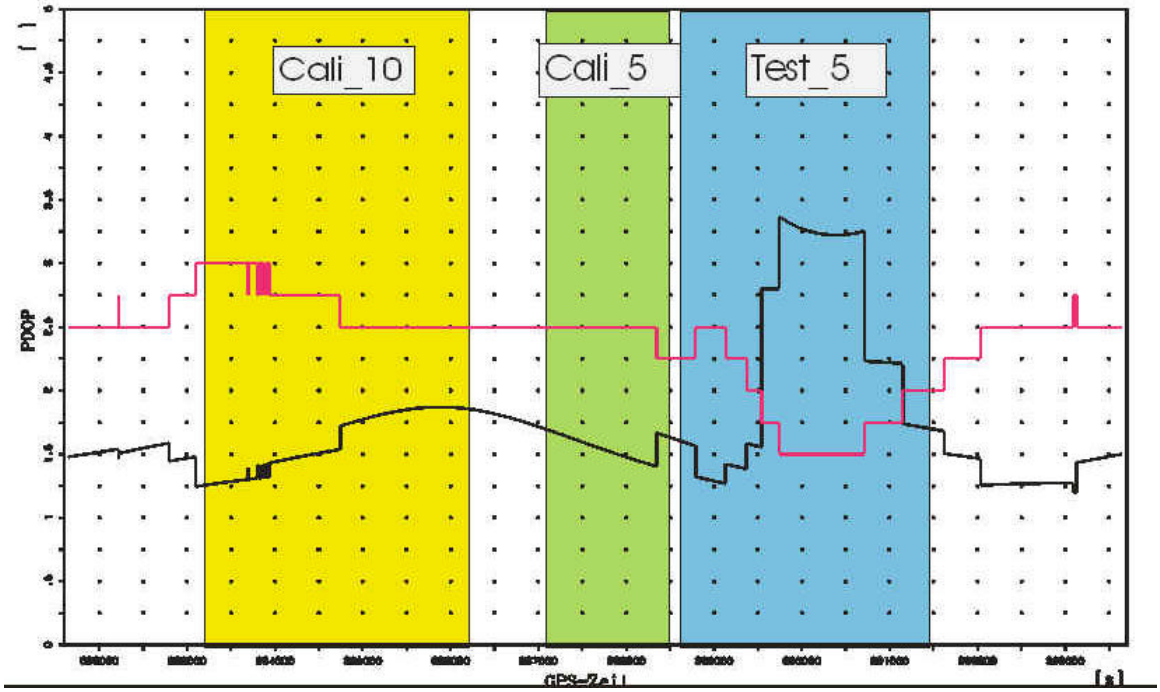

Figure 7: Number of visible satellites (red) and resulting PDOP value (black), FW/IGI flight (elevation mask 5°, SNR >2, signals actually received simultaneously at the reference station and the receiver in the aircraft)

3.3 GPS/IMU pre-processing

From the raw GPS and IMU measurements flight trajectories for the camera projection centres in UTM/EUREF89 in zone 32 with ellipsoidal heights and roll, pitch and yaw values in ARINC 705 convention (ARINC 2001) describing a three-dimensional rotation from local level coordinate system to the body frame of the aircraft were computed. The flight trajectories refer to the camera projection centre, thus the lever arm corrections describing the difference in position between the GPS antenna, the IMU coordinate origin and the origin of the camera coordinate system (more precisely, the entrance node of the camera lens) were taken into account. It should be noted, that a few assumptions were introduced into pre-processing:

- The alignment of the EUREF89 and the WGS84 coordinate systems is assumed to be identical.
- No geoid information was introduced, thus the local Z-axis was assumed to be parallel to the local gravity vector, thus the deflection of the vertical was assumed to be zero.

Pre-processing details are considered propriety information by both, Applanix and IGI. Consequently, within the arrangements made for the test, pre-processing was carried out by the two companies. As mentioned, GPS data were recorded at different reference stations. Initially, four of these GPS data sets were processed to make sure that no problems had occurred during data collection. IMU measurements were not use during these checks. Applanix and IGI judged the results of reference station Fredrikstad, located within the test field, to be well suited for the further investigations. Therefore, it was decided to only use this data set within the OEEPE test. Subsequently, GPS/IMU pre-processing was carried out by Applanix and IGI, respectively. Position and attitude data for the test flights were then delivered to the pilot centre, unfortunately without any information about the quality of the pre-processed GPS/IMU data such as a covariance matrix.

Raw GPS and IMU data were not made available by the companies. Therefore, an investigation into pre-processing, and also into rigorous GPS/IMU/AT approaches must be postponed to a later stage (see, however, Schmitz et al. 2001 for such an approach using the OEEPE test data, albeit with other reference stations).

4 TEST SET-UP

The test consists of two phases. The first phase comprises the determination of so-called system calibration parameters, i. e. the determination of the boresight misalignment (the angular difference between the IMU and the image coordinate systems), and possibly additional parameters modelling GPS shifts, the interior orientation of the camera, GPS antenna offsets, time synchronisation errors etc. and direct sensor orientation. The second phase deals with the integration of the GPS/IMU data into the bundle adjustment, i. e. the integrated sensor orientation itself.

4.1 Phase I: System calibration and direct georeferencing

The first test phase deals with the determination of the system calibration parameters from the information of the calibration flights. Phase I also comprises the direct sensor orientation of the actual test flight based on the GPS/IMU data and the results of system calibration and – as part of the analysis of the results (see chapter 5) - the derivation of object space coordinates. Thus, all elements of direct georeferencing are contained in phase I.
The test scheme of phase I is depicted in figure 8. From the pre-processed GPS/IMU values and the instant of exposure the pilot centre interpolated the position and roll, pitch, yaw angles for each image. The pilot centre also measured image coordinates of GCP and about 25 tie points in each of the calibration flight images using the analytical plotter Planicomp P1. These measurements were checked by the pilot centre using photogrammetric bundle adjustments, and also by Applanix and IGI by performing a system calibration. The object space coordinates of some GCP as determined by IKF were given in UTM/EUREF89 with ellipsoidal heights, the camera calibration protocol was provided by the flight companies.
All these data were then sent out to the test participants[5]. The derived calibration parameters together with the orientation parameters for the calibration flights and the test flight and a detailed report about the work carried out were to be delivered back to the pilot centre.
34 potential test participants asked for the data, 13 participants returned their results in time to be included into this paper[6], refer to table 2. As can be seen, besides the two companies having provided the GPS/IMU sensor systems, three software developers (GIP, inpho, LH Systems), one National Mapping Agency (ICC), one commercial user (ADR) and five research institutes (DIIAR, FGI, IPF, IPI and ifp) have taken part in the test. Thus, with the exception of the University of Calgary, which carried out much of the pioneering work in direct georeferencing (Schwarz 1993; 1995), most parties currently active in this area are represented in the test. Nearly all participants used existing bundle adjustment programmes, partly augmented by additional software development. In this way, besides demonstrating the state-of-the-art in integrated sensor orientation, the distributed data also served as test data for refinements of the existing software, which is well within the goal of technology transfer. For reports of the individual participants see e. g. Alamùs et al. (2001), Forlani, Pinto (2001), Jacobsen, Wegmann (2001), and Ressl (2001).

---

[5] The GPS/IMU data from IGI sent out at first contained an error due to inappropriate consideration of the initial alignment process during GPS/IMU pre-processing. This error was detected by IGI shortly afterwards, and corrected GPS/IMU data were subsequently distributed to the participants. The results presented in this paper refer exclusively to the second data set, the first incorrect data set is not further considered.

[6] A few results arrived at the pilot centre too late to be included into this paper. They are currently being processed and will be published in the final test report.

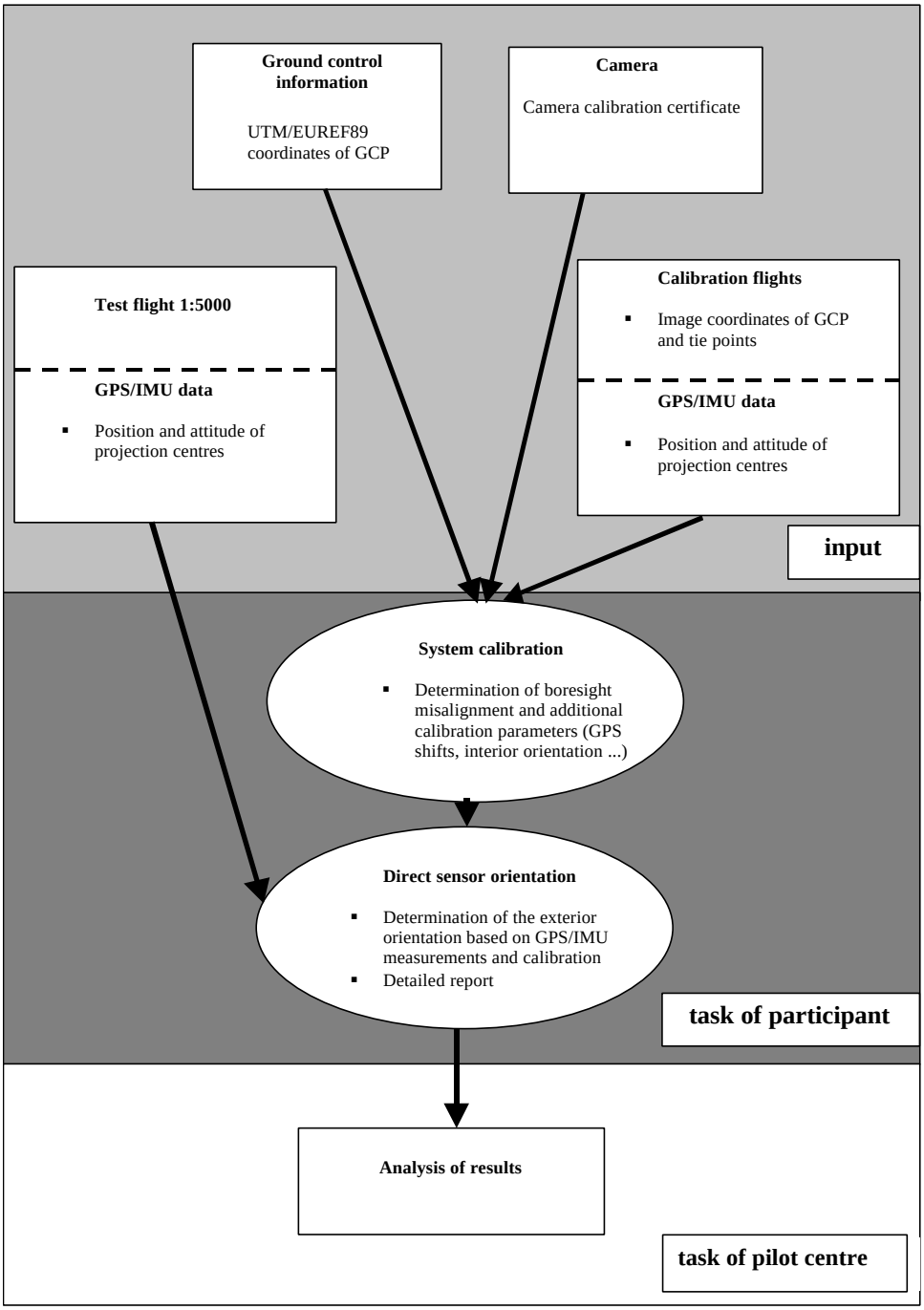

Figure 8: Flowchart of phase I

Test participant	Abbreviation	Used software
Applanix, Canada	Applanix	POS tools
IGI, Germany	IGI	AEROoffice tools and BINGO
ADR, BAE Systems, USA	ADR	BLUH
Finnish Geodetic Institute, Masala	FGI	own development, called FGIAT
GIP, Germany	GIP	BINGO
ICC Barcelona, Spain	ICC	GeoTex/ACX
inpho, Germany	inpho	inBlock
LH Systems, USA	LHS	ORIMA
Politecnico di Milano, Italy	DIIAR	own development
Technical University Vienna, Austria	IPF	ORIENT
University of Hannover, Germany	IPI	BLUH
University of Stuttgart, Germany	ifp	PAT B and own development

Table 2: List of test participants, phase I (note that the same software name does not necessarily imply the same version and thus the same results)

4.2 Phase II: Integrated sensor orientation

The second phase deals with the integration of the GPS/IMU data into the bundle adjustment. After having returned the results of phase I the participants have received image coordinates of tie points and GCP of a subset of the test flight images, namely from a small block and one strip. It should be noted that no object space coordinates of GCP were distributed, and that GCP used in phase I were not used as tie points in phase II. Thus, the participants received only information in image space, but no object space information. This decision was made, because we wanted to explore the advantage of combining GPS/IMU measurements with tie points alone, since (1) tie points can be generated automatically using image matching techniques (see approaches automatic aerial triangulation), and (2) as soon as GCP are included, their influence starts to dominate the results, and thus we end up with a GPS-assisted photogrammetric bundle adjustment.
Combining the received information with the system calibration parameters determined in phase I, the participants have then performed an integrated sensor orientation, refining the exterior orientation (and partly also the system calibration parameters), and estimating the object space coordinates of the tie points and the GCP. These values have subsequently been returned to the pilot centre together with a detailed report describing the adopted model for the integration. Analysis of the phase II results is currently under way.

5 ANALYSIS OF PHASE I RESULTS

5.1 System calibration approaches

The results delivered back to the pilot centre have been analysed and are presented in this chapter. As was to be expected the different participants have used different approaches for computing the system calibration parameters. A description of the standard approach can be found e. g. in Skaloud (1999 and Forlani, Pinto 2001), it will not be repeated here. Although the exact procedures adopted by the participants were not always released in detail, a number of noticeable distinctions could be observed (see also table 3):

– Input information used: some participants used the image coordinates of both calibration flights in one simultaneous adjustment, others performed separate adjustments and subsequently combined the results, while yet others used one calibration flight only. In some cases, the GPS shifts were

determined from only one flight while the boresight misalignment was derived from both. Some participants also deleted the first and the last few images from the computations, arguing that the corresponding GPS/IMU data were not suited for the calibration.

- Determination of the system calibration parameters in a combined bundle adjustment run with the image coordinates of the calibration flights, the GPS/IMU data and the GCP object coordinates as input (denoted as "1 step" in table 3) vs. a comparison of the exterior orientation derived from a conventional bundle adjustment and the GPS/IMU values ("2 steps"), see also Mostafa (2001). Some participants averaged the differences of the photogrammetric and the GPS/IMU result, others used a more sophisticated computational scheme. DIIAR, for example, weighted the influence of the photogrammetrically determined exterior orientation parameters based on the corresponding theoretical standard deviations derived from the bundle adjustment (see Forlani, Pinto 2001). IPI and ifp introduced the GPS measurements into the bundle adjustment in which the three GPS shifts were determined; the misalignment angles were derived in a separate step.
- Number of system calibration parameters estimated in the adjustment: Many participants used the six standard parameters (3 GPS shifts, 3 misalignment angles), which can be computed from only one calibration flight. Some participants also corrected for the parameters of interior orientation and the additional parameters known from camera self-calibration (Ebner 1976; Jacobsen 1980). DIIAR also investigated the time synchronisation between the attitude values and the exposure time by estimating a constant time shift (see Skaloud 1999), but found that no correction needed to be applied (see again Forlani, Pinto 2001). ifp did not consider the computed GPS shifts as calibration parameters and only used the three angular misalignment values.
- UTM vs. local tangential coordinate system: Most participants carried out all computations in the UTM system; LHS transformed the input data into a local tangential system, computed the results, and subsequently transformed them into the UTM system (denoted by * in table 3); DIIAR and ifp processed and delivered results in the local tangential system, IPI processed and delivered results in both systems[7].

Participant	**Procedure**	**Object space coord. system used for the computations**	**Number of system calibration parameters**
IGI	1 step	UTM	6
Applanix	1 step	UTM	6
ADR	2 steps	UTM	6
FGI	2 steps	UTM	18 (6 + 12 add. par.) for IGI ; 19 (6 + focal length + 12 add. par.) for Applanix
GIP	1 step	UTM	21 (6 + 3 f. int. ori. + 12 add. param.)
ICC	1 step	UTM	21 (6 + 3 f. int. ori. + 12 add. param.)
Inpho	1 step	UTM	6 for IGI; 9 (6 + 3 f. int. ori. for Applanix)
LHS	1 step	Local tangential*	6
DIIAR	2 steps	Local tangential	6
IPF	1 step	UTM	11 (6 + 3 f. int. ori + 2 f. rad. distortion)
IPI	2 steps	Local tangential and UTM	21 (6 + 3 f. int. ori. + 12 add. param.)
ifp	2 steps	Local tangential	3

Table 3: System calibration approaches followed by the different participants

[7] The IPI results in table 4 slightly differ from previously published results due to an editing error. The results given here are correct.

5.2 Analysis procedure and overall results

While it is obvious that in object space a comparison between the computed coordinates and those of independent check points can serve to judge the results, it is not clear a priori how to assess the derived orientation parameters themselves. Rather than trying to analyse the GPS/IMU measurements and to quantify their accuracy we have taken a users´ perspective for this test and have looked at remaining y-parallaxes in the resulting stereo models. The reason for this approach was that the most sensitive application for the image orientations in terms of accuracy is that of stereo plotting, which relies on y-parallax-free models. Thus, if the determined exterior orientation is accurate enough for this task, it is also good enough for other tasks.

In order to analyse the participants´ results we have carried out a conventional bundle adjustment for the test flight 1:5.000 in which the image coordinates of the GCP of the test field (49 GCP for Applanix, 41 GCP for IGI) together with 25 tie points per image and a number of object space coordinates served as input. All image coordinates were measured manually, again using the Planicomp P1. The standard deviation of the image coordinates after the bundle adjustment was 4.8 µm for the IGI dataset and 6.2 µm for the Applanix data. These values lie in the expected range; the difference can be explained by the somewhat poorer image quality of the Fotonor/Applanix images. In a second step, we transformed the image coordinates of the GCP into object space via a least-squares forward intersection with the exterior orientation of the participants being introduced as constant values. The resulting object space coordinates were then compared to the known values of the GCP yielding RMS differences. The residuals in image space are accumulated in the σ_o value of the adjustment and can be thought of as a measure for remaining y-parallaxes in stereo models formed using the participants´ exterior orientation (see below for a more detailed discussion). Statistical results of this procedure are given in table 4. In order to compare them with the conventional photogrammetric accuracy without GPS/IMU data the corresponding results are also shown.

Participant	**No. of cal. parameters**	**Applanix**				**IGI**			
		σ_o [µm]	RMS differences at GCP			σ_o [µm]	RMS differences at GCP		
			X [cm]	Y [cm]	Z [cm]		X [cm]	Y [cm]	Z [cm]
Convent. bundle adjustment		6.2	2.2	2.0	6.0	4.8	2.8	2.6	4.3
Applanix	6	22.2	5.9	11.9	32.0	-	-	-	-
IGI	6	-	-	-	-	36.7	15.9	16.1	23.0
ADR	6	32.2	13.4	12.7	18.1	55.5	19.9	16.8	28.8
FGI	19/18	13.6	9.8	10.8	9.2	27.4	11.8	10.1	18.6
GIP	21	14.8	10.7	11.2	8.1	22.9	8.1	8.3	11.2
ICC	21	14.4	5.1	3.0	22.4	24.1	9.0	12.3	22.9
Inpho	9/6	14.8	4.7	3.3	8.2	27.0	10.3	9.8	14.6
LHS	6	-	-	-	-	44.6	13.8	13.1	17.9
DIIAR	7	12.4	3.9	2.5	8.4	22.9	8.8	11.8	13.5
IPF	11	19.5	7.0	3.3	12.0	42.6	12.0	11.7	14.6
IPI (local tang.)	21	16.2	5.5	4.0	7.9	43.0	12.7	12.6	18.4
IPI (UTM)	21	16.1	8.5	3.3	12.3	42.8	12.9	15.7	18.7
Ifp	3	31.3	11.1	8.7	15.1	35.5	14.9	15.6	25.0

Table 4: Numerical results of phase I for each participant ("-" denotes that the result was not delivered to the pilot centre or is still being processed)

The following results can be derived from the figures given in table 4:

- The accuracy potential of direct georeferencing lies at approximately 5-10 cm in planimetry and 10 – 15 cm in height when expressed as RMS values at independent check points, and at 15 - 20 µm when expressed as σ_o values of the over-determined forward intersection in image space.
- These values are larger by a factor of 2 - 3 when compared to standard photogrammetric results.
- IGI and Applanix have not obtained the best results for their respective data sets. This finding suggests that a refinement of their calibration models and software may lead to improved results.
- The results do not significantly depend on the way of computing the boresight misalignment (one or two steps).
- For the IGI data the results do not depend on the chosen object space coordinate system (see the two IPI results), the situation is different, however, for the Applanix data. Here, the RMS values for planimetry and in particular for the height are better in the more rigorous local tangential system than in the UTM system.
- Whereas in the IGI data a dependency on the chosen calibration model was not found, the Applanix results significantly depend of the number of parameters estimated during system calibration. Allowing for a change in the calibrated focal length and the position of the principal point improves the results especially in height, as was to be expected a further refinement using self calibration parameters does not lead to significantly better results. These findings are also reflected in the results presented in table 5 in which for two participants (GIP and IPI) the results for different sets of calibration parameters under otherwise identical conditions are presented. An exception to these findings, however, is the results obtained by DIIAR, as they only used 6 calibration parameters and still obtained excellent results. This may have to do with the weighing scheme used when computing the calibration parameters, however, at this point in time, no conclusive explanation is available for this result.
- The best Applanix results are better by approximately a factor of 2 when compared to the IGI results. While a conclusive explanation for these differences cannot be given, the used hardware (dry-tuned vs. fibre optics gyros) and the less favourable GPS conditions during the IGI flight (see chapter 3) are possible reasons; see also the discussion below.
- The results are not homogeneous with respect to the number of estimated calibration parameters, especially if only six calibration parameters are used; different results are obtained (compare e. g. the results of ADR, inpho and LHS for the IGI flight), but also for more refined calibration models (compare e. g. the results from ICC and inpho for the Applanix data). Again, a conclusive reason for these differences cannot be given due to lacking information about the details of the system calibration.

Participant	**No. of cal. parameters**	**Applanix**				**IGI**			
		σ_o [µm]	RMS differences at GCP			σ_o [µm]	RMS differences at GCP		
			X [cm]	Y [cm]	Z [cm]		X [cm]	Y [cm]	Z [cm]
GIP	6	30.2	13.4	12.3	11.8	28.1	11.6	12.0	15.1
	21	14.8	10.7	11.2	8.1	22.9	8.1	8.3	11.2
IPI (local tang.)	6	33.7	10.3	11.0	16.6	43.8	13.3	13.4	19.2
	9	17.1	6.1	3.8	8.0	43.0	12.7	12.6	18.4
	21	16.2	5.5	4.0	7.9	43.0	12.7	12.6	18.4

Table 5: Detailed results for a varying number of calibration parameters, GIP and IPI

5.3 Local systemtic effects

The results presented so far give a good overview of the potential of direct georeferencing, and the RMS differences are surprisingly small. Thus, direct georeferencing must be seen as a promising candidate for 3D point positioning from airborne platforms. However, tables 4 and 5 contain only average values for the whole block. Next, a more detailed analysis aiming at detecting local systematic effects in location and/or time was carried out. To this end the RMS values in object space where plotted in the XY plane. The plots of one participant (GIP) are presented in the figures 9-12. The figure 9 and 10 show the results for Applanix and IGI achieved with 6 calibration parameters, while figures 11 and 12 show the same information obtained from a calibration with 21 parameters. In the Applanix data set a systematic effect can clearly be seen in the 6 parameter solution, while it has vanished when using 21 parameters. For the IGI results no such systematic effect is visible.
These observations could also be made for other participants´ results and can thus be regarded as representative. The systematic effect shown in figure 9 and its absence in figure 11 conform well with the discussion about the necessary number of calibration parameters above, as does the similarity of figures 10 and 12. Thus, these results again suggest to introduce parameters in the calibration procedure, taking care of differences between the nominal and the actual values for the interior orientation.

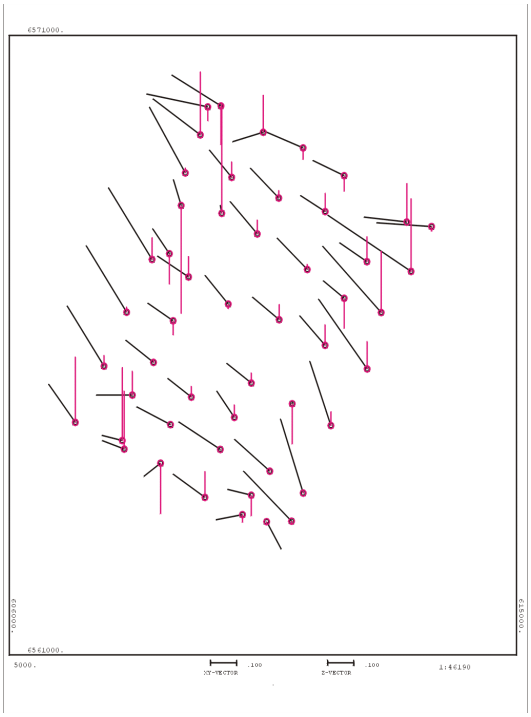

Figure 9: Difference vectors in object space (black: planimetry, red: height), Fotonor/Applanix flight, Participant GIP, 6 calibration parameters

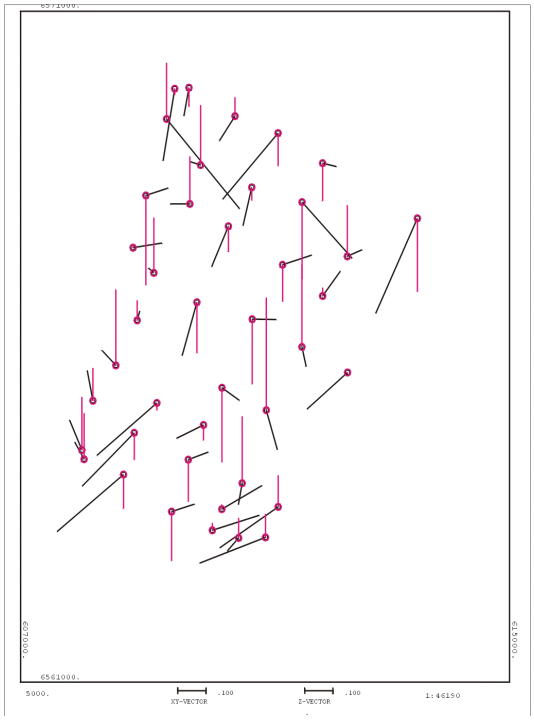

Figure 10: Difference vectors in object space (black: planimetry, red: height), FW/IGI flight, Participant GIP, 6 calibration parameters

Also, the deviations in image space represented by the σ_o values in tables 4 and 5 deserve a closer look. First, we assessed individual models rather than relying on the results of multi-ray points. We computed relative orientations for all models which could be formed from the two test blocks (178 models for Applanix, 106 models for IGI). Table 6 contains the results: the σ_o values from table 5, the average of the RMS y-parallaxes per model, called $\sigma_{o,\,rel}$ and the percentage of models with RMS y-

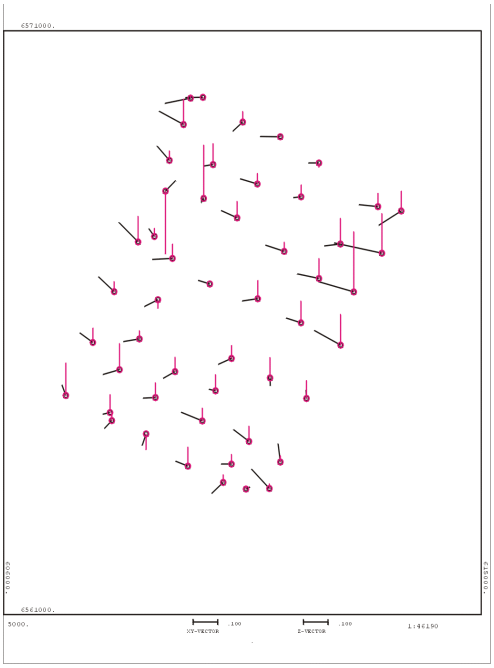

Figure 11: Difference vectors in object space (black: planimetry, red: height), Fotonor/Applanix flight, Participant GIP, 21

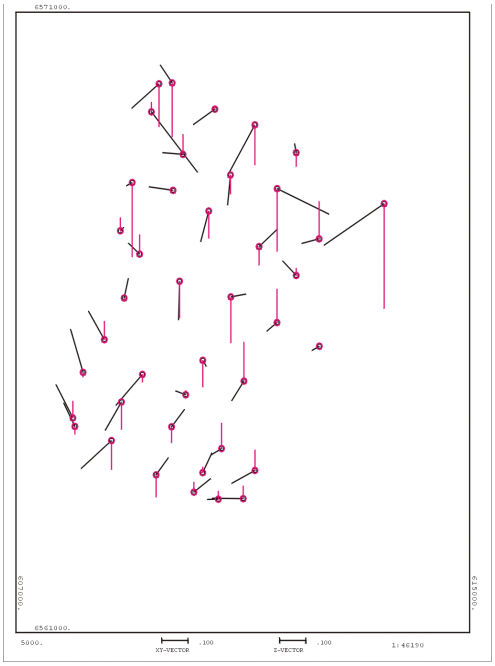

Figure 12: Difference vectors in object space (black: planimetry, red: height), FW/IGI flight, Participant GIP, 21 calibration parameters

parallaxes larger than 10 and 20 µm. These thresholds were chosen because in models with y-parallaxes larger than 10 µm stereo plotting becomes less comfortable, and even cumbersome with y-parallaxes larger than 20 µm.

Participant	**Applanix** (178 models)				**IGI** (106 models)			
	σ_o [µm]	$\sigma_{o,\,rel}$ [µm]	% of models with RMS y-parallaxes		σ_o [µm]	$\sigma_{o,\,rel}$ [µm]	% of models with RMS y-parallaxes	
			> 10 µm	> 20 µm			> 10 µm	> 20 µm
Applanix	22.2	20.2	89	31	-	-	-	-
IGI	-	-	-	-	36.7	36.6	86	55
ADR	32.2	22.6	90	34	55.5	57.5	100	86
FGI	13.6	13.6	85	13	27.4	26.9	75	35
GIP	14.6	16.4	88	15	27.8	27.3	74	36
ICC	14.4	15.4	84	13	24.1	27.0	75	35
inpho	14.8	15.6	86	12	27.0	27.0	74	34
LHS	-	-	-	-	44.6	43.3	98	78
DIIAR	12.4	15.1	79	13	22.9	27.0	74	33
IPF	19.5	16.4	85	15	42.6	43.3	98	78
IPI (local tang.)	16.2	19.3	86	27	43.0	45.4	90	61
ifp	31.3	19.0	76	17	35.5	36.8	86	53

Table 6: Model accuracy in image space, all models of the test blocks

Besides the fact that σ_o indeed seems to be a good approximation for the model accuracy, because in most cases and σ_o and $\sigma_{o,\,rel}$ agree rather well, table 6 suggests that while a number of model orientations from direct georeferencing can in fact be used for stereo plotting, this is not always the case. For both data sets there is a substantial number of models with y-parallaxes larger than 10 µm. In addition, the percentage of stereo models with y-parallaxes larger than 20 µm is rather high for the IGI data set. In order to further investigate this issue plots were created for all participants showing a distribution of the RMS y-parallaxes in the XY plane. As a representative example the plots for one participant (DIIAR)are presented in figures 13 for Applanix and in figure 14 for IGI.

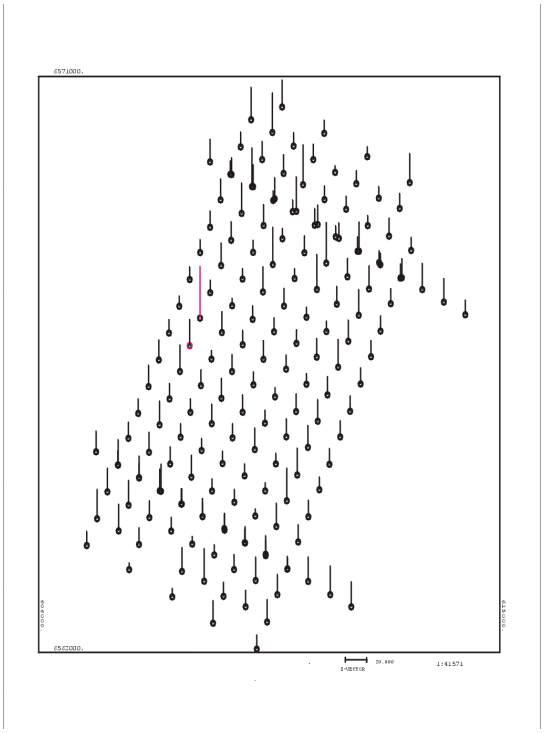

Figure 13: Remaining RMS y-parallaxes in individual stereo models, Fotonor/Applanix flight, participant DIIAR (red vectors show large parallaxes)

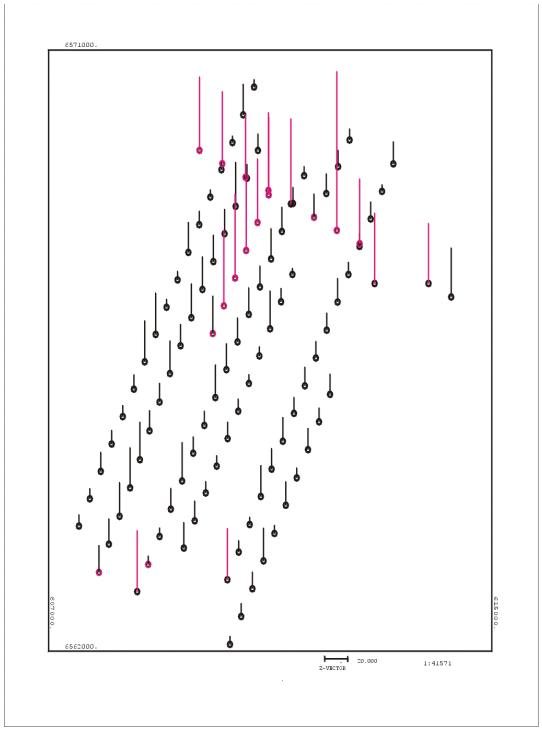

Figure 14: Remaining RMS y-parallaxes in individual stereo models, FW/IGI flight, participant DIIAR (red vectors show large parallaxes)

It can be seen that while for the Applanix data the RMS y-parallaxes are more or less similar across the whole block, for IGI two strips, namely the cross strip and a short strip in the middle of the block show distinctly larger y-parallaxes (see also Forlani, Pinto 2001 for a discussion of this effect).
At first sight this effect is surprising. The photogrammetric data give no evidence that an error in the image coordinates of the tie points can explain it. A possible explanation can be given when referring again to figure 7 and the GPS conditions during the FW/IGI test flight. As is evident from the flight management recordings the two strips in question are the two last strips flown during the complete mission, at a considerable time interval to the other strips of the block. The images in the middle of the block could not be captured before due to clouds, and the cross strip was planned to be the last strip anyway. As was mentioned before, about the second half of the block was captured under unfavourable GPS constellations. The two strips discussed here where flown shortly after the PDOP had returned to a value of about 1.7, however, the time interval between the last good satellite constellation and the acquisition time of the two strips may have been too long to again reach an adequate positioning accuracy.
In order to test this hypothesis these two strips were discarded from the analysis procedure, and the whole process was repeated for some participants. The results are presented in table 7.

Participant	**IGI** 88 models, without the two problematic strips						
	σ_o [µm]	RMS differences to GCP			$\sigma_{o,rel}$ [µm]	% of models with RMS y-parallaxes	
		X [cm]	Y [cm]	Z [cm]		> 10 µm	> 20 µm
IGI	30.1	15.9	14.6	21.7	29.4	86	49
GIP	16.0	6.9	7.9	10.2	18.0	70	26
DIIAR	16.4	7.4	10.6	11.6	17.2	68	22

Table 7: Comparison of IGI results with and without the two questionable strips

When comparing these values to the corresponding entries in table 4 and 6 an improvement can be seen. As was to be expected this improvement mainly concerns the results in image space, since the object space coordinates are of course not only influenced by the models of the two discarded strips. Nevertheless a small improvement is also visible in the RMS differences to the GCP.

5.4 General discussion of the results

The most important finding is the fact that based on the obtained results direct georeferencing has proven to be a serious alternative to conventional bundle adjustment and currently seems to allow for the generation of orthophotos and other applications with less stringent accuracy requirements. However, stereo plotting is not always possible due to the sometimes large RMS y-parallaxes of individual models. It should also be kept in mind, that also the reliability of the results remains a weak point of direct georeferencing due to a lack of redundancy in absolute orientation Systematic errors in the GPS/IMU measurements cannot be detected without the introduction of GCP coordinates.
When analysing the presented figures in more detail it must be kept in mind that a refinement of the interior orientation parameters during the calibration does not necessarily mean that the camera calibration protocol contains incorrect values. It only implies, that the more general models better explain the given input data. For instance, a change in the x-direction of the principal point has nearly the same effect onto the results as a constant error in the time synchronisation between the GPS/IMU sensor and the camera. The same is true for a change in the calibrated focal length and the GPS shift in Z. Only if two calibration flights in distinctly different flying heights are available and are processed simultaneously (as was the case in this test), the latter two parameters are independent and can both be determined.

As mentioned, the reason for the better results with the Applanix data is possibly the difference in the GPS conditions during the test flights. Also the use of dry-tuned gyros in the (today outdated) IGI system may play a role, Applanix had already used a fibre optics gyro in the test. A conclusive explanation for the differences, however, can not be given based on the test data. The better accuracy level of the Applanix data may explain why the results are more sensitive to the chosen calibration model and the object space coordinate system: while the IGI results are dominated by sensor effects, the Applanix data are more effected by the chosen mathematical model and object space coordinate system. To confirm this hypothesis a more detailed analysis is necessary.

Based on the obtained results it is recommended to include the interior orientation parameters into the system calibration whenever possible. If it is not feasible to use two different calibration flights, the calibration should be carried out in the same scale as the actual project. In this case, the GPS shift will also take care of possible changes in the focal length.

As for the object space coordinate system, preference should be given to a local tangential system, because in this case the approach is mathematically more rigorous. A theoretical analysis should be carried out in order to quantify the errors introduced by the approximations inherently contained in the UTM system. If, for whatever reason, a project has to be carried out in a non-cartesian mapping system, however, also the calibration needs to be performed in this system (for details see Jacobsen, Wegmann 2001).

It should also be noted that the test results have been obtained immediately after calibration. Within the test, no statement can be made concerning the stability of the system calibration parameters over time. Currently, it is generally recommended to carry out the system calibration before and possibly also after each block. Since the actual physical reasons for the GPS shift and the possible changes in the interior orientation of the camera are unknown, this recommendation should be followed, at least for high accuracy work.

6 CONCLUSIONS

In the first phase of the OEEPE test on integrated sensor orientation an accuracy potential of direct geo-referencing for 1:5.000 imagery of approximately 5-10 cm in planimetry and 10 – 15 cm in height when expressed as RMS values at independent check points, and of 15 - 20 µm when expressed as remaining y-parallaxes in image space was found. While these values are larger by a factor of 2 - 3 when compared to standard photogrammetric results, they prove that direct georeferencing is a serious alternative to classical and GPS-assisted bundle adjustment and currently allows for the generation of orthophotos and other applications with less stringent accuracy requirements. Stereo plotting, on the other hand, is currently not always possible with such data due to the sometimes relatively large y-parallaxes.

In summary, it can be stated and comes as no surprise that the system calibration itself is more complex than one might think at first. This statement is motivated not only by the fact that direct georeferencing is equivalent to an extrapolation as explained in chapter 1 and therefore comes with all associated difficulties, but also by the fact that not all test participants have given full details of the actual procedure used for investigating the test data. While it is of course understandable that some crucial information is kept confidential, in particular in the commercial arena, this lack of information renders a conclusive interpretation of the results more difficult. Nevertheless, we feel that we could reach the goals set out for phase I of the test.

Future developments in the areas of GPS and IMU sensors and data processing will probably also reduce this problem. The best results in terms of accuracy and in particular in terms of reliability are expected from an integration of GPS/IMU data into the bundle adjustment A particularly important point, which needs to be addressed in this regard, is the choice of a proper stochastic model for the GPS/IMU data. Integrated solutions are investigated in phase II of the OEEPE test; results will be available shortly.

7 ACKNOWLEDGEMENTS

The authors are grateful to the companies Applanix, IGI, Fotonor and Fjellanger Widerøe Aviation for participating in the test and for having acquired and provided the tests data. We would also like to thank the Norwegian Mapping Authority Statens Kartverk, Hønefoss, for making available the measurements of the GPS reference stations and the OEEPE for their support of the project. Thanks are also due to Øystein Andersen and Barbi Nilsen from the Agricultural University of Norway who were responsible for data acquisition and handled this crucial part of the test with great wisdom and care, to Günter Seeber and his team from the Institut für Erdmessung, University of Hannover, for valuable help with the GPS data, and to Adelheid Elmhorst and Karin Kolouch from IPI who have helped tremendously in handling the nearly 700 images in endless hours of work. Last not least, the test would not have been possible without the enthusiastic efforts of the test participants.

8 REFERENCES

Abdullah Q.A., Tuttle M.A. (1999): Integrated GPS-inertial measurement solution as an alternative to aerial triangulation: a case study, Proceedings, ASPRS Annual Convention, Baltimore, pp. 867-876 (on CD-ROM).

Ackermann F. (1986): The use of camera orientation data in photogrammetry – a review, IAPRS (26) 1, 93-99.

Ackermann F. (1994): On the status and accuracy performance of GPS photogrammetry, Proceedings, ASPRS Workshop "Mapping and remote sensing tools for the 21th century, Washington D.C., pp. 80-90.

Alamús R., Baron A., Talaya J. (2001): Integrated sensor orientation at ICC, mathematical models and experiences, OEEPE Workshop "Integrated Sensor Orientation", Institut für Photogrammetrie und GeoInformation, Universität Hannover, Sept. 17/18-2001, 10p. (on CR-ROM).

Applanix (2001): http://www.applanix.com (July-2nd-2001).

ARINC 705: http://www.arinc.com/cgi-bin/store/arinc (July-3rd-2001)

Burman H. (1999): Using GPS and INS for orientation of aerial photography, Proceedings, ISPRS Workshop "Direct versus indirect methods of sensor orientation", Barcelona, pp. 148-157.

Colomina I. (1999): GPS, INS and aerial triangulation: What is the best way for the operational determination of photogrammetric image orientation?, IAPRS (32) 3-2W5, pp.121-130.

Cramer M. (1999): Direct geocoding – is aerial triangulation obsolete?, in: Fritsch D., Spiller R. (Eds.), Photogrammetric Week ´99, pp. 59-70.

Ebner H. (1976): Self calibrating block adjustment, Bildmessung und Luftbildwesen Vol. 44, 128-139.

Forlani G., Pinto L. (2001): Integrated INS/DGPS systems: calibration and combined block adjustment, OEEPE Workshop "Integrated Sensor Orientation", Institut für Photogrammetrie und GeoInformation, Universität Hannover, Sept. 17/18-2001, 13p. (on CR-ROM).

Habib A., Schenk T. (2001): Accuracy analysis of reconstructed points in object space from direct and indirect exterior orientation methods, OEEPE Workshop "Integrated Sensor Orientation", Institut für Photogrammetrie und GeoInformation, Universität Hannover, Sept. 17/18-2001, 6p. (on CR-ROM).

Heipke C., Jacobsen K., Wegmann H., Andersen Ø., Nilsen B. (2000): Integrated sensor orientation – an OEEPE test, IAPRS (33) B3/1, pp. 373- 380.

Heipke C., Jacobsen K., Wegmann H. (2001): OEEPE test on integrated sensor orientation – status report, ASPRS Annual Convention St. Louis, on CD-ROM, 5 p.

Hutton J., Lithopoulos E. (1998): Airborne photogrammetry using direct camera orientation measurements, PFG No. 6, pp. 363-370.

IGI mbH (2001): Computer controlled navigation system and AEROcontrol II, Company information, Kreuztal.

Jacobsen K. (1980): Vorschläge zur Konzeption und zur Bearbeitung von Bündelblockausgleichungen, Wissenschaftliche Arbeiten der Fachrichtung Vermessungswesen der Universität Hannover, Nr. 102.

Jacobsen K. (1997): Operational block adjustment without control points, Proceedings, ASPRS Annual Convention, Seattle, Vol. 2, pp. 238-244.
Jacobsen K. (2000): Potential and limitation of direct sensor orientation, IAPRS (33), B3/1, pp. 429-435.
Jacobsen K., Schmitz M. (1996): A new approach for combined block adjustment using GPS satellite constallations, IAPRS (31) B3, 355-359.
Jacobsen K., Wegmann H. (2001): Dependencies and problems of direct sensor orientation, OEEPE Workshop "Integrated Sensor Orientation", Institut für Photogrammetrie und GeoInformation, Universität Hannover, Sept. 17/18-2001, 11p. (on CR-ROM).
Kruck E., Wübena G., Bagge A. (1996): Advanced combined bundle block adjustment with kinematic GPS data, IAPRS (31) B3, pp. 394-398.
Mader G. (1986): Dynamic positioning using GPS carrier phase measurements, manuscripta geodetica (11/4) 272-277.
Mostafa M. (2001): Digital multi-sensor systems – calibration and performance analysis, OEEPE Workshop "Integrated Sensor Orientation", Institut für Photogrammetrie und GeoInformation, Universität Hannover, Sept. 17/18-2001, 8p. (on CR-ROM).
Ressl C. (2001): The OEEPE-test „Integrated sensor orientation" and its handling within the hybrid block-adjustment program Orient, OEEPE Workshop "Integrated Sensor Orientation", Institut für Photogrammetrie und GeoInformation, Universität Hannover, Sept. 17/18-2001, 12p. (on CR-ROM).
Schenk T. (1999): Digital photogrammetry, Volume I, Terra Science, 428 p.
Schmitz M. (1998): Untersuchungen zur strengen GPS Parametrisierung in der gemeinsamen Ausgleichung von kinematischem GPS und Aerotriangulation, Dissertation, Wissenschaftliche Arbeiten der Fachrichtung Vermessungswesen der Universität Hannover, Nr. 225, 121 p.
Schmitz M., Wübena G., Bagge A., Kruck E. (2001): Benefit of rigorous modelling of GPS in combined AT/GPS/IMU-bundle block adjustment, OEEPE Workshop "Integrated Sensor Orientation", Institut für Photogrammetrie und GeoInformation, Universität Hannover, Sept. 17/18-2001, 15p. (on CR-ROM).
Schwarz K.-P. (1995): Integrated airborne navigation systems for photogrammetry, in: Fritsch D., Hobbie D. (Eds.), Photogrammetric Week ´95, Wichmann, Heidelberg, 139-153.
Schwarz K.-P., Chapman M.E., Cannon E., Gong P. (1993) : An integrated INS/GPS approach to the georeferencing of remotely sensed data, PE&RS (59) 11, 1667-1674.
Skaloud J. (1999): Problems in sensor orientation by INS/DGPS in the airborne environment, Proceedings, ISPRS Workshop "Direct versus indirect methods of sensor orientation", Barcelona, pp. 7-15.
Skaloud J., Schwarz K.-P. (1998): Accurate orientation for airborne mapping systems, IAPRS (32) 2, pp. 283-290.
Toth C. (1999): Experiences with frame CCD arrays and direct georeferencing, in: Fritsch D., Spiller R. (Eds.), Photogrammetric Week ´99, pp. 95-107.
Wewel F., Scholten F., Neukum G., Albertz J. (1998): Digitale Luftbildaufnahme mit der HRSC – Ein Schritt in die Zukunft der Photogrammetrie, PFG No. 6, pp. 337-348.

Web sites about the test:
http://www.nlh.no/ikf/projects/gpsins
http://www.ipi.uni-hannover.de/htm-deutsch/forschung/laufend/oeepe-gps-imu/index.html

DEPENDENCIES AND PROBLEMS OF DIRECT SENSOR ORIENTATION

Karsten Jacobsen, Helge Wegmann
Institute for Photogrammetry and GeoInformation
University of Hannover, Germany
jacobsen@ipi.uni-hannover.de wegmann@ipi.uni-hannover.de

KEY WORDS: direct sensor orientation, boresight misalignment, coordinate systems, inner orientation, combined adjustment

ABSTRACT

The direct sensor orientation has reached a high accuracy level. This and also the fact that we do have an extrapolation from the projection centers to the ground, makes it necessary to take care about all sources of errors. It is not anymore possible to use a not orthogonal coordinate system like the national net. The national coordinate system is not just causing a scale error of the height by the local scale factor, it is also influenced by a change of the height-to-base-relation by the flattening of the curved earth. Also the inner orientation became more important - the temperature depending changes are not compensated like in the case of an exterior orientation with control points. Errors of the mathematical model can only be compensated if the determination of the boresight misalignment will be done under the same condition like the use of the direct sensor orientation. If the image scale will not be the same like during the determination of the boresight misalignment, the boresight misalignment has to be made with 2 different flying altitudes to enable the separation of the inner orientation from the shift values of the exterior orientation.

Even the today reached high accuracy level is not sufficient for the set up of the models. The partially not acceptable y-parallaxes can be reduced to the usual level by a combined adjustment with the direct sensor orientation and image coordinates of tie points; control points are not required.

1. INTRODUCTION

The determination of the image orientation is a basic requirement for every type of photogrammetric data acquisition. The traditional method by means of bundle block adjustment is time consuming and needs a sufficient number of ground control points. The combined adjustment together with projection center coordinates, determined by relative kinematic GPS-positioning is reducing the effort for the ground control but it is still based on image coordinates of tie and control points. The progress of the hard- and software components of inertial measuring units (IMU) during the last years, allows now a direct sensor orientation based on the combined use of IMU and GPS for several applications. The relation between the IMU and the photogrammetric camera (boresight misalignment) has to be determined with a traditional bundle block adjustment. During this process it is also possible to calibrate the camera under operational conditions. The camera calibration and the self calibration by additional parameters in a bundle block adjustment is a well investigated problem, which always has been handled in an ISPRS Working Group from 1976 – 1980. Nevertheless some of the results of the old investigations have not been respected up to now. For the handling of a bundle block adjustment this is not causing problems because several small errors can be compensated by the exterior orientation. This is not anymore the case with the direct sensor orientation, it cannot compensate discrepancies of the focal length with the flying height, if the boresight misalignment between the camera and the IMU has been determined in a different altitude.

The whole process of the direct sensor orientation is very sensitive against a not strict data handling, especially also the chosen coordinate system. The mathematical model, used in photogrammetry, is based on an orthogonal coordinate system. The national coordinate systems are not orthogonal because the coordinates are following the curved earth, nevertheless the data acquisition usually is based on it. In the traditional data handling, the lack of the mathematical model will be compensated by an earth curvature correction. The second order effects are nearly totally compensated by the absolute orientation.

In the case of the direct sensor orientation no absolute orientation based on control points will be done, the absolute orientation is based on the directly determined projection centers and the attitude data, that means, the evaluation of ground points is an extrapolation out of the level of reference. In the case of such an extrapolation, the whole solution must be more strict because errors are not compensated by the solution. Only indirectly we still do have an interpolation

based on the ground points by the boresight misalignment which enables us to compensate or determine some geometric problems.
An up to now not solved problem is the stability of the calibration. It is not well known, how often a system calibration is required. Of course this is depending upon the flight conditions and the careful handling of the hardware components. If components are dismounted, after mounting again, the geometric relations may have changed.

2. BACKGROUND

In the normal case of aerial photogrammetry (view vertical and perpendicular to the base) we do have the simple mathematical relation shown in formula 1.

$$X = \frac{h}{f} \bullet x' \qquad Y = \frac{h}{f} \bullet y' \qquad Z = \frac{b \bullet f}{px}$$

h = flying height above ground
f = focal length
x', y' = image coordinates
b = base (distance of projection centers)
px = x-parallax = x' – x"

formula 1: ground coordinates for normal case

The relation h/f is identical to the image scale number. In the case of an absolute orientation with control points or a classical bundle block adjustment, the scale is determined by the horizontal control points, that means, an error in the focal length will be compensated by the flying height above ground. For the vertical component, the scale is indirectly included in the base, but a deviation of the focal length will directly have a linear influence to the height. So a discrepancy of the focal length will cause an affine deformation of the model with a correct scale in the X-Y-plane but a not correct scale in the vertical direction. For example an error of 15 µm of a wide angle camera (f=153mm) will change the height of a point located 100m above the level of the control points by 15µm / 153mm • 100m = 10mm. This usually will not be recognised. On the other hand, a deviation of the focal length by 15µm will change the distance from the projection centers for a flying height of 1000m (image scale 1 : 6500) by 100mm or 0.1%, that means 10 times the usual vertical accuracy.

The focal length is determined by laboratory calibration under constant temperature condition. During photo flight a vertical temperature gradient in the optics from the cold air to the warm aircraft cannot be avoided. H.-K. Meier (Meier 1978) has investigated this for the Zeiss cameras with the results shown in table 1.

	pressurised cabin, cover glass		lens in free atmosphere, constant temperature 7°C		lens in free atmosphere temperature depending upon air	
flying height	6 km	14 km	6 km	14 km	6 km	14 km
wide angle camera f=153mm	-20µm	-38µm	-36µm	-58µm	-47µm	-80µm
Normal angle camera f=305mm	+12µm	-17µm	-33µm	-28µm	-110µm	-172µm

table 1: change of focal length depending upon flying height and camera operation condition (Meier 1978)

The change of the focal length shown in table 1 depends upon the camera type, the camera operation conditions and the time period in which the camera has been under same temperature condition. By this reason, the values cannot be used directly for a correction of the calibrated focal length. But of course the situation should be respected for the boresight calibration – before taking the photos, the camera should be under constant temperature conditions for a sufficient time.

A complete boresight information should include the attitude relation between the inertial measurement unit (IMU), the constant shifts in X, Y and Z and also the actual inner orientation. The focal length can be determined together with the other elements of the boresight misalignment, if a calibration flight will be done in different height levels. As mentioned before, the computed flying height is linear depending upon the focal length, so an additional information is required and these are the projection center coordinates computed by a Kalman filter of the IMU-data together with the relative kinematic GPS positions. A shift in Z is included in the boresight data. If only one flying height is available and the control points are approximately in the same height level, it is not possible to separate between a shift in Z and a change of the focal length, they are correlated by 100%. The change of the focal length Δf can be computed from the height shift ΔZ with the relation $\Delta f = \Delta Z \bullet f / Z$. If the boresight misalignment will be done in 2 different height levels, in both height levels the same height shift ΔZ is available, but the influence of Δf is different, so it can be separated. Finally Δf is depending upon the vertical difference of the both height levels used for the determination of the boresight misalignment. But also here we do have a limitation, because the focal length may change depending upon the air temperature as mentioned before. So finally we are still limited to a three-dimensional interpolation which will lead to sufficient results if the conditions for projects, using the determined boresight calibration, are done under comparable conditions, that means also similar temperature as a function of the flying height. The use of the determined focal length

also for other projects with an image scale outside the range which has been used for the determination, is still limited, but it is a better estimation of the real condition than the focal length from the calibration certificate. For the location of the principal point we do have a similar condition, but it is not depending upon temperature of the camera system.

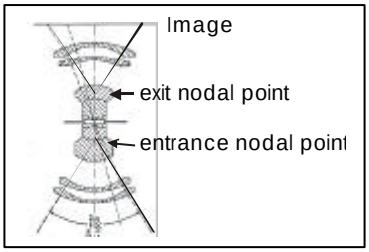

figure 1: definition of projection center

As mentioned, the whole process has to be handled very strictly. This includes also the pre-correction of all used values e.g. by refraction correction and the correct offset from the GPS-antenna to the entrance nodal point of the camera (figure 1) – the projection center in the object space. The rotation of the system camera + IMU against the aircraft is changing the offset, so it has to be recorded. This can be done with a separate gyro-system or in the case of the use of a gyro stabilised platform with a registration of the rotations.

The mathematical model, used in photogrammetry, is based on an orthogonal coordinate system. An orthogonal coordinate system we do have with geocentric coordinates, but the handling of geocentric coordinates, oriented against the equator, has some disadvantages, it is mixing the original height with the horizontal position, so it is better to transform it into a tangential coordinate system. For the data acquisition it is more easy to operate directly in the national than in the tangential coordinate system. Only few photogrammetric operation systems are including internally the transformation from the tangential to the national coordinate system. The traditional photogrammetry is respecting the earth curvature by an earth curvature correction of the image coordinates, but this compensates only a part.

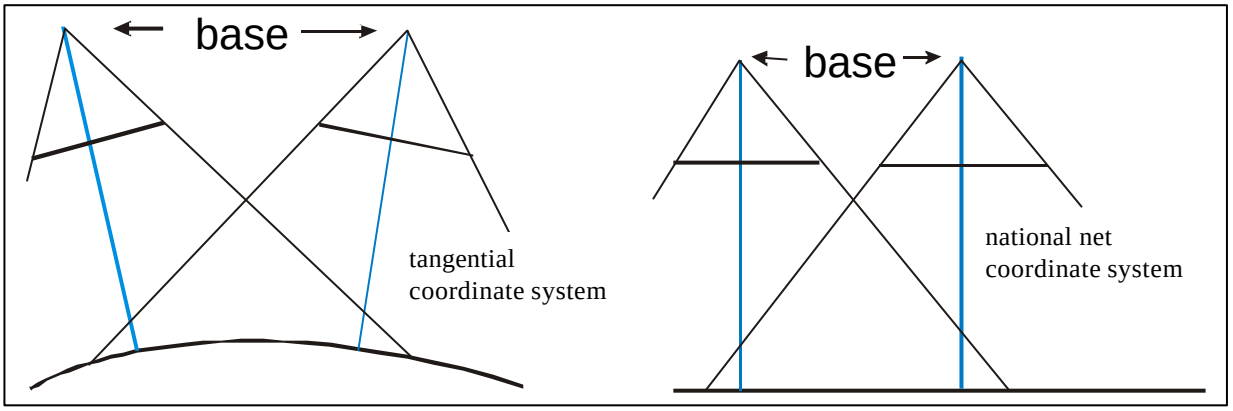

figure 2: influence of earth curvature correction

As it can be seen in figure 2, the real geometry of the photo flight, shown on the left hand side, is changed by the earth curvature correction to the situation shown on the right hand side. By the traditional photogrammetric model orientation, based on control points, this leads to a sufficient situation in X and Y. The influence of the map projection usually can be neglected within one model, it only has to be respected in the case of space images. The vertical component is influenced by the change of the base. Corresponding to formula 1, the height is linear depending upon the base. The base is reduced by the earth curvature correction to the base projected to the height level of the control points, that means the ground.

$$\Delta b = \frac{h}{R} \bullet b \qquad \Delta fe = \frac{h}{R} \bullet f$$

formula 2: influence of earth curvature correction

Δb = change of base by earth curvature correction
Δfe = change of the focal length for the compensation of the second order effect of the earth curvature correction
R = Earth radius

The base reduced by the earth curvature correction is causing a scale change of the height. For a flying height of 1000m above ground, this will change the height of a point located 100m above the level of the control points by 16mm which usually can be neglected, but it is changing the computed flying height above ground by 160mm, which cannot be neglected for the direct sensor orientation. But it can be compensated by a change of the focal length of a wide angle camera (f=153mm) by $\Delta fe = 24\mu m$.

Another effect is based on the map projection. UTM-coordinates do have in the center meridian a scale 1:0.9996. The scale of the reference bundle block adjustment is based on the horizontal control points, so the vertical component will be changed by this scale – a ΔZ of 100m is changed 0.04m or a flying height of 1500m is influenced by 0.6m.

The correct method for the reference bundle block adjustment and the following model handling is the computation in an orthogonal coordinate system. A tangential coordinate system to the earth ellipsoid has the advantage of a more simple weight variation between horizontal and vertical coordinates than a handling in the geocentric coordinate system. If the boresight misalignment including the inner orientation has been determined in an orthogonal system, these results are only valid for this. It is not possible to use such a misalignment for a model handling in the national coordinate system. Only few photogrammetric workstations are able to handle the relations in an orthogonal coordinate system together with a direct output of the results in the national net coordinate system. This is causing a complicate data handling. It is much more simple to have the data acquisition directly in the national net coordinates.

Finally it is not so complicate like in the first view, because also the direct sensor orientation is together with the boresight misalignment not an extrapolation from the projection centers to the ground, the whole system is based on the control points of the reference block and indirectly the points in the project area are determined based on this. If the boresight misalignment will be determined in the national net coordinate system, and the data handling in the project area will be done in the same way, the resulting ground coordinates do have approximately the same accuracy like in the mathematical strict solution, if the reference block has the same scale or scale range like the project area and the scale of the national net coordinates are similar. The mathematical strict handling has the advantage, that it is independent from the national coordinate system, it can be handled also for different net projections and it is much more free in relation to different image scales. But in general it is not easy to estimate all the second and third order effects, by this reason empirical investigations have to be made.

3. USED DATA SET

The empirical investigations have been made with the data of the OEEPE-test “Integrated Sensor Orientation” (Heipke et al 2000). The test field in Frederikstad, Norway, has been flown by companies producing suitable GPS/IMU equipment, namely Applanix of Toronto, Canada, using their system POS/AV 510 and IGI mbH, Germany, with the system Aerocontrol II. Both companies, further named company 1 and company 2 without indication of the real companies, have made calibration flights in the image scales of approximately 1 : 5000 and 1: 10 000 and a block flight for testing the results in the scale 1 : 5000. The targeted control points of the test field are available with an accuracy below +/-1cm for all coordinate components.

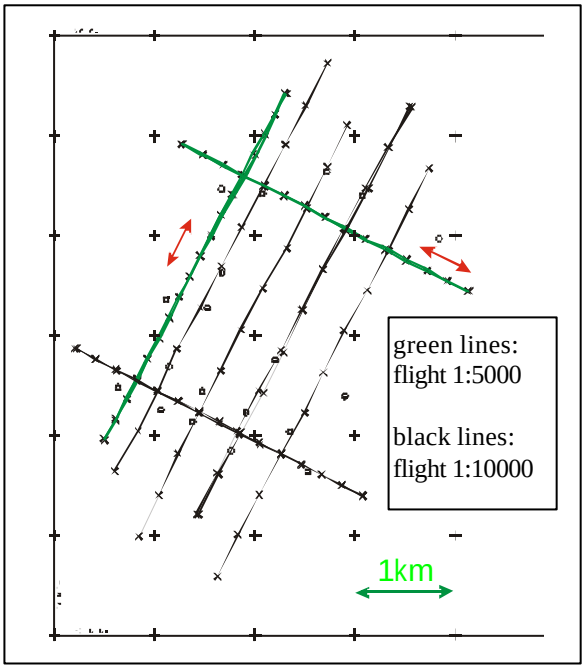

figure 3: calibration flight Friderikstad

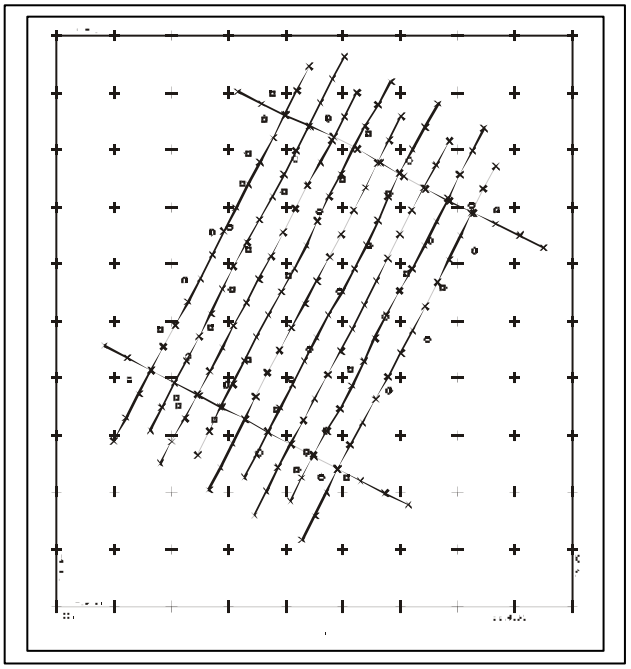

figure 4: test block

The image coordinates have been measured with an analytical plotter Planicomp P1.

4. BORESIGHT MISALIGNMENT

The relation between the IMU and the camera (3 rotations, 3 shifts) have been determined together with the inner orientation, based on a bundle block adjustment with all images of the calibration flights, separately for company 1 and

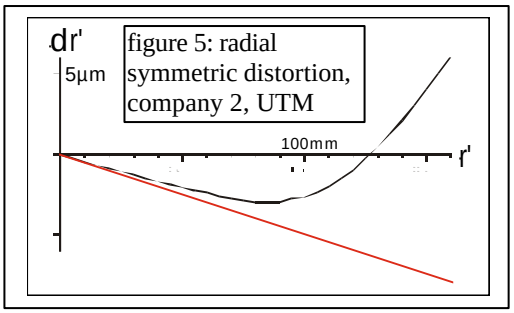

figure 5: radial symmetric distortion, company 2, UTM

company 2. It has been computed in the tangential plane and directly in the UTM coordinate system. In the UTM coordinate system the adjustment has been made with and without earth curvature and refraction correction. The influence of the earth curvature and refraction to the image coordinates can be compensated also by self calibration with additional parameters, but the used Hannover program system BLUH is using, like common, for the compensation of the radial symmetric effect a zero crossing like shown in figure 5. For a radial distance of 146mm and the image scale 1:5000, the refraction correction is –2µm, the earth curvature correction +7µm, so the resulting effect is Δf =+5µm. For the image scale 1 : 10 000 the corresponding figures are –4µm, +15µm, resulting in Δf =+11µm. With pre-correction by earth curvature and refraction correction for company 2, the radial symmetric distortion, determined by self calibration, has not exceeded 1µm, so the radial symmetric effect of the computation without pre-correction shows mainly the compensation of the Earth curvature. The influence to the focal length can be seen as vertical difference between the red line and the correction curve at a radial distance of 153mm. The difference of the focal length computed in the tangential and the UTM-system (see table 2) of 10µm and 7µm for company 2 and 15µm and 6µm for company 1 can be explained by this.

	company 1	company 2
	with self calibration by additional parameters	
tangential coordinate system	-41µm	+13µm
UTM without earth curvature and refraction correction	+20µm	+49µm
UTM with earth curvature and refraction correction	+ 5µm	+39µm
	without self calibration by additional parameters	
tangential coordinate system	+4µm	+1µm
UTM without earth curvature and refraction correction	+18µm	+43µm
UTM with earth curvature and refraction correction	+24µm	+50µm

table 2: correction of focal length computed by bundle adjustment

The tendency of the focal length correction between company 1 and company 2 is the same for the different types of reference block adjustments. The absolute values are of course different – this is dependent upon the changes of the focal length against the laboratory calibration.
The variation against the simplified theory, mentioned before, may be explained by the effect of systematic image errors. In general, table 2 shows also the dependency of the inner orientation to the self calibration. The additional parameters are correlated with the focal length if this is used as unknown in the adjustment. Especially the radial symmetric distortion is affecting the focal length like mentioned before. In general it is not possible to have only an isolated view to the focal length, it has to be seen together with the "systematic image errors" as a system calibration.

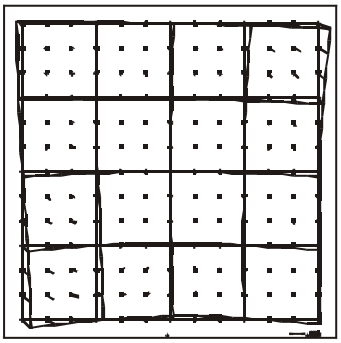
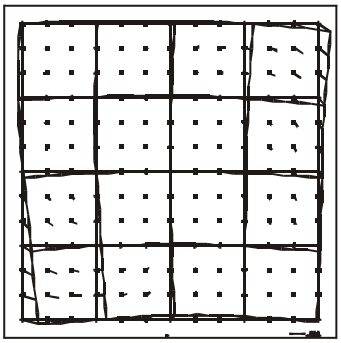
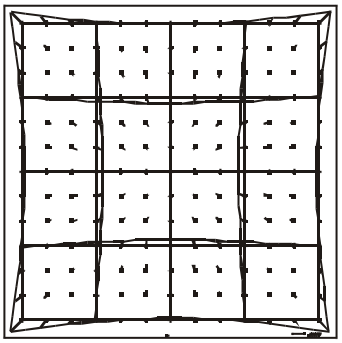

largest vector 25µm 21µm 7 µm

company 2

figure 6: "systematic image errors" figure 7: "systematic image errors" figure 8: "systematic image errors"
tangential coordinate system UTM, without earth curvature correction difference between fig. 6 and 7

The systematic image errors, computed in the different coordinate systems, are similar like shown as example for company 2 in figures 6 and 7. The main difference between both is a radial symmetric effect like shown with enlarged vectors in figure 8.
The differences between the computed focal length have to be seen also together with the shift for the Z-components in the misalignment, both are highly correlated. The location of the principal point is more or less independent from the different types of computation, it is varying only few microns.

The image orientations determined by the calibration flights with the improved focal length, but without influence of the direct sensor orientation information, are used as reference for the determination of the misalignment. The attitude misalignment has to be computed in the IMU-system pitch, roll and yaw with yaw as primary rotation. The difference between the transformed photogrammetric orientation and the IMU-data is the boresight misalignment. The individual discrepancies are indicating the quality of the IMU-data and the photogrammetric orientation. The photogrammetric orientation is also not free of error – the projection center coordinates X0 and Y0 are highly correlated to phi and omega or transformed to pitch and roll (Jacobsen 1999). In the case of narrow angle images, like taken by the digital camera Kodak DCS460, it is not possible to determine the attitude and the shift parameters for the misalignment, the shift values have to be set to 0.0 for a correct determination of the attitude data. This problem does not exist for standard aerial cameras, but the accuracy of the IMU attitude data is today on a level that it should not be neglected.

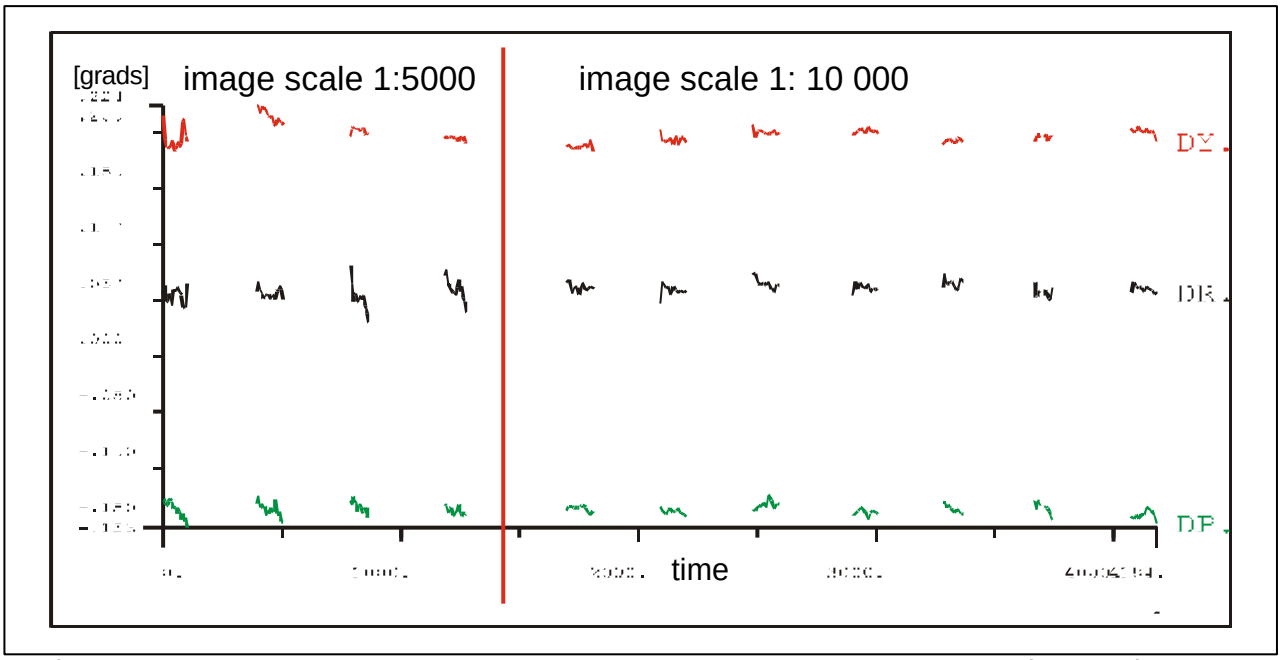

figure 9: attitude discrepancy photogrammetric orientation – IMU (company 2, UTM) as function of time

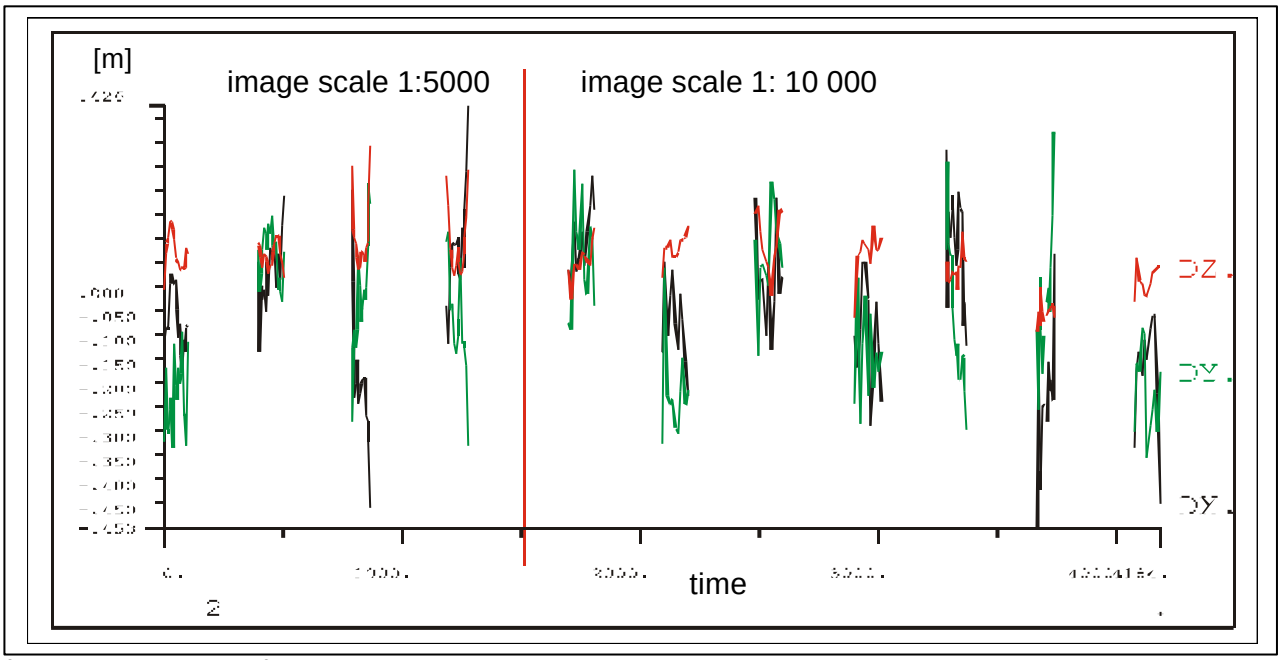

figure 10: discrepancy of projection center coordinates block adjustment – IMU (company 2, UTM)

In figure 9 and 10 the discrepancies of the image orientations determined by bundle block adjustment with program system BLUH against the IMU can be seen. These results are very similar for the data handling in the national coordinate system and the data handling in a tangential plane coordinate system - the values are only shifted. This is reflected also in table 3, showing the mean square discrepancies of the image orientations determined by bundle block

adjustment against the IMU+GPS after shift correction. The shifts are the boresight misalignment. No general discrepancies can be seen between the results in the UTM and the tangential coordinate system and also between both companies. The attitude data are very constant over the time and flight strips. The projection centers are still changing slightly from flight strip to flight strip, but in both cases the results are not improved by a linear function of the time.

	pitch	roll	yaw	X0	Y0	Z0
company 1 UTM	0.0038°	0.0035°	0.0102°	6.7cm	8.1cm	7.6cm
company 1 tangential	0.0029°	0.0039°	0.0106°	6.8cm	7.8cm	6.9cm
company 2 UTM	0.0067°	0.0046°	0.0077°	15.4cm	15.5cm	5.6cm
company 2 tangential	0.0055°	0.0059°	0.0078°	12.1cm	13.6cm	2.5cm

table 3: mean square discrepancies of orientation by BLUH against IMU after misalignment correction

The small differences of the results, based on the data of both companies, can be explained also by the used hardware components, for example in one case a not up to date dry tuned gyro has been used, which would not be done today again. The more complicate data acquisition in the tangential plane seems not be justified, but these figures are just the first indication for this.

5. COMBINED INTERSECTION

The next step of investigation can be made by a combined intersection based on the direct sensor orientation, that means, the IMU-data improved by the boresight misalignment and converted to the photogrammetric definition of the rotations, together with the actual inner orientation adjusted together with the misalignment. The ground coordinates, computed by combined intersection can be checked against the control points, used for the reference adjustment, but also the ground coordinates of all tie points determined by the reference block adjustment just based on control points.

	RMS at control points			RMS at ground points			σ_0
	RMS Xcp	RMS Ycp	RMS Zcp	RMS X	RMS Y	RMS Z	intersection
company 1, UTM	11.3cm	14.7cm	16.3cm	16.6cm	12.8cm	22.3cm	36.7µm
company 1, tangential	11.1cm	15.4cm	16.5cm	16.1cm	12.7cm	21.4cm	38.5µm
company 2, UTM	8.5cm	3.3cm	12.3cm	11.4cm	9.2cm	14.5cm	16.1µm
company 2, tangential	5.5cm	4.0cm	7.9cm	11.6cm	9.6cm	14.6cm	16.2µm

table 4: discrepancies at ground points determined by combined intersection based on direct sensor orientation

Also the results of the combined intersection (table 4) of the reference block do not indicate a major improvement of the more strict computation in the tangential coordinate system in relation to the direct handling in the national coordinate system – here the UTM-system. The discrepancies at the independent control points are smaller than at the not totally independent ground points of the reference adjustment – this can be explained with the number of images per point (figure 11) and the location. The ground points are located in the average in 6.8 photos, the control points in 13 photos. In addition some ground points are located outside the area of the control points, where also the reference adjustment is not so accurate. The accuracy reached with the data of both companies are not indicating mayor differences of the quality of direct sensor orientation – in the case of company 1 several points with poor photogrammetric accuracy, far out of the range of the control points, are included.

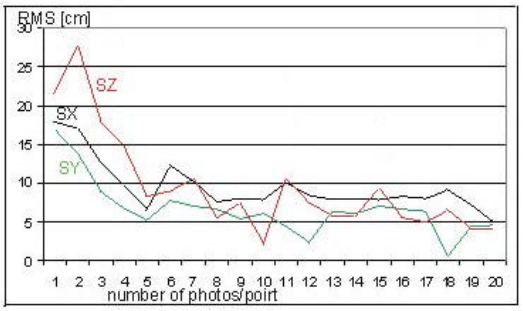

figure 11: accuracy of ground points determined by combined intersection based on direct sensor orientation as function of number of images per point (company 2)

black line: RMSX
green line: RMSY
red line: RMSZ

If the boresight misalignment determined in the wrong coordinate system will be used, the standard deviations are approximately 50% higher.
An independent check of the investigations of course requires an independent data set. This is not totally the case for the OEEPE-test, because the test block has the same location like the reference blocks and the time interval between both is limited, nevertheless, independent photos are available. The block has been handled in the similar way. The misalignment of the reference block has been used for the correction of the block area.

6. COMBINED ADJUSTMENT

As listed in table 4, the sigma0 of the combined intersection based on the direct sensor orientation is in the range of 16µm up to 38µm. This is still a good result, sufficient for several applications like the generation of orthophotos, but it may cause problems for the set-up of stereo models. As a rule of thumb, the y-parallax in a model should not exceed in maximum 30µm, the problems with the stereo view of the floating mark is starting at 20µm. Of course the sigma0 of the combined intersection is not identical to the root mean square y-parallax (Spy) of the model; the y-parallax is computed as difference of 2 coordinates. On the other hand, the orientation elements of neighboured images are correlated, so sigma0 only shows the tendency.

Another problem of the direct sensor orientation is the missing reliability, it can be checked only with the fitting of the final results like orthophotos and to some check points. Like the situation of the model set-up this can be improved by a combined adjustment based on the direct sensor orientation together with image coordinates of tie points, not using control points. In addition of course also the coordinates of the object points determined with image orientations from a combined adjustment will be more precise than just based on the direct sensor orientation.

		direct sensor orientation						combined adjustment		
		models	**Spy**	>10µm	>20µm	>30µm	Spy max	**Spy**	>10µm	Spy max
company 1	UTM	47	**46.6µm**	35	18	8	116.9µm	**9.0µm**	5	14.7µm
company 1	tangential	47	**46.3µm**	38	28	23	115.6µm	**8.7µm**	4	13.1µm
company 2	UTM	47	**21.6µm**	45	19	6	47.5µm	**9.8µm**	15	13.3µm
company 2	tangential	47	**21.7µm**	45	20	8	48.8µm	**9.4µm**	12	13.3µm

table 5: y-parallax of models and number of models exceeding specified limits

Table 5 shows the result of the root mean square y-parallax errors of the model set-up for the images included in the block for phase 2. Between Spy of the model set-up and sigma0 of the combined intersection based on the direct sensor orientation there is a relation between 1.2 and 1.3 (see also table 3). If the orientations are independent, there should be the relation of 1.4. As expected, no significant differences can be seen between handling in the UTM- and a tangential system. The main differences between both companies can be explained by the yaw, which is not so good for company 1 (see table 3). After combined adjustment, there is no more problem with the model set-up and for both companies the results can be accepted for all models, visible also by the maximal Spy for all models.

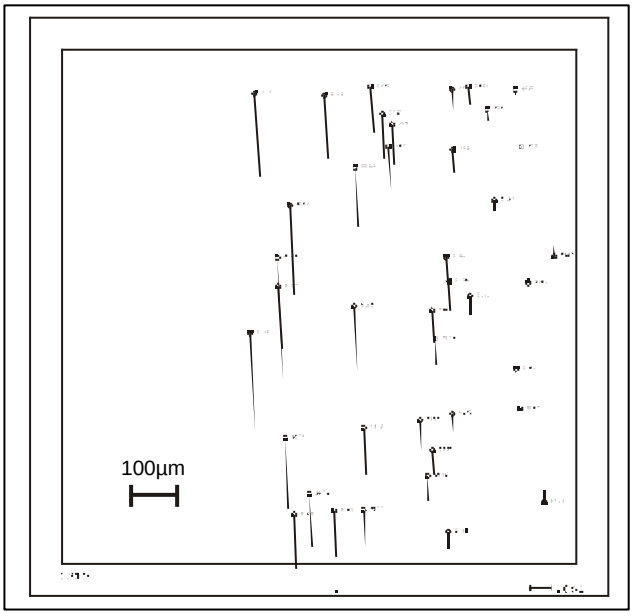

figure 12: y-parallaxes, model 1210/1211 company 1
for model orientation with direct sensor orientation

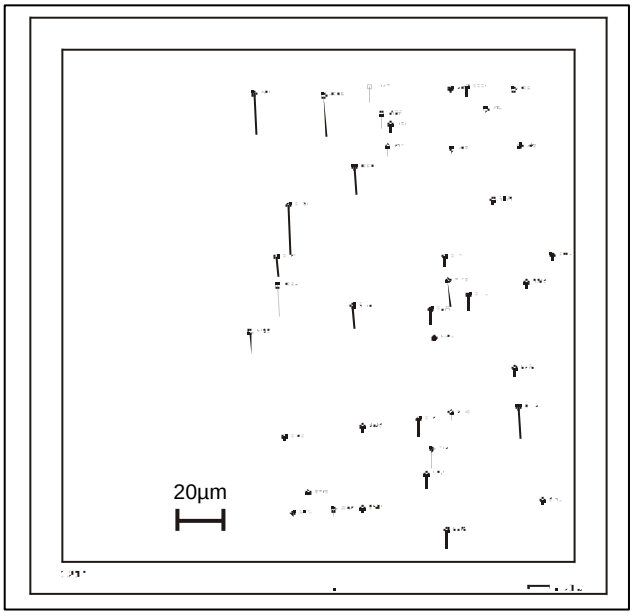

figure 13: y-parallaxes, model 1210/1211 company 1
for model orientation based on combined adjustment

Figure 12 and 13 are showing the y-parallaxes for the model 1210/1211 which has the largest values based on the direct sensor orientation for company 1. After improvement by the combined adjustment, in the whole model there are no

more problems for the stereoscopic handling. In this case, the dominating effect of the yaw is obvious. Of course it is possible to reach a further improvement of the model orientation based on the combined adjustment by a larger weight for the image coordinates, but this is not justified for the complete solution.

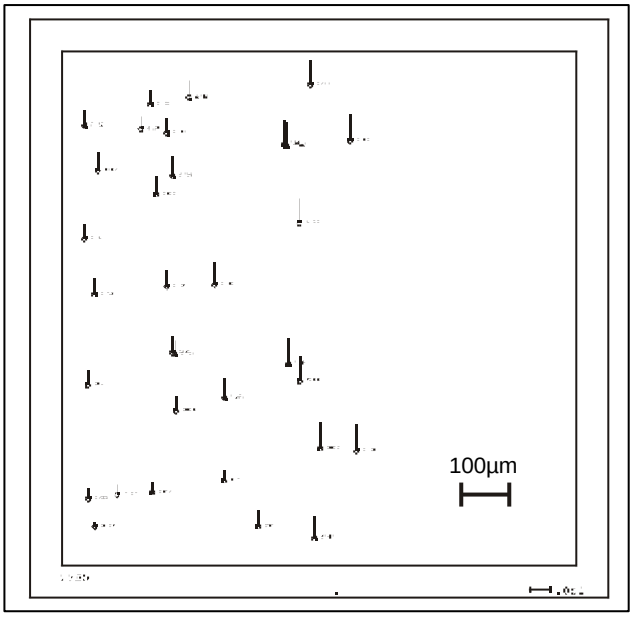

figure 14: y-parallaxes, model 2350/2351 company 2
for model orientation with direct sensor orientation

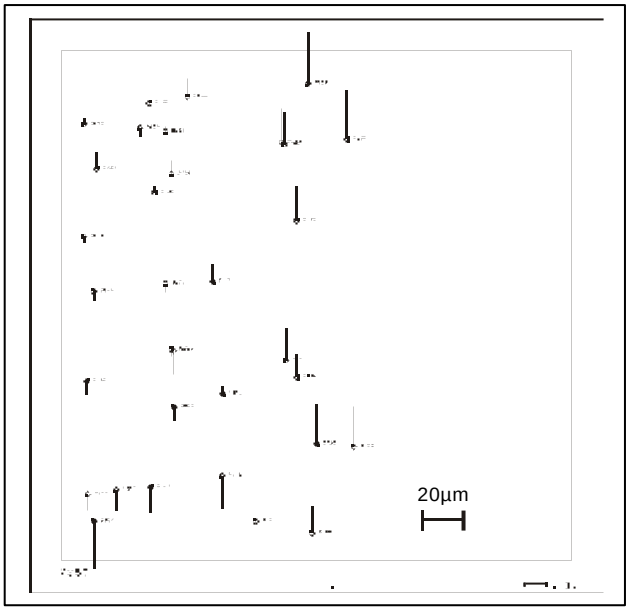

figure 15: y-parallaxes, model 2350/2351 company 2
for model orientation based on combined adjustment

The corresponding extreme case for company 2 is shown in figures 14 and 15. For company 2 the week point is more roll and pitch, visible also in the y-parallaxes based on the direct sensor orientation

		intersection with direct sensor orientation				intersection with combined adjustment		
		SX [cm]	SY [cm]	SZ [cm]		SX [cm]	SY [cm]	SZ [cm]
company 1	block, UTM	14.6	20.1	13.3		11.8	14.5	8.5
	strip, UTM	9.4	5.8	13.7		7.7	6.5	5.3
	block, tangential	13.6	20.0	15.9		11.4	15.5	8.3
	block, tangential	9.3	7.6	14.6		7.7	8.5	5.9
company 2	block, UTM	4.8	3.6	13.0		3.7	3.4	13.0
	strip, UTM	5.1	6.2	15.0		4.7	4.8	14.1
	block, tangential	8.1	3.7	13.8		3.2	1.1	9.5
	block, tangential	5.7	5.6	12.5		7.1	3.9	11.4

table 6: root mean square error at independent check points determined by combined intersection

Based on the combined adjustment of the direct sensor orientation together with image coordinates, but no control points, the random errors of the image orientations can be improved. Only the more local component of the systematic errors can also be improved, but not more. In table 6 on the left hand side the results of an intersection based on the direct sensor orientation determined in phase 1 are listed. These values are not the same like listed in table 3 because of a different selection of images for phase 2. By the comparison of the left hand part with the right hand part of table 6, the improvement of the ground coordinate accuracy by the combined adjustment can be seen. For company 2 there is only a small reduction of the root mean square differences for Z because of a dominating systematic influence.

The root mean square error at independent check points can be separated into the random and systematic component. As systematic component the mean value of the discrepancies has been used, the random component is the root mean square after shift by the systematic component. In general by the combined adjustment together with the image

coordinates, the random part can be improved; for the systematic component control points are required, but they have not been used in phase 2 of the OEEPE-test.

		intersection with direct sensor orientation **random part**			*intersection with direct sensor orientation systematic part*			intersection based on combined adjustment **random part**			*intersection based on combined adjustment systematic part*		
		SXr	**SYr**	**SZr**	*sysX*	*sysY*	*sysZ*	**SXr**	**SYr**	**SZr**	*sysX*	*sysY*	*sysZ*
company 1	block UTM	**10.1**	**11.6**	**13.0**	*10.6*	*-16.3*	*-2.8*	**5.8**	**5.3**	**8.1**	*10.3*	*-13.5*	*-2.6*
	strip UTM	**6.4**	**3.2**	**13.4**	*6.9*	*-4.9*	*2.8*	**4.6**	**3.0**	**5.3**	*6.2*	*-5.8*	*0.4*
	block tang.	**9.7**	**10.8**	**15.2**	*9.5*	*-16.8*	*4.5*	**5.8**	**5.1**	**8.3**	*9.8*	*-14.6*	*-1.2*
	strip tang.	**6.3**	**3.3**	**13.8**	*6.8*	*-6.8*	*5.0*	**4.5**	**3.3**	**5.3**	*6.2*	*-7.8*	*2.5*
company 2	block UTM	**4.6**	**1.1**	**5.8**	*-1.4*	*-3.4*	*11.6*	**2.4**	**1.0**	**5.8**	*-2.8*	*-3.2*	*11.6*
	strip UTM	**4.6**	**5.5**	**8.1**	*-2.4*	*-2.9*	*12.7*	**4.7**	**3.8**	**6.7**	*-0.3*	*-3.0*	*12.5*
	block tang.	**7.9**	**3.2**	**6.7**	*-1.5*	*-1.9*	*12.0*	**2.4**	**1.0**	**5.6**	*2.1*	*-0.5*	*7.6*
	strip tang.	**4.7**	**5.6**	**8.2**	*3.4*	*0.3*	*9.4*	**4.7**	**3.9**	**6.8**	*5.5*	*0.2*	*9.1*

table 7: discrepancies at independent check points determined by combined intersection, separated into random and systematic component

Table 7 shows the improvement of the random component by the combined adjustment and also the only slightly changed systematic part. For company 1 for Z the random part is dominating and for company 2 the systematic part, by this reason there is a more strong improvement of the height by the combined adjustment for company 1. For X and Y in the case of company 1 the systematic part is not negligible and cannot be reduced, only the also not so small random horizontal components are causing also an improvement.

7. CONCLUSION

The accuracy of the direct sensor orientation has been improved to a level where it can be used for several applications. The data acquisition is more simple directly in the national net coordinate system like in a tangential plane coordinate system which corresponds to the mathematical model. Investigations have demonstrated that in spite of the not strict solution, it is possible to handle the problem of the direct sensor orientation also directly in the national net coordinate system. But the handling has to be done consequently, including also the determination of the boresight misalignment. No loss of accuracy could be seen in the case of the investigated limited area with large image scales. The boresight misalignment should not be determined in the tangential plane coordinate system and used in the national net coordinate system or reverse, this is causing a loss of accuracy in any case.

The computation of the misalignment between the IMU and the photogrammetric camera has to include also the calibration of the inner orientation, which has a limited long term accuracy and is dependent upon the environmental conditions. The focal length and also the location of the principal point can only be determined if the calibration flight includes photos taken from different flying heights. If the focal length will not be adjusted, the use of the boresight misalignment is limited to the flying height of the calibration flight.

Only based on the direct sensor orientation, the y-parallaxes for stereo models are out of the tolerance level. A combined adjustment using the direct sensor orientation together with image coordinates of tie points is required for the computation of the settings for stereo models. In addition the random part of the direct sensor orientation will be reduced, leading to a further improvement of the ground coordinates determined by combined intersection.

REFERENCES

Heipke, C., Jacobsen, K.., Wegmann, H., Andersen, O., Nilsen, B. (2000): Integrated Sensor Orientation – an OEEPE-Test, IAPRS, Vol. XXXIII, Amsterdam, 2000

Jacobsen, K. (1997): Operational Block Adjustment without Control Points, ASPRS Annual Convention 1997, Seattle, Volume 2, pp 238 - 244

Jacobsen, K. (1999): Combined Bundle Block Adjustment with Attitude Data, ASPRS Annual Convention 1999, Portland

Jacobsen, K. (2000): Combined Bundle Block Adjustment Versus Direct Sensor Orientation, ASPRS Annual Convention 2000, Washington

Kohlstock, M. (2000): Untersuchung der direkten Sensororientierung, diploma thesis, University of Hannover, 2000

Meier, H.-K. (1978): The effect of Environmental Conditions on Distortion, Calibrated Focal Length and Focus of Aerial Survey Cameras, ISP Symposium, Tokyo, May 1978

GIP Ges. f. Industriephotogrammetrie mbH

Combined IMU Sensor Calibration and Bundle Adjustment with BINGO-F

Erwin Kruck

GIP Gesellschaft für Industriephotogrammetrie mbH
Tännichweg 3 • D-73430 Aalen • Germany

Fon: +49-(0)7361-931434 www.gip-aalen.de
Fax: +49-(0)7361-931435 info@gip-aalen.de

Introduction

Since aerial photos are used for map production – ever since photogrammetry has been a known technique – the estimation of the photo orientation has been a topic of research and development for mechanical engineers, photogrammetrists, mathematicians and software developers. New procedures and formulas have been invented and published all the time to facilitate this work. The wishful thinking to be able to do photogrammetry without this time consuming orientation work is slowly arriving – at least for selected applications – in a step by step fashion.

Actually, methods for direct measuring of orientation angles using inertial measuring units (IMU) of the two companies IGI (company 1 or C1) and Applanix (company 2 or C2) have been investigated in an OEEPE project. From both systems we can expect, that the orientation parameters can be estimated good enough for direct usage without bundle triangulation for the whole block, at least for applications with reduced precision requirements, e.g. for orthophoto production.

All participants of the project received the same data: Photo measurements of a calibration strip with C1= 62 and C2= 66 photos scale 1: 5 000, and a calibration block with C1= 86 and C2= 85 photos scale 1: 10 000. Furthermore the direct estimated projection center coordinates and orientation angles from the GPS/IMU systems for all photos of the block, C1= 284 and C2= 452 photos. From the calibration strips or blocks corrected orientation data have been predicted for all given photos.

The IMU misalignment angles are estimated in a combined adjustment. For the kinematic GPS observations shift and drift parameters have been applied. The mathematical model used will be described. All processing steps will be explained, documented and commented. Recognised problems will be discussed and recommendations for enhancements will be given. It will be summarised, that GPS/IMU application can help to avoid the time consuming bundle triangulation process for applications with lower precision requirements, e.g. for orthophoto production.

Used mathematical model

Because of physical reasons the IMU can never be mounted strictly parallel to the camera system. Therefore an equation system is required to describe the stabile relationship between the IMU and the camera to enable

a simultaneous calibration in the bundle adjustment process. A mathematical rigorous approach has been developed. It has been applied for the OEEPE test fight in Norway.

The best results can always be achieved, if all available data are processed in a single computation step. This is the only way to take correlations as good as possible into account. As well the reliability will be increased and observations and results are better under control. Therefore the three rotation parameters of misalignment between the IMU and the camera have been introduced as additional unknowns in the bundle triangulation software BINGO-F. For this application a global shift has been estimated for all kinematic GPS data.

The following indices are introduced:

G	Superior or ground coordinate system
I	Instrument (i.e. IMU)
P	Photo or photo coordinate system

The instrument **I** measures and records the orientation angles for all photos. The relation between measured rotational angles and the real photo orientations is given in equation (1):

$$\mathbf{R}_G^I = \mathbf{R}_G^P \cdot \mathbf{R}_P^I \qquad (1)$$

where

$\mathbf{R}_G^I$	Rotation from ground to instrument (observables of the IMU Φ, Ω, K).
$\mathbf{R}_G^P$	Rotation from ground to photo (orientation angles φ, ω κ)
$\mathbf{R}_P^I$	Rotation from photo to instrument . (constant) (Misalignment calibration angles dφ, dω dκ or α, β, γ)

Rotational angles cannot be simply added together, if the basic (photo) system is already rotated. In case of terrestrial applications of photogrammetry there is another situation, if a camera is mounted on top of a theodolite and the orientation angles are estimated with the theodolite with vertical standing axes. There we have simply to add the differences between the theodolite and the camera. Those corrections can be understood as small corrections of the measuring pointer of the glass circle of the theodolite. But here in case of the IMU we have to multiply the rotational matrices.

Equation (1) describes the relation between the angles measured from the IMU and the photo orientation. For all three matrices the rotational sequence φ, ω κ is used. From this equation the observation equations (2) for Φ, Ω, K and their partial differential quotients have been established for iterative adjustment with BINGO-F.

$$\begin{aligned} \Phi + v\Phi &= f(\varphi, \omega, \kappa, d\varphi, d\omega, d\kappa) \\ \Omega + v\Omega &= f(\varphi, \omega, \kappa, d\varphi, d\omega, d\kappa) \\ K + vK &= f(\varphi, \omega, \kappa, d\varphi, d\omega, d\kappa) \end{aligned} \qquad (2)$$

The BINGO-F software includes of course all possibilities of full camera calibration, additional parameters, simultaneous estimation of a vector from the projection center to the antenna, corrections for gyro-mount readings, and much more. A complete description is found in the manual and partly as well in the literature [2].

Processing and results

In a first step all provided orientation angles have been converted from roll, pitch and yaw to φ, ω, κ for BINGO-F. The new angles have been corrected for meridian convergence. Therefore all further processing steps can be performed rigorous (with respect to the orientation angles) directly in the UTM coordinate system.

After the first adjustments systematic start-up or warm-up errors have been detected in the residuals of the first strips for both companies. For C1 in the calibration flight 1:5000 and for C2 in the calibration flight 1:10000. C1 provided later an enhanced data set with enhanced filtering with much better results.

The four adjustment processes are showing generally very good results, however, there are some differences. The results of C1 are looking generally slightly better that the results of C2 regarding homogeneity, maximum and RMS residuals of the IMU data and GPS data. An exception are the angle values of calibration flight 1:5000, here C2 has the smaller RMS values than C1.

Regarding the GPS data, we consider that for parts of the block the number of GPS satellites have been smaller for C1 than for C2. Especially for the calibration flight 1:10.000 for C2 with a very good satellite configuration, there are the highest discrepancies. However, we point out: All results are very good, because we are talking about a few decimeters only, as shown in Tab. 1.

	Company 1			**Company 2**		
1:5000	**Line_No.**	**Shifts [mm]**		**Line_No.**	**Shifts [mm]**	
		x	**y**	**z**	**x**	**y**	**z**
Shifts	1087	-44	94	120	2004	-14	-68	353
	1104	-142	79	94	2022	27	47	340
	1121	-45	-2	59	2040	-79	12	331
	1135	-109	117	47	2055	24	10	329
RMS GPS resid.:		23	19	17		15	14	11
Max GPS resid.:		71	45	45		45	42	30
1:10000	**Line_No.**	**Shifts [mm]**			**Line_No.**	**Shifts [mm]**		
		x	**y**	**z**		**x**	**y**	**z**
Shifts	1001	-121	19	31	2076	-68	124	490
	1012	-15	197	30	2087	112	-4	521
	1024	-160	-26	51	2098	-139	74	546
	1035	39	169	94	2109	85	-44	517
	1046	-183	140	162	2120	67	181	488
	1061	70	16	149	2135	-128	-154	396
	1076	-4	141	166	2150	73	-62	462
RMS GPS resid.:		15	17	16		99	75	44
Max GPS resid.:		45	45	51		331	177	133

Tab. 1 GPS shift and drift parameters and GPS residuals

The GPS shift and drift parameters are varying from strip to strip. This is an indication for incorrect fixing of phase ambiguity parameters. A new processing of the originally recorded GPS data should really be able to enhance the results, especially, if this would be done in a processing with GEONAP-K and BINGO-F, where GPS phase ambiguity estimation is integrated in a combined bundle adjustment and therefore much more reliable [2].

A surprise has been the differences in photo measurement precision: 4.0 µm for C1 and 5.8 µm for C2. These differences are related to the aircraft, the camera, the film development, the photo measurement device or the operator, but on no account to the GPS/IMU system. To avoid influences from these differences to the results of this test, the observation weights for each block have been individually adapted and optimised to the real measurement precision. Theoretically this will give the best accuracy. Empirical tests have confirmed this assumption.

These optimised weights have been used to estimate the adjusted misalignment angles of the IM. The measured IMU angles have been introduced with a high standard deviation (and a low weight) of 0.05 grads. The total redundancy in the variance component estimation confirms, that there is nearly no influence of these measurements to the adjustment results.

Tab. 2 gives an overview about all misalignment calibration results. For all four adjustments the RMS residuals (**RMS residuals**), and the maximum residuals (**Max residuals**) of the measured IMU angles as well

as the calibration angles (**rotat. angles**) and their standard deviations (**precision**) are presented. The misalignment angles have to be identical from both photo blocks. This fits in all cases very well within the given standard deviation.

	[mgon]	phi	omega	kappa
Comp.2 / Cal. 1:10000	RMS residuals:	5.0	3.5	5.9
	Max residuals:	11.2	9.4	17.9
	rotat. angles:	-60.6	126.6	-197.1
	precision:	5.3	5.0	5.4
Comp.2 / Cal. 1:5000	RMS residuals:	14.6	11.1	11.2
	Max residuals:	40.4	27.0	20.5
	rotat. angles:	-59.1	130.6	-199.6
	precision:	5.6	5.2	5.7
Comp.1 / Cal. 1:10000	RMS residuals:	3.4	2.8	10.0
	Max residuals:	8.5	9.1	22.2
	rotat. angles:	-10.3	-99.6	66.6
	Precision:	5.1	4.8	5.1
Comp.1 / Cal. 1:5000	RMS residuals:	4.4	3.2	6.7
	Max residuals:	11.7	12.2	15.6
	rotat. angles:	-9.1	-104.0	66.9
	precision:	6.3	5.8	6.3

Tab.2 Results of IMU misalignment calibration using ground control points

In a further trial a processing without ground control points have been done. The results of the IMU misalignment calibration are identical (Tab.3). As well different trials with changes of some parameters resulted in the same angles.

	[mgon]	phi	omega	kappa
Comp.1 / Cal. 1:10000	RMS residuals:	3.4	2.8	10.1
	Max residuals:	12.5	9.5	21.8
	rot angles:	-10.4	-99.6	69.1
	precision:	5.1	4.8	5.1
Comp.1 / Cal. 1:5000	RMS residuals:	5.2	3.6	7.0
	Max residuals:	12.8	14.2	16.0
	rotat. angles:	-9.2	-104.1	67.8
	precision:	6.3	5.9	6.4

Tab.3 Results of IMU misalignment calibration without ground control points

The residuals of all IMU angles are presented in Appendix A. Appendix B is an extract of the BINGO-F processing list file for all four adjustment processes.

The results of further considerations and processings are presented in [3]

Prediction of further orientation data

The results of the bundle triangulations from the calibration Blocks 1:5000 have been used to predict the orientation data of all remaining photos. For this purpose only a global shift was available for the whole block for the position, because there is no information about individual shifts of strips, which did not participate in the calibration process. For the orientation angles, all photo orientations have been multiplied with the calibration matrix.

I.e.: the results sent to the pilot center consists of :

- the original projection centers shifted by three global shift values for X, Y, Z,
- the given orientation angles corrected by a global rotation,
- the new values for the camera constant and principal point as well as some additional parameters.

The adjusted orientation parameters from the calibration block adjustments have not been used here.

Comparison with independent check points

IPI Hannover, the pilot center of this test, estimated the coordinates of independent check points from some photo measurements and the predicted orientation parameters. The results from all test participants are very good and better than RMS ~15 cm in planimetry and ~20 cm in height.

However, before we can conclude, that ALL estimated orientation data is good enough for ortho photo production or other purposes, the distribution and the maximum errors of all single rays compared to the independent check points should be known.

In [1] the pilot center concluded, that the Applanix (C2) results are better than the IGI (C1) results and in the range of some cm. There are several good reasons to plug a very big question mark upon this statement:

- The RMS precision values of adjusted point coordinates from bundle triangulations in photo scale 1:5000 are only about 3 cm in planimetry and 5 cm in height. For scale 1:10000 we have 5 and 10 cm.
- Looking to the variation of shift parameters in Tab. 1, precision values in the range of a few cm cannot be expected and are probably random numbers.
- We detected variations of the principal point position which will effect the ground coordinates probably more than 10 cm. Compare [2].
- The situation of the GPS satellites has been better during the C2 flight time than during the C1 flight time.

It cannot be said, that the computations of the pilot center have not been correct, however, it might be, that not all circumstances of the test have been acknowledged.

Conclusion

Both companies presented very good results. The differences in the results may be more influenced by the GPS coordinates than by the inertial measurement units (IMU). Therefore it is recommended to concentrate on the enhancement of GPS processing. The author presented in [1,2] better processing possibilities. These techniques are highly recommended for further investigations.

References

Heipke, C., Jacobsen, K., Wegmann, H.: The OEEPE Test on Integrated Sensor Orientation – Results of Phase 1. Invited Paper, Photogrammetric Week, Stuttgart, Sept. 2001.

Kruck, E., Wübbena, G. und Bagge, A.: Advanced Combined Bundle Block Adjustment with Kinematic GPS Data. Presented Paper, ISPRS Comm. III/1, Vienna 1996.

Schmitz, M., Wübbena, G., Bagge, A. and Kruck, E.: Benefit of Rigorous Modelling of GPS in Combined AT/GPS/IMU-Bundle Block Adjustment. Presented Paper, OEEPE Workshop, Hannover, Oct. 2001.

Anhang A Residuals of for all IMU angle measurements

Company 1 / Calibration 1:10000

photo	residuals [mgon] phi	omega	kappa	photo	residuals [mgon] phi	omega	kappa
1001	6.4	6.9	7.8	1046	-5.5	0.1	-3.6
1002	4.3	3.3	6.0	1047	0.9	3.0	-3.2
1003	8.5	4.9	4.4	1048	-0.8	2.6	-1.4
1004	0.4	4.6	8.8	1049	2.8	-6.1	-4.0
1005	1.6	1.0	7.5	1050	-0.3	-5.9	-1.1
1006	6.7	-1.1	9.5	1051	0.5	-1.0	-0.9
1007	6.3	0.4	9.0	1052	-1.8	-1.3	-2.2
1008	5.9	2.7	10.1	1053	-0.9	-4.1	0.6
1009	4.5	1.5	12.2	1054	-1.8	-1.1	-0.8
1010	7.9	-2.3	13.1	1055	-0.8	-0.1	-0.5
1011	5.8	0.5	9.6	1056	-0.8	-5.8	1.7
				1057	2.2	-0.1	0.0
1012	-3.2	3.1	14.2	1058	-0.6	0.6	5.4
1013	-0.1	-0.1	12.1	1059	-2.1	2.5	3.1
1014	0.9	1.7	15.6	1060	-0.2	-0.8	3.7
1015	2.2	-1.7	16.6				
1016	6.9	3.0	17.7	1061	-4.8	1.1	-4.5
1017	1.3	-0.7	20.8	1062	0.3	-9.1	-5.4
1018	-0.1	0.6	18.4	1063	-0.5	-3.1	-5.9
1019	0.2	2.6	18.2	1064	-0.8	0.0	-4.9
1020	-2.9	0.3	17.0	1065	0.6	0.2	-5.0
1021	-4.6	1.8	18.6	1066	1.0	-4.1	-4.2
1022	-1.9	0.7	17.4	1067	0.6	-0.5	-3.2
1023	0.7	0.0	17.9	1068	3.2	-1.4	-3.9
				1069	0.6	-0.5	-5.8
1024	-0.1	0.8	0.3	1070	-1.7	1.7	-4.9
1025	1.7	-3.3	-4.2	1071	2.1	0.4	-3.9
1026	0.5	-3.3	-5.0	1072	0.1	-3.5	-5.9
1027	-1.4	-3.8	-8.8	1073	2.3	3.4	-4.0
1028	4.0	-4.4	-7.2	1074	-2.9	1.3	-5.5
1029	5.4	2.5	-7.1	1075	-0.7	0.0	-7.2
1030	3.7	-1.7	-9.3				
1031	4.7	-1.1	-11.3	1076	1.5	-5.4	-22.2
1032	0.1	-0.9	-8.8	1077	-0.4	-2.0	-20.6
1033	0.1	3.5	-6.9	1078	1.1	-0.8	-19.3
1034	2.6	1.9	-6.1	1079	2.0	-1.8	-15.3
				1080	4.7	-0.9	-16.5
1035	-7.9	1.3	-5.8	1081	3.0	-4.2	-15.6
1036	-4.6	0.3	-0.3	1082	4.0	-3.5	-15.4
1037	-2.8	-1.5	1.1	1083	-1.9	-4.2	-13.8
1038	-4.7	0.8	-0.5	1084	6.0	-0.7	-11.8
1039	5.4	0.0	-1.2	1085	1.3	-1.7	-12.3
1040	0.3	0.9	3.2	1086	0.5	1.3	-6.7
1041	4.5	2.8	0.4				
1042	6.0	3.0	1.0				
1043	-0.2	-2.8	7.1				
1044	1.4	-2.1	5.6				
1045	2.9	-4.4	8.3				

RMS resid.:	3.3	2.8	10.0
Max resid.:	8.5	9.1	22.2
rot angles:	-10.3	-99.6	66.6
precision:	5.1	4.8	5.1

Company 1 / Calibration 1:5000

photo	residuals [mgon] phi	omega	kappa
1087	-2.2	0.6	0.3
1088	1.7	1.6	2.1
1089	1.8	0.0	2.6
1090	3.4	0.0	3.8
1091	4.3	-1.4	4.6
1092	8.8	-0.7	4.7
1093	4.0	-3.8	4.1
1094	1.7	-2.9	3.6
1095	0.5	-2.4	2.1
1096	-5.7	-0.6	4.3
1097	-0.2	0.7	7.0
1098	-1.5	1.3	4.7
1099	3.4	0.4	5.2
1100	-1.3	-1.4	4.7
1101	-1.6	-2.1	7.1
1102	-4.7	-2.6	5.1
1103	-6.8	-1.3	6.2
1104	2.4	-1.7	0.4
1105	5.4	-1.5	-1.2
1106	3.9	-0.4	4.8
1107	3.9	0.0	1.2
1108	1.7	-0.6	1.8
1109	-3.4	2.6	0.9
1110	0.5	1.8	4.7
1111	7.2	1.9	-1.1
1112	2.5	3.7	3.4
1113	4.9	2.5	2.1
1114	4.3	1.3	2.5
1115	4.4	-0.9	2.9
1116	5.6	4.4	3.4
1117	4.4	1.5	4.5
1118	3.4	1.3	5.1
1119	2.6	3.6	2.1
1120	-1.1	6.0	3.5

photo	residuals [mgon] phi	omega	kappa
1121	2.7	1.3	-14.7
1122	0.1	-0.3	-9.0
1123	2.1	-6.0	-10.9
1124	5.0	1.0	-11.3
1125	1.7	-2.6	-10.3
1126	4.5	-4.6	-12.2
1127	5.0	-3.4	-10.2
1128	1.4	-0.1	-10.4
1129	2.6	-1.1	-10.6
1130	5.3	-3.4	-10.5
1131	8.9	-0.9	-14.4
1132	3.5	1.0	-10.3
1133	4.5	-9.1	-14.4
1134	9.0	-12.2	-15.6
1135	6.2	-5.2	0.5
1136	7.2	-4.3	2.5
1137	8.3	-4.1	1.1
1138	11.7	1.2	0.1
1139	1.4	1.4	3.3
1140	4.1	1.6	3.4
1141	2.2	-1.4	2.8
1142	5.8	3.7	2.8
1143	1.1	5.6	6.5
1144	2.5	-0.2	3.4
1145	0.1	1.0	9.2
1146	1.1	-3.4	6.7
1147	-0.6	-4.7	5.7
1148	-1.6	-0.1	3.7

RMS resid.:	4.4	3.2	6.7
Max resid.:	11.7	12.2	15.6
rot angles:	-9.1	-104.0	66.9
precision:	6.3	5.8	6.3

Company 2 / Calibration 1:10000

photo	residuals [mgon] phi	omega	kappa	photo	residuals [mgon] phi	omega	kappa
2076	3.6	5.5	-3.2	2120	1.8	7.9	-1.2
2077	4.2	0.8	-5.3	2121	5.3	8.3	-2.9
2078	2.7	4.8	-10.2	2122	4.3	4.5	0.5
2079	2.9	0.1	-9.8	2123	4.6	4.6	-0.3
2080	3.1	2.0	-12.6	2124	4.8	2.7	-1.3
2081	0.7	4.3	-11.1	2125	5.8	3.9	-1.1
2082	6.0	1.4	-9.2	2126	6.3	4.3	-3.1
2083	3.6	3.1	-8.3	2127	6.1	1.4	-6.1
2084	0.2	-2.8	-7.6	2128	6.1	-0.1	-4.8
2085	-2.1	1.9	-10.6	2129	3.4	-0.2	-5.0
2086	-1.0	6.0	-17.9	2130	2.8	-0.9	-2.2
				2131	2.9	-1.3	1.0
2087	-8.4	-8.6	4.4	2132	7.6	-3.5	0.6
2088	-5.7	-0.1	-3.9	2133	4.0	-4.2	-2.1
2089	-2.3	1.0	-4.7	2134	3.5	-6.5	-2.8
2090	-4.1	0.7	-3.5				
2091	1.6	-3.9	-2.5	2135	7.2	-4.8	2.1
2092	2.8	1.7	-5.1	2136	5.2	-8.1	-1.9
2093	5.6	1.6	-2.6	2137	5.3	-3.4	1.8
2094	4.8	0.8	-1.8	2138	7.0	-3.7	-0.4
2095	5.9	1.0	-3.1	2139	6.3	-1.8	3.9
2096	9.7	1.6	-7.7	2140	5.9	1.7	-0.2
2097	11.2	2.4	-10.2	2141	6.6	-0.6	0.5
				2142	1.4	1.9	-0.2
2098	4.5	-0.1	-1.4	2143	5.9	-0.6	1.5
2099	5.7	-4.9	4.1	2144	2.8	-1.6	-1.3
2100	7.2	-2.0	4.0	2145	5.2	0.7	1.6
2101	4.7	-1.9	4.6	2146	3.1	1.5	0.7
2102	5.2	-0.9	2.5	2147	3.7	6.7	3.1
2103	2.8	-2.1	3.5	2148	2.3	7.9	5.9
2104	6.8	-3.2	3.8	2149	-0.1	9.4	1.9
2105	2.9	-3.1	3.7				
2106	0.7	-1.8	5.2	2150	-4.0	-2.5	12.1
2107	-0.8	-3.6	3.3	2151	-2.2	3.2	7.0
2108	-2.7	-3.2	2.9	2152	0.4	-1.8	6.9
				2153	2.3	0.0	6.2
2109	-6.2	-3.3	15.2	2154	2.7	-0.5	6.4
2110	-5.7	-0.8	9.1	2155	5.8	0.2	4.8
2111	-0.3	-2.3	4.9	2156	1.1	-1.4	4.4
2112	-1.4	-0.5	7.6	2157	3.9	0.2	3.1
2113	1.8	-2.7	8.5	2158	4.8	1.2	-0.7
2114	4.7	1.1	4.3	2159	7.5	1.4	-1.2
2115	5.0	0.1	5.7	2160	8.5	0.6	-7.1
2116	5.7	-2.0	9.3				
2117	5.3	2.5	7.8				
2118	7.6	-0.9	7.3				
2119	10.7	-4.8	0.6				

RMS resid.:	5.0	3.5	5.9
Max resid.:	11.2	9.4	17.9
rot angles:	-60.6	126.6	-197.1
precision:	5.3	5.0	5.4

Company 2 / Calibration 1:5000

photo	residuals [mgon] phi	omega	kappa
2004	-7.8	-5.6	-20.5
2005	-9.7	2.6	-17.5
2006	-0.3	-5.8	-14.9
2007	-0.6	-6.4	-15.3
2008	-5.8	1.5	-14.0
2009	-2.0	0.0	-16.4
2010	4.0	-5.3	-16.0
2011	9.1	3.1	-14.0
2012	10.3	4.2	-15.7
2013	15.0	5.2	-15.6
2014	16.8	6.9	-14.5
2015	16.1	7.0	-12.5
2016	21.0	9.5	-11.6
2017	26.7	12.8	-9.6
2018	28.3	9.3	-10.6
2019	35.4	11.8	-11.1
2020	34.9	10.4	-11.0
2021	40.4	21.6	-10.9
2022	33.1	16.5	18.6
2023	36.9	14.8	19.8
2024	29.9	10.7	15.7
2025	28.9	12.5	20.5
2026	22.9	11.9	17.8
2027	21.1	8.6	16.9
2028	14.8	5.9	16.9
2029	13.7	2.8	17.3
2030	10.6	3.1	14.6
2031	10.8	5.5	14.8
2032	6.5	-0.8	16.2
2033	5.3	0.8	11.7
2034	7.2	6.7	10.5
2035	-4.0	-0.4	12.2
2036	-2.6	-1.5	11.1
2037	-0.9	-2.2	9.5
2038	-7.1	-3.3	7.3
2039	-10.6	-2.2	4.4
2040	6.8	-8.1	0.3

photo	residuals [mgon] phi	omega	kappa
2041	3.8	-2.5	1.3
2042	11.6	-4.0	6.6
2043	1.6	-3.7	5.2
2044	2.2	-0.9	4.1
2045	3.4	5.6	3.0
2046	2.8	6.3	5.3
2047	0.6	6.2	3.6
2048	-0.6	11.3	3.6
2049	-6.0	14.1	5.5
2050	-7.0	17.1	6.3
2051	1.0	19.7	3.1
2052	-3.8	23.7	2.6
2053	-6.5	27.0	3.5
2054	-0.4	26.8	1.2
2055	-8.0	25.2	0.5
2056	-2.4	25.6	0.6
2057	-5.5	15.8	-2.2
2058	-2.9	17.6	-2.1
2059	-4.3	14.1	-1.3
2060	-4.5	8.3	-0.7
2061	-2.1	6.4	-3.6
2062	-2.2	8.1	-1.9
2063	1.6	4.8	-5.3
2064	3.1	6.2	-4.3
2065	3.6	-1.8	-5.8
2066	7.2	-0.9	-6.9
2067	2.9	-2.7	-6.0
2068	5.4	-5.5	-11.0
2069	7.8	-6.7	-8.9

RMS resid.:	14.6	11.1	11.2
Max resid.:	40.4	27.0	20.5
rot angles:	-59.1	130.6	-199.6
precision:	5.6	5.2	5.7

Anhang B Extract from the BINGO List Files

```
                        BINGO-F  -  VERS. 4.0 / 10.00d
================================================================================

                              Company 1 / Cali 10
--------------------------------------------------------------------------------
                                        :
                                        :
                                        :
  Summary of image data:
  ----------------------
  No. of points                  :     319
  No. of photos                  :      86
  No. of cameras                 :       1
  Max. measurements per point    :      22
  Max. photo index difference    :      63

                                        :
                                        :
                                        :
          RESULTS OF ADJUSTMENT           SIGMA 0 =        3.79 (1/1000)
================================================================================

          Camera data
--------------------------------------------------------------------------------

 Camera no. 1

     Diff. angle of rotation delta :   -0.0103   -0.0996    0.0666
     +-S                  (1/1000) :       5.1       4.8       5.1

     Additional parameters         :   Format factor =      1.000000

             7         8        17

        0.0165   -0.0055    0.0035


     Mean radial symmetric lens distortion from additional parameters  (1/1000)

     Distortion values; First value for R =  10.0  (= Step width)

         1.8    3.4    4.6    5.5    6.1    6.5    6.4    6.1    5.3    4.3
         2.8    1.0   -1.1   -3.7   -6.7  -10.1


 Correlation between add. parameters in %

   7   100

   8   -63 100

  17    -6   0 100

         7   8  17


 Sigma 0 used for estimation of standard deviations:        3.79 (1/1000)

 Par.no  Parameter value   Standard dev.   Value/Stand.dev   Total correlation
               (1/1000)        (1/1000)

      7           16.5             0.6             29.4            0.41
      8           -5.5             1.0             -5.6            0.41
     17            3.5             0.2             14.8            0.01
```

GPS shift and drift parameters

File	Line_No.	Para.Name	Shift	Drift	+-S	Photos
1	1001	s_X	-0.196		0.030	11
1	1001	s_Y	0.114		0.022	11
1	1001	s_Z	-0.029		0.017	11
1	1001	d_X		-0.029	0.064	11
1	1001	d_Y		-0.015	0.044	11
1	1001	d_Z		-0.048	0.038	11
1	1012	s_X	0.079		0.024	12
1	1012	s_Y	0.100		0.019	12
1	1012	s_Z	-0.034		0.014	12
1	1012	d_X		0.051	0.052	12
1	1012	d_Y		-0.043	0.041	12
1	1012	d_Z		0.037	0.035	12
1	1024	s_X	-0.234		0.024	11
1	1024	s_Y	0.096		0.019	11
1	1024	s_Z	-0.013		0.015	11
1	1024	d_X		-0.111	0.048	11
1	1024	d_Y		0.066	0.040	11
1	1024	d_Z		0.045	0.033	11
1	1035	s_X	0.156		0.031	11
1	1035	s_Y	0.054		0.024	11
1	1035	s_Z	0.030		0.019	11
1	1035	d_X		-0.025	0.063	11
1	1035	d_Y		0.053	0.051	11
1	1035	d_Z		-0.032	0.041	11
1	1046	s_X	-0.061		0.021	15
1	1046	s_Y	0.230		0.020	15
1	1046	s_Z	0.099		0.014	15
1	1046	d_X		-0.075	0.055	15
1	1046	d_Y		0.037	0.061	15
1	1046	d_Z		0.120	0.051	15
1	1061	s_X	-0.036		0.020	15
1	1061	s_Y	-0.066		0.020	15
1	1061	s_Z	0.086		0.014	15
1	1061	d_X		-0.019	0.063	15
1	1061	d_Y		0.055	0.072	15
1	1061	d_Z		-0.048	0.059	15
1	1076	s_X	0.097		0.023	11
1	1076	s_Y	0.039		0.019	11
1	1076	s_Z	0.102		0.015	11
1	1076	d_X		0.018	0.052	11
1	1076	d_Y		-0.014	0.044	11
1	1076	d_Z		0.018	0.036	11

Exterior orientation data

Type	Photo	X	Y	Z	Phi	Omega	Kappa
	+- S (1/1000)						
A	1001	611157.126	6571321.046	1608.147	-1.0285	0.7827	-132.6471
	+-	56.	48.	41.	1.9	1.9	1.9
			:				
			:				
			:				
A	1086	612848.529	6570622.381	1614.551	0.6820	-0.2854	77.0392
	+-	49.	43.	36.	1.7	1.6	1.6

Mean photo scale: 10.0

RMS precision values of photo orientations from Qxx matrix: (1/1000)

41.	36.	26.	1.4	1.3	1.0

Poorest precision values of photo orientations from Qxx matrix: (1/1000)

74.	59.	49.	2.5	2.1	2.3

Listing of object point coordinates suppressed.

	+- S X	S Y	S Z
	(1 / 1 0 0 0)		
RMS precision values of object points:	39.	35.	72.
Poorest precision values of object points:	117.	160.	190.
RMS precision values of control points: (Computed from Qxx matrix)	9.	9.	9.

:
:
:

Residuals of image coordinates list limit = 3.0 * sigma

	Point	Photo	Vx'	Vy'	Rx'%	Ry'%	Wx'	Wy'	Nabla x'	y'
			(1 / 1 0 0 0)						(1 / 1 0 0 0)	
**	2136									
		1012	-3.1	9.9	33	57	-1.3	3.3	9.1	-17.1
		1011	-0.4	3.7	66	62	-0.1	1.2		
		1013	0.4	-7.1	69	66	0.1	-2.2		
		1010	0.2	0.8	59	60	0.1	0.3		
		1014	2.1	1.2	59	66	0.7	0.4		
				:						
				:						
				:						
**	463									
		1005	0.4	-7.8	0	41	unreal.	-3.0	unreal.	18.6
		1006	-0.4	7.9	0	43	-3.0	3.0	331.5	-18.3

Number of skipped photo measurements: 10

Frequency of photo measurement residuals N(0,1) :

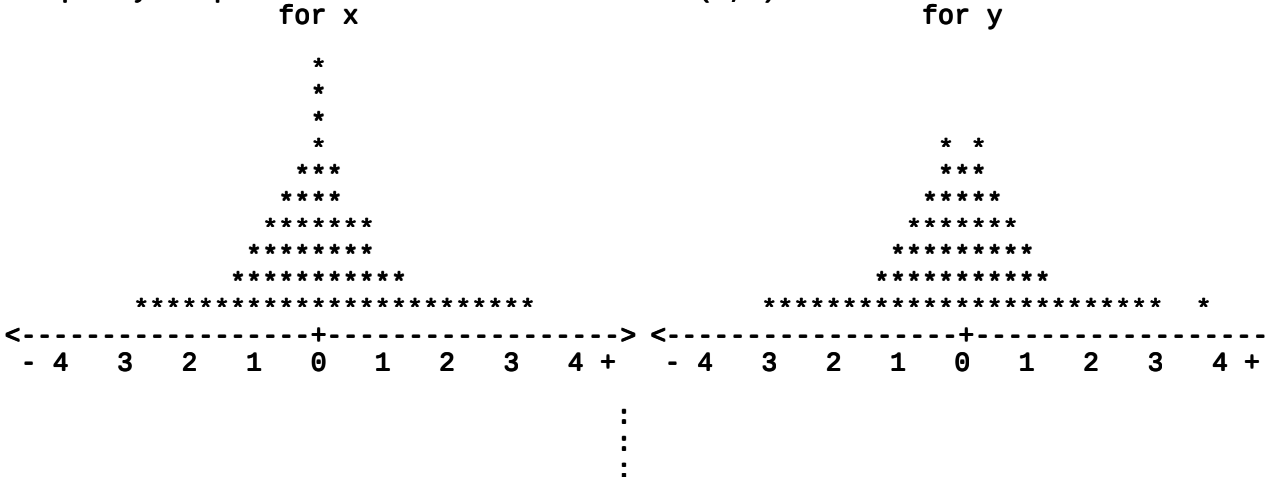

RMS control point residuals:	4.	4.	3. (1/1000)
Maximum control point residuals:	9.	9.	6. (1/1000)
RMS GPS residuals:	14.	16.	13. (1/1000)
Maximum GPS residuals:	37.	44.	47. (1/1000)
RMS IMU residuals:	3.4	2.8	10.0 (1/1000)
Maximum IMU residuals:	8.5	9.1	22.2 (1/1000)

(Computed from real residuals)

A posteriori variance-component estimation

Test value = s(a posteriori) / s(a priori)

Group	Test Value	No. of Obs.	Redundancy
Image coordinates	0.98	4756	3443.19
Coordinates of control points	1.02	39	5.16
Control points only in X	0.98	13	2.16
Control points only in Y	0.92	13	2.18
Control points only in Z	1.35	13	0.82
Image station information	0.13	258	254.83
Exterior orientations incl. GPS	0.87	258	86.82
Sum of all observations	0.95	5311	

BINGO-F - VERS. 4.0 / 10.00d

Company 1 / Cali 5

:
:
:

Summary of image data:

No. of points	:	282
No. of photos	:	62
No. of cameras	:	1
Max. measurements per point	:	12
Max. photo index difference	:	20

:
:
:

RESULTS OF ADJUSTMENT SIGMA 0 = 3.94 (1/1000)

Camera data

Camera no. 1

Diff. angle of rotation delta	:	-0.0091	-0.1040	0.0669
+-S (1/1000)	:	6.3	5.8	6.3

Additional parameters : Format factor = 1.000000

7	8	17
0.0072	-0.0041	0.0021

Mean radial symmetric lens distortion from additional parameters (1/1000)

Distortion values; First value for R = 10.0 (= Step width)

0.9	1.6	2.1	2.5	2.7	2.7	2.6	2.4	2.0	1.6
1.0	0.4	-0.4	-1.1	-2.0	-2.9				

Correlation between add. parameters in %

7	100		
8	-57	100	
17	-3	1	100
	7	8	17

Sigma 0 used for estimation of standard deviations: 3.94 (1/1000)

Par.no	Parameter value (1/1000)	Standard dev. (1/1000)	Value/Stand.dev	Total correlation
7	7.2	0.8	8.9	0.33
8	-4.1	1.5	-2.8	0.33
17	2.1	0.8	2.7	0.00

GPS shift and drift parameters

File	Line_No.	Para.Name	Shift	Drift	+-S	Photos
1	1087	s_X	0.021		0.035	17
1	1087	s_Y	0.096		0.021	17
1	1087	s_Z	0.123		0.023	17
1	1087	d_X		0.085	0.065	17
1	1087	d_Y		0.014	0.046	17
1	1087	d_Z		-0.094	0.053	17
1	1104	s_X	-0.130		0.034	17
1	1104	s_Y	0.034		0.020	17
1	1104	s_Z	0.099		0.023	17
1	1104	d_X		-0.029	0.055	17
1	1104	d_Y		0.055	0.038	17
1	1104	d_Z		0.043	0.045	17
1	1121	s_X	-0.029		0.022	14
1	1121	s_Y	-0.049		0.031	14
1	1121	s_Z	0.081		0.020	14
1	1121	d_X		-0.055	0.056	14
1	1121	d_Y		-0.087	0.077	14
1	1121	d_Z		-0.072	0.067	14
1	1135	s_X	-0.138		0.022	14
1	1135	s_Y	0.117		0.031	14
1	1135	s_Z	0.065		0.019	14
1	1135	d_X		0.071	0.048	14
1	1135	d_Y		0.041	0.066	14
1	1135	d_Z		0.046	0.057	14

Exterior orientation data

Type	Photo	X	Y	Z	Phi	Omega	Kappa
	+- S (1/1000)						
A	1087	606962.493	6563720.224	941.125	-0.3389	-0.3676	75.0705
	+-	44.	38.	35.	2.9	2.6	2.3
			:				
			:				
			:				
A	1148	606661.616	6565349.077	874.296	0.8321	0.0059	174.5469
	+-	38.	39.	35.	2.8	2.7	2.2

Mean photo scale: 5.25

RMS precision values of photo orientations from Qxx matrix: (1/1000)

40.	37.	30.	3.0	2.7	1.5

Poorest precision values of photo orientations from Qxx matrix: (1/1000)

68.	66.	53.	5.2	4.7	2.6

Listing of object point coordinates suppressed.

	+- S X	S Y	S Z
	(1 / 1 0 0 0)		
RMS precision values of object points:	25.	25.	47.
Poorest precision values of object points:	52.	53.	86.
RMS precision values of control points: (Computed from Qxx matrix)	9.	9.	10.

:
:
:

Residuals of image coordinates list limit = 4.0 * sigma

	Point	Photo	Vx'	Vy'	Rx'%	Ry'%	Wx'	Wy'	Nabla x'	y'
			(1 / 1 0 0 0)						(1 / 1 0 0 0)	
*	1415									
		1133	10.9	-20.7		skipped				
		1136	2.6	-1.5	25	54	1.3	-0.5		
		1132	3.7	-3.8	61	67	1.2	-1.1		
		1137	-2.4	3.3	67	67	-0.7	1.0		
		1131	-6.8	-0.7	53	65	-2.3	-0.2		
		1138	-3.5	-5.8	36	57	-1.5	-1.9		
				:						
				:						
				:						
**	877									
		1100	-2.4	-5.5	12	59	-1.7	-1.8		
		1107	21.3	-28.2		skipped				
		1101	4.2	-4.4	59	59	1.4	-1.4		
		1106	9.8	-31.5		skipped				
		1105	3.0	-9.6	16	56	1.9	-3.2	-18.1	17.1

Number of skipped photo measurements: 5

Frequency of photo measurement residuals N(0,1) :

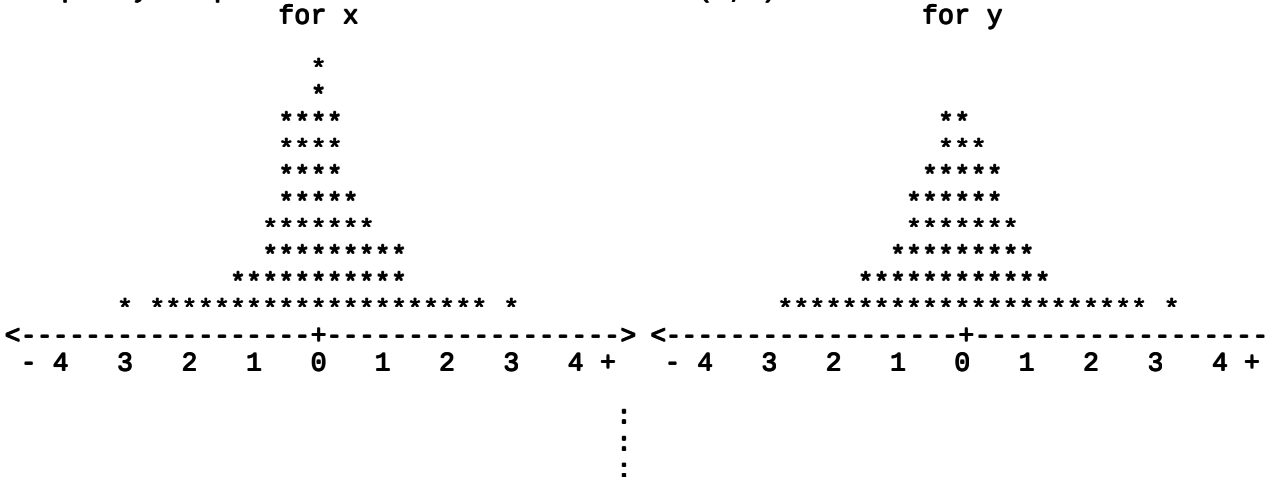

RMS control point residuals:	2.	3.	3. (1/1000)
Maximum control point residuals:	5.	6.	6. (1/1000)
RMS GPS residuals:	18.	17.	17. (1/1000)
Maximum GPS residuals:	51.	43.	45. (1/1000)
RMS IMU residuals:	4.4	3.2	6.7 (1/1000)
Maximum IMU residuals:	11.7	12.2	15.6 (1/1000)

(Computed from real residuals)

A posteriori variance-component estimation

Test value = s(a posteriori) / s(a priori)

Group	Test Value	No. of Obs.	Redundancy
Image coordinates	1.04	2888	1754.45
Coordinates of control points	0.81	21	2.59
Image station information	0.12	186	182.53
Exterior orientations incl. GPS	0.85	186	93.43
Sum of all observations	0.99	3281	

BINGO-F - VERS. 4.0 / 10.00d

Company 2 / Cali 10

:
:
:

Summary of image data:

No. of points	:	321
No. of photos	:	85
No. of cameras	:	1
Max. measurements per point	:	22
Max. photo index difference	:	55

:
:
:

RESULTS OF ADJUSTMENT SIGMA 0 = 5.71 (1/1000)

Camera data

Camera no. 1

Diff. angle of rotation delta	:	-0.0607	0.1265 -0.1972
+-S (1/1000)	:	7.7	7.2 7.8

Additional parameters : Format factor = 1.000000

7	8	17
0.0065	0.0037	0.0004

Mean radial symmetric lens distortion from additional parameters (1/1000)

Distortion values; First value for R = 10.0 (= Step width)

0.3	0.8	1.3	1.9	2.4	2.9	3.2	3.3	3.2	2.7
2.0	0.8	-0.9	-3.1	-5.8	-9.2				

Correlation between add. parameters in %

7	100		
8	-61	100	
17	-5	-1	100
	7	8	17

Sigma 0 used for estimation of standard deviations: 4.00 (1/1000)

Par.no	Parameter value (1/1000)	Standard dev. (1/1000)	Value/Stand.dev	Total correlation
7	6.5	0.5	11.8	0.38
8	3.7	1.0	3.8	0.38
17	0.4	0.2	1.8	0.01

GPS shift and drift parameters

File	Line_No.	Para.Name	Shift	Drift	+-S	Photos
1	2076	s_X	-0.181		0.043	11
1	2076	s_Y	0.322		0.032	11
1	2076	s_Z	0.487		0.026	11
1	2076	d_X		0.101	0.087	11
1	2076	d_Y		0.009	0.059	11
1	2076	d_Z		0.165	0.051	11
1	2087	s_X	0.269		0.038	11
1	2087	s_Y	-0.227		0.030	11
1	2087	s_Z	0.543		0.024	11
1	2087	d_X		-0.316	0.066	11
1	2087	d_Y		0.045	0.054	11
1	2087	d_Z		0.001	0.046	11
1	2098	s_X	-0.175		0.037	11
1	2098	s_Y	0.229		0.029	11
1	2098	s_Z	0.531		0.023	11
1	2098	d_X		0.116	0.068	11
1	2098	d_Y		-0.023	0.053	11
1	2098	d_Z		-0.044	0.044	11
1	2109	s_X	0.212		0.050	11
1	2109	s_Y	-0.244		0.039	11
1	2109	s_Z	0.492		0.031	11
1	2109	d_X		-0.147	0.083	11
1	2109	d_Y		0.025	0.067	11
1	2109	d_Z		0.174	0.055	11
1	2120	s_X	0.210		0.029	15
1	2120	s_Y	0.214		0.028	15
1	2120	s_Z	0.473		0.021	15
1	2120	d_X		-0.086	0.068	15
1	2120	d_Y		-0.275	0.073	15
1	2120	d_Z		-0.067	0.065	15
1	2135	s_X	-0.323		0.029	15
1	2135	s_Y	-0.221		0.028	15
1	2135	s_Z	0.381		0.021	15
1	2135	d_X		0.176	0.080	15
1	2135	d_Y		0.266	0.088	15
1	2135	d_Z		0.147	0.077	15
1	2150	s_X	0.112		0.042	11
1	2150	s_Y	-0.237		0.037	11
1	2150	s_Z	0.493		0.030	11
1	2150	d_X		-0.155	0.069	11
1	2150	d_Y		0.042	0.057	11
1	2150	d_Z		0.069	0.046	11

Exterior orientation data

Type	Photo	X	Y	Z	Phi	Omega	Kappa
	+- S (1/1000)						
A	2076	611152.927	6571368.661	1597.413	-0.6732	-0.6025	65.4712
	+-	87.	71.	62.	2.9	2.7	2.9
			⋮				
A	2160	612820.042	6570553.958	1601.752	-0.8224	0.0688	-122.8481
	+-	69.	62.	52.	2.4	2.4	2.3

Mean photo scale: 9.96

RMS precision values of photo orientations from Qxx matrix: (1/1000)

61.	53.	39.	2.2	1.9	1.4

Poorest precision values of photo orientations from Qxx matrix: (1/1000)

117.	93.	79.	4.2	3.2	3.4

Listing of object point coordinates suppressed.

	+- S X	S Y	S Z
	(1 / 1 0 0 0)		
RMS precision values of object points:	56.	48.	102.
Poorest precision values of object points:	224.	189.	307.
RMS precision values of control points: (Computed from Qxx matrix)	13.	13.	14.

⋮

Residuals of image coordinates list limit = 3.0 * sigma

	Point	Photo	Vx'	Vy'	Rx'%	Ry'%	Wx'	Wy'	Nabla x'	y'
			(1 / 1 0 0 0)						(1 / 1 0 0 0)	
*	100027	Cont.Pt.								
		2089	1.3	-1.7	76	70	0.4	-0.5		
		2107	-3.3	2.4	81	83	-0.9	0.7		
		2111	3.7	-4.1	72	66	1.1	-1.3		
		2151	0.9	-0.2	80	83	0.3	-0.1		
		2090	-4.0	5.5	78	73	-1.1	1.6		
		2106	-1.0	9.5	82	84	-0.3	2.6	1.2	-11.2
		2152	-2.0	2.2	83	84	-0.6	0.6		
		2112	-3.1	11.5	77	63	-0.9	3.6	4.0	-18.1
				⋮						
**	2728									
		2134	2.1	-4.2	41	63	0.8	-1.3		
		2133	3.3	-6.2	41	63	1.3	-1.9		
		2135	1.9	6.3	43	61	0.7	2.0		
		2136	3.9	-16.2	42	62	1.5	-5.1	-9.3	26.1

Number of skipped photo measurements: 4

Frequency of photo measurement residuals N(0,1) :

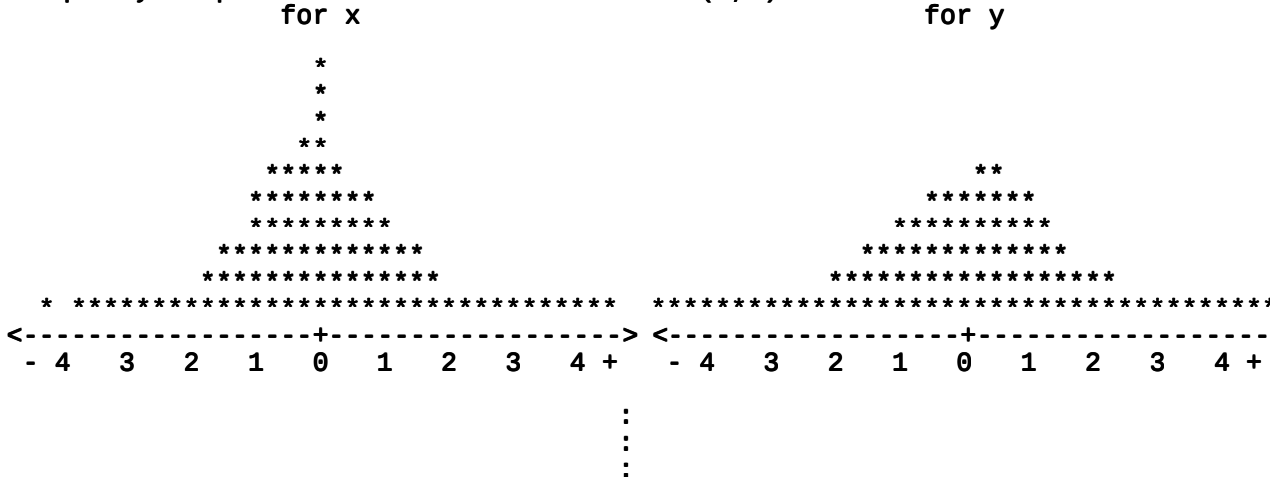

RMS control point residuals:	8.	8.	3. (1/1000)
Maximum control point residuals:	19.	16.	7. (1/1000)
RMS GPS residuals:	24.	20.	19. (1/1000)
Maximum GPS residuals:	62.	56.	44. (1/1000)
RMS IMU residuals:	5.2	3.4	5.9 (1/1000)
Maximum IMU residuals:	10.9	9.4	17.7 (1/1000)

(Computed from real residuals)

A posteriori variance-component estimation

Test value = s(a posteriori) / s(a priori)

Group	Test Value	No. of Obs.	Redundancy
Image coordinates	1.47	5430	4111.69
Coordinates of control points	1.93	39	4.98
Image station information	0.10	255	251.83
Exterior orientations incl. GPS	1.23	255	89.49
Sum of all observations	1.43	5979	

BINGO-F - VERS. 4.0 / 10.00d

Company 2 / Cali 5

:
:
:

Summary of image data:

No. of points	:	301
No. of photos	:	66
No. of cameras	:	1
Max. measurements per point	:	10
Max. photo index difference	:	24

:
:
:

RESULTS OF ADJUSTMENT SIGMA 0 = 5.33 (1/1000)

Camera data

Camera no. 1

Diff. angle of rotation delta	:	-0.0593	0.1306 -0.1996
+-S (1/1000)	:	8.2	7.6 8.2

Additional parameters : Format factor = 1.000000

7	8	17
0.0054	0.0045	0.0014

Mean radial symmetric lens distortion from additional parameters (1/1000)

Distortion values; First value for R = 10.0 (= Step width)

0.2	0.5	1.0	1.5	2.0	2.5	2.8	3.0	2.9	2.5
1.8	0.7	-0.8	-2.9	-5.6	-8.9				

Correlation between add. parameters in %

7	100		
8	-58	100	
17	1	-1	100
	7	8	17

Sigma 0 used for estimation of standard deviations: 4.00 (1/1000)

Par.no	Parameter value (1/1000)	Standard dev. (1/1000)	Value/Stand.dev	Total correlation
7	5.4	0.9	6.2	0.35
8	4.5	1.6	2.8	0.35
17	1.4	0.6	2.2	0.00

GPS shift and drift parameters

File	Line_No.	Para.Name	Shift	Drift	+-S	Photos
1	2004	s_X	-0.112		0.047	18
1	2004	s_Y	-0.080		0.028	18
1	2004	s_Z	0.352		0.034	18
1	2004	d_X		-0.352	0.068	18
1	2004	d_Y		0.161	0.047	18
1	2004	d_Z		0.024	0.060	18
1	2022	s_X	-0.207		0.047	18
1	2022	s_Y	0.216		0.028	18
1	2022	s_Z	0.336		0.034	18
1	2022	d_X		0.367	0.063	18
1	2022	d_Y		-0.150	0.043	18
1	2022	d_Z		-0.045	0.054	18
1	2040	s_X	-0.111		0.030	15
1	2040	s_Y	0.055		0.045	15
1	2040	s_Z	0.296		0.035	15
1	2040	d_X		0.139	0.066	15
1	2040	d_Y		0.366	0.095	15
1	2040	d_Z		-0.044	0.090	15
1	2055	s_X	0.125		0.031	15
1	2055	s_Y	0.097		0.036	15
1	2055	s_Z	0.307		0.030	15
1	2055	d_X		-0.160	0.058	15
1	2055	d_Y		-0.285	0.083	15
1	2055	d_Z		0.052	0.078	15

Exterior orientation data

Type	Photo	X	Y	Z	Phi	Omega	Kappa
	+- S (1/1000)						
A	2004	606941.608	6563696.137	842.563	2.3021	1.6212	-125.8332
	+-	54.	49.	49.	4.1	4.0	3.4
			⋮				
A	2069	606296.163	6565506.724	851.294	0.6505	-0.0087	-26.3226
	+-	53.	57.	54.	4.3	4.6	3.8

Mean photo scale: 5.11

RMS precision values of photo orientations from Qxx matrix: (1/1000)

56.	53.	48.	4.3	4.0	2.3

Poorest precision values of photo orientations from Qxx matrix: (1/1000)

98.	99.	89.	7.7	7.1	3.8

Listing of object point coordinates suppressed.

RMS precision values of object points:	37.	36.	71.
Poorest precision values of object points:	78.	71.	132.
RMS precision values of control points: (Computed from Qxx matrix)	13.	13.	13.

⋮

Residuals of image coordinates list limit = 3.0 * sigma

	Point	Photo	Vx' (1 / 1 0 0 0)	Vy'	Rx'%	Ry'%	Wx'	Wy'	Nabla x' (1 / 1 0 0 0)	y'
*	1473									
		2054	5.6	-1.0	48	70	2.0	-0.3		
		2055	2.4	-8.9	51	71	0.8	-2.6	-4.6	12.4
		2053	-0.5	-0.6	72	74	-0.1	-0.2		
		2056	6.1	10.4	73	74	1.8	3.0	-8.3	-14.1
		2052	4.8	-1.4	46	66	1.8	-0.4		
		2057	1.2	-5.7	48	70	0.4	-1.7		
				⋮						
*	1605									
		2022	-5.0	6.4	37	48	-2.1	2.3	13.4	-13.3
		2023	9.2	-6.0	37	51	3.7	-2.1	-24.2	11.6
		2021	-4.4	0.2	39	50	-1.8	0.1		
		2020	8.5	-0.7	35	53	3.6	-0.2	-23.8	1.4

Number of skipped photo measurements: 3

Frequency of photo measurement residuals N(0,1) :

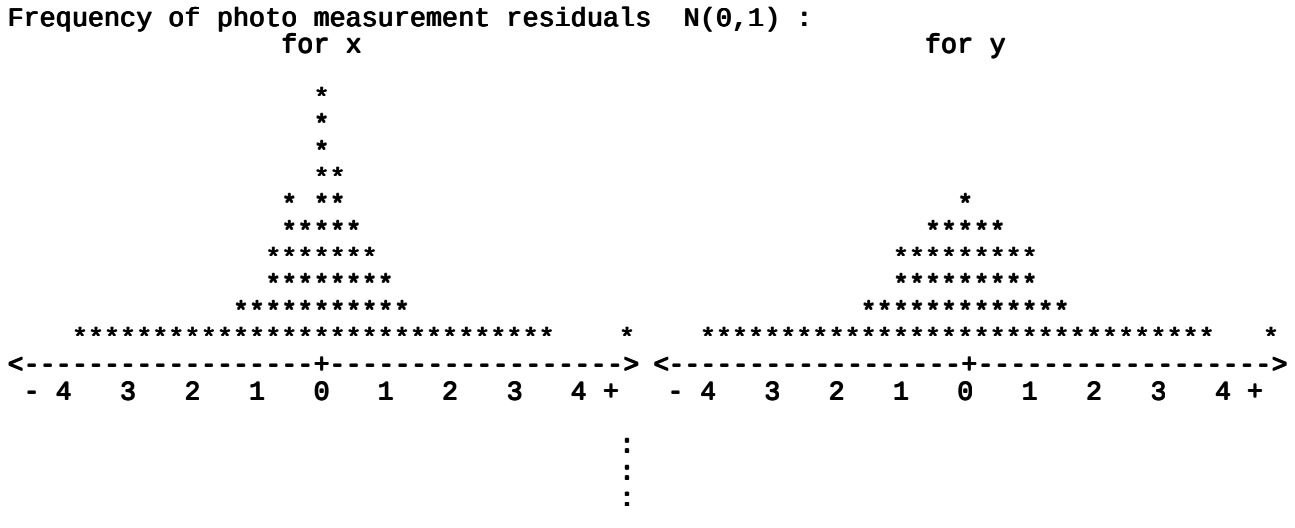

RMS control point residuals:	2.	2.	1. (1/1000)
Maximum control point residuals:	3.	3.	2. (1/1000)
RMS GPS residuals:	22.	21.	12. (1/1000)
Maximum GPS residuals:	52.	65.	29. (1/1000)
RMS IMU residuals:	16.8	12.1	11.2 (1/1000)
Maximum IMU residuals:	46.0	29.0	20.9 (1/1000)

(Computed from real residuals)

A posteriori variance-component estimation

Test value = s(a posteriori) / s(a priori)

Group		Test Value	No. of Obs.	Redundancy
Image coordinates	:	1.42	2962	1749.81
Coordinates of control points	:	0.50	15	1.16
Image station information	:	0.27	198	194.42
Exterior orientations incl. GPS	:	0.93	198	98.61
Sum of all observations	:	1.33	3373	

ISAT Direct Exterior Orientation QA/QC Strategy Using POS Data

Mostafa Madani[1] **and Mohamed Mostafa**[2]

[1] Z/I Imaging Corporation
301 Cochran Rd, Suite 9
Huntsville, Alabama 35824
E-mail: msmadani@ziimaging.com

[2]Applanix Corporation
85 Leek Cr., Richmond Hill
Ontario, Canada L4B 3B3
E-mail: MMostafa@applanix.com

ABSTRACT

This paper describes the quality assurance and quality control (QA/QC) tools currently planned and under implementation in the Z/I ImageStation Automatic Triangulation (ISAT) product for imagery acquired by an aerial camera and Applanix POS/AV™ navigation system. First, a description of the ISAT product with the user interface to the Applanix POSEO package is given. Then, a description on using the EO data in mapping applications is presented. Instead of using the full capabilities of an automatic aerial triangulation, the QA/QC procedure is designed to lessen the amount of work needed to check the quality of the GPS, IMU, and GCP data using different schemes, such as performing a statistical analysis on image/object space intersection using digital images and the GPS/IMU data. Numerical results of using the ISAT's QA/QC strategies on different data sets are also presented.

DIGITAL MULTI-SENSOR SYSTEMS – CALIBRATION AND PERFORMANCE ANALYSIS

Mohamed M. R. Mostafa
Applanix Corporation
85 Leek Cr., Richmond Hill, Ontario, Canada L4B 3B3
Phone: (905) 709-4600 ext 274 E-mail: mmostafa@applanix.com

KEY WORDS: digital camera, multi-sensor systems, GPS, INS, photogrammetry, calibration, sensor integration

ABSTRACT

Currently, the mapping industry is focusing on the implementation of multi-sensor systems for image acquisition and georeferencing. Small format digital cameras are of a particular focus nowadays, due to their numerous advantages and suitability for a number of low- to medium-class applications. Calibration is, however, a critical factor in such a multi-sensor environment. This paper is, therefore, dedicated to present the new developments in calibrating a multi-sensor digital system. The concept of boresight/camera calibration in airborne and terrestrial modes is presented. Data results and analysis of multiple data sets are also presented

1. INTRODUCTION

Over the past few years, the mapping industry has focused on the implementation of the new technologically advanced multi-sensor systems for map production. These systems are currently replacing the traditional aerial mapping systems for some applications such as resource mapping and airborne remote sensing, and are starting to compete in some other applications such as engineering and cadastral mapping. Typically, a multi-sensor digital system consists of one or more digital cameras for image acquisition and a GPS-aided inertial measurement system such as Applanix POS/AV^{TM} system for image georeferencing. These systems require much less operational constraints and a fraction of the post-processing time needed in traditional systems for map production. For a detailed discussion, see Schwarz et al (1993) and Mostafa et al (1997). When using multi-sensor digital systems, a number of new calibration requirements arise, namely camera and boresight calibration. Although digital camera calibration has been researched and well understood in the in the 1990s (c.f., Fraser, 1997; Lichti and Chapman, 1997), and successfully applied (c.f., Mostafa et al 1997; Toth and Grejner-Brzezinska, 1998; Mostafa et al 1999) there is no single government agency that offers certified digital camera calibration service and, therefore, it is currently the responsibility of the mapping firm to calibrate their digital cameras. Boresight calibration, on the other hand, has been done successfully in the past few years in the case of the film-camera traditional systems (c.f., Hutton et al, 1997), but an optimal calibration procedure is not yet available for digital cameras. In the following, this is addressed in some detail.

2. BORESIGHT CALIBRATION CONCEPT

Boresight is the physical mounting angles between an IMU and a digital camera that theoretically describe the misalignment angles between the IMU and the digital camera frames of reference as shown in Figure 1.

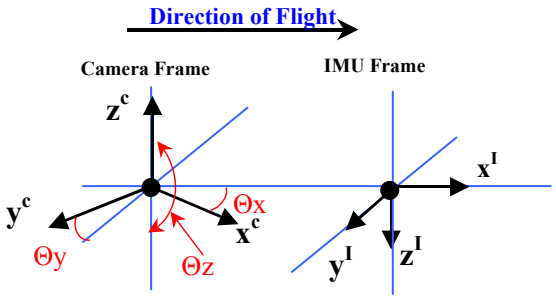

Figure 1 Camera/IMU Boresight

The direction cosine matrix defining the relative orientation of the camera frame with respect to the IMU body frame, $\mathbf{R}_c^b$ is defined in terms of Θ_x, Θ_y, and Θ_z angles between the IMU and the camera frames as:

$$\mathbf{R}_c^b = \begin{bmatrix} 1 & 0 & 0 \\ 0 & \cos\Theta_x & \sin\Theta_x \\ 0 & -\sin\Theta_x & \cos\Theta_x \end{bmatrix} \begin{bmatrix} \cos\Theta_y & 0 & -\sin\Theta_y \\ 0 & 1 & 0 \\ \sin\Theta_y & 0 & \cos\Theta_y \end{bmatrix} \begin{bmatrix} \cos\Theta_z & \sin\Theta_z & 0 \\ -\sin\Theta_z & \cos\Theta_z & 0 \\ 0 & 0 & 1 \end{bmatrix} \quad (1)$$

$$= \begin{bmatrix} \cos\Theta_y \cos\Theta_z & \cos\Theta_y \sin\Theta_z & -\sin\Theta_y \\ \sin\Theta_x \sin\Theta_y \cos\Theta_z - \cos\Theta_x \sin\Theta_z & \sin\Theta_x \sin\Theta_y \sin\Theta_z + \cos\Theta_x \cos\Theta_z & \sin\Theta_x \cos\Theta_y \\ \cos\Theta_x \sin\Theta_y \cos\Theta_z + \sin\Theta_x \sin\Theta_z & \cos\Theta_x \sin\Theta_y \sin\Theta_z - \sin\Theta_x \cos\Theta_z & \cos\Theta_x \cos\Theta_y \end{bmatrix}$$

A key assumption is that the boresight angles remain constant as long as the IMU remains rigidly mounted to the camera, as shown in Figure 2.

Figure 2 IMU Installations on Different Imaging Sensors (Courtesy of Z/I Imaging Inc., and LH-Systems)

To determine the boresight matrix, two methods can be followed. The first method can be summarized as follows:

- Determine each image orientation matrix independently by ground control in an image block using aerotriangulation
- Determine the IMU body-to-Mapping frame matrix independently using the IMU measurements at the moment of image exposure
- Determine the boresight matrix by multiplication (for details, see Mostafa et al 1997; Škaloud et al, 1996).

The second method is to determine a constant boresight matrix implicitly in the bundle adjustment by introducing the three-Θ_x, Θ_y, and Θ_z angles as observable quantities in the adjustment process. The former requires the availability of ground control points (GCP) in the calibration area, while the latter does not require ground control except for quality assurance.

3. AIRBORNE BORESIGHT CALIBRATION

The airborne boresight calibration is currently done by flying over a calibration field that has well distributed and accurate ground control points. Image measurements are collected using an analytical plotter or a SoftCopy workstation. An airborne GPS-assisted aerotriangulation is then done to determine each image attitude with respect to some local mapping frame. For each image frame, the IMU-derived attitude matrix is then compared to the photogrammetric attitude matrix to derive the boresight matrix. Averaging the boresight over a number of images in a block configuration is the last step done to provide accurate calibration and the necessary statistics. This method has been followed successfully for the past few years using the traditional aerotriangulation approach (c.f., Hutton et al, 1997; Mostafa et al, 1997; Schwarz et al, 1993; Škaloud et al, 1996).

Boresight calibration of an IMU/digital camera system differs from that done for a film camera. The main differences are due to the lack of digital camera calibration information and the poor geometry of digital cameras. Therefore, the digital camera calibration and the boresight calibration can either be done sequentially or simultaneously. An example of airborne boresight/camera calibration is presented in the following.

Recently, a more accurate airborne boresight calibration process has been implemented in the Applanix POSEO™ package, where three constant boresight angles are introduced to the least squares filter as observables together with their associated statistical measures; for test results and analysis, see Mostafa et al (2001). The new utility package developed in POSEO is called POSCal. Figure 3 shows a screen shot of the improved POSEO software, Figure 4 shows the main processing options of POSCal, and Figure 5 shows the advanced options of POSCal.

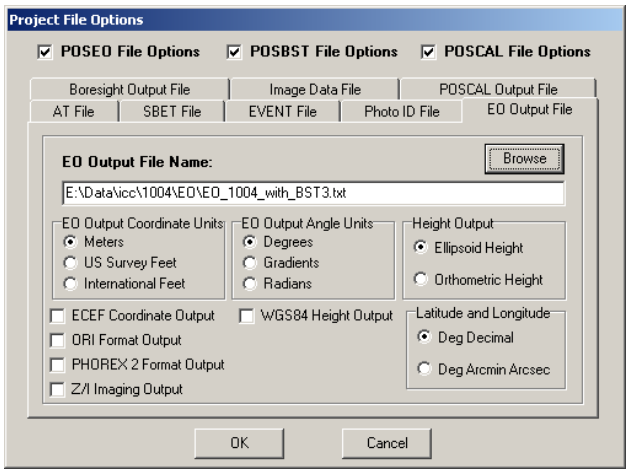

Figure 3 POSEO Data Output Options

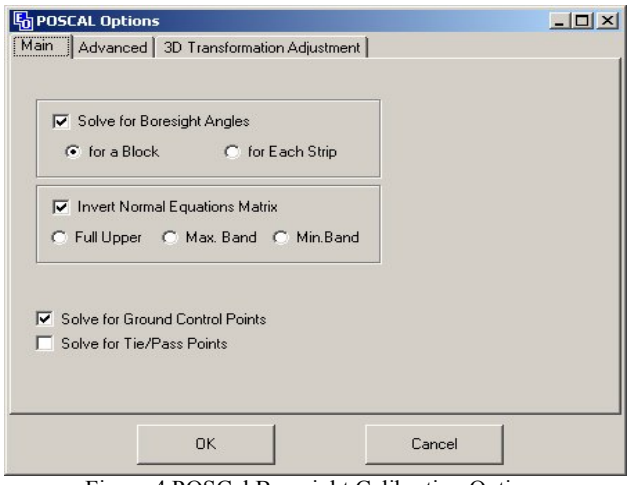

Figure 4 POSCal Boresight Calibration Options

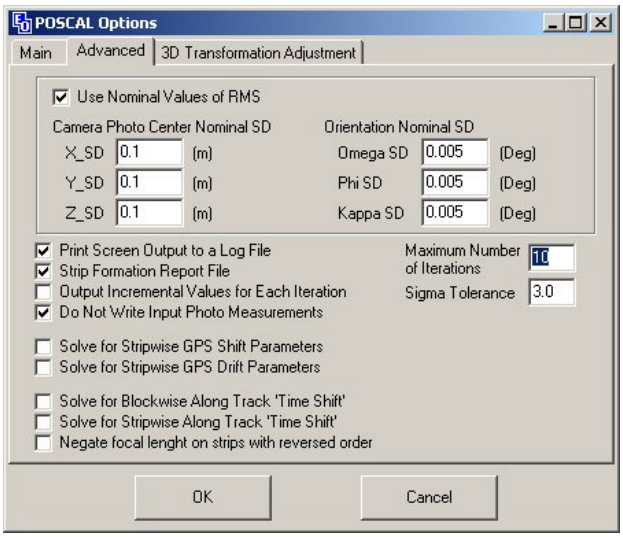

Figure 5 POSCal Processing Options

3.1 OPTECH BORESIGHT/CAMERA INTEGRATED SYSTEM CALIBRATION

In February 2001, a calibration flight (shown in Figure 6) was done to determine the boresight and digital camera calibration parameters of Optech's new integrated digital camera system. The entire system includes Optech's ALTM, a SensorVision 3k x 2k digital camera and Applanix POS/AV™ 410 system.

The camera/IMU boresight and the digital camera were calibrated by flying the system over Square One Mall in Mississauga, Ontario, on two different days using two different flying altitudes as shown in Figure 7. About 60 ground features were surveyed (as shown in Figure 6). In addition, a high accuracy Digital Elevation Model (DEM) was developed using the ALTM and provided by Optech Inc.

Using Applanix POSEO™ package and POSCal™ module, the digital camera and the boresight were calibrated. Almost 50% of the available ground control points were used in the calibration process (Figure 8 shows their residuals) while the other half was used as independent checkpoints. Checkpoint Residuals are shown in Figure 9, while their statistics are shown in Table 1. Note that the RMS values are better than 10 cm in easting and northing and better than 20 cm in height, which gives a quick indication besides statistics that the calibration process was very accurate.

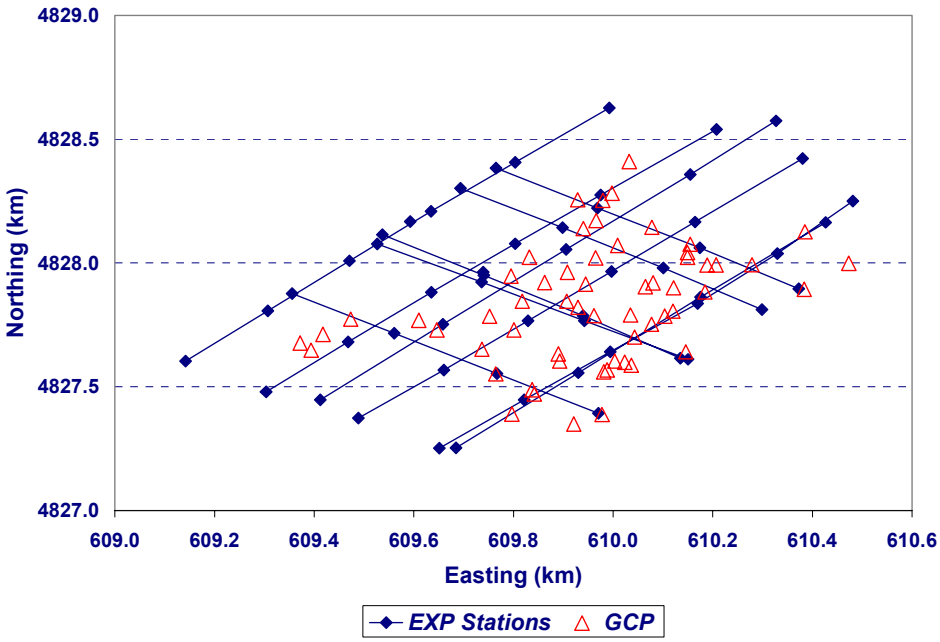

Figure 6 Optech's System Calibration Flight Showing Flight Lines, Camera Exposure Stations, and GCP

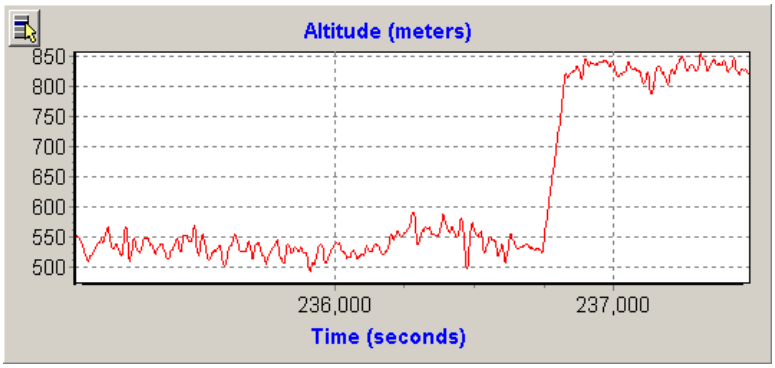

Figure 7 Flight Altitude of Optech's Calibration Flight

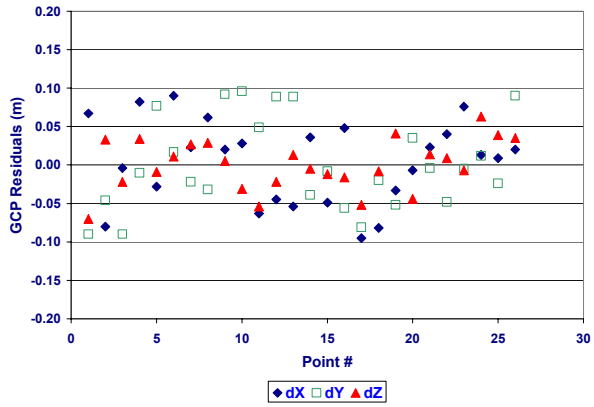

Figure 8 Ground Control Point Residuals During Simultaneous Boresight/Camera Calibration

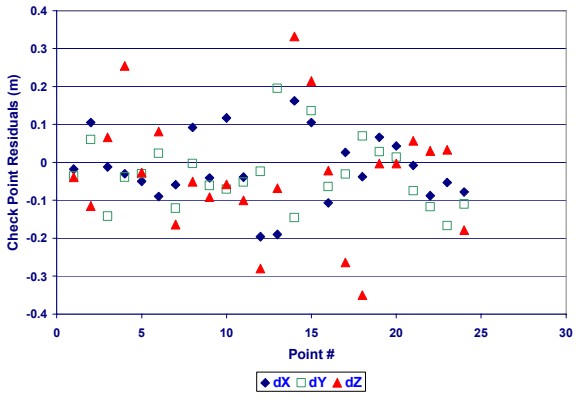

Figure 9 Checkpoint Residuals During Simultaneous Boresight/Camera Calibration

Table 1. Checkpoint Residual Statistics
During Simultaneous Boresight/Camera Calibration

Stat.	X (m)	Y (m)	Z (m)
Mean	***-0.02***	***-0.03***	***-0.03***
Max	0.16	0.20	0.33
Std Dev	0.09	0.09	0.16
RMS	***0.09***	***0.09***	***0.16***

To check the boresight and camera calibration parameters in the actual map production environment, all airborne data (imagery, INS/GPS position and attitude, and calibration parameters) were used in the direct georeferencing mode with no GCP, in order to position points on the ground using photo stereopairs. Then, the resulting coordinates of these points were compared to their independently land-surveyed coordinates. An example of checkpoint residuals is shown in Table 2 for the first day of flight.

To check the stability of the calibrated parameters, a second flight was done using the same integrated system. Applying the calibration parameters derived from Day 1 flight, the calibrated parameters proved to be very stable. Table 3 shows the checkpoint statistics of the Day 2 flight.

Table 2. Statistics of Checkpoint Residuals for Individual Models of Day 1 Flight

Statistics for Model # 6-7			
Coordinate Component	dX (m)	dY (m)	dZ (m)
Minimum	-0.209	-0.108	-0.290
Maximum	0.029	0.110	0.260
Mean	-0.010	0.020	0.091
RMS (m)	0.133	0.044	0.121
Statistics for Model # 7-8			
Minimum	-0.111	-0.189	-0.199
Maximum	0.129	0.195	0.204
Mean	-0.020	0.041	0.081
RMS (m)	0.072	0.120	0.104
Statistics for Model # 8-9			
Minimum	-0.150	-0.198	-0.419
Maximum	0.129	0.185	0.390
Mean	0.016	0.014	0.098
RMS (m)	0.064	0.075	0.195

Table 3. Statistics of Checkpoint Residuals for Individual Models of Day 2 Flight

Statistics for Model # 6-7			
Coordinate Component	dX (m)	dY (m)	dZ (m)
Minimum	-0.198	-0.158	-0.3629
Maximum	0.190	0.141	0.310
Mean	0.030	0.028	0.081
RMS	0.093	0.064	0.151
Statistics for Model # 7-8			
Minimum	-0.110	-0.149	-0.169
Maximum	0.137	0.197	0.204
Mean	-0.032	0.041	0.098
RMS	0.087	0.113	0.114
Statistics for Model # 8-9			
Minimum	-0.201	-0.161	-0.419
Maximum	0.196	0.178	0.390
Average	0.031	-0.014	0.098
RMS	0.106	0.097	0.211

3.2 ADVANTAGES AND LIMITATIONS OF AIRBORNE CALIBRATION APPRAOCH

For a digital multi-sensor system, the airborne calibration is advantageous because of the following reasons:

- Inertial in-flight alignment happens frequently because of manoeuvres, which improves the heading accuracy as shown in Figure 10. As a result of turns, frequent changes of velocity of large magnitude and directions improve the heading accuracy, which is desirable in order to achieve high accuracy of heading boresight calibration. Figures 11 and 12 show the total acceleration and the north velocity of the Optech's calibration flight.
- A calibration flight might have some differences from a regular mapping flight because of the flight pattern required to achieve high accuracy, yet it is the closest to the actual airborne mapping data acquisition environment

The limitations of the airborne approach are:

- Operationally, airborne boresight/camera calibration is sometimes inconvenient
- Digital camera calibration (which is mandatory), is much more difficult when done airborne, even though it is more cost effective and time efficient especially when done simultaneously to boresight calibration

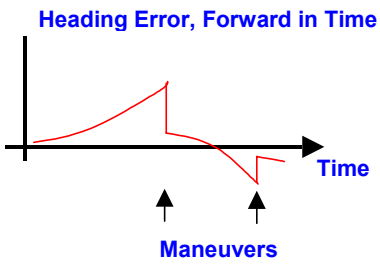

Figure 10 Heading Accuracy Improvements During Maneuvers

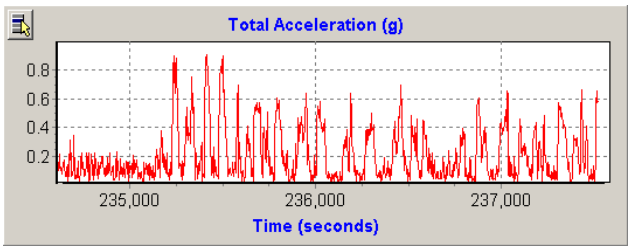

Figure 11 Total Acceleration Frequent Changes During Maneuvers - Optech's Calibration Flight

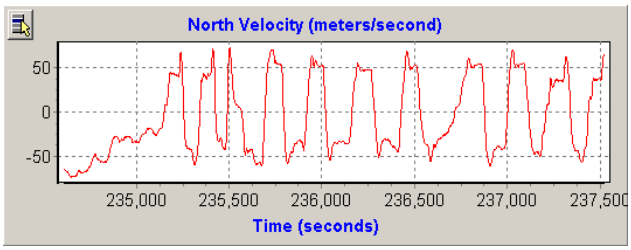

Figure 12 North Velocity Frequent Changes During Maneuvers - Optech's Calibration Flight

4. TERRESTRIAL BORESIGHT CALIBRATION

The reason for calibrating an airborne system in terrestrial mode is to improve the camera calibration by using very large scale photography, by using accurately surveyed targets as reference points, and by using multi-frame convergent photography, all of which cannot be achieved from the air. Although the distances to the targets in terrestrial mode are significantly shorter than in the air and hence the ability to accurately observe angles is much less, early studies (Mostafa and Schwarz 1999) showed that the terrestrial calibration is also a viable approach for boresight calibration.

To satisfy the requirement for both digital camera calibration and boresight calibration, the data has to be collected with some specifications such as:

- Collect GPS/IMU data using a van driven in loops to introduce some manoeuvres for inertial alignment purposes (see Figures 13, 14, and 15)
- Collect convergent imagery to a surveyed target field (see Figure 16) from surveyed ground point close to the calibration cage as shown in Figure 17
- In postmission, process inertial data using coordinate updates and zero velocities to estimate accurate inertial angles of each image

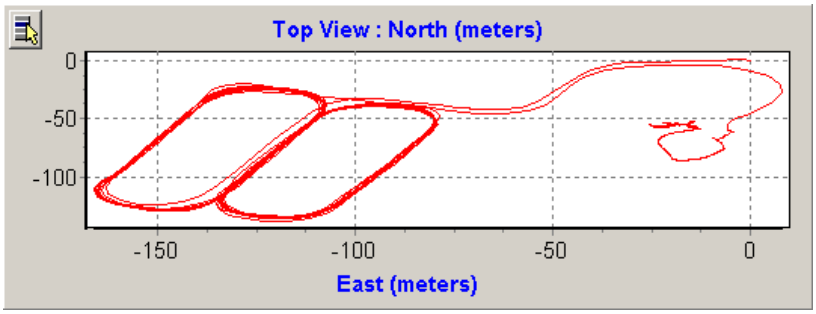

Figure 13 Van Trajectory For Inertial Alignment

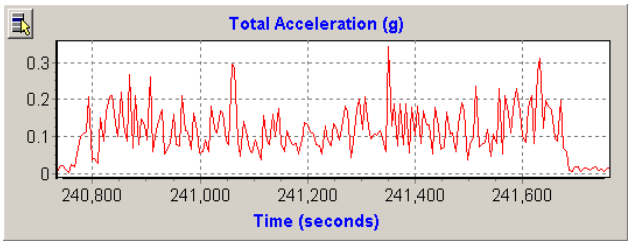

Figure 14 Total Acceleration Frequent Changes During Maneuvers – Van Test

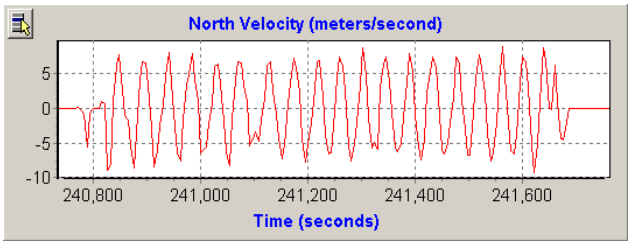

Figure 15 North Velocity Frequent Changes During Maneuvers – Van Test

4.1 Terrestrial Calibration Testing

A van test was conducted using an integrated system consisting of Applanix POS/AV 310 and a 3k x 2k digital camera. The camera and boresight were calibrated using the terrestrial approach. Then, the entire system performance was analysed using both terrestrial and airborne tests.

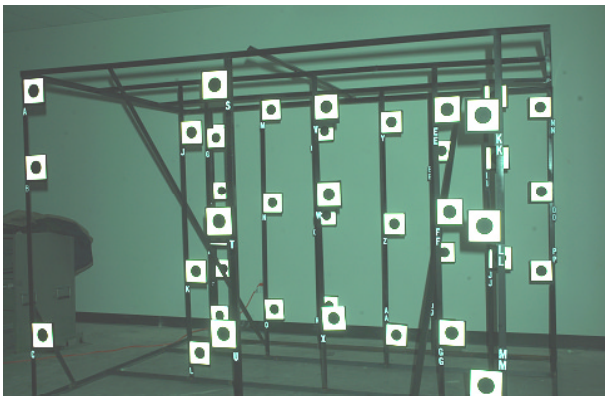

Figure 16 Calibration Cage

Using the same data collected for boresight and camera calibration, the system's performance was analyzed as follows:

1. Consider all the target locations as *unknown*
2. *Compute* target locations using the *known* boresight, camera calibration parameters, imagery, and POS data.
3. *Compare* the resulting target coordinates to the surveyed ones

Checkpoint residuals are shown in Table 4.

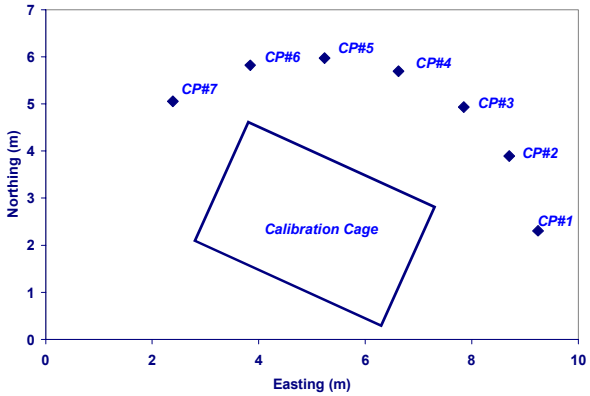

Figure 17 Terrestrial Calibration Layout

Table 4. Statistics of Check Point Residuals

Coordinate Component	*dX*	*dY*	*dZ*
Minimum	-0.0090	-0.0880	-0.0030
Maximum	0.0045	0.0090	0.0045
Average	-0.0010	-0.0010	0.0009
RMS (m)	**0.0037**	**0.0029**	**0.0021**

Note that this accuracy is extremely high because of two reasons. First, about 33 images were used *simultaneously* in a *multi-frame convergent-photography mode* in a bundle adjustment where the object distance is 4 m on average. Such accuracy cannot be achieved when the system is used airborne since the object distance is in the order of kilometres and there is no convergent photography planned. However, it gives a quick indication that the system's calibration is valid. To independently check the system performance a flight test was conducted after the terrestrial calibration. The processing chain included the following:

1. *Refine* image coordinates using camera calibration parameters
2. *Align* the IMU frame to the image frame using boresight data
3. *Apply* image position and orientation to stereo photos to determine ground position in direct georeferencing mode
4. *Compare* ground positions with their reference values (land-surveyed values)

Checkpoint accuracy using individual image models of the test flight is shown in Tables 5 and 6.

Table 5. Statistics of Checkpoint Residuals for Airborne Data - Model 207-208

Coordinate Component	Accuracy (m)
RMS in Easting (m)	0.4
RMS in Northing (m)	0.4
RMS in Height (m)	1.8

Table 6. Statistics of Checkpoint Residuals for Airborne Data Model 209-210

Coordinate Component	Accuracy (m)
RMS in Easting (m)	0.37
RMS in Northing (m)	0.31
RMS in Height (m)	2.00

4.2 Advantages and Limitations OF Terrestrial Calibration

By examining the terrestrial approach and the available test data, the following can be summarized:

- Digital camera calibration in the terrestrial mode is much more controllable than in the airborne mode due to the improved convergent photography.
- Terrestrial Approach is much more cost-effective than the airborne approach
- In terrestrial mode, the heading accuracy of the inertial unit is poorer than that achieved airborne since the changes in velocity magnitude and direction obtained on the ground is limited. This can be seen when comparing Figures 8 and 9 to 11 and 12. Hence the accuracy of the heading boresight calibration will be less than that obtained with the airborne approach

5. CONCLUSIONS

In this paper, digital camera/boresight simultaneous calibration of multi-sensor digital systems has been shown to be determined successfully using two different approaches, namely, airborne and terrestrial. Since digital cameras require calibration and it is currently the responsibility of any mapping company to calibrate them, it is more efficient to calibrate both the boresight and the digital camera simultaneously using the same data set in a bundle adjustment in either airborne or terrestrial mode. Applanix POSEO™ package and POSCal™ utility have been used successfully for this purpose in airborne and terrestrial boresight/camera calibration tests.

ACKNOWLEDGEMENTS

Joe Hutton of Applanix Corporation is gratefully acknowledged for his valuable discussions and for helping with data processing and analysis. Thanks to Paul LaRocque of Optech Inc for allowing publishing the results from Optech's calibration flights.

REFERENCES

Cosandier, D. and M. A. Chapman, 1995. Precise Multispectral Airborne Pushbroom Image Georectification and DEM Generation, Proceedings of ISPRS/IAG/FIG Workshop on Integrated Sensors Orientation, Barcelona, September, 4 - 8, pp. 91-100.

El-Sheimy, N., 1996. The Development of VISAT for GIS Applications, Ph.D. Dissertation, UCGE Report No. 20101, Department of Geomatics Engineering, The University of Calgary, Calgary, Alberta, Canada, 172 p.

Fraser, C.S., 1997. Digital Camera Self Calibration, ISPRS Journal of Photogrammetry & Remote Sensing, 52(1997): 149-159.

Hutton, J., Savina, T., and Lithopoulos, L., 1997. Photogrammetric Applications of Applanix's Position and Orientation System (POS). ASPRS/MAPPS Softcopy Conference, Arlington, Virginia, July 27 - 30.

Lichti, D.D. and M. A. Chapman, 1997. Constrained FEM Self-Calibration, PE&RS, 63(9): 1111-1119.

Moffit, F. and E.M. Mikhail, 1980. Photogrammetry. Harper and Row, Inc, New York.

Mostafa, M.M.R., J. Hutton, and E. Lithopoulos, 2001. Direct Georeferencing of Frame Imagery - An Error Budget. Proceedings, The Third International Mobile Mapping Symposium, Cairo, Egypt, January 3-5.

Mostafa, M.M.R. and K-P Schwarz, 1999. An Autonomous Multi-Sensor System for Airborne Digital Image Capture and Georeferencing, Proceedings of the ASPRS Annual Convention, Portland, Oregon, May 17-21, pp. 976 - 987.

Mostafa, M.M.R., K.P. Schwarz, and P. Gong, 1997. A Fully Digital System for Airborne Mapping, KIS97 Proceedings, Banff, Canada, June 3-6, pp. 463-471.

Schwarz, K.P., M.A. Chapman, M.E. Cannon and P. Gong, 1993. An Integrated INS/GPS Approach to The Georeferencing of Remotely Sensed Data, PE&RS, 59(11): 1167-1674.

Škaloud, J., M. Cramer, and K.P. Schwarz, 1996. Exterior Orientation by Direct Measurement of Position and Attitude, International Archives of Photogrammetry and Remote Sensing, 31 (B3): 125-130.

Toth, C. and D.A. Grejner-Brzezinska, 1998. Performance Analysis of The Airborne Integrated Mapping System (AIMS™), International Archives of Photogrammetry and Remote Sensing, 32 (2):320-326.

Boresight Calibration Without Ground Control

by
Mohamed Mostafa

APPLANIX Corporation
85 Leek Cr., Richmond Hill
Ontario, Canada L4B 3B3
Phone: (905) 709-4600 Fax: (905)709-7153
E-mail: MMostafa@applanix.com

ABSTRACT

This paper summarizes a study conducted to find an optimal camera/IMU boresight calibration procedure without the use of ground control. The study has been done using real sets of data collected by either mapping companies or by the pilot centre of the OEEPE. All data sets were acquired by data a 9" x 9" film camera and by Applanix POS/AV^{TM} system. In addition, all data sets had a good number, distribution, and accuracy of ground control points, quality image measurements, good GPS and IMU data. This allowed starting off with good quality data sets where biases and noises were introduced intentionally for analysis purposes. Different imaging configurations have been studied. For instance, the effect of the number of flight lines have been taken into account to analyse the accuracies obtainable for the boresight angles using one flight line, two flight lines in the same direction, two flight lines in opposite directions, three flight lines, and four flight lines. The effect of the number of images per strip has also been analysed, as well as the effect of the number of image measurements in each single photo. All data sets have been run with and without ground control points where the effect of the number, distribution, and accuracy of ground control points is analysed. The effect of GPS errors has been also analyzed. A summary of the results and analysis is presented together with the relevant references that discussed this topic.

Integrated INS/DGPS systems: calibration and combined block adjustment

G. Forlani*, L. Pinto**

* University of Parma – gianfranco.forlani@unipr.it
** Technical University of Milan - livio@mail.polimi.it

Abstract

Within the OEEPE test “Integrated Sensor Orientation”, a calibration procedure for a INS/DGPS system is presented. The calibration parameters (offset and misalignment angles) are estimateds as a weighted average of the discrepancies between the EO of the calibration block and the INS/DGPS data. The effectiveness of the procedure reflects on the RMS of the differences on the check points computed by direct georeferencing.
The benefits of performing a combined adjustment of collinearity equations and the EO derived by orientation systems is also addressed. A simple functional model of the pseudo-observation equation of the EO elements is discussed, which allow for systematic differences between the photogrammetry-driven solution and the INS/DGPS-driven solution to be adsorbed. Results of the application of the extended model to a large scale block and a strip, each flown with two different systems, are discussed.

1 Introduction

Integrated orientation systems composed by an Inertial Measurement Unit (IMU) and GPS receivers allow direct georeferencing of images. DGPS supplies high precision position and velocity data (below-decimeter accuracies have been demonstrated in aircraft positioning even for large distances between *rover* and *master*); on the other hand, cycle slips in the carrier frequencies may cause accuracy degradation; besides, no accurate attitude information can be provided. An inertial navigation system determine position, velocity and attitude of the carrier thanks gyro and accelerometric measurements with rates up to 100-200 Hz; data accuracy nevertheless degrades quickly because time integration accumulates errors. With these complementary characteristics, their integration in a single system yields better overall precision and increased reliability, compare to the use of separate systems. Thanks to improved performance, a INS/DGPS can supply directly the exterior orientation elements of every image in a block: direct georeferencing with the required accuracy is possible but for the largest image scales and Aerial Triangulation is no longer necessary, claim the manufacturers.

As in GPS-assisted Aerial Triangulation, using an INS/DGPS requires a system calibration to account for the spatial offset beween the IMU and the camera as well as for the time offset, caused by lack of synchronization of the measurement epochs. The objective of the calibration is therefore a time synchronization for the interpolation of the IMU/DGPS navigation data to the middle exposure time of the images and the determination of the offset and misaligment of the IMU/DGPS system with respect to the image reference system.

Calibration parameters are most conveniently determined by carrying out a survey flight over a testfield: by comparing the EO parameter obtained by a bundle block adjustment and the IMU/DGPS data, the transformation parameters can be inferred. First experiences with such systems (Skaloud & Schwarz 1998; Cramer et al. 2000) show that there are correlations with the inner orientation parameters, particularly with the principal distance, which may result in biased estimates of the calibration parameters. From an operational standpoint, another question to be assessed is the time stability of the calibration data, to get hints on how often the calibration procedure should be repeated.

Within the OEEPE a test has been set up aiming to investigate these and other related issues (Heipke et al. 2000). The pilot centre, which coordinates data collection, data distribution to the participants and data analysis, is the Institute of Photogrammetry and Remote Sensing (IPI) of the Hannover University. The test objectives are twofold: to compare and evaluate different calibration procedures by verifying the empirical accuracy of the direct georeferencing and to highlight the advantages of a combined (photogrammetric and direct) determination of the OE parameters.

Figure 1 shows the flight paths of the two survey flights executed at the image scale 1:5000 and 1:10000 respectively over the Fredrikstad testfield (Norway) and devoted to the calibration phase; a third block, flown at the image scale 1:5000 was used in the verification of the calibration and in the combined adjustment (see §4).

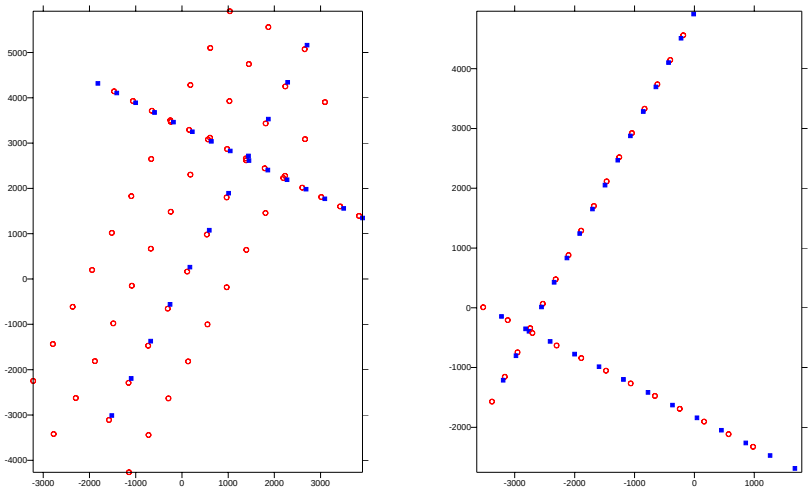

a) b)

Figure 1 – Sketch of the calibration flights: a) 1:10000, b) 1:5000.

Geometrically stable photogrammetric blocks; modern aerial cameras; dual frequency GPS receivers with 0.5 s measurement rate; ground station within a few km; high quality INS's; different image scales, suitable for large scale map production; a testfield with very dense control have been used. As far as the IMU/GPS manufacturers are concerned, Applanix (Canada) with its POS/AV 510-DG and IGI mbH (Germany) with its AEROcontrol II took part into the test.
In the testfield, approximately 5×6 km^2 wide, 51 signalized control points are available, with UTM/EUREF89 and ellipsoidal height determined to an accuracy of about 1 cm. Overall the flights, who took place on October the 7th, 1999 and were executed with 60% forward and side overlap using black and white images, amount to about 700 images.

2 Calibration of the INS/GPS systems

As discussed above, the sensors in the INS/DGPS and the camera are located in different (though possibly very close) positions and provide measured values in distinct reference systems at different times: a system calibration will provide the transformation parameters to relate IMU/GPS data directly to the EO elements of the images.
Calibration procedures have been presented in (Schwarz et al. 1993; Skaloud et al. 1994; Skaloud 1999); by executing a survey flight, the EO parameters obtained by a block adjustment can be compared with the GPS/INS positions and attitudes at the time each image was taken. The differences should be the same for every image of the block: by exploiting data redundancy an estimation process can be used to verify consistency and accuracy.
To this aim, a time interpolation of the IMU/DGPS data to the middle exposure time of each image is performed; accounting for aircraft speed, if sub-decimeter level accuracies are sought, synchronization errors should be kept below 1 ms, while measurement rates of 50 Hz or more are desirable to reduce interpolation errors. In the OEEPE test framework, all preprocessing of GPS and INS observations was performed by the two companies: for each image of the two blocks used for the calibration, the companies provided the position of the origin of the IMU reference system (named body system *b* hereafter) in UTM/EUREF89 and the rotation matrix from *b* to a local level system *l* (i.e. a cartesian frame tangent to the local level surface) interpolated at the nominal exposure time t of the image. The input data for the calibration procedure are therefore the image coordinates of tie and control points

measured for each block, the above mentioned INS/DGPS data and the ground coordinates of the control points in UTM/EUREF89.

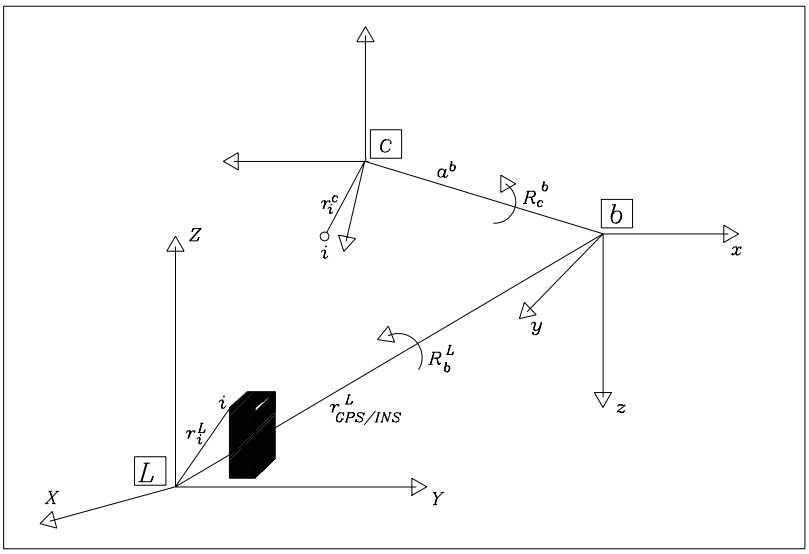

Figure 2 – The different reference systems involved in the calibration of a GPS/INS system

As far as the reference system for the block adjustment is concerned, the choice was up to the test participants; rather than the mapping frame UTM/EUREF89, a local cartesian frame L was chosen, with origin at a ground control point located approximately in the middle of the block, z axis positive upwards, along the ellipsoid normal, and x axis tangent to the parallel (eastwards). Performing the block adjustment in a truly cartesian frame rather than in map coordinates is in our opinion better, since no approximations or corrections need to be introduced to account e.g. for earth curvature.

2.1 Functional model for the calibration

The relation between the INS/DGPS preprocessed data and the EO parameters of the images can be inferred from the equation for the direct georeferencing, in the local frame L, of a point *i* measured in image *j* taken at time t:

$$\mathrm{r}_i^{\mathrm{L}} = \mathrm{R}_{\mathrm{G}}^{\mathrm{L}}\, \mathrm{r}_{\mathrm{INS/DGPS}}^{\mathrm{G}}(\mathrm{t}) + \mathrm{R}_{\mathrm{G}}^{\mathrm{L}}\, \mathrm{R}_l^{\mathrm{G}}(\mathrm{t})\, \mathrm{R}_b^l(\mathrm{t})\, [s_i^j\, \mathrm{R}_c^b \mathrm{r}_i^j + \mathrm{a}^b\,] \qquad (1)$$

where:

- $\mathrm{r}_i^{\mathrm{L}}$: position of point *i* in the ground reference system L;
- $\mathrm{R}_{\mathrm{G}}^{\mathrm{L}}$: rotation matrix from a geocentric reference system G to L;
- $\mathrm{r}_{\mathrm{INS/DGPS}}^{\mathrm{G}}(\mathrm{t})$: position of the origin of the IMU in G at time t, provided by the INS/DGPS;
- $\mathrm{R}_l^{\mathrm{G}}(\mathrm{t})$: rotation matrix from the local level system *l* to G at time t;
- $\mathrm{R}_b^l(\mathrm{t})$: rotation matrix from the body system *b* to local level system *l* at time t, provided by the INS/DGPS;
- R_c^b : rotation matrix from camera system (image coordinate system) *c* to body system *b*;
- r_i^j : image coordinates of point *i* in image *j*, taken at time t;
- $\mathrm{r}_j^{\mathrm{L}}$: position of the projection centre of image *j* in L;

- $s_i^j = \dfrac{\left|\mathrm{r}_i^j\right|}{\left|\mathrm{r}_i^{\mathrm{L}} - \mathrm{r}_j^{\mathrm{L}}\right|}$: scale factor for point *i* in image *j*;
- a^b : position (offset) of the projection centre in the *b* system.

Using two or more images, the object coordinates of *i* can be determined, provided the calibration elements, i.e. the rotation matrix R_c^b and the offset vector $\mathbf{a}^b$ in the body system, which are image- (and time-) independent, are known. For calibration purposes, we notice that R_c^b may be decomposed as follows:

$$R_c^b = R_c^L(t)\, R_L^G\, R_G^l(t)\, R_l^b(t) \qquad (2)$$

where:
$R_c^L(t)$ = rotation matrix from camera system *c* to L at time t;
R_L^G = rotation matrix from L to the geocentric reference system G (EUREF89);
$R_G^l(t)$ = rotation matrix from G to local level system *l*;
$R_l^b(t)$ = rotation matrix from *l* to body system *b*.

Matrices R_L^G and $R_G^l(t)$ are simple functions of the geodetic coordinates of the origin of L and of the projection centres; more exactly, since the local level system is sensitive to the gravity field, the rotation matrices $R_G^l(t)$ are a function of the astronomic coordinates. If there are not strong variations of the gravity field in the block area, though, geodetic coordinates may be used instead. $R_c^L(t)$ is simply the attitude matrix of image *j*, taken a time t, obtained by the bundle block adjustment.
As far as the vector $\mathbf{a}^b$ is concerned, we may compute it as follows:

$$\mathbf{a}^b = R_L^b(t)\, \mathbf{a}^L(t) = R_l^b(t)\, R_G^l(t)\, R_L^G\, \mathbf{a}^L(t) \qquad (3)$$

where:
$\mathbf{a}^L(t) = R_G^L\, r_{INS/DGPS}^G(t) - r_j^L(t)$ is the offset vector in L;
$r_j^L(t)$ is the position of the projection centre of image *j*, determined by the bundle block adjustment.

Equations (2) and (3) are therefore the base of the calibration procedure: for each image *j* of the calibration blocks, the 3 components of the offset vector and the 3 misalignment angles ω, ϕ, κ defining the matrix R_c^b have been computed. To get a proper estimation for each calibration parameter, we should account for the accuracy of the INS/DGPS data as well as for the accuracy of the AT. Since no information was available for the former, only AT results have been used to get a weighted average of $a_x, a_y, a_z, \omega, \phi, \kappa$; the weights are derived from the standard deviations of the EO parameters estimated in the AT. This should yield a more consistent result, since whenever block geometry is weaker (e.g. on the border strips) the EO elements, which may be biased and poorly determined, will count less for the determination of the parameters. For the time being, correlations between EO elements arising from block adjustment have been neglected.

2.2 Calibration results

In a first stage, every block of the two companies has been adjusted separately (Block10_1/2 and Block5_1/2 for image scale 1:10000 and 1:5000 respectively), leading to two estimates for each calibration parameter. Then, a combined adjustment of the 1:5000 and 1:10000 blocks has been performed (Block_1/2), which should properly combine all photogrammetric information available, taking advantage of the better precision of the 1:5000 block as far as projection centres are concerned and of the better precision of the 1:10000 block for the attitude. Table 1 shows the accuracies of the EO elements from the adjustments, for the two companies. Sigma naught is much the same for 1:5000 and 1:10000 but is smaller for Company_1's blocks; so are the standard deviations of the EO parameters.

		RMS(St.dev) EO					
	σ_0	X_0	Y_0	Z_0	ω	ϕ	κ
	[μm]	[mm]			[10^{-4} gon]		
Block 10_1	4.2	81	88	55	32.3	28.1	12.3
Block 5_1	4.4	57	57	46	39.5	39.1	16.3
Block 10_2	5.9	112	116	78	43.2	39.9	16.7
Block 5_2	5.9	84	83	73	59.5	60.4	24.6
Block_1	4.3	69	73	47	32.8	30.2	13.1
Block_2	5.9	96	97	69	47.5	47.5	19.3

Table 1 – Accuracy of the AT (σ_0 and EO) for the calibration blocks

COMPANY_1	BLOCK 10_1		BLOCK 5_1		BLOCK 1	
	Mean	St. Dev	Mean	St. Dev	Mean	St. Dev
a_x (m)	0.065	0.022	0.066	0.028	0.064	0.061
a_y (m)	0.114	0.020	0.064	0.027	0.082	0.058
a_z (m)	0.258	0.084	0.080	0.108	0.154	0.289
dω (deg)	180.0904	0.0005	180.0924	0.0006	180.0910	0.0004
dϕ (deg)	0.0092	0.0009	0.0083	0.0008	0.0089	0.0006
dκ (deg)	-0.0602	0.0009	-0.0596	0.0007	-0.0600	0.0007

Table 2 – Company_1: calibration parameters and their accuracy.

COMPANY_2	BLOCK 10_2		BLOCK 5_2		BLOCK 2	
	Mean	St. Dev	Mean	St. Dev	Mean	St. Dev
a_x (m)	-0.145	0.013	-0.109	0.015	-0.125	0.032
a_y (m)	0.300	0.011	0.123	0.015	0.199	0.030
a_z (m)	-0.154	0.044	-0.137	0.061	-0.140	0.131
dω (deg)	180.1143	0.0004	180.1175	0.0010	180.1152	0.0004
dϕ (deg)	-0.0543	0.0005	-0.0524	0.0007	-0.0538	0.0004
dκ (deg)	-179.8236	0.0005	-179.8208	0.0013	-179.8228	0.0005

Table 3 – Company_2: calibration parameters and their accuracy

Table 2 and 3 show the results of the calibration for Company_1 and Company_2 respectively. As far as the offset is concerned, the a_x and a_y components show an astonishing consistency (dispersion is less than 1.5 cm for Company_2) while for a_z the dispersion is 4 times larger. Nevertheless, the mean value of the component may differ markedly between the two blocks (up to 16 cm in a_z for Company_1) possibly hinting systematic differences whose origin is hard to attribute, since it may depends on photogrammetry as well as on the INS/DGPS. With the exception of the a_z component for

Company_1, these differences are smaller than the accuracy of the EO elements they depend on; still it looks as if the 1:5000 and 1:10000 blocks would “see” a different offset (vector magnitude for Company_1 amounts to about 12 cm Block 5_1 nd to about 29 cm in Block 10_1; to 21 cm and 37 cm respectively for Company_2). This is reflected somehow in the standard deviations of the combined solutions, which exhibit a dispersion considerably larger, because of the differences in mean.
Attitude angles behave more or less the same way as the offsets, as far as differences between mean values are concerned, but seem to tell a slightly different story with respect to the combined solution: the dispersion (internal consistency) of the differences is in fact better than that of each individual block, hinting that there is really an overall improvement by using the combined solution.

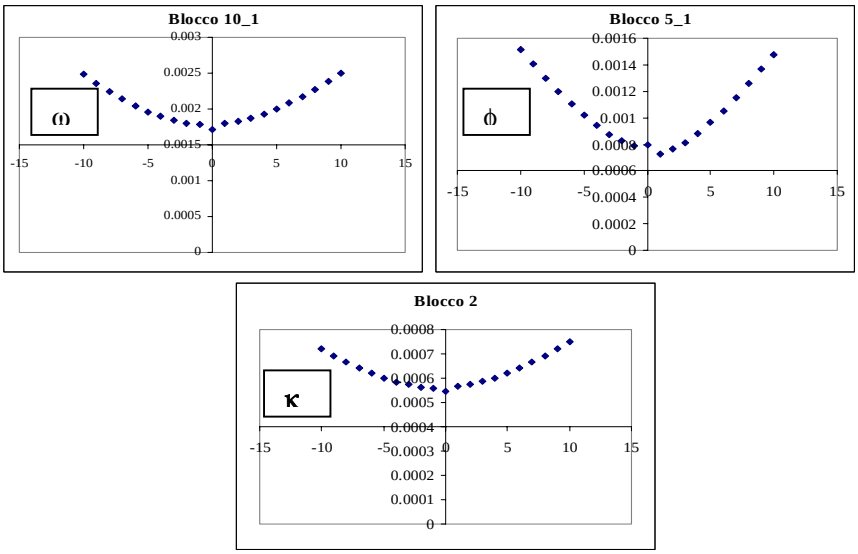

Figure 3 – The st.dev of the misalignment angles as a function of the synchronization offset

In a last calibration stage, we tried to highlight a possible residual synchronization error between the camera release time and the INS/DGPS (Skaloud, 1999). To this aim the rotation matrix R_c^b has been computed by evaluating $R_l^b(t)$ within an interval of 200 ms, symmetric around the nominal exposure time. The IMU angles have been interpolated linearly between the acquisition time of two images with a step of 10ms and the corresponding image attitude angles solved back from the matrices. For each angle, the average value has been computed by the weighted mean described above; if the minimum values of the dispersion of the estimates ω, ϕ, κ (a graphic representation for one of the blocks is shown in Figure 3) does not falls at 0 shift from the nominal time, there is a residual synchronization error. This was (almost) never the case, so the final calibration values of Table 2 and 3 actually refere to the middle exposure time provided with the INS/DGPS data. The lack of evidence in the outcome does not rule out, anyway, a possible small error, because using only data at middle exposure time of the images undermine the sensitivity of the procedure. By using original INS data a much denser sample would be available, thus allowing to focus on a narrower interval around the nominal time with time steps down to e.g. 1 ms, making the error from the linear interpolation negligible. Besides, the offset components may be used as well in the estimation of the synchronization error.

3. Evaluation of the calibration

A full evaluation of the calibration results and of the overall system accuracy on the ground will be performed by the pilot centre, in two ways. First, the coordinates of the ground check points obtained by GPS measurement will be compared with those coming from direct georeferencing by forward intersection from the images of the blocks used in the calibration, whose EO have been derived by INS/DGPS and calibration data. The same procedure will be applied to a new group of test images (a block and a strip, for which only image coordinates have been provided), providing ground coordinates from EO elements independent of calibration. Furthermore, these data will be used to compute the combined adjustment of INS/DGPS data and photogrammetric observations (see §4).

To have at least some sort of check on the calibration, we computed the object coordinates of the points measured in the calibration blocks by forward intersection, i.e. fixing the EO of all images to the values computed by calibration and setting free the GCP used to control the calibration block. Table 5 shows the results of the block adjustment in terms of sigma naught and of the RMS of the changes in the coordinates of the GCP. While σ_0 as expected increases (more for Company_1 than for Company_2) the magnitude of the changes to the coordinates, in absolute terms as well as relative to their accuracy, is quite acceptable, sometimes very small. Since the calibration results may depend to some extent on the GCP, a second series of calibrations was repeated, using fewer control points in the adjustments and computing the differences only for "true" check points; the RMSs remain fairly the same.

Block	σ_0	# GCP	RMS(Δ) GCP		
	[μm]		X [m]	Y [m]	Z [m]
Block 10_1	13.2	13	0.078	0.120	0.208
Block 5_1	11.0	12	0.033	0.082	0.064
Block 10_2	8.8	13	0.092	0.062	0.077
Block 5_2	15.3	12	0.055	0.031	0.058
Block 1	12.6	20	0.036	0.090	0.104
Block 2	14.2	20	0.103	0.055	0.073

Table 5 – Accuracy of the Forward Intersection (σ_0 and RMS on GCP) for the calibration blocks.

3.1 Forward intersection with the test blocks

A forward intersection has also been performed with the data of the 2nd test phase (image coordinates and INS/DGPS data) and the calibration parameters (see §4 for data description). Here no reference for the ground coordinates of the image points is provided, so only the increase of sigma naught with respect to a free net solution and the standard deviations can be computed (see Table 6).

		RMS (st.dev) tie points		
Block	$\sigma_{0(fw)}/\sigma_{0(free)}$	X [m]	Y [m]	Z [m]
Block 1	5.1	0.112	0.104	0.220
Block 2	3.1	0.051	0.050	0.101
Strip 1	2.9	0.061	0.051	0.119
Strip 2	3.4	0.079	0.063	0.151

Table 6 – Accuracy of the Forward Intersection (σ_0 and RMS) for the test blocks

In addition, residuals of the collinearity equations, particularly for multi-ray points, may show inconsistencies. In Block 1, which has the highest increase in sigma naught, several images of the cross strip show large standardized residuals; in Block 2 a border image has many as well: this is

likely to come not from photogrammetric observation errors, but from the INS/DGPS data. Strip 1 and 2 do not show any suspicious residual.
Although the results, at least for Block 1 and 2, clearly need some further editing, e.g. setting freesome EO of the images with large residuals, we kept the object coordinates as they were obtained. Lacking true reference values, we used these coordinates as reference for the combined adjustment, to highlight the differences of the ground with respect to a “blind” forward intersection.

4. Combined adjustment of the INS/DGPS data and AT

As mentioned in the introduction, the second test phase is devoted to the study of the mutual support of AT and INS/DGPS, through the combined adjustment of photogrammetric and INS/DGPS data. This second series of adjustments is performed on a 1:5000 image scale and on a 1:5000 single strip (see Fig. 4); only image coordinates and INS/DGPS data have been provided. Though at a first sight contradictory with the very purpose of integrated orientation systems, which is direct georeferencing, a combined adjustment may help to improve reliability issues, mainly those connected to possible systematic errors, which may be hard to detect otherwise.

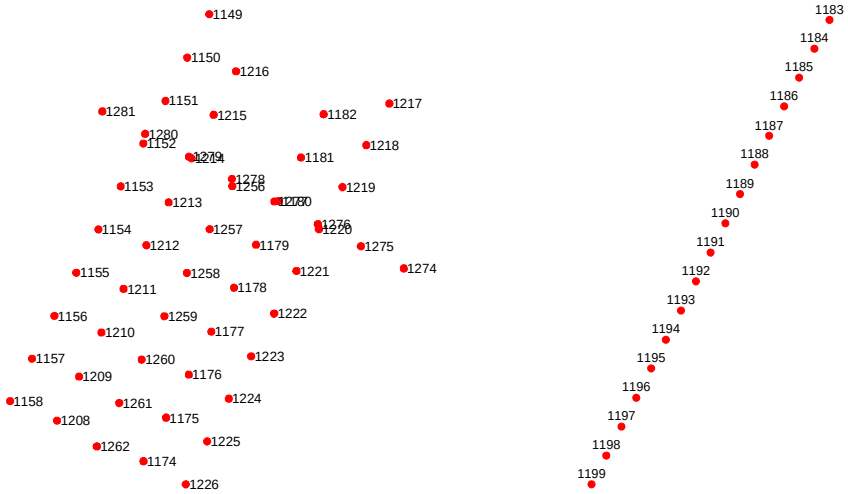

Figure 4 – The test block and the strip used in the combined adjustments

Extending the functional model of the bundle block adjustment with pseudo-observation equations of the calibrated EO parameters measured by the INS/DGPS, a combined solution can be derived. Since the INS/DGPS-derived EO come from a preprocessing stage, they are in fact correlated values; if available, at least the 6x6 covariance matrix of each image should be included. Though it deserves attention, this point was not further investigated, because of lack of information on the pre-processing. In the test we therefore proceeded by assigning uncertainties to position and attitude data based on the system specification provided by the manufacturer and on the results of the calibration. This approach to the combined adjustment is inherently more flexible than simple forward intersection and should allow to identify inconsistencies in the orientation data, which should not spread into the image coordinates or bias the ground coordinates.
As a preliminary step, in order to assign the accuracy of the photogrammetric observations, the blocks have been adjusted with minimum constraint, with a weight reproduction technique.

Accuracies of 5 cm were assigned to projection centres positions; as far as attitude angles are concerned, 10 arc seconds were assigned to ω and ϕ, 15 arc seconds to κ.
By setting free the orientation values whose standardized residuals would be rejected by data snooping, σ_0 become consistent with that of the minimum constraint adjustment; overall, results show an increase in the accuracy of the ground coordinates of the tie points with respect to the forward intersection by a factor of about 2.
In Block 1 systematic strip-dependent components, mainly in the attitude, show up in the residuals of the pseudo-observation equations of two strips. For the image at the end of the cross strip, all residual are very large: this look therefore as a gross-error in all IMU/GPS data (or at least so with respect to photogrammetry). In Block 2, the k angle of aborder image has a standardized residual larger than 7: once removed, no significant systematic pattern can be observed. As far as the strips are concerned, relatively large standardized residuals show up at the end of the strip. Removing them, anyway, does not solve the problem: residuals go up in the next image.

4.1 The extended model for the pseudo-observation equations

Direct pseudo-observation equation of the EO parameters, though effective in revealing inconsistencies between photogrammetry and INU/GPS data, are not very flexible, since they can only properly cope with gross errors. The functional model, in analogy with that of the GPS-assisted AT (Forlani, Pinto, 1994), has been extended introducing a linear drift term, dependent on an ordering parameter such as time or distance along the strip, for each EO component. This may adsorb at least part of possible bias of the GPS solution coming from errors in fixing the ambiguity and maybe a time-dependent drift of the INS solution.
The adopted functional model is therefore made of the collinearity equations and of the following equations:

$$X_{INS/DGPS} = X_{PC} + TX_{Strip} + aX\ A_{Strip} \qquad \sigma(X_{INS/DGPS})$$
$$Y_{INS/DGPS} = Y_{PC} + TY_{Strip} + aY\ A_{Strip} \qquad \sigma(Y_{INS/DGPS})$$
$$Z_{INS/DGPS} = Z_{PC} + TZ_{Strip} + aZ\ A_{Strip} \qquad \sigma(Z_{INS/DGPS})$$
$$\omega_{INS/DGPS} = \omega_{PC} + D\omega_{Strip} + a\omega\ A_{Strip} \qquad \sigma(\omega_{INS/DGPS})$$
$$\phi_{INS/DGPS} = \phi_{PC} + D\phi_{Strip} + a\phi\ A_{Strip} \qquad \sigma(\phi_{INS/DGPS})$$
$$\kappa_{INS/DGPS} = \kappa_{PC} + D\kappa_{Strip} + a\kappa\ A_{Strip} \qquad \sigma(\kappa_{INS/DGPS})$$

where:
$X,Y,Z,\omega,\phi,\kappa_{INS/DGPS}$ = pseudo-observed values of the E.O. parameters of each image, measured by the INS/DGPS data and corrected with the calibration parameters;
$X,Y,Z,\omega,\phi,\kappa_{PC}$ = E.O. parameters of the block images
$TX,TY,TZ,D\omega,D\phi,D\kappa_{Strip}$ = terms modeling possible offsets of the INS/DGPS data with respect to the position and attitude of the images as determined by the photogrammetric block structure;
A_{strip} = an ordering parameter of the images along the strip (e.g. exposure time or abscissa along the strip)
$aX,aY,aZ,a\omega,a\phi,a\kappa$ = the coefficients of the linear term of the trend, for each EO parameter;

$\sigma(X,Y,Z,\omega,\phi,\kappa_{INS/DGPS})$ = the accuracy of each pseudo-observed value

Introducing new equations and additional parameters a rank deficiency analysis is to be performed, to avoid singularities or ill-conditioning in the normal system. If no shift or drift parameters are used, the rank deficiency of the collinearity equations is filled by the pseudo-observevations; since they carry some uncertainty, there is a low amount of ill-conditioning. It was therefore decided, since no INS/DGPS observation is in principle better than any other, to use a minimum norm constraint on the X,Y,Z coordinates of the projection centres, independently of the number and type of additional parameters. As far as the 3 shift on TX, TY, TZ are concerned, each introduces a rank deficiency in a

single strip; the same applies to a block, even if strip-wise parameters have been used, because the ties between strips make up for that. As far as attitude angles are concerned, there is ill-conditioning due to poor control of the rotation along the strip direction. This can be seen in Strip 1 and 2, which are oriented NE-SW: when either Dω or Dϕ are introduced, there is no ill-conditioning; if both are used, ill-conditioning is significant (Dω or Dϕ are correlated 100%) and this also affect the XY ground coordinates of the tie points. Using Dκ in single strips or blocks does not introduce ill-conditioning.

4.2 Strategy for the combined block adjustment

Three main issues where dealt with in the combined block adjustment: the selection of weights for the different observations, the rejection of outliers, the significance of additional parameters. Lacking the reference coordinates of tie points, the comparison is based on the consistency of the two datasets measured by sigma naught, by the estimated standard deviations of the object coordinates and on the changes to the coordinates computed by forward intersection.
As mentioned before, in order to assign weights to the observations in the combined block adjustment, first every block or strip of the two Companies has been adjusted, by using the collinearity equations only, with minimal constraint (fixing 7 parameters only). With a weight reproduction technique, an estimate of the empirical accuracy of the photogrammetric observations has been computed.
As far as the accuracies of the INS/DGPS parameters are concerned, 5 cm were assigned to projection centres positions, 10 arc seconds to ω and ϕ, 15 arc seconds to κ.
In a first series of adjustments, no additional (stripwise) parameter have been introduced; the results are the same as those already described using only the “reduced” pseudo-observation equations.
In a second stage the additional parameters were introduced. Only offsets have been introduced, based on the pattern of the residuals. As a rule, only those who proved to be significant have been retained. Results with and without additional parameters are summarized in Table 7.
With respect to the forward solution, the coordinates of the objects points change by up to 6 cm on average and from 5 to 10 cm in dispersion. Overall, the changes are relevant though not significant in average with respect to the accuracy of the object coordinates. Testing the significance of the change for each coordinate, though, we find that 51% of X, 41% of Y and 29% of Z coordinates has changed in Block1, 53% of the X coordinates has changed in Block2, 22% of the Y coordinates has changed in Strip1, 47% of the Y coordinates has changed in Strip2. Plotting the spatial distribution of the changes show locally systematic patterns. Whether these changes actually improve the precision of the object coordinates cannot be claimed without reference values. The use of additional parameters does anyway improve some other quality measure or statistics of the block adjustment. The estimated accuracy of the object points, with respect to the solution without offset parameters, improves slightly on average, while the maximum standard deviations (the worst determined coordinate) improves by about 10%. While this is not the case for all blocks in the forward intersection, the residuals of the collinearity equations all get 0 mean; their st. dev. again with respect to the forward intersection, decreases by a factor from 2 to 6. Moreover, analysing the differences between the ground coordinates of the block obtained by forward intersection with the Companies, we find that the RMS amount to 20 cm, while it drops to 12 cm between the two combined solutions.
Since the actual precision of the INS/DGPS data is not easy to evaluate, an attempt has been made to estimate it with a weight reproduction technique. This affects the significance of the offset parameters and leads to very optimistic values (too optimistic!) for the accuracies of the measured orientation:
therefore the initial accuracies were maintained. Anyway the solution, in terms of object coordinates, does not look too sensitive to changes in the INS/DGPS accuracy values, at least for the blocks; shift in average amount to just a few mm, even less in dispersion even setting the accuracy of projection centres to 20 mm and of ω and ϕ to 10 arc seconds. The same changes in accuracy for the strip lead to variations of the mean up to 5 cm.

Block	Add. param.		Diff. to FW (mm)		Estimated st.dev. (mm)	
			Mean	St.dev.	RMS	MAX
Block 1	NO	X	-1	101	31	197
		Y	-23	92	31	219
		Z	5	109	60	494
	YES	X	-17	100	30	180
		Y	-26	89	30	200
		Z	-9	120	56	445
Block 2	NO	X	-22	63	30	86
		Y	2	48	30	87
		Z	10	91	54	105
	YES	X	-63	58	31	85
		Y	6	49	30	86
		Z	7	89	54	104
Strip 1	NO	X	7	51	35	72
		Y	15	47	32	64
		Z	14	69	55	80
	YES	X	6	50	33	69
		Y	16	57	31	61
		Z	14	68	52	76
Strip 2	NO	X	-6	80	54	110
		Y	-55	101	49	112
		Z	-3	79	84	125
	YES	X	6	63	48	100
		Y	-85	79	43	99
		Z	-4	75	79	119

Table 7 – Results of the combined adjustment with and without additional parameters.

5 Conclusions

A calibration procedure for integrated orientation systems has been presented, where the discrepancies between the EO of the calibration block and the INS/DGPS data are weighted according to the accuracy of the EO elements, and its application to different blocks discussed. From the (admittedly little) set of reference points, the weighting seems to be effective; an extension of the method would be possible if more details about the processing of the orientation data were available (i.e. the attitude parameters from INS with rate of 50 Hz in order to investigate a possible time shift).
The benefits of the mutual support of photogrammetric observations and of the position and orientation data has been investigated, to highlight improvements in the accuracy of the georeferentiation and in the reliability of the system. An extended model for the combined adjustment has been presented and its application to a test and a strip block discussed. A more complete answer to the worthiness of integrating AT and orientation data may only come from the comparison with ground reference data: for the time being, some preliminary conclusion can be drawn and some guessing is possible. It seems that an improvement in accuracy (estimated st.dev of object coordinates) can actually be achieved and that it may be significant (we found improvements by a factor 2). As far as reliability is concerned, the use of the extended model proved effective in adsorbing gross and

systematic discrepancies between the photogrammetric solution and the navigation solution. If this actually improve the precision of the object coordinates cannot be claimed without reference values.
Overall, as already assessed in previous experiences, integrated orientation system show an impressive performance and will certainly see their use to increase dramatically; proper processing of the navigation data and a good GPS satellite configuration are anyway crucial. The question of reliability, therefore, still remain open. Commercial companies would probably resist performing a combined adjustment with AT, because avoiding AT is the very reason they may be willing to buy such systems.It is apparent, though, that only AT (either followed by a block adjustment with fixed EO or, better, by a combined adjustment) can highlight systematic errors. A compromise solution for photogrammetric blocks may be perhaps to fly one (or two) additional cross strip and verify the inner consistency of the navigation data by computing, by forward intersection, a significant number of object coordinates located in the cross strip, where redundancy is higher. For single strips, though, there seems to be little alternative to flying again all or part of the strip.

References

Cramer M., Stallmann D., Haala N. (2000): *Direct georeferencing using GPS/INS exterior orientation for photogrammetric applications*. In: Int. Arch. of Photogrammetry and Remote Sensing, Vol. 33, Part B3/1, 198-205.

Forlani G., Pinto L. (1994). *Experiences of combined block adjustment with GPS data*. Int. Archives of Photogrammetry and Remote Sensing, Vol. 30 Part 3/1, Muenchen, 219-226.

Heipke C., Jacobsen K., Wegmann H., Andersen Ø., Nilsen B. (2000) - *Integrated Sensor Orientation – an OEEPE Test*. In: Int. Arch.of Photogrammetry and Remote Sensing, Vol. 33, Part B3/1, Amsterdam, 373-380.

Schwarz K.P., Chapman M.A. Cannon M.W. Gong P. (1993) - *An Integrated* INS/GPS *Approch to the Georeferencing of Remotely Sensed Data*. In: Photogrammetric Engineering & Remote sensing, Vol. 59, No. 11, 1667-1674.

Skaloud J., Consandier D., Schwarz K.P., Chapman M.A. (1994) - *GPS/INS Orientation Accuracy Derived From A Medium Scale Photogrammetry Test*. In: International Symposium on Kinematic Systems in Geodesy, Geomatics and Navigation – KIS 94, Banff, Alberta, Canada, 30 August – 2 September, 341-348.

Skaloud J., Schwarz K.-P. (1998): Accurate orientation for airborne mapping systems, In: Int. Arch. of Photogrammetry and Remote Sensing, Vol. 32, Part B2, 283-290.

Skaloud, J. (1999) - *Optimizing georeferencing of airborne survey systems by INS/DGPS* - PhD Thesis, Dept. of Geomatics Eng., The University of Calgary, Calgary.

THE OEEPE-TEST 'INTEGRATED SENSOR ORIENTATION' AND ITS HANDLING WITHIN THE HYBRID BLOCK-ADJUSTMENT PROGRAM ORIENT

Camillo Ressl
Institute of Photogrammetry and Remote Sensing
University of Technology, Vienna
car@ipf.tuwien.ac.at

Abstract

In this paper we present the experiences we made as participants in the OEEPE test 'Integrated Sensor Orientation' by using the hybrid block-adjustment program ORIENT. For the calibration phase of this test we will explain the parameter model chosen for the calibration of the participating GPS/IMU systems. The calibration was carried out in the UTM system as well as in a Cartesian tangential system. The differences in the results in these two systems will be examined. During the application phase (1:5.000, 150 mm) direct georeferencing (with fixed exterior orientation) and a combined bundle block were performed and then the intersected tie points were compared, yielding approx. 6 cm in plane and 11 cm in height (s.d.), which is better than one would deduce by comparing the corresponding σ_0 (17 vs. 6 (µm/image)). One problem with GPS/IMU data is their reliability, which also showed up during this test in one gross error and discontinuous changes in the misalignment.

1. Introduction

The first and most important step for doing object reconstruction with a set of (aerial) photographs is image orientation; i.e. the determination of the images exterior orientation (XOR). The interior orientation (IOR) is generally given by means of the protocol of a labor calibration. Up to now this orientation is generally done in an 'indirect' way by means of an aerial triangulation (AT) using control and tie points and their observations in the images. In the last few years another – more 'direct' – way for image orientation, by means of the Global Positioning System (GPS) and some Inertial Navigation System (INS) (resp. a Inertial Measurement Unit (IMU)), has been developed. This also termed *integrated sensor orientation* has lots of benefits for Photogrammetry which can result in a large temporal (= financial) gain; (Colomina 1999), (Cramer 2000):

- Theoretically, no control and tie points are required
- Free block geometry
- Reduction of the number of images
- Image interpretation does not require full block triangulation
- Support for matching during automatic aerial triangulation

Besides that, there are also some potential error sources. 'These include the Kalman filtering of the GPS/IMU data for noise reduction, the determination of parameters for systematic position and attitude corrections of the GPS/IMU data, the stability of these parameters over time, especially the stability of the attitude values between the IMU and the camera (the so-called *misalignment*), the time synchronization between the various sensors, issues related to the correlation between the interior and the exterior orientation parameters of the imagery, and the quality of the resulting exterior orientation parameters for subsequent stereoscopic plotting' (Heipke et al. 2000).

To investigate the potential of integrated sensor orientation, the European Organization for Experimental Photogrammetric Research (OEEPE) has initiated a large test in the year of 2000. 'The test is expected to demonstrate to which extent integrated sensor orientation using GPS and IMU with and without aerial triangulation is an accurate and efficient method for the determination of the exterior orientation parameters for large scale topographic mapping' (Heipke et al. 2000). The test is

carried out with two different GPS/IMU systems. One is the system AeroControl II of IGI mbH from Hilchenbach, Germany, with a Zeiss RMK Top camera (termed as *Comp1*). The other one is the system POS/AVC 510 DG from Applanix of Toronto, Canada, with a Leica RC 30 camera (termed as *Comp2*). The principal distance of both *analog* cameras is approximately 150 mm.

As test field the one of Fredrikstad, Norway, was chosen. It measures approximately 5 x 6 km^2 and is equipped with 52 well distributed ground control points. The test was split into two phases: Phase 1 was the 'calibration phase', during which two calibration flights for each company in the scales 1:5.000 and 1:10.000 were to be handled. In phase 2 another flight in the scale 1:5.000 (termed as *test flight*) was to be handled with the aim to apply the system parameters determined in phase 1 to this flight and perform a) direct georeferencing and b) a combined AT. All three flights (starting with the two calibration flights) were performed for each company on the same day in October 1999.

Each company processed their own GPS/IMU data.[1] The image measurements (ground control and tie points) were performed using analytical plotters by the Institute for Photogrammetry and GeoInformation (IPI), Hannover, which also acted as a pilot center for the OEEPE test. For each phase, different data were delivered to the test participants and different tasks were to be performed by them. One of these test participants was the Institute of Photogrammetry and Remote Sensing (I.P.F.), Vienna, and in the following it will be presented, how the tasks of this test can be solved using the hybrid block adjustment program ORIENT (Kager 1989), which has been developed at the I.P.F.

2. ORIENT and its functional model[2]

The hybrid bundle block adjustment program ORIENT is written in FORTRAN and has been developed at the I.P.F. for more than 20 years (Kager 1989). The term *hybrid* means that ORIENT offers the possibility to simultaneously adjust different kinds of observations by least squares:

- perspective image (frame) coordinates
- coordinates of push and whisk broom scanners (of 1 or 3 lines)
- Synthetic Aperture Radar image coordinates
- control points
- model coordinates
- geodetic (polar) measurements (e.g. tachymeter observations)
- fictitious observations: points belonging to planes or to polynomial surfaces
- fictitious observations: points belonging to straight lines, circles, or to any intersecting curve of two polynomial surfaces
- fictitious observations: points belonging to 3D spline curves
- observed mapping parameters (e.g. projection center or rotational parameters of an image)

Adjustment is based on the Gauss-Markoff-Model – also known as *adjustment by indirect observations*. ORIENT assumes the observations to be uncorrelated. Additionally, ORIENT offers two blunder detection techniques :

- Robust estimation by iterative re-weighting of observations (using a-priori normalized residuals)
- Data snooping (using a-posteriori normalized residuals)

---

[1] Comp1 discovered a mistake in their data processing and therefore made a 2nd data processing (Heipke et al. 2001), which was delivered to the test participants *after* the end of phase 1. This data will be termed '*Comp1b'* in the following and the 1st processed data will be termed '*Comp1a*'.

[2] This chapter is entirely based on the ORIENT introduction as given in (Rottensteiner 2001).

Since the observations' weighting depends on their (a-priori) accuracies, ORIENT has included the technique of *variance components analysis* (VCA) to check the plausibility of the a-priori accuracies.

The mathematical model of adjustment in ORIENT is based on a very strict concept in using basically the same mapping function for all types of observations (except for the 3D splines). This mapping function expresses the relation between the above mentioned observations and the unknowns (i.e. object points and mapping parameters). Since the observations are made in a 3D Cartesian *observation* coordinate system (*u, v, w*) and the unknown object points are to be determined in a 3D Cartesian *object* coordinate system (*X, Y, Z*), this mapping function is the transformation (depending on the mapping parameters) between these two coordinate systems. The basic formula for this transformation is the spatial similarity transformation. In ORIENT it is formulated in the following way:

$$\mathbf{p} - \mathbf{p_0}(\mathbf{a}) = \lambda \cdot \mathbf{R}^{\mathbf{T}}(\boldsymbol{\Theta}) \cdot (\mathbf{P} - \mathbf{P_0}) \tag{1}$$

with

$\mathbf{p} = (u, v, w)^T$: the *observed* point

$\mathbf{p_0} = (u_0, v_0, w_0)^T$: the interior reference point

$\mathbf{a}$: additional parameters modifying the interior reference point (e.g. camera distortion)

λ : the scale factor between observation and object coordinate system

$\mathbf{R}(\boldsymbol{\Theta})$: a 3×3 rotational matrix parameterized by three rotational angles $\boldsymbol{\Theta}$, like (Roll, Pitch, Yaw)[3]

$\mathbf{P} = (X, Y, Z)^T$: the object point corresponding to $\mathbf{p}$

$\mathbf{P_0} = (X_0, Y_0, Z_0)^T$: the exterior reference point

The mapping parameters are made of $\mathbf{p_0}$, $\mathbf{a}$, λ, $\boldsymbol{\Theta}$ and $\mathbf{P_0}$. All of these parameters may be determined in the adjustment. Basically, these groups of parameters appear in the mapping functions of all observations types, but they might obtain different interpretations and/or be given constant default values. It shall be emphasized that it is possible to

1. keep single groups of parameters fixed for *each* observation type,
2. declare several observation coordinate systems to share groups of mapping parameters (e.g., two perspectives may be declared to have the same rotational parameters if the photos were made using a stereo camera) without having to formulate condition equations, just by manipulating the data base.
3. Declare groups of parameters constant for *individual* observation coordinate systems.

All data in ORIENT are stored in so-called *rooms*, which are uniquely defined by their types and identifiers: the observations are stored in *observation rooms* (e.g. PHOTO rooms, MODEL rooms or SPLINE rooms) and the mapping parameters are stored in *parameter rooms* (e.g. ROT rooms, SCALE rooms, IOR room or APDAR rooms). All rooms that are necessary to describe a particular type of observation in ORIENT are addressed by reference using the identifiers.

If we now stick explicitly to the problem of integrated sensor orientation, the following types of observations occur:

- perspective image (frame) coordinates

  For this kind of observations, considering equation (1), $w \equiv 0$; (u_0, v_0, w_0) is made of the principal point (u_{pp}, v_{pp}) and principal distance f; and λ varies from one image point to another (it is pre-eliminated by dividing the first two equations by the third, this way yielding the well known formula of the perspective transformation[4]). Explicitly, $\mathbf{p_0}(\mathbf{a})$

[3] The definition of Roll, Pitch and Yaw in ORIENT differs from ARINC 705 in the following way: $\text{Roll}_{\text{Orient}} = \text{Roll}_{\text{ARINC 705}}$, $\text{Pitch}_{\text{Orient}} = -\text{Pitch}_{\text{ARINC 705}}$, $\text{Yaw}_{\text{Orient}} = 100^{\text{gon}} - \text{Yaw}_{\text{ARINC 705}}$.

[4] See e. g. (Kraus 1997), which also gives a general introduction to the topic of bundle block adjustment.

means $u_0 = u_{pp} + \Sigma a_i \cdot du_{0,i}(u', v')$, $v_0 = v_{pp} + \Sigma a_i \cdot dv_{0,i}(u', v')$ and $w_0 = f + \Sigma a_i \cdot dw_{0,i}(u', v')$. $u' = \frac{u - u_{pp}}{\rho_0}$ and $v' = \frac{v - v_{pp}}{\rho_0}$ are normalized image coordinates and ρ_0 is a normalization radius. In this way the modification of the interior reference point (e.g. the camera distortion) is described by the sum of polynomial functions $du_{0,i}$, $dv_{0,i}$ and $dw_{0,i}$ of the reduced image coordinates. For each index i there is such a set of functions and a_i is the corresponding additional (e.g. distortion) parameter. Table 1 gives the parameters a_i which were used in the OEEPE test together with the corresponding functions $du_{0,i}$, $dv_{0,i}$ and $dw_{0,i}$ and a geometrical interpretation. As it was already mentioned, additional parameters are stored in ADPAR-rooms.

i	**$du_{0,i}(u', v')$**	**$dv_{0,i}(u', v')$**	**$dw_{0,i}(u', v')$**	**Geometric interpretation**
3	$u' \cdot (r^2-1)$	$v' \cdot (r^2-1)$	0	Radial distortion; 3rd degree
5	$r^2+2 \cdot u'^2$	$2 \cdot u' \cdot v'$	0	Tangential (asymmetric) distortion
6	$2 \cdot u' \cdot v'$	$r^2+2 \cdot v'^2$	0	Tangential (asymmetric) distortion
41	1	0	0	Interior GPS excenter[5]
42	0	1	0	Interior GPS excenter
43	0	0	1	Interior GPS excenter

Table 1: Some of the additional parameters in ORIENT ($r^2 = u'^2 + v'^2$).

- ground control points

  For this kind of observations, considering equation (1), $\mathbf{p_0}(\mathbf{a})$ and $\mathbf{P_0}$ both equal to (0, 0, 0) (or to an special *reduction point*), $\lambda \equiv 1$ and $\boldsymbol{\Theta} \equiv (0, 0, 0)$.

- observed projection centers (realized in ORIENT as models)

  For this kind of observations, considering equation (1), $\mathbf{p_0}(\mathbf{a})$ is constant (and merely serves as a reduction point for numerical considerations). The seven remaining parameters describe a spatial similarity transformation of the GPS/IMU projection centers and can be interpreted as corrections for remaining errors after the datum's transformation between WGS84 and EUREF89, but only $\mathbf{P_0}$ was considered, whereas λ and $\boldsymbol{\Theta}$ were fixed to 1 resp. (0, 0, 0). Since this $\mathbf{P_0}$ describes a translation of the GPS/IMU projection centers as a whole, $\mathbf{P_0}$ will be termed as *exterior GPS excenter* in the following.

- observed rotational parameters (realized in ORIENT as observed mapping parameters)

  For this kind of observations, considering equation (1), $\lambda \equiv 1$, $\boldsymbol{\Theta}$ and $\mathbf{P_0}$ both equal to (0, 0, 0). The interpretation of **p** and **P** has a bit changed. They don't mean *points* in the usual sense, but stand for triples of rotation angles. **p** holds the observed GPS/IMU Roll, Pitch and Yaw values, whereas **P** holds the unknown rotation angles of the respective photo. $\mathbf{p_0}(\mathbf{a})$ is used as additional excenter for the rotations' observations (*misalignment*).

3. Phase 1 – The calibration of the systems

Both companies made two calibration flights at scales 1:5.000 (2 + 2 strips with 60 images totally) and 1:10.000 (5 + 2 stripes with 85 images totally). The data delivered to the test participants in August 2000 included the image measurements for the calibration flights performed by IPI (fiducial

[5] The effect of this interior GPS excenter is identical to the lever arm correction.

transformed and distortion corrected) together with the IOR (0, 0, *f*), the GPS/IMU processed data (linearly interpolated for exposure time and lever-arm corrected, so yielding observations for the images' XOR) and the coordinates of 20 ground control points, with an accuracy of ± 1.5 cm. The aim of phase 1 was to compute the system calibration for each company and to return the results to the pilot center till the end of October 2000.

For each company a separate ORIENT project was created. The observed projection centers for each of the 11 strips were imported into ORIENT as 11 separate models. The observed rotation angles were realized as special rooms, which are addressed by each photo in ORIENT. Because the accuracies for the image measurements and the GPS/IMU data were missing, it was first tried to get some plausible estimates for them. The accuracies for the image measurements were obtained by computing the relative orientation for all images of each company (with fixed IOR). This yielded an accuracy of 4.1 µm for the images of Comp1 (Zeiss RMK Top) and 5.6 µm for those of Comp2 (Leica RC 30). Due to this relatively large difference of 1.5 µm between these two cameras, it was tried to improve the results by including distortion parameters. For the Zeiss RMK Top only one radial distortion parameter (adp3) was found to be significant (with very small effects of 1 µm as average and a maximum of 8 µm) resulting in an image accuracy of 4.0 µm. For the Leica RC 30, however, large tangential distortion parameters (adp5&6) were found. The adp6 had effects of 16 µm as average and a maximum of 40 µm. Furthermore it would have induced a significant change in the y-coordinate of the principal point in the range of 60 µm. Since these quantities are highly improbable for metric cameras (and as it turned out later, adp6 differs between phase 1 and phase 2) it was finally decided not to include these two tangential distortion parameters (adp5&6) – although this simple model of two additional parameters improved the image accuracy of the Leica camera to a value of 4.7 µm. After phase 1 a summary paper by the IPI was published (Heipke et al. 2001) where the worse accuracy of the Leica camera was ascribed to the poorer image quality.

The accuracies for the GPS/IMU data were found by an adjustment with GPS excenters and ROT excenters for each of the 11 strips, so that no systematic errors in the GPS/IMU data could disturb the results. Using the above mentioned VCA, the arbitrary chosen a-priori accuracies were adapted to fit to the a-posteriori ones. The IOR was kept fixed at their given values, since any errors in the IOR would be compensated by the free GPS/IMU excenters. For this adjustment (and all the following ones) the data of *both flights* were used. In Table 2 the estimated accuracies are listed:

	Comp1a	Comp1b	Comp2
PHO $\sigma_x = \sigma_y$	4 µm	4 µm	6 µm
GPS $\sigma_X = \sigma_Y = \sigma_Z$	5 cm	5 cm	5 cm
IMU	35/35/110 ^{cc}	35/35/80 ^{cc}	35/35/80 ^{cc}
GCP $\sigma_X = \sigma_Y = \sigma_Z$	1.5 cm	1.5 cm	1.5 cm

Table 2: Estimated accuracies for the observations of phase 1

Then, with these accuracies, the next step was to choose the appropriate model for the system calibration. Since both scales (more precisely, the paths) of the calibration flights were suitable for doing the calibration (except for the determination of the principal distance, which had to rely on both) the appropriateness of a chosen model could be checked, by comparing the results obtained for both scales. Due to the combined processing of the GPS and IMU data, the observations for the images' projection centers and rotation angles were assumed to be free of gross errors (due to cycle slips etc.), so for all ORIENT-models (containing the observations for the projection centers) of one height level only one common (exterior) GPS excenter was specified. The same was done with the observed rotation angles. The IOR was fixed at (0, 0, *f*). This model will be termed **M1**. Table 3 holds the values for the GPS and IMU excenters of both scales. Table 3 is followed by the plots of the GPS residuals (shifted for better distinction) and of the IMU residuals (with the excenter included).

Outstanding attributes in Table 3 and in the plots are the strip characteristics in the GPS plane residuals in both companies (although the GPS excenter's plane components in both scales do not differ very

much – perhaps due to averaging effects) and the jump in the GPS excenter's height component of Comp1 (indicating a wrong principal distance). It is also interesting to see how the IMU accuracy of Comp1 improved by the 2nd data processing.[6] The existence of a strip systematicness in the GPS plane residuals implies rather the existence of an *interior* GPS excenter (defined in the system of the camera and therefore changing its effect in the object system in dependence of the flight direction) than an *exterior* GPS excenter.

	scale	global GPS-exc. (X/Y/Z) [m]			ROT-exc. (Roll/Pitch/Yaw) [gon]		
Comp1a	5k	0.045	-0.075	0.100	0.0947	0.0044	-0.1201
Comp1a	10k	0.034	-0.101	0.270	0.0915	0.0023	-0.1017
Comp1b	5k	0.036	-0.077	0.095	0.1029	0.0100	-0.0670
Comp1b	10k	0.021	-0.092	0.272	0.1013	0.0108	-0.0663
Comp2	5k	-0.016	0.000	-0.130	-0.1329	0.0599	0.1989
Comp2	10k	-0.058	0.013	-0.148	-0.1324	0.0628	0.1969

Table 3: Exterior GPS excenter and ROT excenter of model **M1**

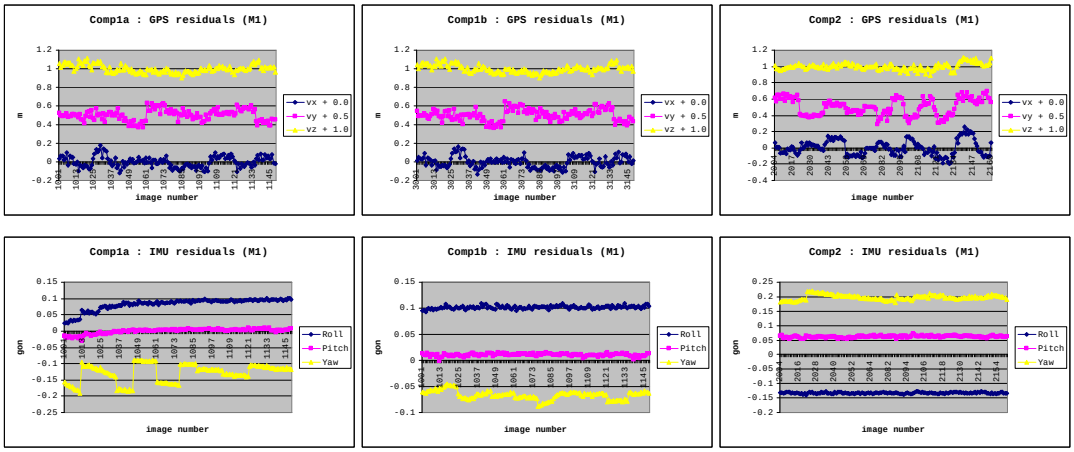

Figure 1: GPS and IMU residuals of model **M1**

So, in the 2nd model **M2** the exterior GPS excenter is replaced by an interior one. In ORIENT, this means that the GPS-model's exterior reference point $\mathbf{P_0}$ is fixed and all images of the same scale point to the same ADPAR-room, which includes the adpars 41-43 (c.f. Table 1). The IOR remains fixed at (0, 0, *f*). Table 4 holds the values for the GPS and IMU excenters of both scales. Table 4 is followed by the plots of the GPS residuals (shifted for better distinction). The plots of the IMU residuals do not differ much from the ones above.

In the residual plots, it can be clearly seen, that the strip systematicness is removed. But now it is interesting to see, that the y-component (orthogonal to the flying direction) of the interior GPS excenter in both scales differs by a factor 2. This implies, that rather a change in the principal point is necessary. So, in the 3rd model **M3** the interior GPS excenter's plane components are fixed at (0, 0) and the principal point in each scale is allowed to be free (while *f* still being fixed). Table 5 holds the

[6] As it can be clearly seen in the IMU residual plot, there had to be an error in the 1st processing of Comp1's GPS/IMU data. This data, however, had to be calibrated somehow, so as a makeshift, for Comp1a the GPS/IMU data of the first strips were not used for the calibration phase.

changes in the principal point, the interior GPS excenter's z-component, and the IMU excenters of both scales.

	scale	Interior GPS-excenter [m]			ROT-excenter [gon]		
Comp1a	5k	0.0740	-0.056	-0.095	0.0939	0.0033	-0.1201
Comp1a	10k	0.065	-0.135	-0.276	0.0882	0.0018	-0.1018
Comp1b	5k	0.068	-0.062	-0.093	0.1021	0.0092	-0.0670
Comp1b	10k	0.049	-0.138	-0.273	0.0989	0.0102	-0.0665
Comp2	5k	0.108	0.115	0.124	-0.1307	0.0579	0.1990
Comp2	10k	0.141	0.291	0.155	-0.1269	0.0603	0.1970

Table 4: Interior GPS excenter and ROT excenter of model **M2**

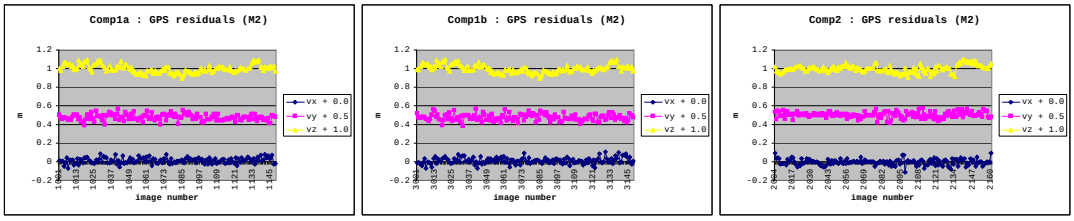

Figure 2: GPS residuals of model **M2**

	scale	princ. point [mm]/int. GPS-exc. z[m]			ROT-excenter [gon]		
Comp1a	5k	0.014	-0.010	-0.095	0.0939	0.0033	-0.1201
Comp1a	10k	0.006	-0.013	-0.276	0.0882	0.0018	-0.1018
Comp1b	5k	0.013	-0.011	-0.093	0.1021	0.0092	-0.0670
Comp1b	10k	0.005	-0.014	-0.273	0.0988	0.0102	-0.0665
Comp2	5k	0.021	0.023	0.124	-0.1307	0.0579	0.1990
Comp2	10k	0.014	0.029	0.154	-0.1268	0.0603	0.1970

Table 5: Principal point, interior GPS excenter's z and ROT excenter of the model **M3**

From Table 5 it can be seen, that the y-coordinate of the principal point in both scales fit together much better than the y-component of the interior GPS excenter in **M2**. On the other hand, the x-coordinates of the principal points differ in the range of factor 2, whereas the x-components of the interior GPS excenter in **M2** show almost no differences. This means, that not only a change in the principal point needs to be modeled but also the x component of the interior GPS excenter (which can be interpreted as an error in the time synchronization of the GPS/IMU system and the camera).

	IOR [mm]			Glob GPS exc. [m]			Loc [m]	ROT exc. [gon]			Adp []
	x	y	z	X	Y	Z	Adp41	Roll	Pitch	Yaw	Adp3
Comp1a	-0.003	-0.013	153.693	0.051	-0.081	-0.080	0.086	0.0932	0.0025	-0.1173	-3.9E-03
Comp1b	-0.003	-0.013	153.692	0.037	-0.079	-0.089	0.078	0.1003	0.0097	-0.0666	-3.9E-03
Comp2	0.010	0.027	153.387	-0.025	0.005	-0.107	0.046	-0.1284	0.05931	0.1977	----

Table 6: Values of the final calibration model (computed in the UTM)

The results of the models **M1** – **M3** led to the final model, which is made of the parameters in Table 6 common for both scales (and whose values where determined by a bundle adjustment using the data of both calibration flights). All computations during this calibration phase were carried out in two systems: the UTM system (zone 32) and a Cartesian tangential system (*TangSys*) defined at the center of the test area.[7] In both systems the same values for the interior GPS excenter, the ROT excenter, the Adpars and the planar components of the IOR and the exterior GPS excenter were obtained, whereas in UTM the height component of the exterior GPS excenter were smaller by less than 1 cm (which is negligible), but the principal distances were larger by approx. 40 µm.

These differences are caused by the different scales in height and plane in UTM. The scale in height is 1:1 (meaning the ellipsoidal heights are used in UTM 'as they are'), whereas the planar scale is caused by the distortions of the UTM projection and depends on the location of the project's area relative to the central meridian of the specific zone. So, for the center of the given area the scale factor is approx. $\tau = 0.99975$, meaning that the planar situation in the projection is compressed. In the adjustment, these two different scales are realized in plane and height by the ground control points and the GPS observations for the projection centers. If this scale difference is not removed, height errors may occur. With the free principal distance f, however, the height scale can be aligned to the planar one and f is changed into f/τ. For more details concerning this problem see (Ressl 2001).

Another interesting result: the (by the pilot center resp. calibration protocol) *given* value for the principal distance f for the Leica RC 30 camera (Comp2) fitted closely to the *computed* value in the Cartesian tangential system, whereas the *given* value for the Zeiss RMK top (Comp1) fitted closely to the *computed* value in UTM.

After the system calibration the GPS/IMU data of the test flight (which was also delivered to the test participants) were corrected by the calibration parameters and returned (along with the calibration parameters) to the pilot center.

4. Phase 2 – Integrated bundle block adjustment

The aim of phase 2 was to apply the system calibration of phase 1 to an independent flight. This third flight (the test flight), made of 9 + 2 strips, was flown by each company directly after the 2nd calibration flight. Its scale is 1:5.000 and it consists of 180 images for Comp2 and a smaller number of 130 images for Comp1 (due to bad weather conditions). Phase 2 started in March 2001 and the results where due at the end of May. The GPS/IMU data of this flight were already delivered to the test participants together with the data for phase 1. The only data that were additionally delivered, were the measurements in the images of the test flight (approx. 25 tie points per image); but not for all images. Out of all images a sub-block (5 + 1 strips) of 50 images and a single strip of 17 images were selected by the pilot center – both were to be handled separately.

All throughout phase 2 the phase 1 corrected GPS/IMU data of the test flight were used. For the block and strip data of each company the following three scenarios were applied:

1. The GPS/IMU data of the test flight are kept fixed and are used as the XOR of the images. Then an overdetermined spatial intersection for the tie points is computed (direct georeferencing).
2. A combined AT is performed, using the GPS/IMU data together with the image measurements. In this case the GPS/IMU data are used as observations for the images' XOR.
3. Same as 2); additionally a change in the misalignment is modeled.

Afterwards the coordinates of the intersected tie points of scenarios 1 and 3 were compared.

---

[7] The IMU rotations are related to a temporary system of the aircraft (local horizon, ARINC 705). For UTM the Roll and Pitch angels were adopted and the Yaw angels were corrected by the actual value of the meridian convergence. For the TangSys all three angels had to be transformed.

4.1 Overdetermined spatial intersections with fixed XOR and IOR (direct georeferencing)

For this scenario the corrected GPS/IMU data was used as the XOR of the images and kept fixed. The overdetermined spatial intersection for the tie points resulted in the following σ_0 (µm in the image):

	Comp1a	Comp1b	Comp2
σ_0/Block	43	27	17
σ_0/Strip	17	11	14

If one compares these values with the accuracy of the image measurements of approx. 6 µm, one discovers a decrease in accuracy of 200 % - 700 %. This comparison, however, is not correct, because the GPS/IMU data are disturbed by accidental (or even systematic) errors and are kept fixed. Therefore, the residuals of the image coordinates have to compensate for these GPS/IMU errors and this will result in larger image residuals and hence a large σ_0 (see also section 4.4). Further, it is interesting to see, that the strip version yielded significantly smaller σ_0 – the reason for this will be explained at the end of section 4.3.

4.2 AT with free and observed XOR and IOR

For this scenario, the XOR and (common) IOR for the images are allowed to be free. The GPS/IMU data are used as observations for the XOR (with the accuracies of Table 2). The calibrated values of the IOR (determined in phase 1) are used as observations for the IOR ($x_0 \pm 0.002$ / $y_0 \pm 0.002$ / $f \pm 0.003$). The following roots of the reference variance σ_0 (µm in the image) were obtained:

	Comp1a	Comp1b	Comp2
σ_0/Block	6.2	5.8	6.1
σ_0/Strip	3.7	3.6	6.2

These values can be compared with the accuracy of the image measurements of 6 µm (for Comp2) and 5 µm (for Comp1). During the bundle block for each company, the a-priori accuracies of the GPS/IMU measurements were checked using ORIENT's VCA. It delivers for each group of observations a factor, which describes the ratio between the a-priori and a-posteriori accuracies. If these factors are 'close' to 1, one can be quite sure, that the assumed a-priori accuracies are plausible and that finally the weighting of the observations is correct.

For the block versions of Comp1a and Comp1b the VCA delivered factors in the range of 3 for the Roll and Yaw angles, whereas for Comp2 these factors where close to 1. These high factors for Comp1 implied a change in the misalignment, for that reason another bundle block with an additional misalignment for each company was computed. For the strip versions of Comp1, the VCA-factor were always close to 1. The strip of Comp2, however, yielded a higher factor of 1.6 for Pitch and Yaw.

4.3 AT with free and observed XOR and IOR and an additional misalignment

With an additional misalignment in the adjustment the following σ_0 (µm/image) were obtained:

	Comp1a	Comp1b	Comp2
σ_0/Block	5.0	5.0	6.1
σ_0/Strip	3.4	3.4	5.9

Now for all companies the VCA delivered factors close to 1, except for the Yaw of the block version of Comp1b. Since this was a little bit surprising, the residuals of the rotations angles were plotted.

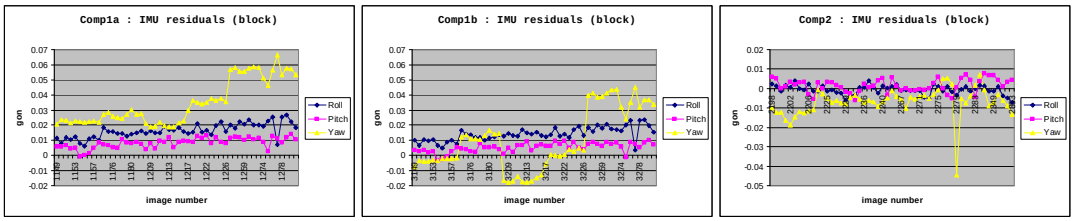

Figure 3: Residuals of the GPS/IMU rotations of phase 2

These plots clearly show the following facts:

- In both data processings of Comp1 *irregularities* in the Yaw angle occur at the strip endings. In all three angles a linear trend can be seen clearly. For Roll and Pitch this linear trend can effectively be replaced by an additional misalignment. Comparing the Yaw-residuals of the 1st (erroneous) and 2nd (correct) data processing, it is interesting to see, that the mean value of the Yaw-residuals got closer to zero (which was expected), whereas the extent of the Yaw-residuals (max – min) increased (which was not expected). So, as a makeshift, the accuracy of the Yaw angles of the 2nd data processing was set from 80^{cc} to 160^{cc}.
- The Yaw angles of Comp2 included one *gross error* (the value for image 2279), which was eliminated during all adjustments.

The following table holds the values for the additional misalignments (with an accuracy of ~ 15^{cc}).

[gon]	Comp1a	Comp1b	Comp2
Block	0.0163/0.0083/0.0348	0.0141/0.0052/0.0098	-0.0005/0.0015/-0.0068
Strip	0.0000/0.0045/0.0141	0.0000/0.0019/-0.0095	0.0000/0.0052/0.0112

These irregularities in the IMU-data of the block version of Comp1 are the reason, why the strip version of the direct georeferencing (in section 4.1) yielded significantly smaller σ_0 for Comp1, since in one single strip no such irregularities occur. On the other hand, for Comp2, whose IMU-data is systematic free, the strip and block version of the direct georeferencing yielded similar values.

Another interesting fact could be observed with the IOR of Comp1. The value for y_0 computed in phase 1 did not fit to the data of phase 2 (Δy_0 = 25 µm). This is not a result of the additional misalignment in Roll, since y_0 of phase 1 doesn't fit to phase 2 either, when all angle observations are excluded from the adjustment and only the GPS observations are used. So, perhaps, there was an error in the GPS data. The y_0 coordinate of the principal point, however, was allowed to be free, although – perhaps – it only removes the symptoms but not the cause.

4.4 Comparison of the intersected tie points of the direct georeferencing with the tie points of the AT with additional misalignment

The following table holds the statistics of the differences of the tie points of scenario 1 and 3. For Comp2 637 (block) and 322 (strip) tie points were compared, for Comp1 549 (block) and 257 (strip). For the block version, the standard deviations for Comp2 are the smallest (6 cm in plane, 11 cm in height), for the 2nd data processing of Comp1 they are larger by approx. 3 cm. The mean values of Comp2 are caused by the small additional misalignment. For the strip version the standard deviations of the 2nd data processing of Comp1 are the smallest. For Comp2 quite large mean values and standard deviations in the tie point differences can be spotted. They are caused by the changes in the misalignment of Pitch and Yaw. The Yaw residuals also show a clear linear trend (plot not included).

[m]	Comp1a			Comp1b			Comp2		
Block	X	Y	Z	X	Y	Z	X	Y	Z
Mean	0.020	-0.013	-0.018	-0.001	0.001	-0.016	-0.015	-0.018	0.018
Std. dev.	0.150	0.141	0.158	0.098	0.087	0.125	0.069	0.058	0.107
Strip	X	Y	Z	X	Y	Z	X	Y	Z
Mean	0.026	0.055	0.003	0.012	0.028	0.004	-0.024	-0.075	-0.006
Std. dev.	0.051	0.078	0.075	0.046	0.056	0.070	0.064	0.088	0.096

Let's take a closer look at the block version of Comp2. The AT with additional misalignment resulted in a σ_0 of 6 (µm in the image). The 3-fold tie points of this scenario have a standard deviation of 3 cm in plane and of 6 cm in height. The direct georeferencing scenario resulted in a σ_0 of 17 (µm in the image). This would mean, that 3-fold tie points would have an accuracy 2.8 times worse than the bundle method. The differences of the tie points, however, show a standard deviation of (only) 6 cm in plane and 11 cm in height. This means, that the *results of the direct georeferencing scenario fit to those of the bundle scenario* much better, than one would think just by judging the σ_0:

We think, that there are mainly two reasons, why for this test (and especially for Comp2) direct georeferencing delivers results comparable with those of the bundle method:

- The GPS/IMU data for the block of Comp2 are free of systematic errors, whereas the Comp1 data (even the 2nd data processing) show some kind of strip systematicness in the rotation observations.
- The accuracy of the GPS/IMU data (GPS: ± 5 cm, Roll/Pitch: ± 35cc, Yaw: ± 80cc) transformed to the ground (GPS: ± 5 cm, Roll/Pitch: ± 5 cm, Yaw: ± 7 cm) is in the range of the image measurements' accuracy (6 µm) transformed to the ground (3 cm).

Because of these two reasons it seems plausible, that the impact of the superposing – on the ground similarly distributed – accidental errors of the GPS/IMU data and of the image measurements can be widely absorbed by larger and approximately normally distributed residuals of the image coordinates.

The GPS/IMU data of both Comp1 processings are affected by systematic errors (occurring strip by strip). The image residuals can not fully absorb these systematic errors, because they demand strip-systematic image residuals. This, however, is not possible within a least squares adjustment, which tries to distribute the whole system's contradiction over all observations according to their weights.

The fact, that for Comp2 the direct georeferencing scenario delivers similar results to the bundle scenario, does not mean, that the latter can be fully replaced by the former one. Two reasons mainly speak against that:

- Direct georeferencing does not deliver useful accuracy estimates. As we saw, the direct results appear much more accurate than one may deduce from their σ_0.
- If systematic errors (like for Comp1) or gross errors (like for Comp2) are in the GPS/IMU data, then the intersected points will be false according to that. These types of errors can be detected using conventional bundle methods (when at least three images are used at once).

5. Conclusions

In this article it was presented how the task of the OEEPE test 'Integrated Sensor Orientation' can be solved using the hybrid bundle block adjustment program ORIENT. The results of the two phases can be summarized in the following way. The *main* result of this test is:

- The usage of GPS/IMU data free of systematic errors as fixed values for the images' XOR (direct georeferencing) yields for the given block with the scale 1:5.000 coordinates for the tie points similar to those of the corresponding integrated AT (standard deviations of the differences: 6 cm in plane and 11 cm in height). This is somehow surprising when comparing the σ_0 of both

versions: σ_0(AT) = 6 and σ_0(direct) = 17 (µm in the image). The reason for these large differences in the σ_0 is caused by the fact, that with direct georeferencing the residuals of the image measurements have to compensate for the errors of the fixed GPS/IMU data. One must be aware of the fact, however, when adapting these results for other projects of direct georeferencing, that the results during this test were obtained by performing an *overdetermined* intersection for the *whole* block – which is perhaps not what a novice may understand as 'direct georeferencing', who would rather use the GPS/IMU data to perform stereo restitution from image *pairs* right away (cf. end of this section).

Among the *secondary* results the following can be stated:

- The IMU data of the block version showed one gross error (for Comp2) and partly linear trends together with clear discontinuities in the misalignment at strip endings (for Comp1). The IMU data of the strip version showed a linear trend for the Yaw values of Comp2.
- The IOR of Comp1 showed a somewhat peculiar behavior. The y_0-coordinate, that was determined for Comp1 during the calibration phase, did not fit to the data of the test flight in phase 2 and changed by $\Delta y_0 \sim 25$ µm. We assume, that this is rather a compensation for some error in the GPS data of phase 2, since Δy_0 occurs independently on the usage of the IMU data.

This OEEPE test demonstrated the high potential of integrated sensor orientation and it is undoubtable that its importance in image orientation will increase over the next years. Today, however, there are still some open problems this technique has to cope with (see section 1), including the reliability of the GPS/INS data and the stability of the misalignment as the most important ones. These latter problems showed up also during this test. As a consequence, *total* direct georeferencing without any tie and control points by immediate stereo restitution using GPS/IMU data is still not possible (due to the large y parallaxes in the image (Heipke et al. 2001)).

A thinkable solution would be to perform a calibration flight (in two scales) *before* and *after* each project to determine the misalignment and its linear trend and to interpolate the misalignment for each time of exposure. Discontinuous changes in the misalignment during the project flight, however, can not be detected by this method, either. This calibration flight is also inevitable regarding the IOR, since the principal distance may differ largely from its labor calibrated value because of atmospheric influences. And, as it emanated during this test, also the choice of the underlying coordinate system (map projection vs. Cartesian tangential system) is of importance concerning direct georeferencing.

6. References

Colomina, I. (1999) *GPS, INS and Aerial Triangulation: What is the best way for the operational Determination of Photogrammetric Image Orientation?*, IAPRS, Vol. 32, Part 3-2W5, „Automatic Extraction of GIS Objects from Digital Imagery", Munich, September 8 – 10.

Cramer, M. (2000) *Genauigkeitsuntersuchungen zur GPS/INS-Integration in der Aerophoto*-grammetrie, Dissertation, Fakultät für Bauingenieur- und Vermessungswesen, Universität Stuttgart.

Heipke C., Jacobson K., Wegmann H., Andersen O., Nilsen B. (2000*) Integrated sensor orientation – an OEEPE test*, IAPRS (33) B3/I, pp. 373 – 380.

Heipke C., Jacobson K., Wegmann H. (2001*) The OEEPE test on integrated sensor orientation – results of phase 1*, in: Photogrammetric Week 2001 (to be published)

Kager H. (1989) *ORIENT: A Universal Photogrammetric Adjustment System*. In Grün/Kahmen (Editors): Optical 3-D Measurement Techniques, Wichman Verlag, Karlsruhe.

Kraus K. (1997) *Photogrammetry 2 – Advanced methods and applications*, Dümmler Bonn.

Ressl C. (2001) *Direkte Georeferenzierung von Luftbildern in konformen Kartenprojektionen*, Österreichische Zeitschrift für Vermessung und Geoinformation, 89. Jahrgang, Heft 2

Rottensteiner F. (2001) *Semi-automatic extraction of buildings based on habrid adjustment using 3D surface models and management of building data in a TIS*, PhD-thesis, Institute of Photogrammetry and Remote Sensing, Technical University, Vienna, Geowissenschaftliche Mitteilungen Nr. 56

Benefit of Rigorous Modeling of GPS in Combined AT/GPS/IMU−Bundle Block Adjustment

Martin Schmitz, Gerhard Wübbena, Andreas Bagge

Geo++®
Gesellschaft für satellitengestützte geodätische und navigatorische Technologien mbH
D−30827 Garbsen, Germany

Erwin Kruck

GIP
Gesellschaft für Industriephotogrammetrie mbH
D−73430 Aalen, Germany

Abstract

The benefit of a rigorous GPS modeling in the combined bundle block adjustment has already been investigated some years ago. However, the closed GPS approach is only used operationally in the subsequent processing with the GEONAP −K package for GPS data and with the BINGO−F package for the combined adjustment. Recently, the BINGO−F package has been extended for the combined adjustment of additional IMU (Inertial Measurement Unit) data.

The rigorous GPS approach in a combined GPS/block adjustment uses the actual GPS constellation for the determination of projection center and does not rely on approximative shift and drift parameters, which are generally applied. The advantage is the geometrical constraint of the projection centers within the complete block or at least between individual strips under unfavorable GPS conditions. Changes in satellite constellation do not affect the combined adjustment. The geometrical information from GPS for neighboring strips or the complete block is maintained and strengthen the combined adjustment. The theory of the rigorous GPS modeling will be discussed.

For the integrated sensor orientation the correct modeling of all sensor is an essential task. The rigorous GPS approach in a combined bundle adjustment together with IMU and photogrammetric data will consequently also benefit. The European Organization for Experimental Photogrammetric Research (OEEPE) has conducted a multi−site test for the integrated use of AT (Aerial Triangulation), GPS and IMU data. Based on the test, analysis are presented, which focus on the effects of the GPS modeling in the combined bundle block adjustment with the GEONAP−K and BINGO−F software packages.

1 Introduction

The integration of the Global Position System (GPS) into photogrammetric projects is commonly applied. Besides GPS navigation and GPS ground control surveys, the major interest is the determination of the coordinates of the projection center as part of the photogrammetric exterior orientation. The combined GPS/block adjustment used for this task is a state−of−the−art technique and is used operationally in aerial triangulation.

A further reduction of costs is expected from the integration of Inertial Measurement Unit (IMU) data to determine the complete exterior orientation including the orientation angles of the camera during aerial triangulation. These new attempts make it necessary to analyze the currently used models of the integrated AT/GPS adjustment.

The current constellation of GPS of 29 satellites tends to neglect remaining problems in the general processing of kinematic GPS data. There are still GPS constellation changes during a flight from strip to strip. The so−called shift & drift approach is often applied in the combined GPS/block adjustment, which has the task to account for systematic GPS errors. Discontinuities in the determined GPS trajectory are caused by constellation changes, while time dependent changes originate from unreliable or false ambiguity resolution. The effects can only be approximated by the shift and drift parameters, while the strips are not too long and the magnitude and variations of the errors are not too high. There exists also a high correlation of the shift and drift parameter with other parameters of interest, which makes it impossible to estimate such parameters correctly.

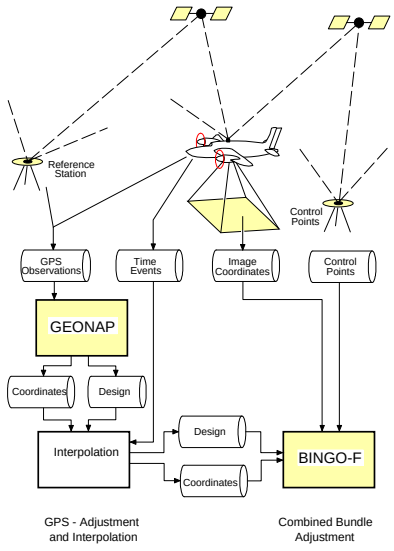

Figure 1: Data flow of GEONAP−K and BINGO−F (from Kruck et. al. 1996)

A mathematical model performs generally best, if a closed functional relationship is used or remaining approximation errors are small. If the approximation error may reach the magnitude of the actual error component, the individual error must be separated and adequately modeled for

highest accuracy requirements. The philosophy of separation error components is incorporated into the rigorous GPS modeling approach in the combined bundle adjustment with the GPS processing package GEONAP −K and the bundle block adjustment BINGO−F.

A rigorous GPS modeling is applied in the combined block adjustment to overcome the approximation of the shift & drift approach and the correlation with other parameters. In addition, the geometric strength of the GPS positions is maintained and the geometric information in the combined GPS/block adjustment is constrained from this fact. The approach is also termed CPAS (Combined Phase Ambiguity Solution) in the combined GPS/block adjustment with BINGO−F. The rigorous GPS model has been described by Kruck et. al. (1996), Jacobsen, Schmitz (1996) and Schmitz (1998). Empirical results are discussed in e.g. Okamoto (1998).

The European Organization for Experimental Photogrammetric Research (OEEPE) has conducted a multi−site test for the integrated use of AT, GPS and IMU data (Heipke et. al. 2000). The original idea of this paper was the description, application and discussion of the rigorous GPS model using GEONAP−K and BINGO−F using the test data. For this purpose, the data including the recorded raw data of all GPS receivers is required. Although, the description and investigation of all available techniques and methods is the goal of the OEEPE test, the necessary data was not accessible through the pilot center. The presented analysis uses the photogrammetric and GPS raw data of the IGI flight from the OEEPE test, which has been provided by IGI. Some analysis are presented from the complete photogrammetric data of the test, but the IMU data are not used. For detail on the OEEPE test, objectives, participants and configuration see Heipke et. al. (2000, 2001).

2 Systematic GPS Coordinate Errors

Static GPS and realtime application of GPS can routinely achieve an accuracy at the few centimeter level, and, for certain applications even well below one centimeter (i.e. Wübbena, Lahr 2000). In contrast to static GPS measurement, no accumulation of measurements is possible in the determination of a kinematic trajectory. Therefore the processing of kinematic GPS station is still a challenging task. The accuracy of kinematic GPS for dynamic application depends on the distance to the reference station, the used observable and also on the processing strategy. In the following, always the highest accuracy requirements for the GPS processing is assumed.

The distance dependent errors are the ionosphere, troposphere and orbits. With increasing distances to the GPS reference station, the reliable ambiguity resolution becomes more difficult. Ambiguity resolution is the key issue to get an accuracy at the several centimeter level. The distance dependent errors can be modeled in the GPS processing package GEONAP−K.

Additional systematic GPS coordinate errors are generally caused in high dynamic kinematic applications by false ambiguity fixing, unresolved ambiguities and changes in the satellite constellation. The quality of the ambiguity resolution is steadily improving, but satellite constellation changes generally occur during a flight. Avoiding a loss−of−signal can be attempted during curve flights of the plane, but signal interruptions are often still present in the data. Automated data reduction in the GPS processing may introduce additional constellation changes not expected from the visibility of satellites at the kinematic station.

The magnitude of shift and drift effects in dynamic GPS applications depends on the actual geometric GPS conditions. The measure for this are the dilution of precision (DOP) values of GPS, which are generally given for geometry, called GDOP, or the position, called PDOP. Values of 3 or

less indicate very good conditions. Nowadays, the GPS satellite constellation is mostly favorable, so that the amplification by a poor DOP values is today mostly small. The effect must also be compared with the actual accuracy requirements of the photo flight or the intended accuracy for georeferencing.

Nevertheless, the GPS processing software must be capable to account for all possible error components. GEONAP−K allows a simultaneous multi−station, multi−frequency adjustment of the undifferenced GPS observable, which make the ambiguity resolution and the modeling GPS error components much more flexible. A closed simultaneous adjustment of several reference stations and several kinematic stations is possible, which is ideally suited applied with permanent reference station data. Combined adjustment of single and dual−frequency GPS data allows the ionospheric correction of e.g. a single frequency receiver in the photo flight airplane. Table 1 compares different scenarios of a local reference station, one remote reference station and a reference station network and some options to model systematic GPS errors.

Kinematic GPS Processing	***local reference station***	***remote reference station***	***reference station network***
ambiguity resolution	possible	difficult	possible
distance dependent errors:			
• ionosphere	ignore, eliminate	ignore, eliminate	model, eliminate
• troposphere	(model)	(model)	(model)
• orbit	(PE)	(model, PE)	(model, PE)
remaining systematic effects:			
• shift, drift errors	(approximate,) model	(approximate,) model	(approximate,) model
costs	high	low	low

Table 1: Photo flight configuration of GPS reference stations and comparison of different aspects of processing and costs

The use of a local reference station is favorable for the ambiguity resolution and therefore for the accuracy and simplicity of processing, but it is very cost intensive. The use of remote reference stations, which generally operate permanently, reduce the logistical and operational burden dramatically as well as the cost. However, ambiguity resolution and distance dependent errors increase and degrade the accuracy level. An additional improvement is gained from several reference stations, which can be processed as a reference station network. It is then possible to achieve ambiguity resolution over longer distances, while e.g. applying ionospheric modeling. Orbit improvement techniques can also be introduced in a network, without the delay of precise ephemeris (PE). Some GPS error components may be ignored, but may then introduce addition coordinate errors. The remaining systematic GPS effects cannot be approximated or modeled without any redundant observation and is therefore part of the combined GPS/block adjustment.

3 Modeling of Remaining Systematic GPS Coordinate Effects in the combined GPS/Block Adjustment

It is a common procedure in the combined GPS/block adjustment, to reduce all efforts in the GPS processing and to approximate all systematic GPS errors as a lump sum, while applying shift and drift parameters. The method is often called shift & drift approach. This is the false strategy considering highest accuracy by separating and correctly modeling individual error components. To point out the major important aspects, the generally applied approximative shift & drift approach for correction of systematic GPS errors will be discussed in comparison to the rigorous GPS modeling approach.

All distance dependent GPS errors can best be modeled in the GPS processing, exceptionally with a sufficient number of reference stations and an adequate software package. Remaining systematic GPS effects due to the high dynamic photo flight and its presence in the GPS data require an adequate modeling, especially with respect to the combined adjustment of GPS and aerial triangulation.

The basic concept of the shift & drift approach is a linear regression of the systematic GPS effects and errors. The Systematic effects of the GPS coordinates (and often systematic error from atmosphere and orbits) are approximated by constant and time dependent coordinate corrections generally for every strip or simplified for the complete block. It is generally not accounted for effects due to satellite constellation changes in the combined adjustment nor in the GPS processing.

The best choice for the formulation of the combined GPS/block adjustment is the object space. The centered GPS coordinates correspond to the coordinates of the projection center. The coordinates of the external orientation from photogrammetric data can be used as redundant observation in the adjustment and vise versa. The formulation of the combined adjustment in the image space is also used, but has the major disadvantage, that the linear dependence of image coordinates (internal orientation) and projection center (external orientation) are used to express changes of external orientation by changes of the internal orientation in the image space. As a consequence, the separation from other parameters is difficult due to high correlation and is only possible, when it is applied for different time dependent parts of the data set.

When the shift and drift parameters are used strip wise, no geometric GPS relationship between strips exists anymore. Every strip or sub−block with an individual set of shift and drift parameters is completely independent from each other, because the introduced parameters destroy the geometric constraints from GPS. Even neighboring strips or repeated strips are completely independent concerning the GPS data, if individual shift and drift parameters are applied and the GPS position are translocated and scaled.

The systematic GPS errors can generally not be determined from a sub−set of data for a complete trajectory of a moving GPS receiver. Therefore uncertainties will remain, if no adequate modeling or configuration of the photo flight is used. Also the general accuracy requirements must always taken into account for the processing strategy. To be able to control the error behavior of the systematic GPS errors at least one, favorable some ground control points must be available.

4 Rigorous GPS Model for Combined GPS/Block Adjustment

In the following, the rigorous GPS model for the combined GPS/block adjustment is described.

The redundant information of the coordinates of the projection center from photogrammetric data and GPS can be used in the combined adjustment. The general distance dependent errors of GPS have been correctly modeled in the GPS processing. Additionally, GPS position correction due to the remaining shift and drift effects are required. A simplified design matrix for a GPS adjustment model can very easily computed from elevation and azimuth of all satellites used for the position estimation in the GPS processing. To estimate a position correction of the GPS trajectory, only the not reliably resolved ambiguity have to be known for every position. Range corrections for these satellites are introduced as unknown into the combined adjustment, which give with the design information a coordinate correction using strictly the functional model of the actual GPS constellation. Reliably resolved ambiguities of the GPS processing are unchanged and are still used for the GPS coordinate correction, but must not explicitly be known.

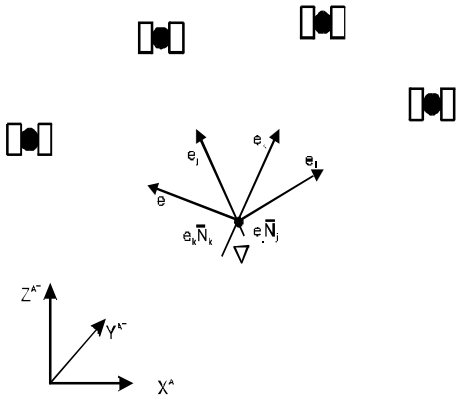

Figure 2: Principle of rigorous GPS modeling in combined GPS/block adjustment: projection center • AT and ∇ GPS

The principle of the rigorous GPS model is displayed in Figure 2. The design information actually gives the unit vectors **e** in direction to the GPS satellites i to l. For the unresolved ambiguity term N of satellite j and k, a range correction is then estimated.

The coordinate corrections are computed using design information and estimating the ambiguity terms within the combined GPS/block adjustment. There exists a difference in the datum between GPS and the reference system of the photogrammetric object space. Therefore, a term for a datum transfer is required in addition to the remaining systematic GPS effects. The GPS positions are considered as observations in the combined block adjustment. The complete model for the rigorous GPS modeling in the combined GPS/block adjustment reads:

$$\mathbf{X}_p{}^{AT}{}_i = \mathbf{X}_A{}^{GPS}{}_i + \mathbf{dX}_D + (\mathbf{QA}^T\mathbf{P})_i \times \mathbf{N}_i + \mathbf{R}_i\,(\varphi\omega\kappa) \times \mathbf{dX}_A$$

The GPS coordinates $\mathbf{X}_A{}^{GPS}$ of a position i are transferred to the coordinates of the exterior orientation applying $\mathbf{X}_P{}^{AT}$ the eccentricity of the GPS antenna $\mathbf{dX}_A$ with the rotation matrix of the camera $\mathbf{R}(\varphi\omega\kappa)$, the datum difference $\mathbf{dX}_D$ and the position correction of the rigorous GPS model computed from the design ($\mathbf{QA}^T\mathbf{P}$) and the unsolved ambiguity term vector **N**. The GPS coordinate correction term actually accounts for range correction from the current satellites constellation.

Generally, the number of additional parameters for the correction of systematic GPS effects is smaller compared with a shift & drift approach, because not all signals are lost during every curve flight. Hence, only a minimum of required parameters has to be estimated in the adjustment.

The datum difference (datum transformation) can be described as translations only, or can be incorporated with a complete seven−parameter−transformation depending on the actual data set. The orientation angles φωκ are used from the exterior orientation or from an IMU data, to reduce the GPS positions given for the antenna phase center to the photogrammetric projection center. In modern systems also the crap angle is measured and can correctly applied.

The complete GPS design information for a rigorous modeling is accessible by elevation and azimuth of the GPS satellites used for the GPS position computation. Additionally, a book keeping of GPS ambiguity terms and their state (fixed or unfixed) is required. The actual vector **N** contains only a counter and a sign to indicate the state. Both information are at hand during the GPS processing. They must be available to estimate coordinate correction in a combined GPS/block adjustment and define the interface between GPS and block adjustment. The GEONAP−K GPS processing package uses undifferenced GPS observable, which makes the handling and processing of the design and ambiguity data very easy. For the use in the block adjustment the design information and the coordinates must be interpolated to the actual event of the photo.

5 Geometric Strength and Parameter Separation through Rigorous GPS Model

GPS gives absolute positions with very high relative accuracy between positions. Therefore the GPS positions can introduce geometric information between individual strips of the complete block. This geometric information is only available, if an adequate model is used. As already pointed out, the very essential geometric information is destroyed by multiple shift and drift parameters in the combined GPS/block adjustment.

The geometric constraints through the rigorous GPS model allows the reduction of ground control points and it is not necessary to have cross strips for the block. The shift & drift approach requires cross strips to overcome the loss of the geometric information inherent in GPS. Even the reduction of side lap is feasible for the rigorous GPS modeling.

The correlation between the interior orientation, namely the focal length and the coordinates of the principal point, datum transformation parameters and shift parameters is very high. Some block adjustment packages even use this high correlation to model systematic GPS errors in the image space instead of the actual object space.

The shift and drift parameters must be distinguished from the transformation parameter between the local coordinate system and the satellite reference system. It is essential to determine the transformation parameters for the block. Shift parameters applied to a complete block and translations of a datum difference cannot mathematical be separated.

From the high correlation of parameters, shift parameters can also not distinguished from changes of the interior orientation. However, the rigorous GPS approach can separate such error components as the model using the actual satellite constellation and in particular the introduced coordinate corrections due to unresolved ambiguities is different compared to the photogrammetric parameters of the image space.

The correlation between the principal coordinates of the interior orientation with the horizontal component of the GPS positions is getting higher for vertical photographies and hence for a flat terrain. Empirical analysis show, that almost no correlation between these parameters exists in the rigorous modeled GPS/block adjustment. Therefore, the rigorous GPS approach is independent of the topology of the actual terrain.

To get the best geometric condition in the combined GPS/block adjustment, the high relative accuracy of the GPS position has to be maintained. The modeling is independent on the length of the strips and the magnitude and variations of the errors. This is a major aspect of the rigorous GPS modeling approach.

6 Rigorous GPS Modeling Using OEEPE Data Set

Photogrammetric data and GPS data of the IGI photo flight, which is part of phase I, system calibration and direct georeferencing of the OEEPE test, is used. The GPS conditions during the photo flight were in some parts unfavorable, because the weather condition did not allow the flight according to the intended mission planning. The positioning quality of GPS derived from the actual used satellite constellation in the kinematic GPS processing varies from PDOP 1.2 to 4.9.

The GPS processing is based on data from three reference stations (fred, rade, moss) and the kinematic station (figi). The network of reference station gives redundancy, better availability and allows enhanced processing for ambiguity resolution and distance dependent GPS error. The trajectory has been computed in the ETRF89 datum defined by the coordinates of station fred. The coordinates of the GPS antenna were transferred into the UTM projection on the WGS84 ellipsoid and interpolated for the recorded event times of the photos. The uncertainty of the GPS position at the stage of the combined adjustment consists of several different parts. These are the GPS processing, the time synchronization of events and the interpolation. While the accuracy of the processing is in the order of 0.05−0.10 m, the accuracy of the events is only 0.5 ms. From the velocity of the airplane of ca. 100 m/s during the flight, an uncertainty of up to 5 cm results from the time synchronization. The interpolation error is expected to be small due to the overall recording interval of 2 Hz for the GPS data. The eccentricity of the GPS antenna is applied in the block adjustment, because the additional orientation information from AT or IMU can be applied. The eccentricity vector is generally assumed to be precisely known. The datum transformation can approximately done in a first step before the combined adjustment. The local datum differences are best estimated in the combined GPS (block adjustment itself having generally additional data.

Figure 3 shows the available satellites from the original recorded RINEX data on three reference stations and the kinematic station, as well as the actual used satellites of the kinematic station.

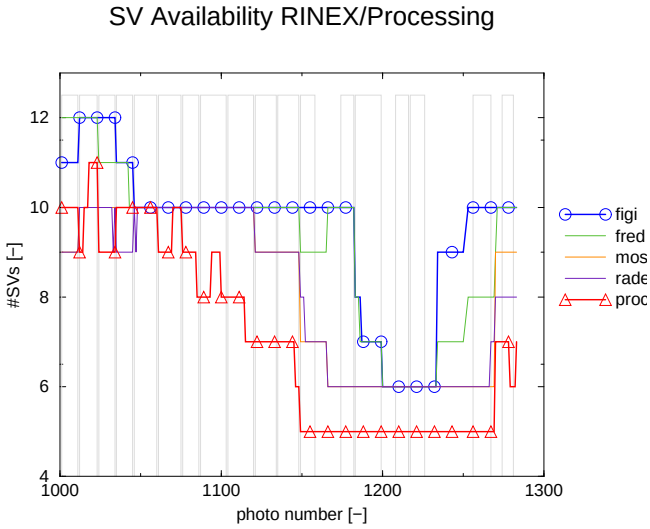

Figure 3: GPS satellite constellation and strips

Absolute results from the combined processing with GEONAP−K and BINGO−F cannot be presented from the present data, because independent check points are not published in phase I, calibration photo flights and georeferencing. Therefore, a kind of extended data set is used in one adjustment, which consists of available data from both companies participating with a GPS/IMU system in the OEEPE test. According to phase I, the exterior orientation may be estimated from these calibration data sets.

The analysis of the complete IGI block applying the rigorous GPS model (CPAS) show in some parts of the block very large misclosures. There are obviously systematic effects in the residuals of the projection center as shown in figure 5. The effects cannot be eliminated with a complete self−calibration of the camera and additional parameters. Therefore some detailed analysis of the GEONAP−K processing and the estimated coordinates were executed, which showed no errors or causes from the GPS data or processing. Investigations concerning any problems in the determination of image coordinates had also no result.

The residuals of the IGI block apparently originate from the coordinates of the principal point of the camera. This became obviously after numerous analysis and investigation of the photogrammetric data, also together with other researchers (Cramer 2001). The capability of the rigorous GPS model approach to separate between individual parameters of interest is used to determine corrections for the principal point. The systematic effects of figure 4 disappear completely after applying different camera parameters for parts of the block (see table 4). There are major differences especially in the y−component of the principal point, which are high significant considering the standard deviation. Afterwards, the complete block does not show any significant residuals (figure 5).

For verification of this findings, all four individual block provided in phase I (calibration flight 1:5000, calibration flight 1:10000, block and strip) of both companies are processed as a free network with self−calibration of the principal point. Table 3 shows the variations of the principal point for several different adjustment strategies in the block adjustment. The standard deviation indicates, that the corrections of the principal points are not significant. However, there is a general trend, which agrees with the results of table 2.

Block Name	***xH'***	***yH'***	***S xH'***	***S yH'***	***Remarks***
C1 − CPAS adjustment with 3 camera numbers	+3.9	−12.8	+1.2	+1.2	Cam1
	+11.0	+12.7	+2.3	+2.4	Cam2
	+10.2	+7.9	+3.4	+3.4	Cam3: Cass2

Table 2: Estimated principal point xH', yH' and standard deviation from combined GPS/block adjustment with ground control points

Block Name	***xH'***	***yH'***	***S xH'***	***S yH'***	***Remarks***
C1 – part of block, divided by used cassette	−5.9	−0.8	+10.5	+11.4	Cam1: Cass1
	+0.1	+13.3	+22.4	+23.9	Cam2: Cass2
C1 − complete block, divided by used cassette	−1.0	−8.9	+5.0	+5.1	Cam1: Cass1: 202 photos
	−11.2	+7.7	+19.2	+21.1	Cam2: Cass2: 15 photos
C1 − all photos	−0.1	−6.6	+4.7	+4.8	Cass1: 202 photos Cass2: 15 photos
C1 – calibration 1:5000/1:10000	+1.6	−10.3	+5.5	+5.5	Cass1: all photos
C1 − Block+Strip	−2.1	+5.1	+8.6	+9.2	Cass1: 54 photos Cass2: 15 photos

Table 3: Estimated principal point xH', yH' and standard deviation from free network bundle block adjustment, IGI data, company 1

Block Name	***xH'***	***yH'***	***S xH'***	***S yH'***	***Remarks***
C2 – all photos	+11.3	+18.8	+4.5	+4.7	
C2 – Calibration 1:5000/1:10000	+14.0	+20.9	+6.1	+6.1	
C2 − Block+Strip	+19.7	+22.9	+7.4	+7.8	

Table 4: Estimated principal point xH', yH' and standard deviation from free network bundle block adjustment, Applanix data, company 2

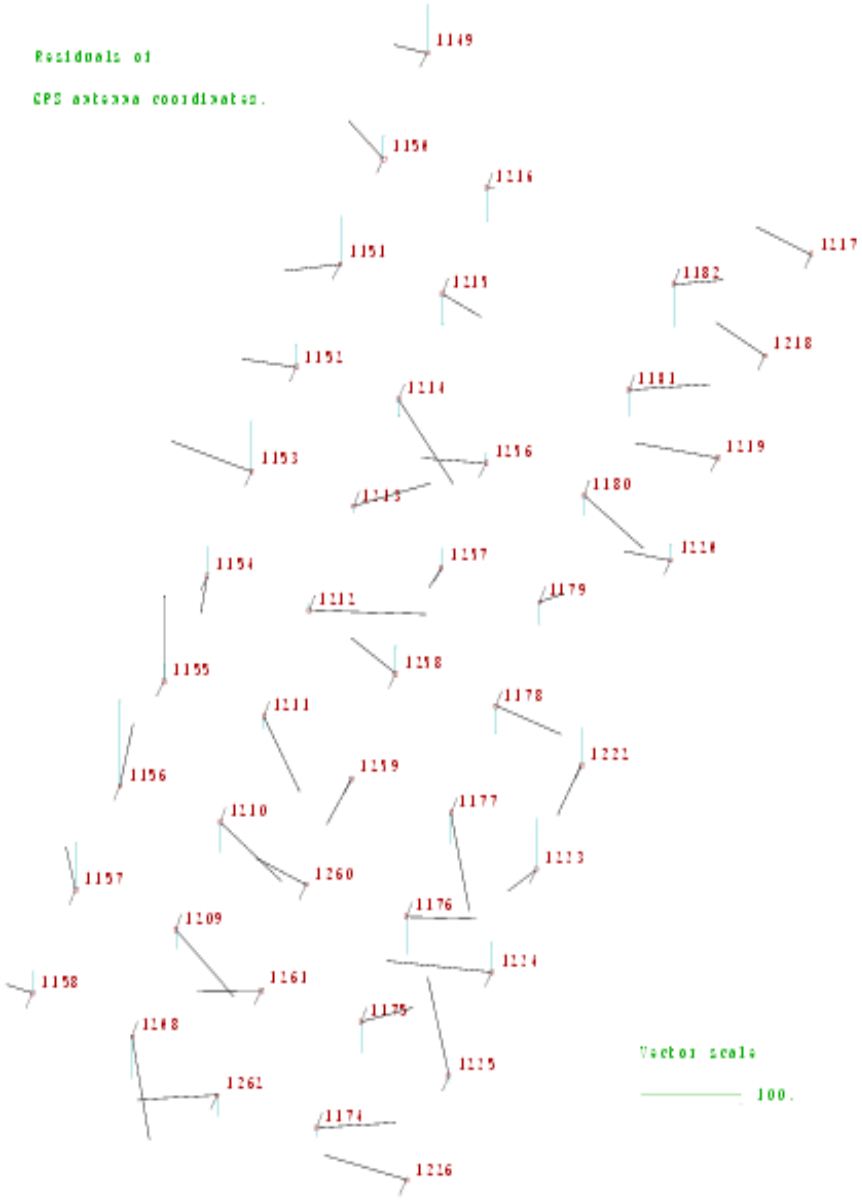

Figure 4: Section from the complete IGI photo flight with large systematic effects (horizontal and vertical residuals, small vectors indicating flight direction), units are mm

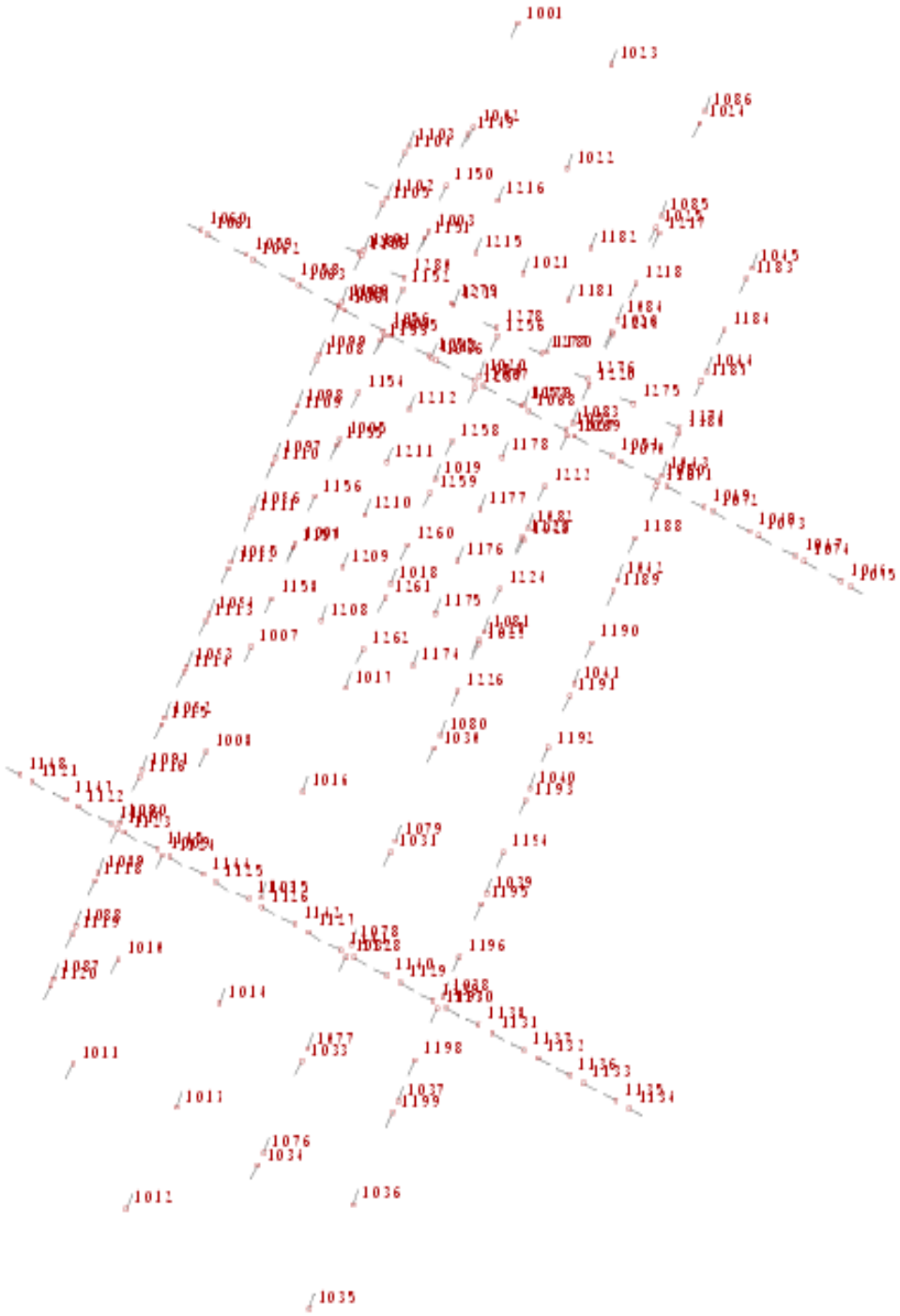

Figure 5: Complete block of IGI photo flight (horizontal and vertical residuals, small vectors indicating flight direction)

Table 4 shows the variations of the principal point for several different adjustment strategies in the free network block adjustment of company 2. The principal point is significantly determined and is verified within the different block configurations.

Generally, comparable misclosures are present in the processing of the complete Applanix block using the provided GPS coordinates for the projection centers (not shown). However, the residuals vanish after introducing one set of unknowns for the principal point of the camera in the adjustment. For the size of the principal point corrections see table 4. The processing and comparison with the rigorous GPS model was not possible, because the GPS raw data were not available.

While the principal point of the IGI block shows again large differences (table 3), the principal point of the Applanix block is stable (table 4). In the free network processing only the photogrammetric data is used. Hence, the GPS/IMU processing results of IGI and Applanix do not have any influence on the results.

The selection of the partial blocks is somehow arbitrary, leading to the not solvable question of the adequate choice for the determination of the different locations of the principal point. Some processing results even indicate, that for some part of the block the differences in the principal point coordinates are much higher.

7 Benefits of Rigorous Modeling of GPS

The benefits of coordinate corrections from the rigorous GPS modeling in the combined GPS/block adjustment have been discussed in the previous chapters. The restriction in the available data made absolute results using independent control points not yet possible. However, from the discussed theory, analysis and from our empirical experiences, the following list summarizes the major advantages of a rigorous GPS modeling in the combined GPS/block adjustment:

- correct modeling of all GPS errors
- independent of strips
- considers the actual GPS model
- considers drift and GPS constellation changes
- reduced number of unknowns
- relative accuracy of GPS coordinates is maintained
- no crossing strips required
- enables separation of systematic GPS errors from i.e. datum parameters, additional parameters of interior orientation
- reduction of side lap possible

8 Aspects for Integration of AT/GPS/IMU

The current attempts in aerial triangulation are to integrate GPS and IMU data for georeferencing. The interest is again to reduce the costs of a photogrammetric survey by substituting photogrammetric data by IMU data. Our experiences with the rigorous GPS modeling show, that also a simultaneous, combined adjustment of GPS/IMU/AT can benefit from a closed approach. It might be necessary to develop special configurations of ground control points and special procedures for the time sequence of flying strips. One particular calibration flight is considered as

not sufficient to model remaining systematic GPS position effects adequately. It might work for certain accuracy requirements, but technical development and adoption of techniques for other applications and accuracy specifications proceed, which makes further investigations useful.

Nevertheless, the correct GPS modeling of remaining error requires the knowledge of the processing involved in all processing steps. The integration of IMU and GPS data must be known at least in some details to decide upon the model to be used in the combined adjustment. On the one hand the IMU data can be used solely as a sensor of orientation in addition to GPS for positioning, on the other hand the IMU data can be integrated for positioning and coupled with GPS data for a combined trajectory. In the latter case, the rigorous model as well as simple shift & drift approximation for remaining systematic GPS errors might fail without the knowledge of the processing.

The accuracy of orientation data from an IMU is generally not sufficient to significantly constrain the external orientation of AT. However, the intention of the use of IMU data is the transfer of exterior orientation with a reduction of ground control points and photogrammetric data. It is essential for this task, that the parameter of interior orientation can be separated from the exterior orientation. The calibration of the camera's principal point must be accurate to 20 µm, because in dependency of the actual photo scale significant errors are possible for the coordinates in object space. Again, there exists a high correlation between IMU data and the principal point. The separation of these error components is only practicable with the rigorous GPS model in the combined adjustment.

9 Conclusion

The rigorous GPS modeling in the combined GPS/block adjustment has been explained. The advantages and benefits of the approach and comparisons with the shift & drift approach have been discussed. The rigorous GPS model in the combined GPS/block adjustment uses the actual GPS satellite geometry and keeps the geometric relationship between individual strips and the complete block. The strengthening of geometry becomes obvious as crossing flight strips can be completely dropped, even for blocks with few control points. The rigorous GPS approach allows to estimate GPS position corrections for a complete block using strictly the functional GPS model. Hence, the correlation with other parameters of interest is significantly reduced, which allows to account for individual error components of the block adjustment.

The use of IMU data in the combined block adjustment is encouraging, although no actual IMU data has been used in this paper, benefits for a closed adjustment of GPS/IMU/AT from the rigorous GPS modeling are expected. Additional investigation and analysis is required in this respect.

At the time of writing, the data of the OEEPE test is restricted. There are no independent checks for absolute comparisons available or other useful comparisons of the rigorous GPS modeling using GEONAP−K/BINGO−F were possible. The check points will be made available in a later phase of the OEEPE test, and will then be used to completed and report the investigations.

After numerous investigation and analysis of the photogrammetric part of the OEEPE test data, it must be assumed, that differences in performance and accuracy of the two data set within the OEEPE test might be caused by the provided photogrammetric data and not necessarily by differences of the GPS/IMU systems of the companies IGI and Applanix. There are a lot of steps involved from picture taking to image coordinate determination, which in general are all capable to introduce the detected effect. However, the principal point is an essential part of the

photogrammetric coordinate determination of the OEEPE test, which even can make results indeterminate as long as a varying principal point location is actually considered possible. A likely cause has not been brought up here and is left for discussion within the actual OEEPE test.

References

Cramer, M. (2001). Personal Communication with E. Kruck. University of Stuttgart, Institute of Photogrammetry/GIP mbh, August.

Heipke, C., K. Jacobsen, H. Wegmann, O. Andersen, B. Nilsen (2000). Integrated Sensor Orientation − An OEEPE Test. IAPRS, Vol. XXXIII, Amsterdam.

Heipke, C., K. Jacobsen, H. Wegmann (2001). The OEEPE Test on Integrated Sensor Orientation − Results of Phase I. Pre−print of paper submitted to Photogrammetric Week 2001, University of Stuttgart.

Jacobsen, K., M. Schmitz (1996). A New Approach of Combined Block Adjustment Using GPS−Satellite Constellation. International Archives of Photogrammetry and Remote Sensing, Vol. XXXI, Part B3, Vienna, 355−359.

Kruck, E., G. Wübbena, A. Bagge (1996). Advanced Combined Bundle Block Adjustment with Kinematic GPS Data. International Archives of Photogrammetry and Remote Sensing, Vol. XXXI, Part B3, Vienna, 394−398.

Schmitz, M. (1998). Untersuchungen zur strengen GPS Parametrisierung in der gemeinsamen Ausgleichung von kinematischem GPS und Aerotriangulation. *Wissenschaftliche Arbeiten Fachrichtung Vermessungswesen an der Universität Hannover*, Nr. 225, Hannover.

Okamoto, A. (1998). Large Scale Aerial Photogaphy and Triangulation Project in Toyonaka City Area. Presentation held at the Seminar of the Japanese Association of Precise Survey and Applied Technology, May 1998, Tokyo.

Wübbena, G., B. Lahr (2000). Grundlagen und Begriffe GPS. *Eisenbahningenieurkalender (EIK) 2000*, Jahrbuch für Schienenverkehr und Technik, VDEI, 317−333.

COMPARISON BETWEEN DIRECT CAMERA ORIENTATION MEASUREMENT AND BUNDLE BLOCK ADJUSTMENT DETERMINATION

Artur João Seara – Head of the Photogrammetric Division of IPCC, Portugal

ABSTRACT

IPCC, the Portuguese NMA, has been executing several blocks in aerotriangulation (AT) with GPS in flight observations support. Since one of our flight suplliers, IMAER, has a GPS/INS Applanix system POS/AV 310, we decided to compare the results coming from the direct measurements, after being processed and converted to our reference system, with the results of the bundle block adjustment with GPS. We used a block with:

- 134 photographs,
- 12 main strips, direction N-S
- no cross strips
- 32 full control points plus 11 height control points
- mean flying height of 788 meters
- lens principal distance of 153.073 mm
- mean photo scale of 1/5100
- average overlap of 62%
- average sidelap of 10%

The differences **in** Ω, Φ, and K were determined for all of the photograps as well as in X, Y, and Z, in the national terrain system – Ellipsoid Hayford, Projection Gauss, Datum 73.

1. Introduction

Since 1998 IPCC has been receiving exterior orientation parameters, directly derived from GPS/INS in flight measurements, from one of our aerial photography suppliers, IMAER. This data, in the beginning, appear to be rather incomplete and carrying large errors. Since 1999 the data has become more reliable and we decided to do some comparison between the GPS/INS data and the one resulting from block adjustment. Here we describe the results of a block whose aerial triangulation (AT) output was computed in a production environment, aiming the stereoplotting at large scale, 1/1000 and 1/2000.

2. Main aspects of the work

The photo flight of the area of this study took place in September 2000 and has the following properties:

Number of photographs: 134

Number of strips (GPS profiles): 12, designated as 7, 8S, 8C, 9S, 9C, 10S, 10C, 11S, 11N,12S, 12N and 13S

No cross strips

Mean flying height:788 m

Focal length: 153.073 mm

Mean overlap: 62%

Mean sidelap: 10%

Camera: Leica RC 30

GPS/INS: Applanix POS/AV 310.

Ground control:

11 vertical points with a a priori standard deviation of 0.05 m

32 total points with the same a priori accuracy

Perspective centers X, Y and Z coordinates, coming from GPS/INS were used as observations with a a priori standard deviation of 0.18 m. These coordinates were given to IPCC already in the terrain system we use in our mapping, this means, International Ellypsoid, Gauss-Kruger Projection and a National planimetric and altimetric datum.

In Annex we have a draft of the flight with the strips and the position of the ground control.

AT equipment:

Artificial points were used, marked with WILD PUG.

Observations were carried out in a LEICA AC1 analytical plotter.

Adjustment performed with LEICA Orima-TE and CAP-A bundle block program.

According to Applanix, the 310 GPS/INS model has an absolute accuracy of 0.05 to 0.30 m in the X, Y and Z parameters, 0.013 degrees in Roll and Pitch and 0.035 degrees in heading. The 410 and 510 models are more accurate but IPCC has no flights with these systems.

3. Exterior orientation results

First we compared the exterior orientation parameters (X, Y, Z, W, F, K), for all the 134 photographs in the block. The bundle block adjustment computed the following average Standard Deviation for the exterior orientation parameters:

X - 0.19 m

Y – 0.14 m

Z – 0.10 m

Ω – 0.009 degrees

Φ – 0.011 degrees

K – 0.004 degrees.

The ranges and mean values of the differences between the GPS/INS data and the AT data are in Table I. In this table as well as in the next ones, the units are meters and degrees.

TABLE I – REAL AND ABSOLUTE DIFFERENCES FOR THE WHOLE BLOCK

	DX	DY	DZ	D Ω	DΦ	DK	|DX|	|DY|	|DZ|	|DΩ|	|DΦ|	|DK|
from	-0.984	-1.535	-0.833	-0.034	-0.050	-0.052	0.003	0.117	0.001	0.000	0.000	0.000
to	0.929	1.177	0.296	0.030	0.067	0.041	0.984	1.535	0.833	0.034	0.067	0.052
average	0.062	-0.213	-0.228	-0.001	0.004	-0.009	**0.368**	**0.771**	**0.251**	**0.010**	**0.021**	**0.012**

The values in bold represent the mean error, this is, the average of the absolute values of the differences. As we can see the mean error in Y is large; also in X and in F we have not very good values.

Knowing that the GPS in flight data has usually a behaviour that can be rather different from profile to profile, we made a comparison for each of them. As stated before we have in this block 12 profiles. Tables II to XIII show the results profile wise.

TABLE II – DIFFERENCES FOR STRIP 7 (24 PHOTOS)

	DX	DY	DZ	DΩ	DΦ	DK
from	-0.140	-1.319	-0.222	-0.030	-0.050	-0.024
to	0.732	-0.785	0.296	0.017	0.015	0.006
average	0.275	-0.981	0.022	-0.007	-0.014	-0.007

TABLE III – DIFFERENCES FOR STRIP 8S (11 PHOTOS)

	DX	DY	DZ	DΩ	DΦ	DK
from	0.096	-1.097	-0.279	-0.034	-0.008	-0.020
to	0.434	-0.729	0.008	0.005	0.017	0.005
average	0.274	-0.892	-0.108	-0.009	0.004	-0.006

TABLE IV – DIFFERENCES FOR STRIP 8C (14 PHOTOS)

	DX	DY	DZ	DΩ	DΦ	DK
from	-0.754	0.335	-0.240	-0.022	0.019	-0.052
to	-0.152	0.924	-0.086	0.006	0.043	0.010
average	-0.388	0.478	-0.177	-0.004	0.035	-0.011

TABLE V – DIFFERENCES FOR STRIP 9S (14 PHOTOS)

	DX	DY	DZ	DΩ	DΦ	DK
from	-0.532	0.224	-0.425	-0.011	-0.004	-0.026
to	0.050	0.945	-0.153	0.020	0.043	0.000
Average	-0.235	0.678	-0.260	0.004	0.017	-0.019

TABLE VI – DIFFERENCES FOR STRIP 9C (13 PHOTOS)

	DX	DY	DZ	DΩ	DΦ	DK
from	0.245	-1.297	-0.401	-0.031	-0.036	-0.010
to	0.594	-0.655	-0.162	0.016	0.009	0.041
Average	0.357	-1.012	-0.304	0.004	-0.012	0.003

TABLE VII – DIFFERENCES FOR STRIP 10S (7 PHOTOS)

	DX	DY	DZ	DΩ	DΦ	DK
from	-0.040	-0.847	-0.745	-0.020	-0.007	-0.022
to	0.201	-0.528	-0.439	0.000	0.020	-0.004
average	0.089	-0.711	-0.568	-0.010	0.010	-0.013

TABLE VIII – DIFFERENCES FOR STRIP 10C (9 PHOTOS)

	DX	DY	DZ	DΩ	DΦ	DK
from	-0.626	0.117	-0.833	-0.007	-0.022	-0.017
to	-0.355	0.570	0.037	0.030	0.038	0.022
average	-0.479	0.381	-0.352	0.013	0.017	-0.001

TABLE IX – DIFFERENCES FOR STRIP 11S (8 PHOTOS)

	DX	DY	DZ	DΩ	DΦ	DK
from	-0.065	0.609	-0.727	-0.022	-0.035	-0.017
to	0.553	0.903	-0.302	0.006	-0.006	-0.004
average	0.340	0.729	-0.457	-0.005	-0.024	-0.009

TABLE X – DIFFERENCES FOR STRIP 11N (7 PHOTOS)

	DX	DY	DZ	DΩ	DΦ	DK
from	-0.133	-1.535	-0.372	-0.009	-0.006	-0.040
to	0.288	-0.996	-0.156	0.027	0.017	-0.013
average	0.093	-1.222	-0.272	0.012	0.005	-0.028

TABLE XI – DIFFERENCES FOR STRIP 12S (8 PHOTOS)

	DX	DY	DZ	DΩ	DΦ	DK
from	0.445	-0.988	-0.353	-0.020	-0.038	-0.019
to	0.920	-0.521	0.110	0.012	-0.007	0.007
average	0.616	-0.736	-0.272	-0.007	-0.018	-0.007

TABLE XII – DIFFERENCES FOR STRIP 12N (7 PHOTOS)

	DX	DY	DZ	DΩ	DΦ	DK
from	0.552	0.252	-0.252	-0.011	-0.033	-0.021
to	0.929	0.574	-0.158	0.017	-0.011	-0.011
average	0.699	0.402	-0.193	0.007	-0.026	-0.016

TABLE XIII – DIFFERENCES FOR STRIP 13S (12 PHOTOS)

	DX	DY	DZ	DΩ	DΦ	DK
from	-0.984	0.298	-0.562	-0.011	0.019	-0.029
to	-0.252	1.177	-0.195	0.014	0.067	0.024
average	-0.559	0.762	-0.364	0.004	0.043	-0.002

Looking at the tables above it is easy to detect a systematic deviation in some of the parameters. Since we had the AT output, it was evident a direct relation between the Y differences and the Y drift parameter computed by the block adjustment for the GPS profiles. Besides this almost general systematic deviation in Y, also we consider as being systematic some differences in the parameters of other profiles. Being so, it was made a new comparison for the strips taking out the systematic differences, for some parameters, as follows:

Profile 7 – X and Y

Profile 8S – Y

Profile 8C – X, Y and Φ

Profile 9S – Y

Profile 9C – X and Y

Profile 10S – Y and Z

Profile 10C – X, Y and Z

Profile 11S – Y and Z

Profile 11N - Y

Profile 12S – X and Y

Profile 12N – X and Y

Profile 13S – X, Y and Φ .

This procedure brings, of course, better results for the strips and also for the whole block. Table XIV shows the differences as in Table I but with these new values.

TABLE XIV – ABSOLUTE DIFFERENCES FOR THE WHOLE BLOCK

	|DX|	|DY|	|DZ|	|DΩ|	|DΦ|	|DK|
from	0.001	0.000	0.001	0.000	0.000	0.000
to	0.553	0.464	0.481	0.034	0.050	0.052
Mean error	**0.177**	**0.136**	**0.149**	**0.010**	**0.015**	**0.012**

As one can see from this table, the mean errors, in bold, got considerably better in X, Y, Z and F, showing that, in average, one can produce photogrammetric products, in scales as large as 1/2000, with this data from GPS/INS since there is an efficient elimination of systematic errors; however the highest values in the middle row indicate that there are areas with large differences allowing only tasks at the scale 1/5000 or smaller.

4. Point measurement

Next, some points were measured in a digital photogrammetric station introducing the exterior orientation coming from GPS/INS and from AT. The selection was made on the photographs that showed larger differences, specially in Y coordinate. After the interior orientation has been made it was possible to measure the points in 3D on the stereo models formed by some pairs of photographs. In 6 models we measured 7 or 8 points per model and the differences were computed as shows Table XV. Again it is notorious the systematic differences in Y coordinate in 5 of the 6 stereo models.

TABLE XV – DIFFERENCES IN X, Y, Z FOR THE POINTS MEASURED

STRIP NUMBER	MODEL NUMBER	POINT NUMBER	DX	DY	DZ	|DX|	|DY|	|DZ|
7	19/18	77225	-0.10	0.50	-0.30	0.10	0.50	0.30
		74002	-0.40	0.60	-0.20	0.40	0.60	0.20
		77226	0.00	0.60	0.10	0.00	0.60	0.10
		70018	-0.10	0.70	0.20	0.10	0.70	0.20
		78226	0.30	0.70	0.10	0.30	0.70	0.10
		76002	0.10	0.70	-0.10	0.10	0.70	0.10
		78225	0.20	0.90	-0.50	0.20	0.90	0.50
		70019	0.00	0.60	-0.30	0.00	0.60	0.30
	Average for model		0.00	0.67	-0.13	**0.15**	**0.67**	**0.23**
8C	45/46	87215	0.05	-0.61	-0.14	0.05	0.61	0.14
		78215	0.01	0.33	-0.23	0.01	0.33	0.23
		87216	0.08	-0.37	0.43	0.08	0.37	0.43
		80046	0.13	-0.11	0.43	0.13	0.11	0.43
		88216	-0.13	-0.48	0.37	0.13	0.48	0.13
		88215	0.05	0.09	0.25	0.05	0.09	0.25
		80045	0.33	-0.86	0.29	0.33	0.86	0.29
	Average for model		0.07	-0.21	0.20	**0.11**	**0.41**	**0.31**

8S	66/65	78205	0.12	0.85	0.01	0.12	0.85	0.01
		10903	-0.20	0.91	-0.24	0.20	0.91	0.24
		78206	-0.49	1.15	-0.07	0.49	1.15	0.07
		80265	-0.24	1.17	0.20	0.24	1.17	0.20
		88206	-0.13	1.26	0.34	0.13	1.26	0.34
		88205	-0.50	0.94	-0.11	0.50	0.94	0.11
		80266	-0.30	0.99	-0.18	0.30	0.99	0.18
	Average for model		-0.25	1.04	-0.01	**0.28**	**1.04**	**0.16**
11	200/201	117206	0.02	-0.35	0.53	0.02	0.35	0.53
		117207	0.57	-0.22	-0.39	0.57	0.22	0.39
		110201	0.04	-0.27	0.45	0.04	0.27	0.45
		118207	-0.37	-1.05	0.00	0.37	1.05	0.00
		118206	0.23	-0.82	-0.05	0.23	0.82	0.05
		124001	0.09	-0.59	-0.20	0.09	0.59	0.20
		110200	0.04	-0.67	0.86	0.04	0.67	0.86
	Average for model		0.09	-0.57	0.17	**0.19**	**0.57**	**0.38**
9C	36/35	88215	0.22	0.83	0.03	0.22	0.83	0.03
		88216	0.29	0.93	-0.15	0.29	0.93	0.15
		90035	0.02	1.05	-0.05	0.02	1.05	0.05
		98217	-0.37	1.15	-0.26	0.37	1.15	0.26
		98216	-0.26	1.48	-0.34	0.26	1.48	0.34
		907215	-0.46	1.14	-0.04	0.46	1.14	0.04
		90036	-0.14	1.06	-0.05	0.14	1.06	0.05
		90254	-0.12	0.85	-0.02	0.12	0.85	0.02
	Average for model		-0.10	1.06	-0.11	**0.24**	**1.06**	**0.12**
9S	44/45	88206	-0.49	-1.11	0.12	0.49	1.11	0.12
		97207	-0.18	-1.11	0.08	0.18	1.11	0.08
		882071	-0.23	-1.24	0.70	0.23	1.24	0.70
		90245	-0.15	-0.71	-0.22	0.15	0.71	0.22
		98207	-0.03	-1.06	0.03	0.03	1.06	0.03
		98206	-0.04	-1.02	0.38	0.04	1.02	0.38
		90244	-0.06	-1.07	0.41	0.06	1.07	0.41
	Average for model		-0.17	-1.05	0.21	**0.17**	**1.05**	**0.28**

In bold we have the mean error per model in X, Y and Z.

5. Conclusions

The occurrence of some systematic differences, treated as drift parameters in the bundle block adjustment, may lead to the conclusion that these were not completely overcome in the processing of the GPS/INS data of this project or some calibration procedure has failed. On the other hand, having in mind that this is not the best GPS/INS system from Applanix (310), may be with the 410 or 510 models better results would be achieved. Anyway, for scales 1/10000 or smaller one could work with all the photographs of the block with the data coming from GPS/INS. It looks like that, sooner or later, may be sooner, flights with GPS/INS will allow direct introduction of exterior orientation parameters, with accuracies enough for large scale mapping, making easier and shorter the flight planning, besides avoiding ground control and AT

ANNEX

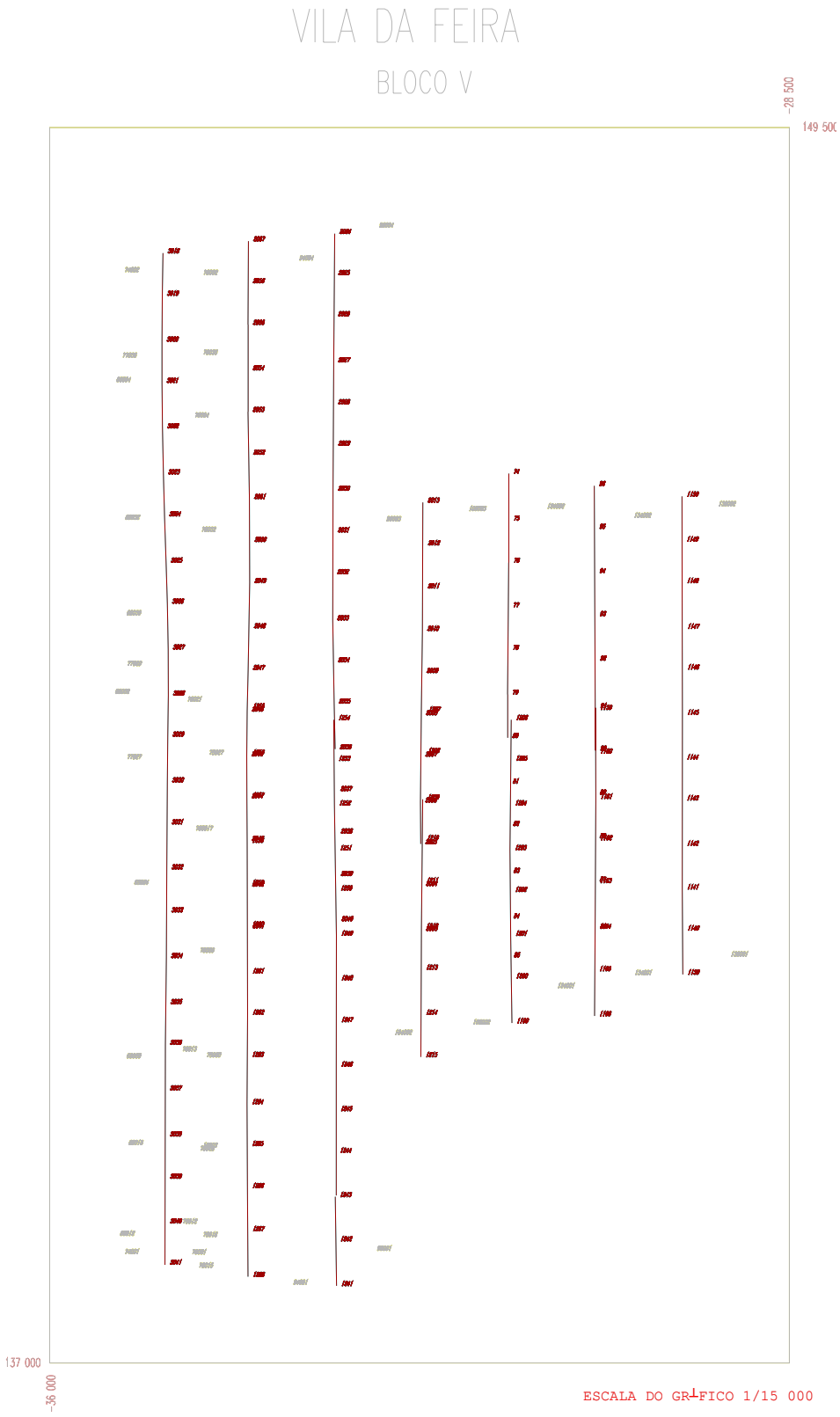
VILA DA FEIRA
BLOCO V
-28.500
149.500
137.000
-36.000
ESCALA DO GRÁFICO 1/15 000

Handheld Mobile Mapping system for Helicopter-based Avalanche Monitoring

Julien Vallet
Swiss Federal Institute of Technology
Institute of Geomatics, Photogrammetric lab.
CH 1015 Lausanne - Switzerland
Phone: +41 21 693 2775
Fax: +41 21 693 5720
Email: julien.vallet@epfl.ch

Key Words: Photogrammetry, Navigation, Handheld, GPS, IMU, Avalanche mapping.

ABSTRACT

The study of avalanches requires techniques that can provide accurate and sporadic geo-referenced data. When facing difficult accessibility of the terrain and large mapping areas, the aerial photogrammetry offers the best solution to this problem. Nevertheless, in this specific domain, the classical photogrammetry reaches its limits when volumes of snow are the parameters to be determined. The difficulties of installing durable signalization in such areas initiated the development of a system that uses navigation solution to determine the parameters of exterior orientation. It integrates light aerial camera and GPS/INS components to a platform that is free of the helicopter in 6 degrees of freedom. Experimental studies performed in the avalanche test site of "Vallée de la Sionne" allow determining the correct ratio between the system accuracy versus its flexibility. The system should be light and flexible whereas the accuracy of the camera projection centre needs to be determined with an accuracy of 15-20cm and 0.005-0.01° in position and attitude, respectively. The paper presents the design of the system setup on a solid handheld platform, a summary of the results obtained with just GPS integration and a comparison with standard Bundle Block Adjustment.

1. INTRODUCTION

In the specific domain of snow transportation (avalanche, wind), accurate data concerning the snow cover needs to be quickly and sporadically acquired over inaccessible and dangerous areas. Procedures combining Aerial triangulation, DGPS are commonly used to provide DTM and volume measurements. Although those techniques need only a minimum of Ground Control Points (GCP's) (Ackerman, Schade 93), the avalanche and winter environment make the establishment of any signalization a slow and dangerous process (Fig.1). Moreover, it is difficult to maintain permanent and visible signals throughout all the winter, due to frequent avalanches and quickly changing of snow cover. The Swiss Federal Institute for Snow and Avalanche Research (SFISAR), managing several avalanche study sites in the Alps. Among them, the studies conducted in "Vallée de la Sionne" (Issler, 99) require a mapping system that does not need GCP's establishment and that can be mounted on standard mountain's helicopter in a few minutes.
To avoid the use of any GCP's in the photogrammetric process, the six parameters of the exterior orientation has to be measured directly onboard by navigation sensors. The potential of using DGPS and inertial integration for this purpose has been strongly demonstrated during the eighties (Schwarz et al. 84, Hein et al. 88) and finally found practical and industrial applications in the mapping system during the second half part of the nineties (Abdullah, 97). Its application field has widened to non-photogrammetric system as pushbroom scanner, laser scanner or Synthetic Aperture radar (SAR).

Although the utilization of the Laser Scanner or airborne SAR is very attractive for snow mapping, due to the independence in contrast and illumination, their cost, limited setup flexibility and size led to a design of a system that integrates an optical aerial handheld camera and a small lightweight INS/GPS.

In following, the design of the system in development will be presented. The emphasis will be on the unique setup of all instruments for such a dedicated task. Finally, results of the test with GPS will be presented.

Fig. 1 : Difficulties to setting up the GCP in the avalanche environment

2. MAPPING REQUIREMENTS

In the Swiss Alps and particularly in the large avalanche test site located in "Vallée de la Sionne", the method of photogrammetry is used to precisely measure the surface of the snow cover before (when possible) and after the avalanche, and to map the boundaries of avalanche events. This allows an estimation of the released mass of snow in the starting and deposition zones. Its periodic mapping revealed following constraints that are not easy to fulfil by the standard procedures:

- An undisturbed cover of fresh snow has very small contrast. Hence, a precise measurement of the snow cover in the release zone before the triggering is difficult. Therefore, a full sunny illumination with optimal incidence angle is necessary to provide sufficient contrast.
- An artificial avalanche release cannot be planned sooner than 3 days in advance. Therefore, the implementation of a mapping procedure must be quick and flexible.
- The pictures of the release zone must be acquired before 9.00 a.m. since the likelihood of a successful triggering quickly decreases after 10 a.m.
- The surveying and placement of GCP's in the release and deposition zones is very difficult, since these points must be placed on exposed rocks that remain clearly visible even after a heavy snowfall and out of reach of the avalanche runoff. Temporary signalization is not conceivable since it is extremely dangerous to access the site during experiments and may result in systematic errors between the events (e.g., unsuitability due snow settlement).

2.1. Snow Height

The accuracy required on the snow height measurements is 10% of the snow depth and therefore will depend on the thickness of the snow layer. That varies considerably between the deposition and the release zones.

In the release zone, the thickness seldom exceeds 3m and therefore a high accuracy of 15-30cm is needed. Experiments show that the lack of contrast due to fresh snow generates a random noise of 60cm on single point measurement (Vallet et al. 2000). However, although this noise seems critical for a 3D-modelisation of the snow pack, its influence on the final volume is strongly reduced when averaged over larger area. Also, the determination of the height of the fracture line is less sensitive to the errors in absolute orientation because this measurement is relative and involves only one image pair. Hence, two types of errors affect the mapping accuracy in the release area: First and mainly, the systematic errors in parameters of exterior orientation (either bad or insufficient distribution of GCP's

or errors in navigation sensors providing these parameters), second, the lack of contrast that directly influences the plotting accuracy.
In the deposition zone, the main parameter of interest is the accumulated snow volume and its distribution. As contrast is usually excellent in this zone, the plotting accuracy is at the level of few centimetres. Therefore, the quality of the exterior orientation is the crucial factor affecting the accuracy of volume measurements in this zone. Since the required accuracy depends on the volume and snow distribution (i.e., absolute snow height), a precise measurements at the level of +/-20-30cm on snow height are required for small avalanches whereas for large avalanches, an accuracy of 50cm is sufficient.

2.2 Exterior orientation requirements

Simulations studies (Vallet, et al. 2000) revealed that an accuracy of 10-20cm for projection centre and 20"-30" for camera attitude allow ground accuracy of 15-30cm.
Considering a DGPS/INS system that provides navigation parameters with an accuracy of 10-20 cm and 20"-30", respectively, the errors in position and attitude have similar effect on the ground coordinates. Such system should be feasible to implement while satisfying the overall requirements of 15-30cm mapping accuracy.

3. SYSTEM DESIGN

The topography of an avalanche area is composed of steep slope in the release zone that decreases toward deposition. To acquire of pictures with constant scale, oblique and vertical photographs are taken. Therefore, the system has to be adjustable at flight to allow capture both type of imagery. For this reason, we propose to keep the camera-INS-GPS frame free from the helicopter. Such setup has an advantage of dampening vibrations with the body instead of employing a complex dampening system (silent block, springs, gyro) on the helicopter.
The choice of a helicopter as the system carrier is justified by its capability to fly close to the ground at low speed. This allows capturing large-scale photographs and provides better flight line navigation flexibility.

3.1. Navigation Component

An embedded GPS receiver and a small, tactical grade strapdown inertial system (LN-200) with fibre-optic gyros are integrated into a loosely coupled real-time aiding loop over the VME (Versa Module Eurocard) bus. The system is capable of performing the real-time code differential aiding and all raw measurements are stored on the hard disk for intense post-mission filtering including carrier-phase differential GPS/INS integration. The GPS receiver provides the L1 and L2 carrier phase data at 10 Hz while the raw inertial measurements are stored at 400 Hz. The high data rate should guarantee that all platform frequencies are recovered without the effect of aliasing. Hence, the camera absolute position and orientation can be found by interpolation between two neighbouring navigation solutions after considering the relative offsets existing among the devices. According to recent studies (Cramer 1999, Skaloud, 1999) such systems should fulfil the accuracy requirement for the parameters of exterior orientation.

3.2. Imagery Component

In order to fulfil the required flexibility while preserving a sufficient image quality, a light handheld Linhof Aerotechnika camera has been selected (Figure 2). This camera stores up to 200 colour, large format photographs (4x5 inch) and has a 90mm wide angle lens. Its total weight reaches 8kg. The Linhof is not a metric camera because the "pseudo" fiducial marks are not clearly defined and that affects the determination of the principal points. Insertion of precise marks has been performed using small diffractive diffusers in the four corners of the picture frame.

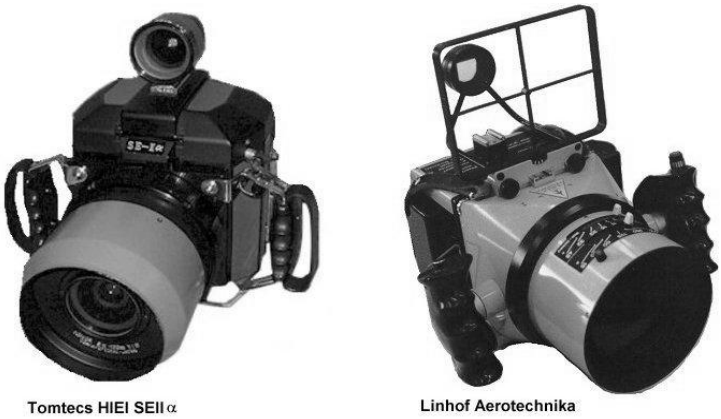

Fig. 2: Both Tomtecs and Linhof handheld light aerial camera

Another handheld camera in consideration is the Tomtecs HIEI G4 with 370 colour pictures capacity, 5x5 inch format and 90mm lens. Although it is a metric camera, its weight of 13 kg ranks it as a second choice.

Furthermore, some type of digital camera is considered to arrive with a fully digital mapping system. Even if the chip's format is still to small, tests are performed to compare the noise level with an analogue camera.

3.3. Synchronization

The GPS and INS data are synchronized over the VME bus at the level of 1 µs in the GPS time frame. The event of camera exposure is also brought in as a pulse to the VME bus and the accuracy of the time stamping driven by an interrupt is at the level of few µs.

For the Linhof camera, the triggering of the shutter was planned to be performed by a switch but several tests revealed that the delay between the switch pulse and the real shutter aperture was changing with temperature at a level of 6-7ms for a range 20°C à 0°C.

Since the temperature of the camera changes during the flight, a shutter aperture with electro-optical solution was implemented. Four photodiodes detect the shutter aperture and send trough integrated circuit a TTL signal to Event input of the GPS receiver. The event is recorded at the falling front edge of a 10ms wide pulse. Overall, this method allows synchronization to be better than 2 ms, which corresponds to the aperture speed at 1/500 sec. The Tomtecs camera is synchronized by a Mid Exposure Pulse signal fed by PPS and NMEA signals.

3.4. Helicopter Mount

Placing a sensor in an airborne carrier is a non-trivial task. A poor sensor mount is most likely to alter the performance of the whole system and errors of such type may be very difficult to correct for (Skaloud, 1999). In this case, the requirements on sensor placing are motivated by following objectives:

- to minimize the effect of calibration errors on lever-arm corrections,
- to avoid any differential movements between sensors,
- to minimize noisy vibrations of the helicopter.

- to enable manual orientation of the camera towards the mountain face and to capture oblique as well as vertical imagery.

Fig. 3 : Tomtecs camera mounted with GPS antenna. The INS is mounted under the camera. During the picture session, the block camera-antenna is only hold by the operator.

Addressing the first objective, short distances between the sensors reduce the impact of uncertainties in the lever-arm corrections. This especially affects the positioning component of direct-georeferencing.
For this reason the IMU is mounted directly over the top of the camera through a common platform which carries also the GPS antenna (Figure 3-4). Stiffness and lightness of the antenna mast is assured by a carbon pipe of 21mm.

On the other hand, small differential movements mainly alter the attitude performance. This undesirable effect should be prevented by the rigidity of the steel-aluminium-carbon holder connecting all system components. The first version of the camera holder implements no vibration dampers and these are dampened through the body of a person handholding this lightweight system during the picture session (Fig 5).

During the transition flight the systems is stiffly mounted outside the helicopter on a steel frame (Fig. 3). At the beginning of the picture session, the INS-GPS-camera block is removed from the steel frame through the side door and becomes totally handheld by the operator.

Fig. 5: The camera is held and the vibrations are dampened by the body of the operator.

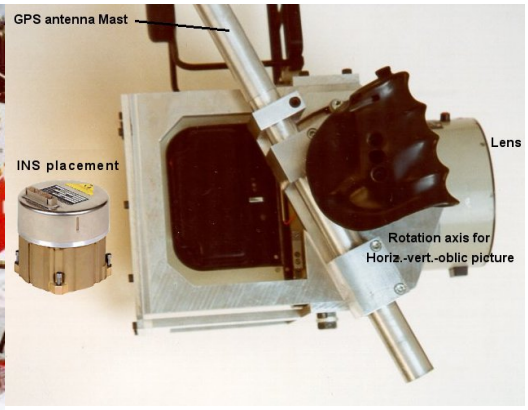

Fig. 4: Detailed views of the camera frame with the INS position and possible rotations for the GPS mast.

Manual control allows fulfilling the last requirements on orientation towards the mountain face around the omega angle. To capture either oblique or vertical picture, the camera can rotate around the Phi axis in relation to the GPS mast, which remains more or less vertical. This angle cannot be adjusted during the flight to keep the offset parameters constant. Its adjustment is preformed prior to the flight according to type of photographs to be captured.

Safety cables limit the vertical motion of the antenna below the rotor and secure the system in case of emergency. The frame has been designed as light as possible for handholding in collaboration with a helicopter company.

A second GPS antenna is placed on the tail of the helicopter to aid the inertial system with the GPS-derived azimuth.
The helicopter Alouette III (Fig. 3) has been chosen because of its sliding door and the absence of skis, that gives free view angle from ground to sky. Moreover, this type of helicopter is designed for mountaineering flight (e.g. powerful turbine, light weight, maneuverability). Data acquisition is centralized in the cockpit of the helicopter. The required time to mount the whole system is about 20 minutes.

3.5. System Calibration

The calibration of all sensors used in the integrated system is an essential step prior to a survey mission. System calibration can be divided into two parts: calibration of individual sensors and calibration between sensors. The calibration of the individual sensors may include the calibration for camera interior orientation, INS calibration for constant drifts, biases or scale factors, GPS antenna multipath calibration, etc. An extensive literature exists on each of these topics. Calibration between sensors involves determining the relative orientation difference between the camera and the inertial system as well as the constant synchronization offset inherently present due to data transmission and internal hardware delays. For that purpose, it is essential to use a well-determined block with images of strong geometry to derive the parameters of exterior orientation by means of a bundle-adjustment with an accuracy of 10-15 cm in position and 20 arc seconds (~ 0.005°) in attitude. For this purpose a permanent calibration test field is going to be established near the airport so the calibration can be performed routinely before and after each mission. The targets will be permanent ground marks and building corners that stay clear throughout the winter.
Shift offsets between GPS antenna, IMU center and projection center are directly measured with a theodolite with an accuracy of 5 mm.

3.6 Costs

Another aspect of the design was to minimize the cost. Although navigation sensors are quite expensive (INS above all), the global cost of this system is inferior to 80'000 US$. In comparison with other potential system as Laser scanner (1 Mio US$) or standard aerial camera, this system is relatively cheap. With the use of GPS only the cost could be reduce for half.

4. TEST OF GPS EXTERIOR ORIENTATION AT “VALLÉE DE LA SIONNE”

Photogrammetric avalanche mapping is a difficult task but four years of experiences at the “Vallée de la Sionne” have demonstrated the feasibility of the method (Vallet, 2000). The placement of GCP’s being the crucial problem, we investigate in ways to perform the exterior orientation with a minimum of GCP’s.

As IMU was not ready to install, we decided to make a test with only one GPS antenna and the Tomtecs camera.. Indeed, it is possible to determine the entire exterior orientation parameters using two strips with a large side overlap with only GPS data. The second strip serves to determine the omega angle (roll) which can not be fixed with one single line.

4.1. Experimental procedure

We use for this test the GPS receivers Leica SR500 with 10Hz data rate sampling. Reference station is situated near the test field. The base line is about 1.5 km and the height difference is about 1000m (Fig. 6).
We flew over the avalanche site according four lines:

- 2 strips in the release area forming a block with a side overlap of 70%. The scale is about 1:4000 for the first line and 1:4500 for the second line. In order to respect the winter condition, we took oblique pictures. The ground is partly covered of snow (May) but allow tie point measurements with a good distribution. The area is signalized with 21 aluminum plates determined by terrestrial measurements (theodolite) with an accuracy of 10 cm. Those points are impossible to determine by GPS survey because they are located in cliffs.
- 2 strips in the deposition area. The scale is about 1:6000. The fact that the helicopter deviated from the planned line involves a poor geometry block. The presence of shadow in this area obliged to decrease the speed aperture of the shutter to 1/125 sec instead of 1/500 sec. It results in some blur pictures. For those reasons, those strips have not been used. The deposition area is signalized with 20 aluminum plates measured by GPS.

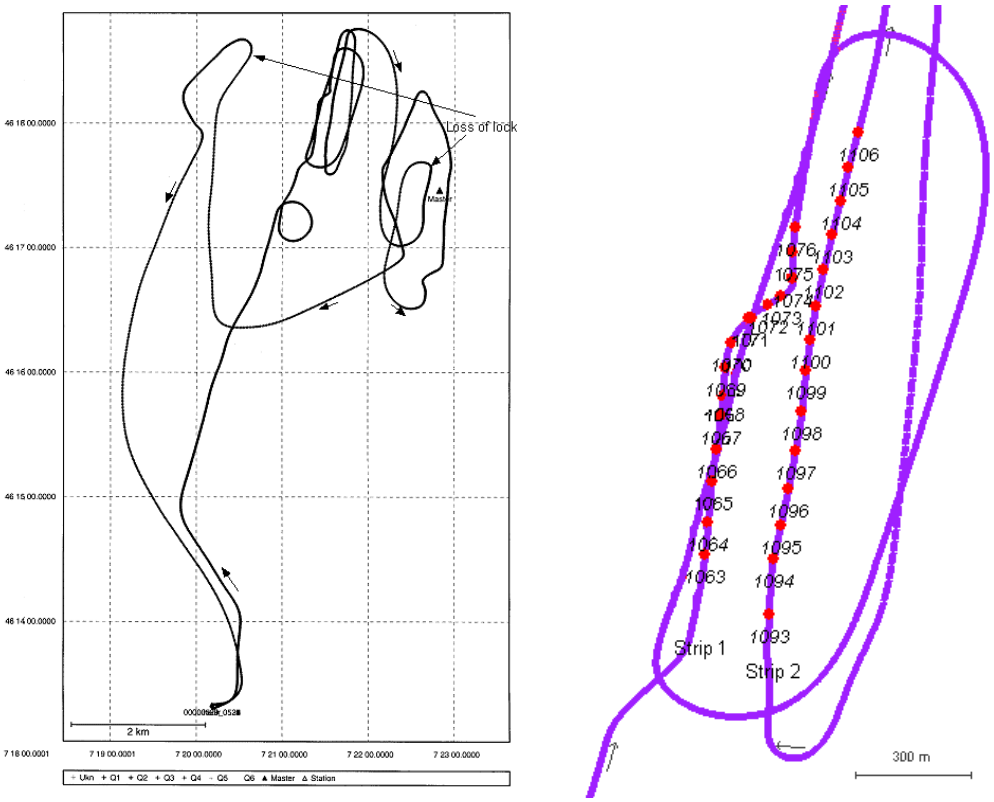

Fig. 6 : Map of the flight. Entire Flight (left) and Detail for the release area with the camera position(right).

During the transition flight, from the airport to the interest area, the camera was mounted on the helicopter frame. Astonishingly, the feared vibrations was not so important. It is probably due the weight of the system (15kg) giving some inertia. At each picture session, the set camera-GPS antenna was removed from the frame and all the vibrations were damped by the operator. Due to the high weight of the Tomtecs G4 camera, the system was re-mounted on the helicopter frame between each line. We expect to avoid this with the lighter Linhof camera.

The main purpose is to see which precision on the GCP's residuals we can obtain with the measurements of the camera position by GPS with as less control points as possible. In this way, we have the block in the release area which meets the requirements (2 strips, 70% side overlap) for GPS adjustment without control points.

Pictures have been scanned with the DSW200 scanner, with a pixel size of 10 microns. 130 tie points and 21 GCP's have been manually measured on the block of 15 images with Socet Set of LH systems. The offset ***e'*** between the GPS antenna and the projection center was determined with theodolite measurements and with an accuracy of 5 mm.

4.2. Results

We have used the software GRAFNAV for the GPS computation and BINGO-F for all the block adjustments. Time marks are printed on the picture (Tomtecs, 2001). All the angles are given in the PHI, OMEGA, KAPPA sequence.

4.2.1. GPS results:

Six satellites were available during all the flight. We detect two loss of lock. One just before the third line in a quick turn, probably due to the inclination of the helicopter and another one before returning (turn) (fig. 6). We did not encounter any problem of reception through the propeller. We used only L1 to compute the position until the first loss of lock. Ambiguities were fixed until this point and the positions of the antenna for each picture in the strips 1 and 2 has been determined with an accuracy of 5-7cm.

4.2.2. Triangulation results

In order to have a point of comparison, we have computed first a standard aerial triangulation (AT) with all the GCP's and tie points (tab. 1). As we had not the real calibration sheet of the camera HIEI-G4, we computed also a self-calibration parameters to determine the focal length ***c'*** and the position of principal point of symmetry (***x', y'***). Those computed values have been used after for all adjustment.
We have made several kinds of computation with the GPS data:

- GPS data and 3 GCP's
- GPS data and 3 GCP's with SHIFT and DRIFT parameters
- GPS data and 3 GCP's with SHIFT parameter
- GPS data without any GCP's
- GPS data with 1 GCP
- GPS data and all GCP's

All the results figure in the following tables 1 and 2.

Adjustment type	Sigma [µm]	RMS X,Y [m]	RMS Z [m]	RMS Φ [g]	RMS Ω [g]	RMS K [g]
AT	7.44	0.09	0.08	0.014	0.01	0.0085
GPS-3GCP	8.62	0.03	0.03	0.009	0.006	0.007
GPS-3GCP shift	8.17	0.10	0.12	0.023	0.007	0.010
GPS-3GCP Shift/drift	7.87	0.14	0.15	0.029	0.0111	0.014
GPS	7.98	0.03	0.02	0.011	0.0067	0.008
GPS-all GCP	8.17	0.03	0.02	0.006	0.005	0.006
GPS-1GCP	8.10	0.03	0.02	0.009	0.006	0.007

Tab. 1 : Sigma and RMS values on the exterior orientation parameters for each type of computation

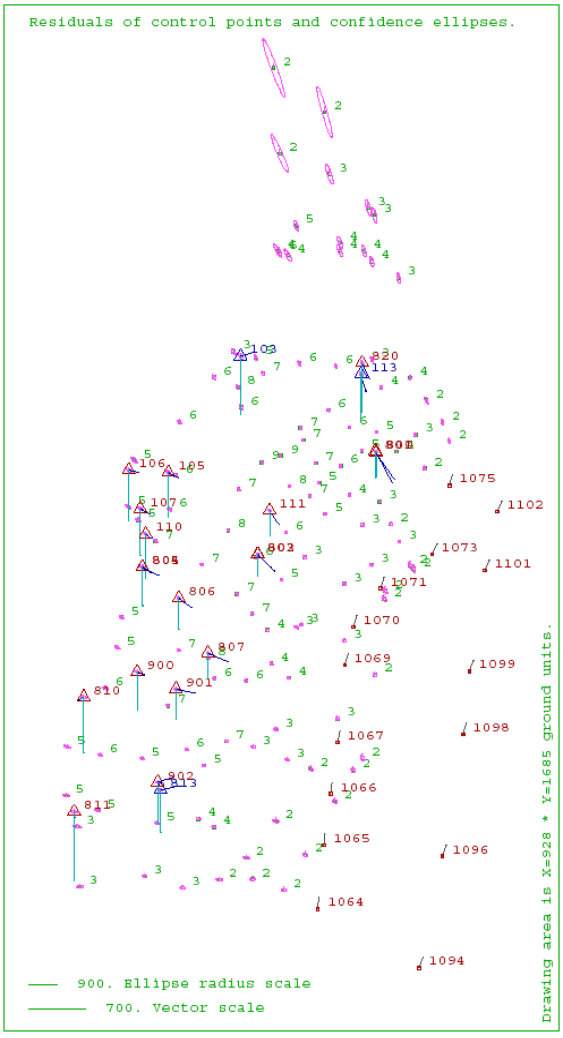

Fig. 7 : Residuals on the GCP's for the adjustment with GPS data only.
The systematic error in Z appears clearly.

The different RMS of the table 1 shows that the block is stable because the RMS on the angles are small (~30 arc second). There is no floating solution. The same kinds of adjustment have been performed on a single line (except without GCP's) but the Phi angle show an instability (RMS PHI= 0.1 g).

Adjustment type	RMS X [m]	RMS Y [m]	RMS Z [m]
AT	0.08	0.07	0.20
GPS-3GCP	0.08	0.08	0.26
GPS-3GCP shift	0.07	0.13	0.20
GPS-3GCP Sft/dft	0.09	0.15	0.24
GPS	0.16	0.15	0.49
GPS-all GCP	0.05	0.12	0.19
GPS-1GCP	0.09	0.11	0.31

Tab.2 : RMS values of the residuals on Control points for each type of computations.

The table 2 shows that it is possible to obtain an accuracy of 30cm on the ground control point with only one determined control point. The graphical analysis of the residuals shows a systematic error (fig. 7).
For the computation without any GCP's, we determine the residual shift with a Helmert transformation on the control points and the final residuals on the control points. The computed shift is similar to the shift self computed with GCP's. Except for the standard triangulation (AT), this shift of 10 cm in planimetry and 40-50 cm in altimetry appears in each adjustment (tab.3).

The origin of this residual systematic error on the GCP's (or Check points) is hard to find. We have tried to modify both the focal length ***c'*** and the principal point coordinates but while the sigma increases, the shift does not change.

Adjustment type	Shift X [m]	Shift Y [m]	Shift Z [m]
GPS-3GCP shift	*0.05*	*0.01*	*-0.53*
GPS	0.10	0.22	-0.46
GPS-1GCP	0.10	0.21	-0.45

Tab. 3 : *Self-computed* / a posteriori s determined with Helmert 3D transformation on the GCP's shift.

The other source could come from the fact that the GCP's have been determined by tacheometric survey. A shift between both way of measurements could explain it. But for now, it is impossible to say exactly where this shift comes from.

Once the effect of this shift is removed, either by self-computation or by Helmert, the residuals on the control points do not exceed 10 cm in planimetry and 15cm in altimetry.

If we used the 1 GCP' in the adjustment, the residuals are the same after the Helmert (8cm X,Y and 12cm Z).

4.2.3. Comparison between GPS adjustments and Aerial Triangulation (AT)

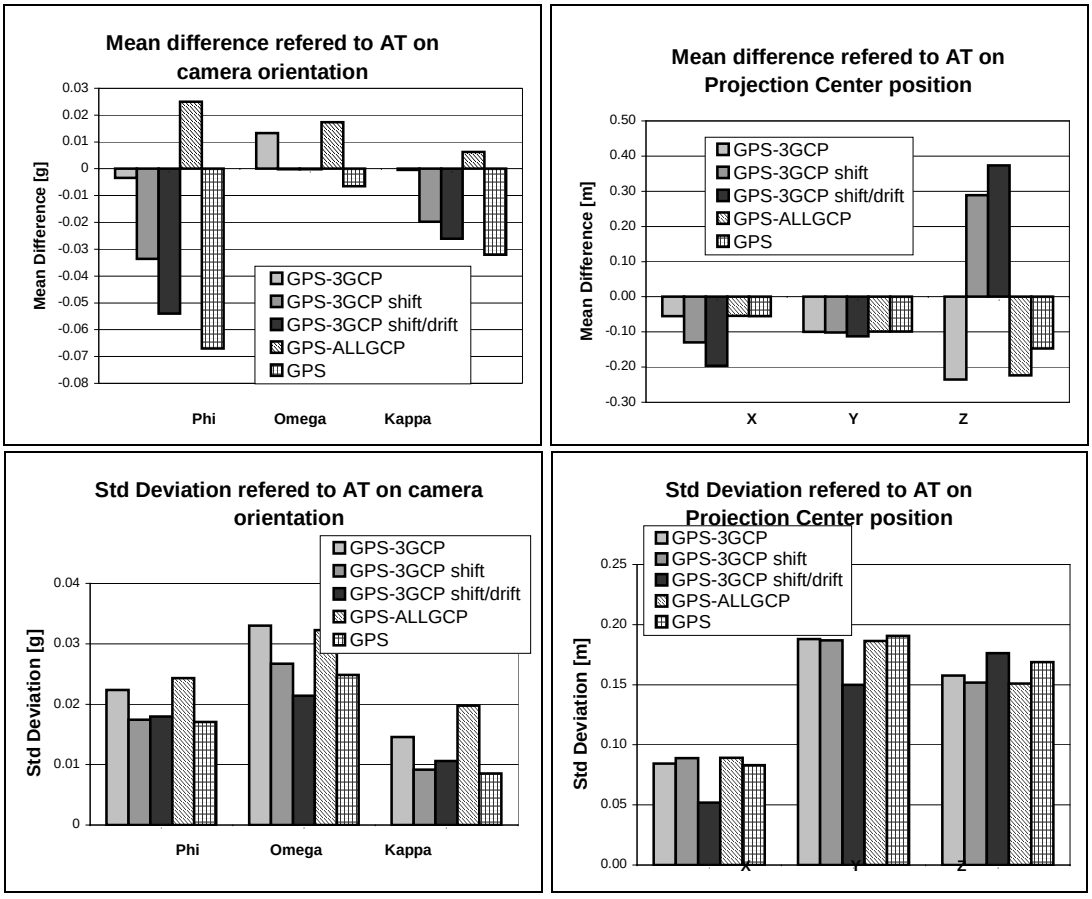

Fig. 8 : Comparison of the exterior orientation parameters between the different types of GPS adjustment and the AT. First line of graphics shows the systematic deviation regard to AT whereas the second line shows the standard deviation of the orientation parameters for each type of adjustment regard to AT.

The comparison between the use of external data (GPS) to determine the orientation parameters and a standard Aerial triangulation confirms the presence of a systematic error (Fig. 8).

If the residuals on the GCP's do not vary a lot in relation to the sort of adjustment, the differences on the orientation parameters change significantly and systematically. For example, we can see that Phi systematically changes of –0.05 gon for the GPS adjustments. This systematic deviation of the angles is balanced by the computed shift (either self computed or Helmert). This phenomenon is easily understandable: the value of Phi is near 60 gons. A variation of 0.05 gon at 450m gives involves a shift in Z of 35 cm and 10 cm in X,Y (the slope is more or less perpendicular to the optical axis).

For the position, the systematic error is less significant with values about 10-15cm. We reach, on one hand, the limits of the accuracy of the GPS in Kinematic mode, and on other hand, the accuracy of the control points.

If we compare the coordinates of the tie points between each kind of adjustment with AT, the systematic component does not exceed 13 cm in X,Y and 20 cm in altimetry (shift effect removed). Standard deviation is about 10 cm in X,Y and 15 cm in Z. Without the removal of the shift, systematic component reach 35 cm in Z with no GCP's and 28 cm with one control point.

5. CONCLUSION

The goal of this test was to answer to the question: what is the minimum of necessary GCP's with GPS data to get exterior orientation parameters providing an accuracy of 20-30cm on ground measurements with a light handheld system?

Those results showed that with GPS, it is possible to obtain an accuracy of 15cm without GCP's. The use of 3 GCP's does not increase significantly the accuracy but gives a control. Even if there is a shift on the GCP's residuals, we have to keep in mind that the final aim is to measure volume by differentiation between two flights. It means that if the shift stays constant between two flight, its effect on the volume measurement will be insignificant. Obviously, it is crucial to control if the shift is constant. In this way, we recommend to use one or two ground control points. If possible, the control points should be measured by GPS in order to remove the eventual shift between two coordinates systems.

We can also infer that with 2 strips, it is possible to perform stable exterior orientation with GPS data without any GCP's whereas it is well known that on one single strip the roll angle can not be determined.

Another crucial aspect of this test is that the reception of GPS signal is not affected by the propeller. Neither loss of lock nor cycle slip were detected because of the propeller obstruction. Nevertheless, the GPS constrains the way of piloting the helicopter. The pilot has to care to make flat turns with the helicopter, otherwise satellites can be lost.
Moreover, the variation of the refraction coefficient around the propeller due to a variation of the air density is unknown. Its on the propagation of the carrier phase is also unknown.

Finally, from a practical point of view, the handheld system meets our expectations. It is enough flexible to take both vertical or oblique photographs and the feared vibrations during the transition flight were largely lower than we thought. It is a positive aspect for the future IMU integration. These latest integration is yet to be tested over the upcoming weeks and first results hope to be presented at the time of the workshop.
We have now an operational handheld system that meets the needs of the avalanche volume mapping. Indeed, the minimal number of ground control points can be reduced to two. This will allow us to determine snow volumes in the runoff area, where it was previously impossible.

AKCNOWLEDGMENT

We thank Dr. W. Ammann, Dr. U. Gruber and F. Dufour of the Swiss Federal Institute for Snow and Avalanche Research of Davos for their active participation in this research project.

The Helicopter company Air Glacier in Sion is thanked for providing their expertise during the design and testing stages of the system.

Tomtecs AG. in Japan is also thanked for lending us their HEIE G4 Camera for all of our tests and developments.

REFERENCES

Abdullah Q, (1997). Evaluation of GPS-Inertial Navigation system for airborne photogrammetry.

Ackermann, F., Schade, H. (1993). Application of GPS for aerial triangulation. Photogrammetric Engineering and Remote Sensing, Vol. 59, No. 11, pp. 1625-1632.

Cramer, M. (1999). Direct Geocoding – is Aerial Triangulation Obsolete? Photogrammetric Week 47, Stuttgart, September 20-24, pp. 59-70.

Hein, G.W, Baustert G., Eisfeller, B., Landau H. (1988). High Precision Kinematic GPS Differential Positioning: Experiences, Results, Integration of GPS with a Ring Laser Strapdown Inertial System, Proceedings of ION-GPS 88, Colorado Springs, Colorado. September 19-23.

Issler, D. (1999). European Avalanche Test Sites. Overview and Analysis in view of coordinated experiments. Mitteilungen #59, 1999. SLF Davos.

Schwarz, K.P., Fraser C.S., Gustafson, P.C. (1984). Aerotriangulation without Ground Control, International Archives of Photogrammetry and Remote Sensing, Vol. 25, Part A1, Rio de Janeiro, June 16-29.

Skaloud, J. (1999). Optimizing Georeferencing of Airborne Survey Systems by INS/DGPS, UCGE Report 20126, Department of Geomatics Engineering, The University of Calgary.

Vallet, J , Gruber, U (2000). Avalanche mass balance measurements at Vallée de la Sionne. Annals of glaciology Vol. 32. International Glaciology Society. Innsbruck, May 22-26.

Vallet, J , Skaloud, J, O, Koelbl, B, Merminod (2000). Development of a Helicopter-Based Integrated System for Avalanche Mapping and Hazard Management. ISPRS congress 2000 Amsterdam proceedings.